

This item was submitted to [Loughborough's Research Repository](#) by the author.
Items in Figshare are protected by copyright, with all rights reserved, unless otherwise indicated.

Designing neuronal networks with chemically modified substrates: an improved approach to conventional in vitro neural systems

PLEASE CITE THE PUBLISHED VERSION

PUBLISHER

© Maria de las Mercedes Pardo Figueres

PUBLISHER STATEMENT

This work is made available according to the conditions of the Creative Commons Attribution-NonCommercial-NoDerivatives 4.0 International (CC BY-NC-ND 4.0) licence. Full details of this licence are available at: <https://creativecommons.org/licenses/by-nc-nd/4.0/>

LICENCE

CC BY-NC-ND 4.0

REPOSITORY RECORD

Pardo-Figueres, Maria M.. 2019. "Designing Neuronal Networks with Chemically Modified Substrates: An Improved Approach to Conventional in Vitro Neural Systems". figshare. <https://hdl.handle.net/2134/27941>.

Designing neuronal networks with chemically modified
substrates: an improved approach to conventional *in vitro*
neural systems.

By

Maria de las Mercedes Pardo Figueres

A thesis submitted in partial fulfilment of the
requirements for the award of

Doctor of Philosophy

Loughborough University

August 2017

TABLE OF CONTENTS

ABSTRACT.....	VIII
ACKNOWLEDGMENTS	X
LIST OF FIGURES	XII
LIST OF EQUATIONS	XVIII
LIST OF TABLES	XIX
 1 INTRODUCTION	 1
1.1 Neurons	2
1.1.1 Overview of the nervous system.....	2
1.1.2 Neuronal structure and nerve impulse	4
1.1.3 Neuronal synapses	6
1.2 Neurons in culture	7
1.2.1 Surface modification for material enhancement	8
1.2.2 Directing neuronal outgrowth	12
1.2.3 Surface engineering techniques for neuronal guidance	13
1.2.4 Most popular scaffolds for neuronal orientation in vitro	17
1.3 Chemical modifications on planar substrates	19
1.3.1 Self-assembled monolayers (SAMs).....	19
1.3.1.1 Silane self-assembled monolayers	20
1.3.2 Polymer brushes.....	22
1.3.3 Effect of chemical surface properties on cell behaviour.....	29
1.3.3.1 Engineering approaches used to create surface chemical patterns	32
1.4 Aim of the Thesis.....	37
2 GENERAL METHODS	38
2.1 Methods for surface modification	39
2.1.1 Surface cleaning.....	39

2.1.2	Formation of 3-aminopropyltriethoxysilane (APTES) by chemical vapour deposition (CVD).....	40
2.1.3	Deposition of α -bromoisobutyryl bromide (BIBB) onto APTES-functionalised surfaces	40
2.1.4	Polymerisation of 2-hydroxyethyl methacrylate (HEMA) from BIBB-functionalised surfaces.....	41
2.1.5	Polymerisation of methyl methacrylate (MMA) from BIBB-functionalised surfaces	42
2.1.6	Polymerisation of 3-sulfopropyl methacrylate (KSPMA) from BIBB-functionalised surfaces.....	42
2.1.7	Polymerisation of [2-(methacryloyloxy)ethyl]trimethylammonium chloride (METAC) from BIBB-functionalised surfaces.....	43
2.2	Patterning methods.....	44
2.2.1	Photolithography.....	44
2.2.2	Soft lithography: Micromolding in Capillaries (MIMIC).....	45
2.3	Techniques for surface analysis	46
2.3.1	Fourier transform infrared (FTIR)	46
2.3.2	Atomic force microscopy (AFM)	48
2.3.3	Water contact angle (WCA).....	49
2.3.4	Ellipsometry	50
2.3.5	X-ray Photoelectron Spectroscopy (XPS)	52
2.4	Cell culture methods	53
2.4.1	Cell culture: SH-SY5Y's	53
2.4.2	Cell culture: C2C12's	54
2.4.3	Cell passaging	54
2.4.4	Cell counting.....	55
2.4.5	Cryopreservation of cells	55
2.4.6	Resuscitation of cryopreserved cells.....	56
2.5	Techniques for biological analysis.....	56

2.5.1	Principle LIVE/DEAD® Cell Viability staining	56
2.5.2	Procedure LIVE/DEAD® Cell Viability staining	57
2.5.3	Principle alamarBlue® assay	58
2.5.4	Procedure alamarBlue® assay	60
2.5.5	Principle Quant-iT™ PicoGreen® dsDNA Assay.....	60
2.5.6	Procedure Quant-iT™ PicoGreen®.....	60
2.5.7	Principle Reverse transcription polymerase chain reaction RT-qPCR	61
2.5.7.1	Primer design and specificity of the primers	63
2.5.7.2	RNA extraction	65
2.5.7.3	Relative quantification PCR	66
2.5.7.4	RT-qPCR procedure.....	68
2.5.8	Principle Immunocytochemistry	68
2.5.9	Staining procedure	69
2.5.10	Image analysis.....	70
2.5.11	Statistical analysis	72
3	GENERATION OF CHEMICALLY MODIFIED SURFACES	73
3.1	Introduction.....	74
3.1.1	Objectives of the chapter	78
3.2	Methods.....	79
3.3	Results.....	79
3.3.1	X-ray Spectroscopy (XPS).....	80
3.3.2	Fourier transform infrared spectroscopy (FTIR)	88
3.3.3	Water contact angle (WCA).....	89
3.3.4	Brush thickness	91
3.4	Discussion	92
3.4.1	Surface preparation	93
3.4.2	Surface characterisation	93
3.5	Chapter summary	95
4	NEURONS CULTURED ON CHEMICALLY MODIFIED SURFACES	97

4.1	Introduction.....	98
4.1.1	SH-SY5Y cells as a neuronal model on chemical modified substrates	99
4.1.2	Objectives of the chapter	101
4.2	Methods.....	101
4.2.1	General procedure for LIVE/DEAD® staining of mammalian cells.....	101
4.2.2	Assessment of metabolic activity: General procedure for alamarBlue®.....	101
4.2.3	Proliferation assay: Quant-iT PicoGreen dsDNA assay	101
4.2.4	Morphological and biochemical assessment of neuronal differentiation	101
4.2.4.1	Neurite length general procedure.....	101
4.2.4.2	RT-qPCR.....	102
4.2.4.2.1	MAPT gene expression	102
4.2.5	Effect of PHEMA brush thicknesses on cell behaviour.....	102
4.2.6	Statistical analyses	102
4.3	Results.....	103
4.3.1	Effect of chemical surface modifications on cellular viability	103
4.4	Cellular metabolism and proliferation	110
4.4.1	Assessment of metabolic activity on chemically modified surfaces	110
4.4.2	Assessment of cell proliferation on chemically modified surfaces	112
4.5	Effect of PHEMA brush thicknesses on cell behaviour.....	113
4.6	Effect of surface coatings on neurite outgrowth and differentiation of SH-SY5Y cells.....	116
4.7	Correlation between neurite length and water contact angle	119
4.8	Discussion	120
4.8.1	Effect of surface chemistry on cell behaviour	120
4.8.1.1	Different thicknesses for PHEMA in cell culture	123
4.8.2	Chapter summary	123
5	CREATING CHEMICAL PATTERNS FOR NEURITE GUIDANCE	125
5.1	Introduction.....	126
5.1.1	Micropatterning surfaces and the ability for cell confinement	127

5.1.2	Objectives of the chapter	128
5.2	Methods.....	128
5.2.1	Binary coating formation (Binary sample)	129
5.2.2	Binary sample under cell culture conditions.....	129
5.2.3	Photolithography via dry film photoresist: fabrication of masters for MIMIC and direct patterning	129
5.2.4	Fabrication of PDMS moulds for MIMIC technique.....	130
5.2.5	Creating BIBB/PKSPMA patterns by MIMIC technique.....	131
5.2.5.1	BIBB/PKSPMA patterns formed by MIMIC technique under cell culture conditions.....	131
5.2.6	Photolithography via wet film photoresist.....	132
5.2.6.1	Mask design	132
5.2.6.2	Photolithography process via wet film photoresist.....	132
5.2.6.3	SU-8 10 photoresist.....	132
5.2.6.4	S1813 photoresist.....	133
5.2.7	Chemical pattern via wet film photoresist	133
5.2.7.1	PKSPMA as the starting surface.....	133
5.2.7.2	BIBB as the starting surface	134
5.2.7.3	Non-coated glass slide as the starting surface.....	135
5.3	Experimental set up of SH-SY5Y on different channel widths.....	136
5.4	Statistical analysis.....	136
5.5	Results.....	137
5.5.1	First attempts in cell spatial constraining: binary sample.....	137
5.5.2	Photolithography via dry film photoresist	143
5.5.3	Patterning SH-SY5Ys using soft lithography MIMIC technique	144
5.5.4	Photolithography via wet film photoresist.....	147
5.5.5	MIMIC with wet film photolithography masters.....	147
5.5.6	Conventional photolithography	148
5.5.6.1	PSKPMA as the starting surface.....	148

5.5.6.2	BIBB as the starting surface	150
5.5.6.3	Non-coated glass slide as the starting surface.....	151
5.6	Discussion	159
5.6.1	Controlling cell confinement from cm to μm sizes.....	160
5.6.2	Does cell density and channel width affect cell rearrangement within the pattern	161
5.6.3	Chapter summary	162
6	INTERACTIONS BETWEEN NEURONS AND MYOTUBES IN A CHEMICALLY PATTERNED CO-CULTURE	164
6.1	Introduction.....	165
6.1.1	The effect of retinoic acid on skeletal muscle	166
6.1.2	Objectives of the chapter	167
6.2	Methods.....	167
6.2.1	Effect of repulsive and attractive coatings on C2C12's.....	168
6.2.2	Differentiation media optimisation for C2C12's and SH-SY5Y's: reduction in serum percentage	168
6.2.3	Differentiation media optimisation for C2C12's and SH-SY5Y's: ATRA dose effect	169
6.2.4	Co-culture experimentation with SH-SY5Y's and C2C12's using chemical patterning and physical barrier.....	170
6.2.4.1	Co-culture experimentation with SH-SY5Y's and C2C12's without a physical barrier.....	171
6.2.5	Statistical analysis.....	172
6.3	Results.....	172
6.3.1	Repulsive and attractive coatings on C2C12's	172
6.3.2	Differentiation media optimisation for C2C12's and SH-SY5Y's: reduction in serum percentage	174
6.3.3	Differentiation media optimisation for C2C12's and SH-SY5Y's: ATRA dose effect	180

6.3.4	Co-culture experimentation with SH-SY5Y's and C2C12's	183
6.4	Discussion	192
6.4.1	Media compatibility and attempts to co-culture with patterned neurons.....	192
6.4.2	Chapter summary	194
7	DISCUSSION	195
7.1	General discussion	196
7.2	Key findings.....	198
7.3	Limitation of this work	201
7.4	Future directions	202
7.5	Conclusions.....	204
8	REFERENCES	206
9	APPENDICES.....	232
9.1	LIVE/DEAD® assay optimisation	233
9.2	alamarBlue® assay optimisation	235
9.3	Guidance to estimate brush thickness	238
9.4	List of abbreviations	239
9.5	Achievements related to this thesis.....	245

ABSTRACT

Highly organised structures are known to be part of the complex neuronal network present in the nervous system, where thousands of neuronal connections are arranged to give rise to critical physiological functions. Conventional *in vitro* culture methods are useful to represent simplistic neuronal behaviour, however, the lack of such organisation results in random and uncontrolled neurite spreading, leading to a lack of cell directionality and in turn, resulting in inaccurate neuronal *in vitro* models.

Neurons are highly specialised cells, known to be greatly dependent on interactions with their surroundings. Therefore, when a material surface is modified, drastic changes in neuronal behaviour can be achieved. The use of chemically modified surfaces *in vitro* has opened new avenues in cell culture, where the chaotic environment found in conventional culture methods can be controlled by the combination of surface modification methods with surface engineering techniques. Polymer brushes and self-assembled monolayers (SAMs) are a convenient surface modification tool for cell culture applications, since their properties can be finely tuned to promote or inhibit cellular adhesion, differentiation and proliferation. Thus, when precisely combined with patterning techniques, a control over neuronal behaviour can be achieved.

Neuronal patterning presents a system with instructive cues that can be used to study neuron-neuron communication by directing single neurites in specific locations to initiate synapses. Furthermore, although this area has not been much explored, the use of these patterned brushes could also be used in co-culture systems as a platform to closely monitor cell heterotypical communication.

This research demonstrates the behaviour of SH-SY5Y neurons on a variety of SAMs and polymer brushes, both in isolation and combination to promote cellular spatial control. APTES and BIBB coatings promoted the highest cell viability, proliferation, metabolic activity and neuronal maturation, whilst low cell adhesion was seen on PKSPMA and PMETAC surfaces. Thereafter, PKSPMA brushes were used as a potential cell repulsive coating and its combination

with micro- patterning techniques (photolithography and soft lithography) resulted in a system with instructive cues for neuronal guidance, where neuronal directionality was obtained.

In the final chapter of this thesis, a chimeric co-culture system was developed where the patterned SH-SY5Y cells were co-cultured with C2C12 myoblasts in an attempt to obtain an organised neuronal-muscle co-culture system. Whilst preliminary observations showed first stages of a patterned neuronal-muscle co-culture, future work is necessary to refine and improve the patterned co-culture process.

ACKNOWLEDGMENTS

Firstly, I would like to thank my supervisors Professor Mark P. Lewis and Dr Steve D. R. Christie for all the support and knowledge I have received throughout this project. Thank you for accepting me as your PhD student despite my little background in biology and for showing me the amazing world of cells! Thanks to Paul Roach for his help and assistance on the photolithography equipment and to the miniCDT group for those constructive meetings where I mastered my oral presentation skills!

I would especially like to thank Dr Darren Player and Dr Neil Martin for teaching me all the cell lab skills from scratch. I would not have known where to start if you guys were not there with all the good banter and patience since day one. Your encouragement and support made this lab the greatest to work in. Special thanks go to Neil for the continuous advice out and inside the lab whenever I needed a chat, for dealing with my innumerable Spanglish corrections and for always being there really. OCK!

I have met so many great people in my years at Loughborough University that I could fill pages and pages of acknowledgments, as all of them have contributed to making these years worthy. I have been lucky to work in two different labs where I have felt at home since day one. Thanks the cell group for all the bio-banter and numerous pints after long round table meetings, and to the chemistry group for all those evenings at the Moon and Bell. Especially to Vanessa, for all those chats over coffee breaks and for showing me all the tricks that Word was hiding from me when I was writing up my thesis. To Alberto, for being my partner in crime from the 1st year of university until the last day of my PhD. I don't know where I would be now if you weren't in luffs to lift me up with your silliness-*¡Zapato en reactor!*

Special mentions go to Alex, for making me believe enough in myself to apply for this PhD and for pushing me to read all those books in English. To my friends from Spain: Flor, Angela, Abel, San... whose continuous support in hard times kept me going. To Mark, whose help and understanding made the end of this journey a bit easier.

To my mum, always cheerful and smiley despite everything. To my brother, I do not know where to start. Thank you for being there not matter what. For the enormous economic and moral support I had from you when I decided to start this adventure. For all the stupid jokes you and mum told me to cheer me up when I was not at my best time. I would certainly not be the person I am if I hadn't had you as my big brother.

This is for you both.

LIST OF FIGURES

Figure 1.1. Overview of the nervous system. Adapted from Reece <i>et al.</i> (2010).....	3
Figure 1.2. Characteristic neuronal structure.....	5
Figure 1.3. Neuromuscular junction.	7
Figure 1.4. Organised vs. disorganised neuronal environments.	13
Figure 1.5. Main classification of micro-nano fabrication techniques for their use in biological patterns.....	14
Figure 1.6. Microcontact printing process for neuronal patterning.	17
Figure 1.7. Structure of self-assembled monolayers.....	20
Figure 1.8. Process to produce silane self-assembled monolayers on glass surfaces.	22
Figure 1.9. Polymer brush structure.....	23
Figure 1.10. Polymer brush conformations.....	24
Figure 1.11. “Grafting from” and “grafting to” approaches.	26
Figure 1.12. ATRP mechanism.....	27
Figure 1.13. ARGET-ATRP mechanism.	28
Figure 1.14. Effect of surface potential in cell culture.	31
Figure 1.15. Use of photolithography for chemical patterning.....	33
Figure 1.16. Effect of soft lithography patterns on cell culture..	34
Figure 2.1. Surface cleaning under UV/ozone photo reactor.....	39
Figure 2.2. Deposition of 3-aminopropyltriethoxysilane (APTES) onto glass surfaces/silicon wafers.....	40
Figure 2.3. Deposition of α -bromoisobutyryl bromide (BIBB) onto APTES-functionalised glass surfaces/silicon wafers.	40

Figure 2.4. Polymerisation of 2-hydroxyethyl methacrylate (HEMA) from BIBB-functionalised glass surfaces/silicon wafers.	41
Figure 2.5. Polymerisation of methyl methacrylate (MMA) from BIBB functionalised glass surfaces/silicon wafers.	42
Figure 2.6. Polymerisation of 3-sulfopropyl methacrylate (KSPMA) from BIBB functionalised glass surfaces/silicon wafers.	42
Figure 2.7. Polymerisation of [2-(methacryloyloxy)ethyl]trimethylammonium chloride (METAC) from BIBB-functionalised glass surfaces/silicon wafers.	43
Figure 2.8. Schematic of photolithography principle	45
Figure 2.9. Micromolding in capillaries (MIMIC) principle.	46
Figure 2.10. Schematic of FTIR principle	47
Figure 2.11. Schematic of AFM principle.	48
Figure 2.12. Water contact angle in a smooth surface	50
Figure 2.13. Schematic of ellipsometer principle.	51
Figure 2.14. Schematic of XPS principle.....	52
Figure 2.15. Hemocytomer grid used for cell counting.	55
Figure 2.16. LIVE/DEAD® Cell Viability principle.....	57
Figure 2.17. AlamarBlue® principle.	59
Figure 2.18. Standard curve used to determine [dsDNA] using the fluorescence of Quant-iT™ PicoGreen®.....	61
Figure 2.19. Three step process in RT-qPCR	62
Figure 2.20. MAPT melt curve.	65
Figure 2.21. Immunocytochemistry principle for direct and indirect fluorescence.....	69
Figure 2.22. Analysis of neurite length.....	71

Figure 2.23. Analysis nuclei alignment	72
Figure 3.1. Effect of surface chemical functionalities in cell culture.	75
Figure 3.2. N1s high resolution spectra of A) UV/ozone glass slide and B) APTES functionalised surface..	81
Figure 3.3. Curve-fitted XPS spectrum of Br3d core-line recorded for BIBB functionalised glass slide.	82
Figure 3.4. XPS analysis of PHEMA brushes.	84
Figure 3.5. XPS analysis of PMMA brushes.	85
Figure 3.6. XPS analysis of PMETAC brushes.	86
Figure 3.7. XPS analysis of PKSPMA brushes.	87
Figure 3.8. FTIR characterisation of polymer brushes.	89
Figure 3.9. Images of water droplets (2 μ L) during water contact angle measurements for CTRL (non-coated glass), SIOH, APTES, BIBB, PHEMA, PMMA, PKSPMA and PMETAC.	90
Figure 3.10. PKSPMA brushes deposited on silicon wafers	92
Figure 4.1. Main factors affecting cell behaviour.	98
Figure 4.2. Figure 4.2. Representative fluorescence micrographs LIVE/DEAD® staining of SH-SY5Y after 1 and 3 days cultured on the different chemical surfaces.	105
Figure 4.3. Representative fluorescence micrographs LIVE/DEAD® staining of SH-SY5Y after 5 and 7 days cultured on the different chemical surfaces	106
Figure 4.5. SH-SY5Y's cell viability (%) on the different chemical coatings at days 1, 3, 5 and 7.	108
Figure 4.6. Average number of SH-SY5Y's counted per field of view on the different chemical surfaces at days 1, 3, 5 and 7	109

Figure 4.7. Comparative light micrographs illustrating the proliferation rate prior performing the alamarblue® assay on the different chemical surfaces.	111
Figure 4.8. Metabolic activity assessed by alamarBlue® fluorescence on SH-SY5Y's.	112
Figure 4.9. Proliferation rates assessed by DNA quantification from Quant-iT™ PicoGreen® fluorescence of SH-SY5Y's.....	113
Figure 4.10. SH-SY5Y's cultured on PHEMA samples generated at different polymerisation times.....	115
Figure 4.11. Effect of PHEMA film thicknesses on cell behaviour.	116
Figure 4.12. Representative phase contrast micrographs illustrating neurite outgrowth.....	117
Figure 4.13. Average neurite length measured on BIBB, APTES, PMMA, SIOH and the control (non-coated glass).	118
Figure 4.14. Expression of MAPT gene on modified surfaces. MAPT codes for tau protein involved in microtubule stabilisation.....	119
Figure 4.15. Relationship between WCA vs. average neurite length	120
Figure 5.1. Macroscopic images of the photomasks used and the master fabricated with PDMS cast on top.	130
Figure 5.2. MIMIC process.....	131
Figure 5.3. Schematic describing the photolithographic process for obtaining a PKSPMA/APTES pattern.	134
Figure 5.4. Schematic describing the photolithographic process for obtaining a PKSPMA/BIBB pattern.	135
Figure 5.5. Schematic describing the photolithographic process for obtaining a PKSPMA/glass pattern	136
Figure 5.6. FTIR spectrum of PKSPMA (pink) and BIBB (black) binary sample.....	138

Figure 5.7. XPS analysis of S2p and Br3d core level spectra of PKSPMA (pink) and BIBB (black).	140
Figure 5.8. Interface of BIBB/PKSPMA binary sample.....	141
Figure 5.9. SH-SY5Y cells were grown on the binary sample and stained after a week in GM..	142
Figure 5.10. Photolithography with dry film photoresist.....	143
Figure 5.11. Macroscopic image of a MIMIC patterned sample with BIBB/PKSPMA.	144
Figure 5.12. XPS spectrum of A) PKSPMA area and B) BIBB area.	145
Figure 5.13. MIMIC patterns under neuronal cell culture	146
Figure 5.14. MIMIC patterns with high resolution features	148
Figure 5.15. PKSPMA/APTES patterns	149
Figure 5.16. APTES/PKSPMA patterns under cell culture.	149
Figure 5.17. BIBB/PKSPMA patterns under culture.....	150
Figure 5.18. BIBB/PKSPMA patterns in cell culture after hard baking.....	151
Figure 5.19. Schematic of the photolithographic procedure to obtain PKSPMA/glass patterns.	152
Figure 5.20. AFM height profiles showing the patterned PKSPMA polymer brush samples on glass for A) 5 μm and B) 10 channel widths.	153
Figure 5.21. Patterns with 5 and 10 μm channel width under cell culture.	153
Figure 5.22. AFM height profiles showing the patterned PKSPMA polymer brush samples on glass containing approximately A) 20, B) 50, C) 75 and D) 100 μm channel widths for cell growth.	154
Figure 5.23. SH-SY5Ys patterned in channels of 20 μm width.	155
Figure 5.24. SH-SY5Y cells seeded at 5000, 10000 and 150000 cells/ cm^2 in 20 μm , 50 μm , 75 μm and 100 μm wide channels.	157

Figure 5.25. Analysis of SH-SY5Y's patterns at different cell densities (5000, 10000 and 15000 cells/cm ²) and channel widths (20, 50, 75 and 100 μ m).	158
Figure 5.26. Patterned SH-SY5Y cells seeded at 10000 cells/cm ² in 20 μ m wide channels.....	159
Figure 6.1. Experimental set-up for co-culture.	171
Figure 6.2. Experimental set-up for co-culture with no barrier at the interface.	172
Figure 6.3. Effect of BIBB and PKSPMA surfaces in C2C12's.	173
Figure 6.4. Phase contrast micrographs of C2C12's after 3 days in various DM.....	175
Figure 6.5. Phase contrast micrographs of SH-SY5Y's after 3 days in various DM	176
Figure 6.6. Fluorescence micrographs of C2C12's myoblasts and myotube morphology analysis after 3 days in various DM.....	177
Figure 6.7. Fluorescence micrographs of SH-SY5Y's and neurite length analysis after 3 days in various DM.	179
Figure 6.8. Fluorescence micrographs of C2C12's myoblasts and myotube morphology analysis at different ATRA concentrations after 3 days in DM.	181
Figure 6.9. Fluorescence micrographs of SH-SY5Y's and neurite length at different ATRA concentrations after 3 days in DM.	182
Figure 6.10. Co-culture of C2C12's and SH-SY5Y's with a physical barrier to separate cell populations.....	183
Figure 6.11. Co-culture with a PDMS barrier at the co-culture interface. A PDMS "wall" was used to stop the C2C12's (left) and SH-SY5Y's (right) from mixing.....	185
Figure 6.12. Attempts to create a neuron-muscle interface when culturing with a PDMS wallm.	186
Figure 6.13. Attempts to create a neuron- muscle interface by seeding cell droplets on different sides of the sample.	187

Figure 6.14. Attempts to create a neuron- muscle interface by seeding cells at different time points.....	188
Figure 6.15. Unpatterned areas covered by C2C12's and SH-SY5Y's.	190
Figure 6.16. Patterned neuronal areas covered by C2C12's and SH-SY5Y's.....	191
Figure 7.1. Alternative designs for neuron-muscle co-culture experimentation.	203
Figure 9.1. Representative fluorescence microscope images of SH-SY5Y for dye optimisation..	234
Figure 9.2. Optimisation of alamarBlue® assay for different cell densities for SH-SY5Y's.....	236
Figure 9.3. Optimisation of alamarBlue® assay at different incubation periods for SH-SY5Y's..	237
Figure 9.4. Colour chart to estimate brush thickness. Film with refractive index 1.5 on silicon.	238

LIST OF EQUATIONS

Equation 2-1. Young Laplace equation	49
Equation 2-2. Fundamental equation of ellipsometry	51
Equation 2-3. Fundamental equation in X-ray photoelectron spectroscopy	52

LIST OF TABLES

Table 1.1. A summary of a selection of studies where neuronal cells were examined under various physical and chemical modifications	11
Table 1.2. Selection of studies based on different patterning techniques for the immobilisation of cells and biomolecules	36
Table 2.1. Parameters used for primer design.....	63
Table 2.2. Primer sequences used in this thesis	64
Table 2.3. Example of data analysis carried out using the $2^{-\Delta\Delta C_T}$ method	67
Table 3.1. Effect of surface charge and wettability on various cell types	77
Table 3.2. Main considerations when comparing SAMs and polymer brushes for thin film formation.....	78
Table 3.3. Chemically modified surfaces used highlighting their functional group and surface wettability	79
Table 3.4. Percentage composition of Si2p, C1s, O1s, N1s and Br3d after the cleaning, silanisation and initiator deposition	81
Table 3.5. Percentage of Si2p, C1s and O1s atomic composition after the polymerisation of the brushes	83
Table 3.6. Average water contact angle for each surface	91
Table 5.1. Main characteristics of the Ordyl dry film photoresist	130
Table 5.2. Atomic composition of Si2p, C1s and O1s determined by XPS on both sides of the binary sample (half BIBB and half PKSPMA).....	139
Table 6.1. Composition of different media used for the co-culture of SH-SY5Y's and C2C12's	169

Table 6.2. Composition of different media used with differing concentration of ATRA for the co-culture of SH-SY5Y's and C2C12's.....	170
--	-----

1 Introduction

1.1 Neurons

1.1.1 Overview of the nervous system

The nervous system (NS) is comprised of a highly organised network that is responsible for transmitting and receiving information from and to various parts of the body. The NS is mainly divided by the central nervous system (CNS) and the peripheral nervous system (PNS) (Figure 1.1). The CNS, which includes the brain and spinal cord, contains a substantial network of nerve fibres extending through the limbs and organs that interpret the signals received from the PNS (Schmidt and Leach, 2003; Roach *et al.*, 2007). The PNS is responsible for sending information to the CNS regarding the stimuli received from the surroundings (sensory division), thus triggering an action (motor division, e.g. muscle contraction due to pain) (Sherwood, 2001; Fowler, *et al.*, 2013). The PNS motor division system is divided into subsystems: the autonomic and somatic systems. The autonomic system oversees functions regarding the autonomous control of the body such as breathing or heartbeat, and it is further subdivided in the sympathetic and parasympathetic systems. The sympathetic nervous system is triggered under stressful circumstances, commonly known as the *fight or flight* response, where the body gets prepared to confront threatening situations by activating functions such as an increase in heart rate or sweating. Normally, for the neuronal network to reach certain organs, various neurons are connected together to send the information. Thus, preganglionic cells are in charge to send the information to postganglionic cells, which in turn will send the information to the target organ. Visceral organs, blood vessels, cardiac and smooth muscle are involved in this system (Sherwood, 2001). In contrast, the parasympathetic nervous system is responsible for resetting the functions triggered by the sympathetic system. After a stressful situation, the parasympathetic system will be in control of slowing the heart rate or lowering the blood pressure, processes frequently referred to as the *rest and digest* response (Lodish *et al.*, 2000; Alberts *et al.*, 2002; Schmidt and Leach, 2003).

The somatic system controls the voluntary movement of the body and the response to stimuli from the external environment (Figure 1.1). For example, when you notice the presence of a spider on your arm, the upper motor neuron (a set of neurons is necessary to reach the target)

will receive the stimuli from the CNS. This will be carried to the lower motor neuron located in the ventral horn of the spinal cord, ultimately releasing the information. The lower motor neuron will then proceed to synapse the muscle, resulting in the movement of the arm. The main components involved in this system include sense organs, skeletal muscle, bones, joints and skin (Alberts *et al.*, 2002; Fowler, *et al.*, 2013).

The nervous tissue behind the nervous system is packed with neurons and neuroglia, and although the latter are more abundant, neurons are the main functional component involved in the system (Purves *et al.*, 2001; Reece *et al.*, 2010).

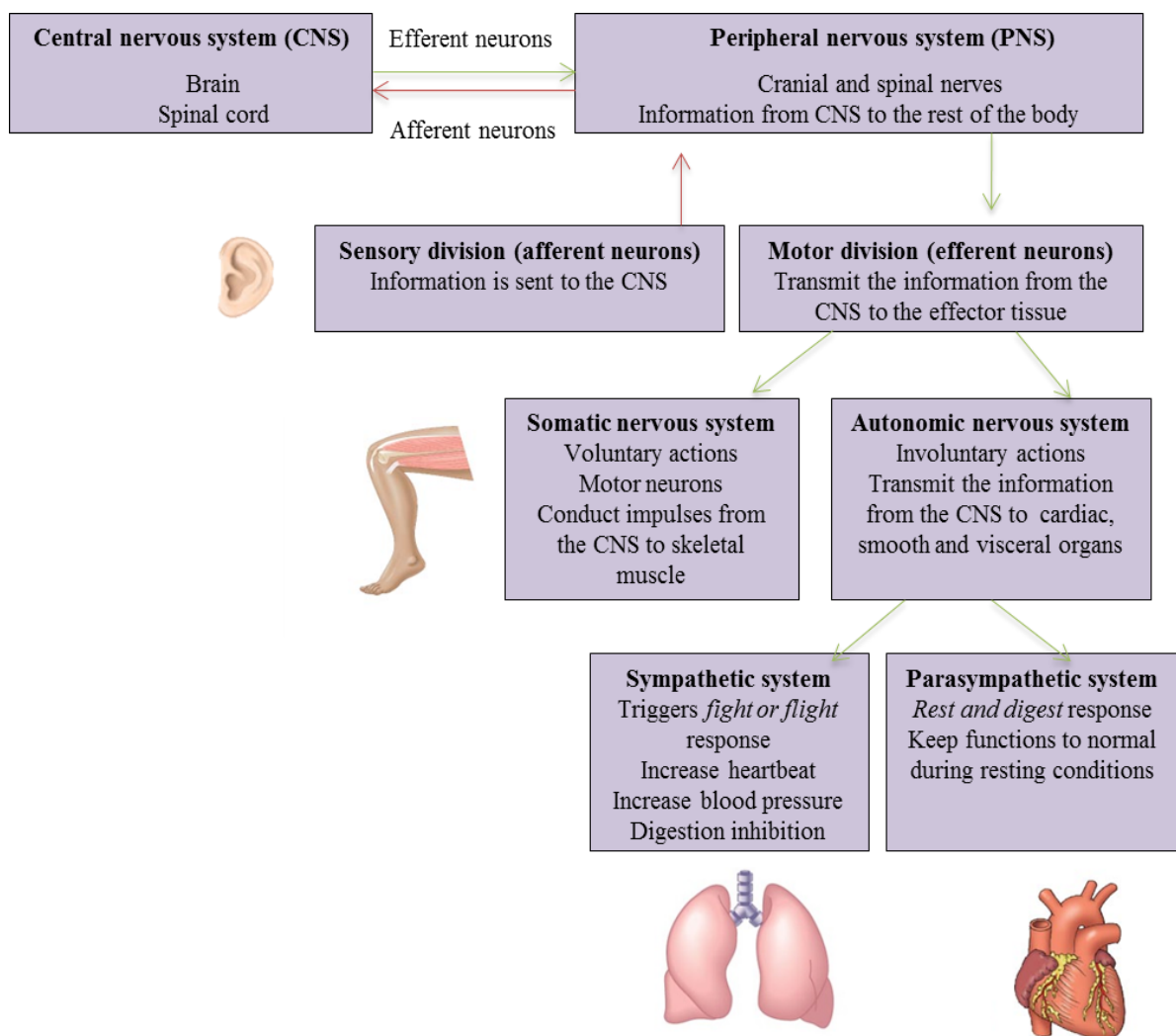


Figure 1.1. Overview of the nervous system. Adapted from Reece *et al.* (2010).

1.1.2 Neuronal structure and nerve impulse

Neurons are the essential cellular component in the NS organisation, comprising the main functional element responsible for coordinating several functions involved in the nervous system (Alberts *et al.*, 2002; Schmidt and Leach, 2003). These highly specialised cells are responsible for transmitting information by electrical and chemical signals. Depending on the flow of information, neurons can be classified either as afferent (sensory) or efferent neurons (motor) (Figure 1.1). The sensory neurons transmit the impulses from sensory receptors to the CNS. Alternatively, motor neurons receive the information from the CNS to trigger signals within the body. Interneurons can flow information in both directions (Lodish *et al.*, 2000; Purves *et al.*, 2001).

Neurons can vary in shape and size due to the different functions these cells conduct. However, the structure of a neuron is typically characterised by a cell body (soma) containing the nucleus and various short extensions emerging from the cell body, called dendrites. These protrusions contain several branches aimed to receive the signals from other neurons (Alberts *et al.*, 2002; Kanning, *et al.*, 2010; Reece *et al.*, 2010). One of the dendrites will grow significantly longer, becoming an axon (Figure 1.2). The initiation and outgrowth of the axon involves a reorganisation between the actin cytoskeleton and the microtubule network, where microtubules form a tight bundle and actin filaments organise themselves to form the growth cone. The growth cone is characterised by a “sheet like” structure called lamellapodia. From this structure, small “fingers” called filopodia will extend to contact the surroundings, acting as sensors and identifying the different cues in the surrounding environment (Purves *et al.*, 2001). The role of the axon takes place during the transmission of neuronal information. Dendrites receive electrical impulses from other neurons or sensory cells and thereafter, the axon transmits such impulses away from the soma to the axon terminal, triggering synapses with target cells (Lodish *et al.*, 2000; Sherwood, 2001). The nerve impulses are triggered by a change in the membrane potential. The inside of the neurons is known to be negatively charged relative to the outside surroundings (polarised state), creating a resting potential maintained by the sodium and potassium pumps at a value of approximately -70 mV. When the stimulus received is large enough to surpass a threshold strength (-55 mV, *all or nothing* phenomenon), an action potential near the axonal hillock is triggered (Alberts *et al.*, 2002).

This prompts the opening of the voltage-gated ion channels within the membrane, resulting in a flow of positively charged sodium ions into the neuron, reducing the resting potential value and thus depolarising the cell. Due to such a dramatic change, the sodium channels close and the potassium channels open to release positive ions, returning the membrane to its normal resting potential. The membrane then undergoes a hyperpolarisation state until it returns to the resting level. There is a refractory period after every action potential where the membrane cannot respond to stimulus, thus avoiding signals in both directions (Lodish *et al.*, 2000).

The speed of the action potential can vary depending on the axon diameter, resistance and whether the neuron is wrapped in a myelinated sheath. The myelinated sheath is formed by Schwann cells in the PNS and oligodendrocytes in the CNS (Purves *et al.*, 2001). Myelinated neurons are able to carry impulses faster and more effectively by a saltatory process, as the voltage gated channels are only found at the nodes of Ranvier (see Figure 1.2).

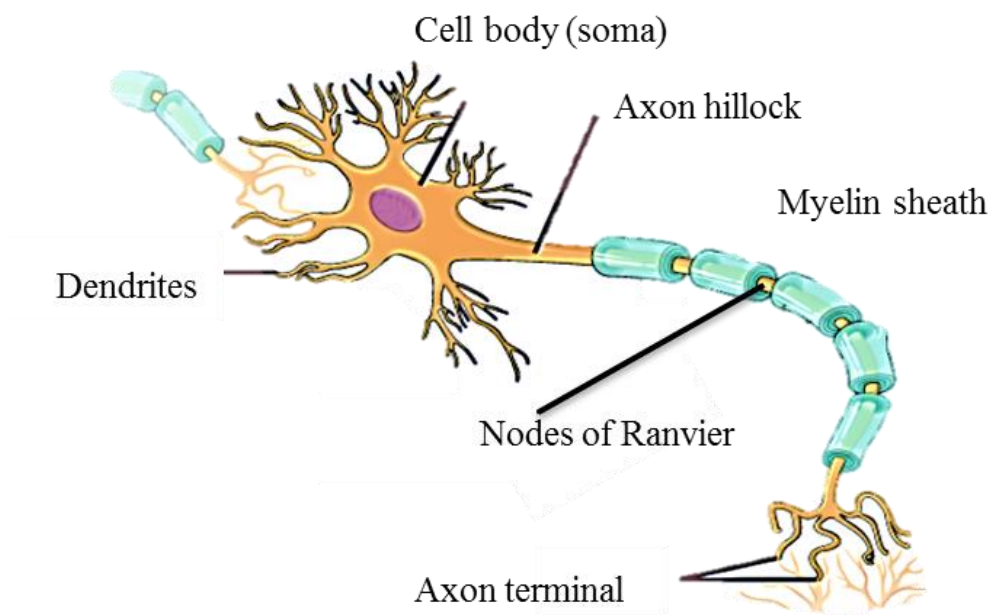


Figure 1.2. Characteristic neuronal structure. The axon terminal is responsible for transmitting the signals that travel down the axon to other neurons or efferent cells, whereas the dendrites receive the stimulus from other cells. Adapted from Fowler *et al.* (2013).

1.1.3 Neuronal synapses

The main mechanism underlying the nervous system is the continuous communication between cells by synapsing. Synapses are the connections established between neurons or another cell to pass necessary information (Campbell, N.A., & Reece, 2008). The synapses can be classified either as electrical or chemical. Electrical synapses are more unusual however, they are faster than chemical synapses. In order to transmit electrical signals, pre and postsynaptic cells are connected by gap junctions and the flow of ions is transmitted (Purves *et al.*, 2001). Alternatively, chemical synapses are slower but more precise. The presynaptic cell contains synaptic vesicles loaded with chemical transmitters, which are released from the axon terminal to the postsynaptic cell in a small region called the synaptic cleft (Lodish *et al.*, 2000; Purves *et al.*, 2001). Once the action potential reaches the axon terminal, the voltage-gated calcium channels open, releasing a flow of calcium ions to the cytoplasm. This in turn triggers the fusion of the synaptic vesicles with the membrane, releasing the neurotransmitters into the synaptic cleft. These neurotransmitters will reach the postsynaptic cell, binding to their receptors and triggering a change on its electrical membrane potential (Alberts *et al.*, 2002). Depending on the neurotransmitter released and which receptors it binds to, the postsynaptic cell can be excited or inhibited. Excitatory neurotransmitters produce a slight change in the membrane by making it more positive on the inside and thus depolarising it. When the neurotransmitter is inhibitory, the potential becomes more negative on the inside, hyperpolarising the membrane (Alberts *et al.*, 2002). A neuron can receive various signals from different cells and thus, the sum of all the signals will trigger the final response, either inhibitory or excitatory. One of the most commonly known neurotransmitters is acetylcholine, considered an excitatory neurotransmitter involved in the neuromuscular junction (NMJ) by triggering muscle contraction (Figure 1.3) (Lodish *et al.*, 2000; Purves *et al.*, 2001). Ultimately, once the neurotransmitter has carried out its function, specific enzymes are the responsible to inactivate the process.

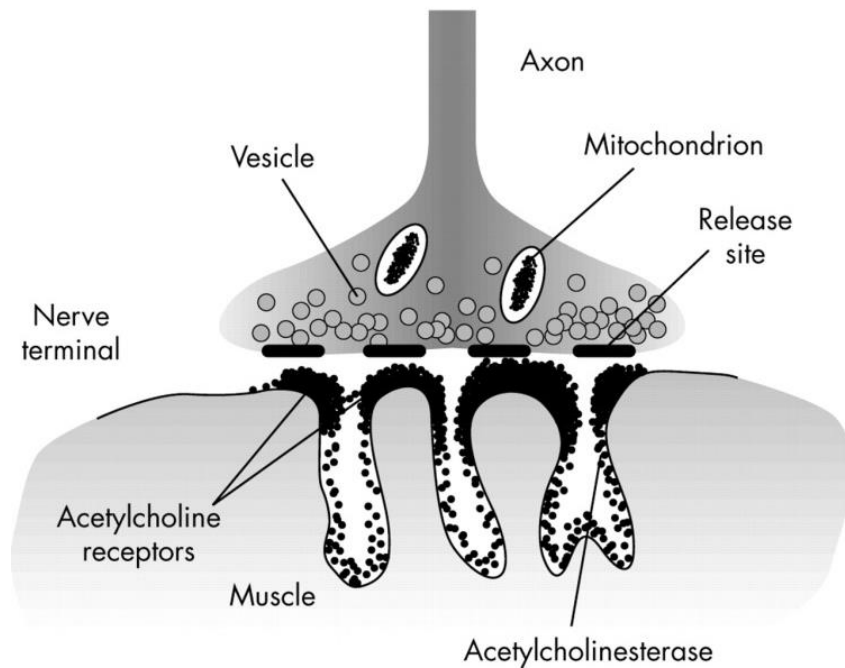


Figure 1.3. Neuromuscular junction. Chemical synapse between a motor neuron and a muscle fibre (Chan and Ho, 2000). Once the neurotransmitter has been released from the nerve terminal, acetylcholine will bind to the acetylcholine receptors present in the muscle. Acetyl cholinesterase will be the responsible to breakdown acetylcholine to inactivate the process.

1.2 Neurons in culture

Efforts to recreate the mechanisms underpinning nervous system physiology have been achieved by using conventional *in vitro* culture systems (Gordon *et al.*, 2013). Cultured neurons have been shown to maintain cellular and molecular properties *in vitro*, undergoing processes such as differentiation and polarisation, and thus providing a potential tool for studying neuronal behaviour (García, 2005; Roach *et al.*, 2007; Kovalevich and Langford, 2013). Conventional *in vitro* systems are based on the observation of a number of cells performing random connections on culture dishes or well plates. These platforms are typically made of polystyrene or glass, due to their transparency under the microscope and low cost (Stanton, 2014). Whilst standard neuronal cultures on these platforms are essential for studying neuronal behaviour, the simplicity of these homogeneous surfaces may elicit an unnatural cell response. This is because such simplicity translates in a poor representation of the environmental cues that cells encounter and respond to *in vivo* (Charest, 2007; Chen *et al.*,

2014). Thus, the disorganised environment created in these platforms translates in a lack of cellular directionality *in vitro* which could affect cell functionality, ultimately limiting many applications within bioengineering (Charest *et al.*, 2006; Chen *et al.*, 2014).

1.2.1 Surface modification for material enhancement

The interaction of the cells with the extracellular environment leads to the ultimate morphology, differentiation and cell growth. The initial response when a material is used in *in vitro* culture is the arrival of water molecules on the surface, forming a water shell. Following this, the adsorption of proteins and other molecules from the media takes place. According to the Vroman effect, the highest mobility proteins will arrive first to the surface and will be likely replaced by less motile proteins, with a more affinity for the surface. Depending on the surface characteristics and the surrounding environment (pH, ionic strength), the deposited proteins are likely to change their conformation from the initial to the final adsorption (Vroman *et al.*, 1980). The interaction between the cells and these proteins is mediated by transmembrane proteins called integrins, which bind to extra-cellular proteins with short amino acid sequences, such as RGD (Massia and Hubbell, 1991). Due to this known interaction, the use of small peptides have been attached onto biomaterial surfaces, in order to analyse cell spreading and focal adhesion contacts (IKVAV, RGD, etc) (Tong and Shoichet, 2001; Tugulu *et al.*, 2007). After such protein adsorption, the cells will reach the surface, interacting with the surface through a protein layer, forming cell-surface interactions (Roach *et al.*, 2007; Ventre *et al.*, 2012).

In the pursuit of influencing a controllable cell response, material scientists have been attempting to find the “perfect” surface (depending on the purpose of the application) by modifying the properties of the surface material for their use in culture (Thevenot *et al.*, 2008). The differing properties on the surface material are of great importance in cell culture, as the degree of protein adsorption and consequently the different cell response will be triggered by such features (Roach *et al.*, 2007; Mager *et al.*, 2011). To this end, efforts have been made to modify surface characteristics by a range of diverse techniques, effectively creating instructive extracellular microenvironments and in turn enhancing positive cell

outputs such as adhesion, proliferation, differentiation and migration (Roach *et al.*, 2010; Ventre *et al.*, 2012; Krishnamoorthy *et al.*, 2014).

Material surface modification can be classified in two main categories: chemical modification and physical modification (including mechanical and topographical properties). Chemical or biochemical molecules are incorporated onto the material surface to alter material properties such as wettability, surface charge and chemical functionality, and in turn either promote or inhibit cellular adhesion, growth and differentiation (Charest *et al.*, 2006; Thevenot *et al.*, 2008; Hayes *et al.*, 2011). This type of modification has been very advantageous to fabricate a wide range of materials with different properties for cell culture assays (Lih *et al.*, 2015). For neurons, coatings typically carrying amine groups such as poly-L-lysine (PLL) have been shown to promote positive cell responses (Khan and Newaz, 2010). Chemical modifications will be discussed in more detail in Section 1.3.

Physical cues involve variations in the topography and the mechanics of the surface material such as the formation of grooves, pits, ridges, etc. and also changes in surface roughness and stiffness (Khan and Newaz, 2010; Tonazzini *et al.*, 2014). In a study presented by Engler *et al.*, (2006), mesenchymal stem cells (MSCs) were shown to go down sspecific lineages depending on the stiffness of the substrate. For the softest substrates, MSCs showed a branched morphology and the upregulation of various neuronal markers. However, with moderate stiff matrices, these cells expressed various myogenic markers, whereas the stiffest substrates promoted the upregulation of osteogenic markers. The formation of microstructures on the surface has also shown to have an impact on cell behaviour, and its been widely used in the field of biosensors and cell-based assays (Jung *et al.*, 2001). Research studies have shown the effects of changes in surface functionality on different cell types, elucidating that different cell types respond in their own manner to similar instructive cues (Arima and Iwata, 2007). Albeit some of the surface features affecting cell behaviour have been analysed, the mechanisms underpinning why cells react in such a manner to the different cues is not fully understood (Senaratne *et al.*, 2005; Krishnamoorthy *et al.*, 2014). A collection of the main studies regarding neuronal behaviour on various surface properties has been highlighted in Table 1.1. The studies presented indicate a profound effect of chemical

and physical modifications on neuronal behaviour, aiding to gain a further understanding of the neuronal-material crosstalk.

Table 1.1. A summary of a selection of studies where neuronal cells were examined under various physical and chemical modifications.

Cell type	Property studied	Surface	Effect	Reference
PC-12 cells	Chemical modification: wettability gradient	Polyethylene (PE) surfaces	PC-12 adhered to moderate hydrophilic surfaces (50-60 degrees). Neurite length was also greater in this wettability range	Lee <i>et al.</i> (2003)
E 18 rat cortical neurons	Chemical modification: different end groups	Gold-coated glass with NH ₂ -terminated SAMs, COOH terminated SAMs and a mixture of both.	For the carboxyl-terminated SAMs and the 1:1 mixture of the amino- and carboxyl-terminated SAMs, significant cell adhesion was not observed whereas amine (NH ₂)-terminated SAMs enhanced favourable cell adhesion	Palyvoda <i>et al.</i> (2008)
Neural stem cells	Mechanical modification: stiffness	PDMS substrates with different stiffness	Soft substrates prepared with similar stiffness to the stiffness of the brain promoted differentiation of neural stem cells	Teixeira <i>et al.</i> (2009)
Nigra cells	Physical modification: roughness	Si wafer with different degree of etching	Cells on rough Si samples adhered and survived much better than on the untreated surfaces, forming neuronal networks	Fan <i>et al.</i> (2002)
E 18 rat cortical neurons	Physical cues	Poly-L-lysine-coated silicon surfaces containing fields of pillars	Neurite length was significantly longer on pillars with the smallest inter-pillar spacing (gaps) and 2µm pillar widths	Dowell-Mesfin <i>et al.</i> (2004)

1.2.2 Directing neuronal outgrowth

During tissue formation and development, cells will encounter and respond to a complex milieu of chemical, physical and biochemical cues in their microenvironment, triggering specific cell behaviour. Researchers have been attempting to mimic such signals *in vitro* by modifying surfaces of cell culture materials, aiming to enhance cell response affecting adhesion, migration, proliferation and cellular differentiation (Tuft, 2014). Highly organised structures have been well known to be part of the complex neuronal network presented in the nervous system (Figure 1.4A), where thousands of neuronal connections are arranged to give rise to critical physiological functions. Conventional *in vitro* culture methods are useful to represent simplistic neuronal behaviour, however, the lack of such organisation *in vitro* results in random and uncontrolled neurite spreading, where neuronal guidance is not apparent (Kleinfeld *et al.*, 1988; In *et al.*, 2005). Consequently, when mimicking neuronal connections *in vitro*, the disorganised environment observed certainly differs from the highly organised network shown *in vivo*, resulting in inaccurate neuronal models (Figure 1.4B). The complex organisation required for neuronal directionality is essential to recreate the mechanisms underpinning neuronal development and neural regeneration. When nerve damage occurs in mice at the PNS, the regenerating axons seem to retrace their original path before injury, reaching original branch points and innervating the same fibres, thus suggesting that organisation and directionality are required (Nguyen *et al.*, 2002).

Materials that incorporate well-defined oriented cues with specific geometries could be a useful tool to prevent random signalling between neurons and heterotypic cells, in turn monitoring cell-cell interactions closely. This could facilitate the study of the biology underpinning nervous system physiology. In addition, the use of a well-organised system could facilitate the directionality of neuronal outgrowth towards specific targets, thus being relevant in areas such as neuroprosthetics or lab on a chip processes (Peyrin *et al.*, 2011; Biffi *et al.*, 2012).

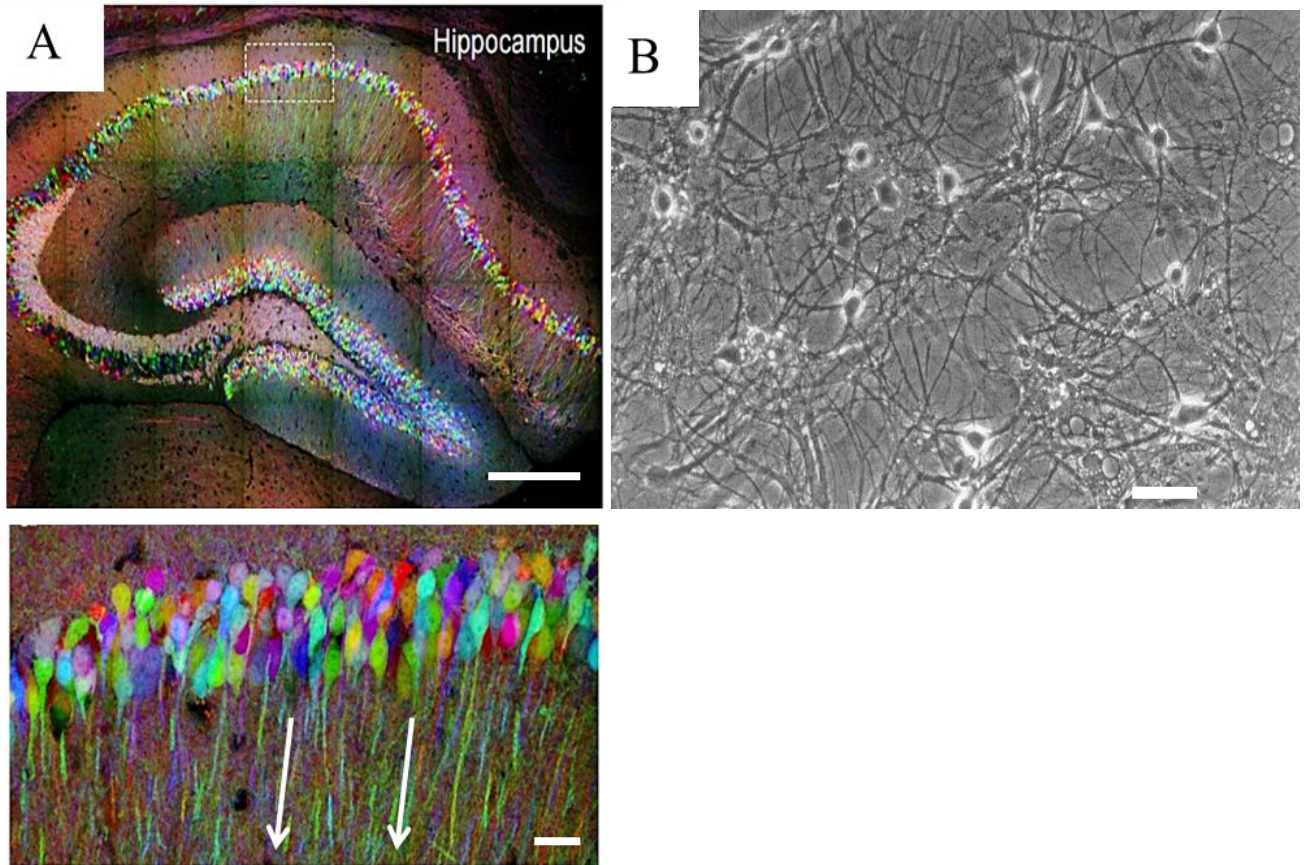


Figure 1.4. Organised vs. disorganised neuronal environments. A) Brainbow: Hippocampus in mice. An organised neuronal assembly can be observed with neurons pointing towards the same direction. Scale bar= 150 and 40 μm . Adapted from Livet *et al.* (2007). B) Hippocampal neurons *in vitro*, where the random neurite spreading has been illustrated. Scale bar= 150 μm . Adapted from Gibbs *et al.* (1997).

1.2.3 Surface engineering techniques for neuronal guidance

Advances in biological approaches along with developments in micro-nano fabrication have facilitated the combination of microengineering techniques in cell culture to control neuronal growth and directionality (Mahoney *et al.*, 2005; Offenhausser *et al.*, 2007; Staii *et al.*, 2009). Artificial neuronal networks are normally based on the confinement of neuronal cells in order to achieve a well-defined architecture for the study of neuronal signalling and synapse formation (Gomez *et al.*, 2007). The numerous engineering techniques used to create specific surface patterns has been growing over the last decade (Chen *et al.*, 2012; Poudel *et al.*, 2012). Although it is beyond of the scope of this introduction to detail every technique, the most

common used surface engineering techniques known for the formation of biological patterns have been classified in three main groups: traditional techniques, writing techniques and soft lithography (see Figure 1.5).

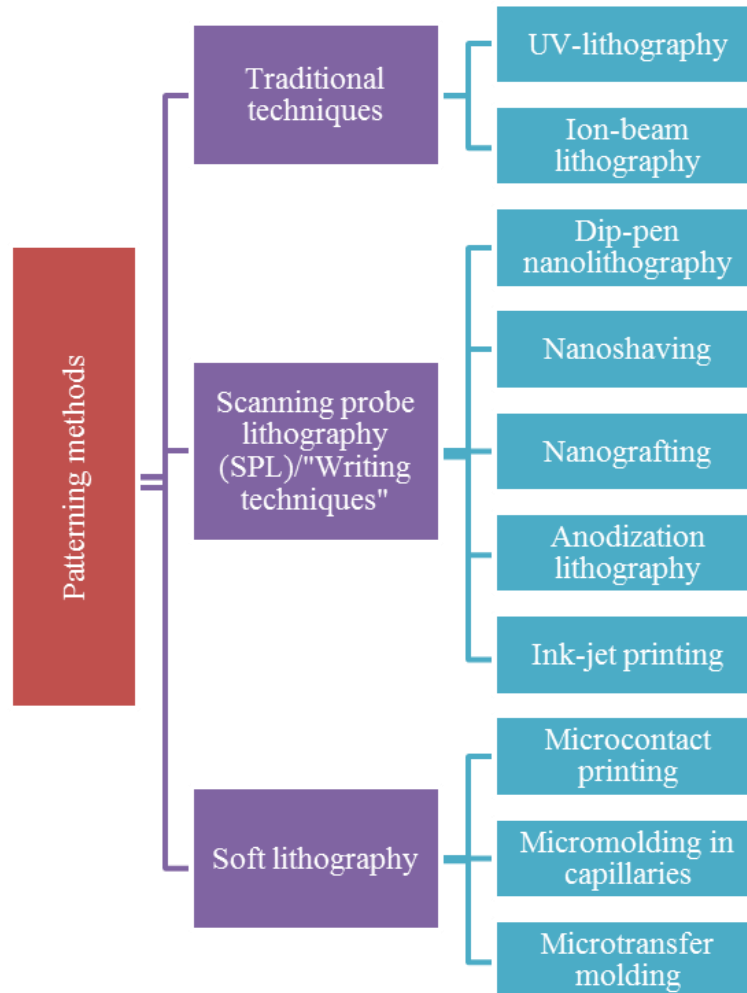


Figure 1.5. Main classification of micro-nano fabrication techniques for their use in biological patterns.

Traditional lithography techniques refer to a group of methods that allow the formation of patterns through irradiation with an energy source. The pattern is often recorded by a “resist” that is sensitive to the energy source (Ito, 1999; Ito *et al.*, 2000; Falconnet *et al.*, 2006; Chen *et al.*, 2012). The methods are classified depending on the energy source used, and thus this category can include X-Ray lithography, UV-lithography, electron beam, ion beam and many more (Chen *et al.*, 2012; Olivier *et al.*, 2012). Conventional lithographical techniques have

been widely used for cell patterning, particularly by creating topographical and chemical patterns (Dowell-Mesfin *et al.*, 2004; Senaratne *et al.*, 2005). Topography has been observed *in vivo* (e.g. the fibre bundles of proteins such as collagen and rough surfaces such as crystal deposit) and thus it is unsurprising that engineering techniques have been used to provide cues on surface materials to promote neuronal directionality (Ventre *et al.*, 2012; Yu *et al.*, 2008; Lee *et al.*, 2007). Topographical patterns are based on the fabrication of geometries such as grooves, pits or islands of different width, length (pitch) or depth (height) at the micro-nano scale (Khan and Newaz, 2010; Ballester-Beltran *et al.*, 2015; Metavarayuth *et al.*, 2016). These types of patterns can include structures with a clear orientation of the pattern for cell alignment (i.e. grooves or ridges), or the random location of pits or protrusions, which are more commonly used to regulate cell functions (Ballester-Beltran *et al.*, 2015).

Directionality and neurite outgrowth have been achieved through the use of lithography techniques. Mahoney *et al.* (2005) cultured PC-12 neuronal cells on microgrooves of 20-60 μm wide and 11 μm deep produced by photolithography. Neurons were best oriented in channels with a width of 20-30 μm , whereas neurites extended along the channel axis in the wider grooves. Likewise, Rajnicek *et al.* (1997) used two types of neuronal cell lines (Xenopus spinal cord neurons and rat hippocampal neurons) to examine differences in neuronal guidance by the presence of parallel grooves of various widths (1, 2 and 4 μm) and depths (14 nm-1100 nm) produced by electron beam lithography. The authors indicated that both cell types showed different growth patterns in response to dimensions of the grooves. Xenopus spinal cord neurites grew parallel to 1 μm wide grooves and as deep as 14 nm, whereas hippocampal neurons grew parallel to wide (4 μm) and deeper grooves (520-1100 nm). In terms of chemical patterns created by traditional techniques, this methodology has been utilised for patterning polymers and proteins for selective cell adhesion. Zhou *et al.* (2013) prepared patterned poly(PEGMA-ran-MAETAC) brushes by photolithography on silicon wafers to culture hippocampal neuronal cells. The random copolymer was used for cell attachment and protein adsorption, whilst a background of polyethylene glycol was chosen as a repellent surface for cells. Thus, hippocampal neurons were constrained in the poly(PEGMA-ran-MAETAC) brush and obtained a greater neurite outgrowth when

compared to neurons cultured on poly-L-lysine. The main techniques utilised to obtain chemical patterns have been further discussed in Section 1.3.3.1.

Alternatively, scanning probe lithography methods, often called “direct writing techniques” use a scanning tunnelling microscope or atomic force microscope tip to produce the pattern on the substrates at a nanometre scale (Olivier *et al.*, 2012; Hon *et al.*, 2008). These techniques have focused more on the pattern of biomolecules instead of cell patterning (Arrabito *et al.*, 2013; Lee *et al.*, 2003; Lee *et al.*, 2002) and therefore will not be further discussed in this section.

The last group contains the so-called soft lithography. These methods replicate microstructures with the use of an elastomeric material (“soft material”, hence the name) created by the use of conventional lithography. Depending on the use that is given to the elastomeric material (as a stamp or as a mould), different methodologies have evolved (Falconnet *et al.*, 2006). When the PDMS relief structure is used as a mould for pattern transfer, the main methodologies include micromolding in capillaries (MIMIC) or microtransfer molding (μ TM) (Kim *et al.*, 1996; Zhao *et al.*, 1996; Lindquist *et al.*, 2012). Alternatively, microcontact printing uses the elastomeric material to produce a stamp with the patterned structure that is inked with a precursor liquid and stamped onto the substrate to transfer the pattern (Xia and Whitesides, 1998). These techniques are commonly used in cell and protein patterning for several advantages such as the good control over the surface chemistry and cellular environment (Kane *et al.*, 1999). Belkaid *et al.* (2013) used microcontact printing by stamping poly-L-lysine onto coverslips in order to pattern primary murine hippocampal and cortical cells. The authors obtained linear and octagonal patterns with highly aligned neurons in them (see Figure 1.6).

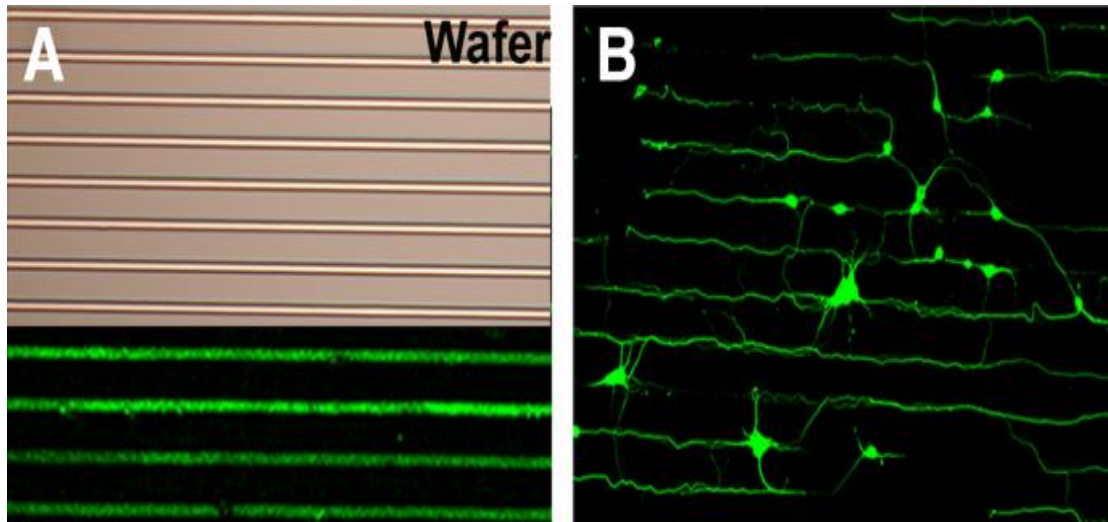


Figure 1.6. Microcontact printing process for neuronal patterning. A) Dimensions of the pattern with 10 μm thick lines separated by a pitch of 60 μm . B) Primary hippocampal neurons plated on micropatterned PLL and immuno-stained for neuron-specific β tubulin III. (20x magnification). Adapted from Belkaid *et al.* (2013).

1.2.4 Most popular scaffolds for neuronal orientation *in vitro*

Several scaffolds have been developed over the years by using various strategies and manipulating their material properties to achieve neuronal directionality. “Natural” components such as collagen or laminin are normally preferred in normal culture conditions due to the bioactivity and the presence of cell recognition sites. However, the use of synthetic materials are more adaptable for these systems due to the controllable physical and biochemical properties, and the wide range of materials that can be used for specific applications (Dadsetan *et al.*, 2009). Due to this, a large emphasis has been placed on synthetic scaffolds, such as the use of micro and nano fibres. Fibres have been used for neuronal alignment due to their topographical effects, which includes fibre size ranging from nano to micro scale and porosity (Roach *et al.*, 2007; Metavarayuth *et al.*, 2016). They can also vary in composition and the type of polymer used, thus the chemical effect is also present. Micro and nano fibres can be prepared by self-assembly, phase separation or electrospinning, although the latter is the most commonly used, being the fastest and cheapest technique (Shah *et al.*, 2016). Electrospun nano and micro poly(L-lactic acid) fibres (PLA) have been used for neuronal cell culture of neuronal stem cells (NSCs). Albeit nanofibers obtained higher differentiation rates than microfibers, they were both shown to promote

elongation and neurite outgrowth along the fibre direction, independently of the fibre diameter (Yang *et al.*, 2005). Although these scaffolds are widely used, they often lack consistency due to a wide range of parameters to consider upon formation of the scaffold, resulting in variability on the fibre formation. Alternatively, the use of nanotubes has been also used for cell guidance either by its topographical features or by its conductive, chemical or mechanical properties (Roach *et al.*, 2010). Carbon nanotubes (CNT) have been utilised in this area due their conductive properties (Arslantunali *et al.*, 2014).

Another common method used to achieve neuronal directionality is closely related to soft lithography processes (see Section 1.2.3). An elastomeric material (e.g. PDMS) with a relief structure is placed against a surface to form microchannels, phenomenon known as microfluidics. Microfluidics have been widely used in this area for the flexibility in their design, allowing studies of single cell processes or complex co-cultures (Paguirigan and Beebe, 2009; Mehling and Tay, 2014; Zahavi *et al.*, 2015). However, these systems can carry some limitations such as the PDMS adsorption of undesired chemicals from the media, evaporation, or leaching. In addition, the shear stress due to the flowing of the media could also bias neuronal function (Goubko and Cao, 2009; Peyrin *et al.*, 2011).

Although the scaffolds discussed above achieve neuronal directionality, chemical patterns provide distinct advantages such as eliminating the use of PDMS or the issue of media flow sheer stress. In addition, chemical patterns are more reproducible upon production and can be produced using several different materials (Charest, 2007, Wei *et al.*, 2012, Sheng *et al.*, 2015). Furthermore, chemical patterning could be used to create a system whereby different chemical combinations can have multiple functionalities, and therefore, patterned surfaces could be designed so one area elicits a certain response, such as enhancing cell differentiation, whilst another area could be used to prevent cell attachment. With the use of such patterns, bioactive materials could be specifically design to obtain spatial control of cell growth for regenerative medicine or to produce bio inert surfaces for certain areas of an implant.

1.3 Chemical modifications on planar substrates

The microenvironment found in the outside of the cells contains several chemical, biological and physical cues that contribute to cell functions such as adhesion, proliferation, migration, etc. Hence, the strategy of modifying a material surface to enhance performance for its use on cell culture is of great importance to promote cellular response and obtain a control on their behaviour (Senaratne *et al.*, 2005; Moroni *et al.*, 2014). When cells are cultured on synthetic materials, water, molecules and various proteins from the media will interact *a priori* with the surface before the cell does (Roach *et al.*, 2007; Ventre *et al.*, 2012). Thus, the surface properties will determine whether the interaction with such molecules is favourable and therefore whether the cell starts building more complexes connections mediating cell attachment or inhibiting such function (Stevens and George, 2005; Roach *et al.*, 2010; Ventre *et al.*, 2012).

Surface chemistry plays an important role in how the biological systems respond (Yu *et al.*, 2008). For example, tissue-contact biomedical devices are known to elicit adverse reactions such as infection or inflammation when the biomaterial surface does not provide optimum surface properties. Likewise, various surface coatings have proved to enhance diverse cell response in *in vitro* cultures (Krishnamoorthy *et al.*, 2014). Although many surface modification approaches have been used for years, the use of self-assembled monolayers (SAMs) and polymer brushes have emerged as potential techniques to tailor different chemical properties onto surfaces in an effort to control cell-material interaction (Raynor *et al.*, 2009).

1.3.1 Self-assembled monolayers (SAMs)

SAMs refers to a thin ordered molecular assembly that is normally attached to the surface by the adsorption of a surfactant (Ulman, 1996). The adsorption can take place on bare, clean surfaces of glass, metals and polymers either in solution or by vapour phase, forming a layer on the surface (Raynor *et al.*, 2009; Stanton, 2014). The adsorbed units organise themselves to become more stable than the unassembled components. SAMs are a popular method of surface modification due to their simple and packed structure (Olivier *et al.*, 2012). The main structure of a SAM is comprised of three main components: the end-group, the backbone and

the head group (see Figure 1.7). In the biomaterials field, the end group is of potential interest because of the wide range of end groups that can be used to modify surface properties such as wettability, charge, cell repulsion etc. (Ulman, 1996). In addition, the type of end group can be used to add further layers or as an initiator anchor point for surface initiated polymerisation, which would lead to more robust and thicker layers. The backbone is normally comprised by alkyl groups which help to assemble the monolayer by Van der Waals and hydrophobic forces (Lafranzo, 2013). The head group must have an affinity for the surface of interest to promote strong adsorption, such as thiols on gold (alkylthiol SAMs) and silanes on glass or oxidised plasma polymers (silane SAMs) (Ulman, 1996; Edmondson *et al.*, 2004; Senaratne *et al.*, 2005).

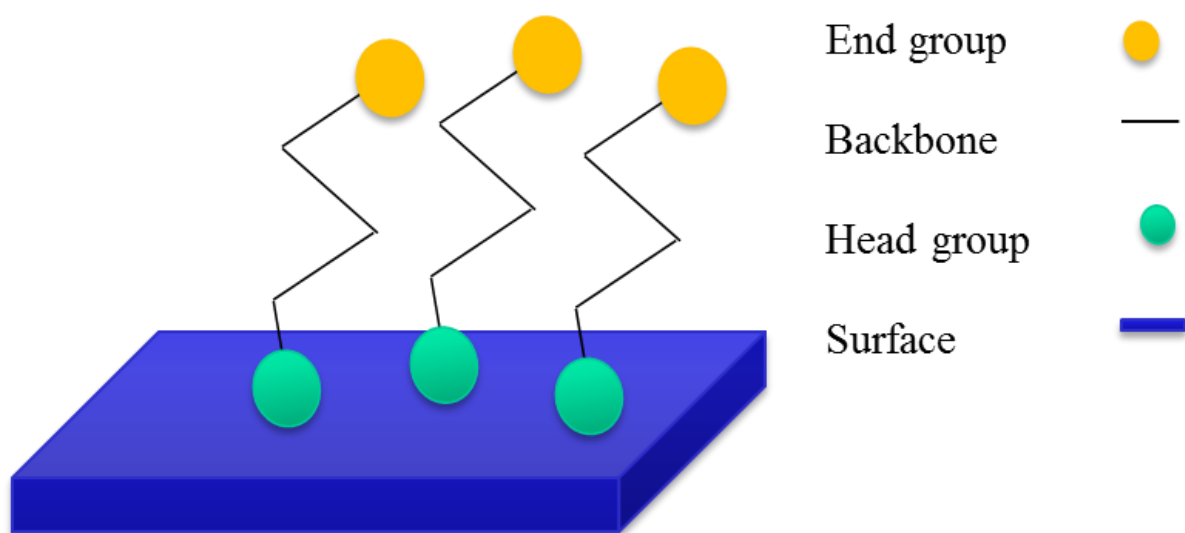


Figure 1.7. Structure of self-assembled monolayers. The end group (yellow), back bone (black line) and head group (green) are the main structural points of the monolayer chains.

1.3.1.1 Silane self-assembled monolayers

Silanes are used as a tool to modify surfaces by providing hydroxyl groups for bonding, a phenomenon known as silanisation. Polymer, silicon and metal oxides can be used for silanisation. The most commonly used silanes are chlorosilanes or alkoxy silanes however, the latter is more commonly used as chlorosilanes are more reactive (especially to water) and typically result in less ordered layers (Advincula *et al.*, 2006; Albutt, 2013; Stanton, 2014). The process to produce alkoxy silanes SAMs occurs by the hydrosilation of the alkoxy groups,

forming silanol groups. Self-condensation between monomers can occur at this point forming silane oligomers (see Figure 1.8) (Howarter and Youngblood, 2006; Pasternack *et al.*, 2008; Barbey *et al.*, 2009). The following step involves the hydrogen bond and condensation of the silanes with the hydroxyl groups of the surface and other silanol molecules, where the bonds are formed. Although the process in theory may sound simple, forming well-defined SAMs is a complicated task, as the amount of water involved in the reaction can determine the quality of the SAM. An excess or complete absence of water can lead to imperfections in the monolayer, as only small amounts of water are needed for the assembly. Likewise, the presence of contaminants can alter the formation of the SAM. In addition, functional end groups can obstruct the silanisation process, by forming hydrogen bonds first with the hydroxyl groups of the surface (Albutt, 2013). Nevertheless, with the appropriate procedure this problem can be minimised since the ease of formation and the ability to use SAMs in a wide range of applications make them a very good candidate for surface modification.

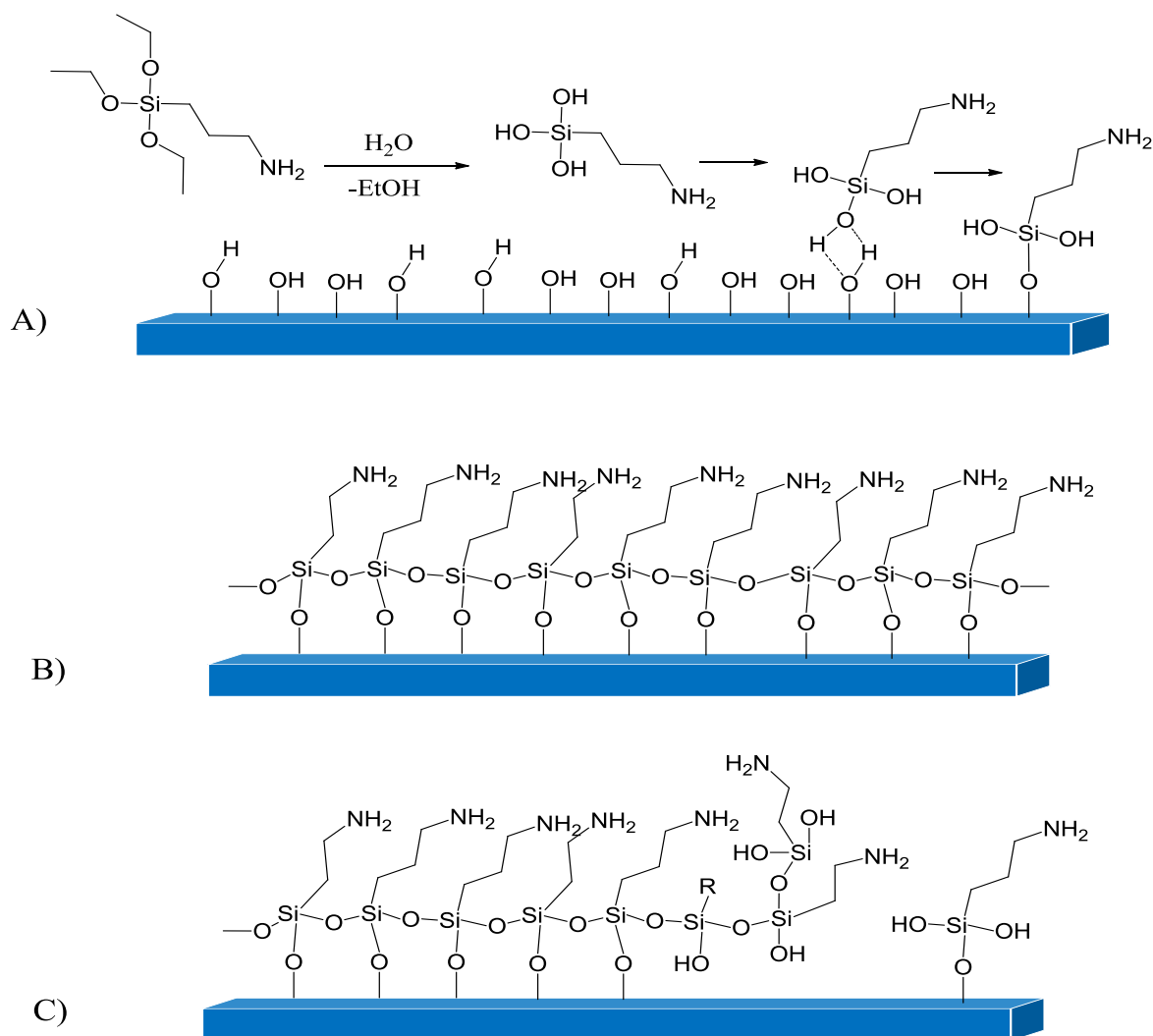


Figure 1.8. Process to produce silane self-assembled monolayers on glass surfaces. A) Hydrosilylation of the alkoxy groups results in the formation of silanol groups. B) The hydrogen bond and condensation of the silanes with the hydroxyl groups of the surface and other silanol molecules occurs, creating such structure. C) Defects on the surface during monolayer formation can occur due to contamination of water excess.

1.3.2 Polymer brushes

Polymer brushes have also been used in biological applications as a potential tool to modify surfaces (Krishnamoorthy *et al.*, 2014). Polymer brushes have a more complex structure when compared to SAMs; these films are based on long polymer chains attached by one end to a surface or interface (Milner, 1991). The film is densely packed and the polymer chains

are forced to stretch away from the surface. The chain stretching results in a height (h) of the polymer chains larger than the radius of gyration of the chain, avoiding overlapping between the chains (Senaratne *et al.*, 2005). These stretched chains are known as polymer brushes (see Figure 1.9).

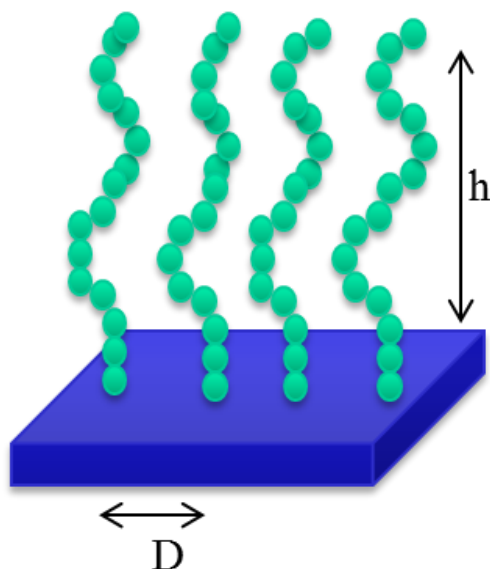


Figure 1.9. Polymer brush structure. D is the parameter defined as the distance between the chains grafting points and h represents the height of the polymer chains.

Depending on the distance between the chain grafting sites (D), the chains can adopt different architectures. When the grafting density (number of chains per area) is low, the chains are more separated from each other and therefore D is larger than the radius of gyration of the grafted chain. Due to the lack of steric repulsion, the chains are not forced to move away from each other, adopting the form of a “mushroom” (Zhao and Brittain, 2000; Brittain and Minko, 2007). As the grafting density increases, the radius of gyration will exceed the value of the grafted chain sites. This will translate in the stretching up of the chains to avoid repulsion with their neighbours, adopting the brush configuration (see Figure 1.10).

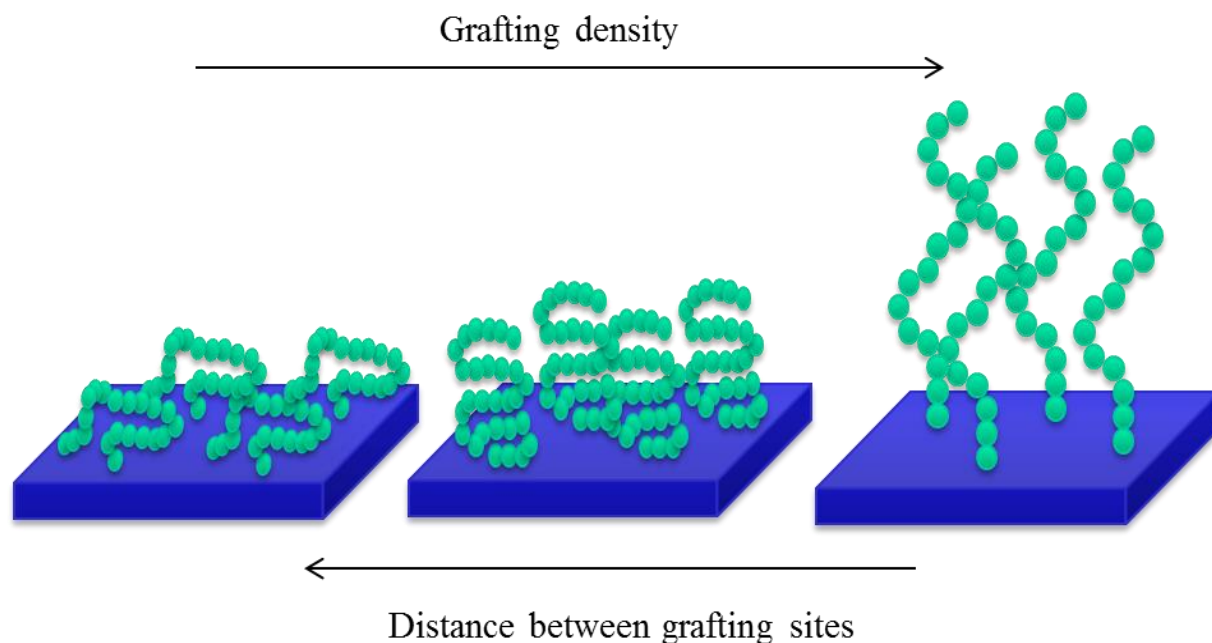


Figure 1.10. Polymer brush conformations. Left) Mushroom conformation. When chains are not forced to stretch away, a mushroom conformation is adopted. In the middle, a transition state is formed between these two conformations where repulsions start to force the chains to move up. When repulsions between chains are too high, a brush conformation is adopted (right).

The synthesis of polymer brushes can be carried out either by “grafting to” or “grafting from” approach (Barbey *et al.*, 2009). In “grafting to”, polymer brushes are formed by growing polymer chains in solution and then attaching them to the surface (Brittain and Minko, 2007). Brushes can be prepared in this method either *via* chemical bond formation or by physisorption of block copolymers. Physisorption occurs in the presence of selective solvents or selective surfaces (Edmondson *et al.*, 2004; Brittain and Minko, 2007). The copolymer with affinity for the surface will adsorb onto the substrate whilst the other block will be designed to interact with the solvent, giving selective solvation. In this manner, one of the blocks will interact more actively than the other with the surface of interest (Figure 1.11A) (Brittain and Minko 2007; Edmondson *et al.*, 2004). One of the main drawbacks of this technique is that physisorbed blocks are not always stable depending on the conditions of solvent and temperature. In addition, they can be moved away and replaced by other adsorbents, resulting in poor control of polymer growth (Edmondson *et al.*, 2004; Brittain and Minko, 2007; Ibanescu, 2015). When synthesis is performed covalently by “grafting to”, end-

functionalised polymers already prepared react with a substrate containing reactive sites with affinity for the polymer chains, forming the polymer brush (see Figure 1.11B) (Brittain and Minko, 2007; Barbey *et al.*, 2009; Zhu, 2012). This method has proved problematic as the reactive sites on the surface are difficult to reach once the first chains have been attached, resulting in a low grafting density and low film thickness (Zhao and Brittain, 2000; Mittal, 2012; Zhu, 2012).

Alternatively, “grafting from” method, also called “Surface-initiated polymerisation” (SIP) is a potent technique that has been widely used due to its good control in functionality, density and thickness of polymer brushes (Edmondson *et al.*, 2004; Azzaroni, 2012). For this strategy, the surface of interest must be modified *a priori* with an initiator coating so the polymerisation can be carried out *in situ* (Edmondson *et al.*, 2004). The initiator anchored to the surface is then exposed to a solution or vapour containing the monomer (depending on the polymerisation method), linking the free monomer to the initiator and forming the desired functionalised brush (see Figure 1.11C) (Edmondson *et al.*, 2004).

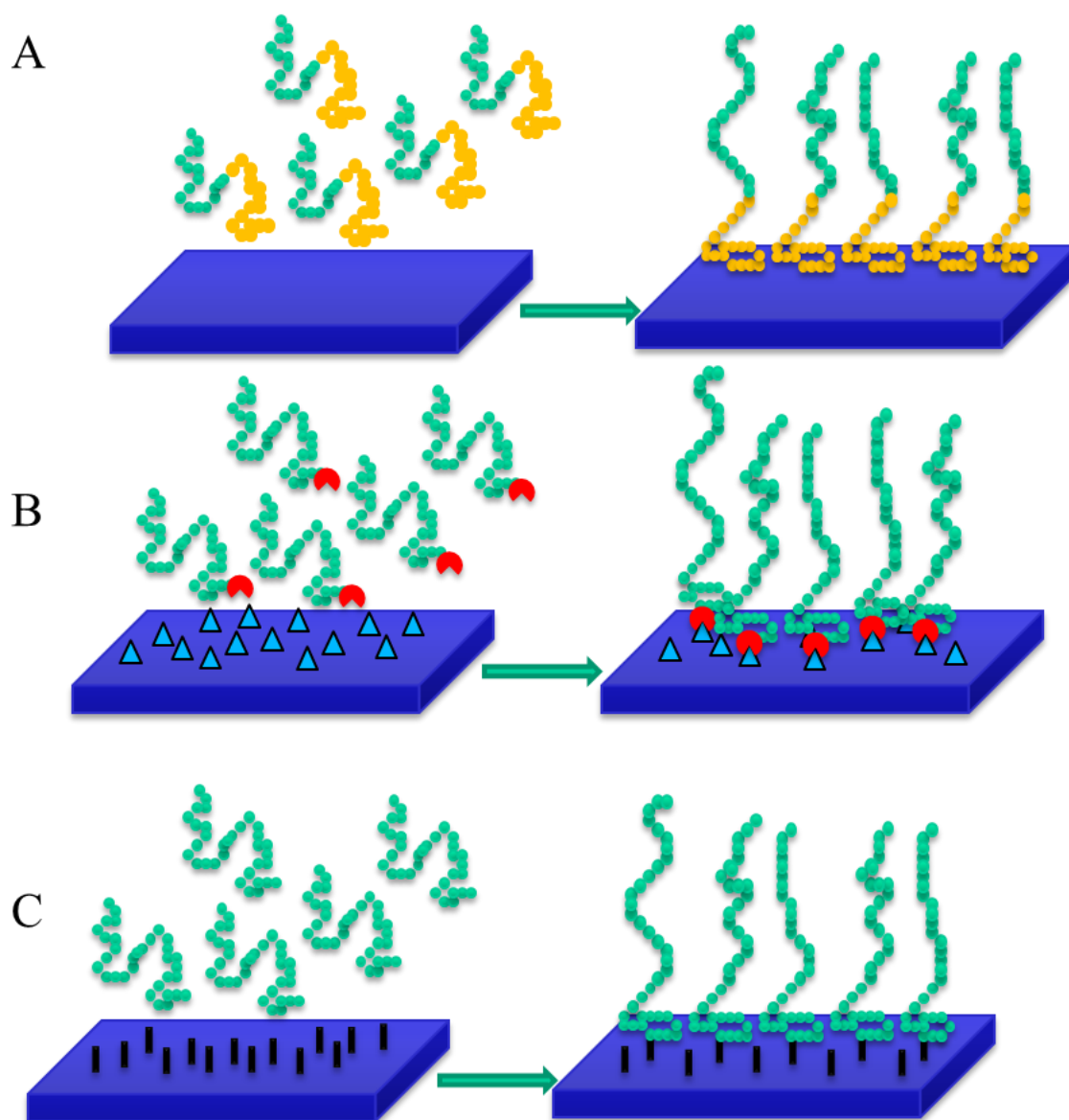


Figure 1.11. “Grafting from” and “grafting to” approaches. A) “Grafting to” approach *via* physisorption. Block copolymers (green and yellow) are prepared and one of the blocks (yellow) will have more affinity for the surface whereas the other block (green) will positively interact with the solvent. Consequently, the yellow block polymer will adsorb onto the surface, forming the anchor points. B) “Grafting to” approach *via* chemical bond (chemisorption). Polymer chains are presynthesised in solution with end groups (red balls) which will anchor to the surface by reacting with the active sites on the surface (blue triangles) for polymerization (Barbey *et al.*, 2009; Brittain and Minko 2007). C) “Grafting from” approach. An initiator self-assembled monolayer (black stick) is anchored prior to polymerisation. The monomer in solution (green) will react with the initiator, forming the polymer brushes *in situ* (Barbey *et al.*, 2009; Brittain and Minko 2007).

The grafting methods can be implemented with most polymerisation techniques such as ring-opening metathesis polymerisation (ROMP), atom transfer radical polymerisation (ATRP), nitroxide-mediated radical polymerisation (NMP), activators regenerated by electron transfer ATRP (ARGET-ATRP), etc. (Barbey *et al.*, 2009; Chen *et al.*, 2012; Olivier *et al.*, 2012). Among them, ATRP is one of the most used techniques for the synthesis of polymer brushes *via* SIP (Edmondson *et al.*, 2004). ATRP was first reported by Kamigaito (1995) and Matyjaszewski (1995), and so far the method has been an extremely versatile and robust technique in the chemical field (Matyjaszewski and Xia, 2001; Barbey *et al.*, 2009). When brushes are prepared by the “grafting from” method followed by ATRP, the term surface initiated atom transfer polymerisation is used (SI-ATRP) (Edmondson *et al.*, 2004). This polymerisation is based on a reversible redox reaction where a metal complex catalyst ($\text{Mt}^{\text{m}}/\text{L}$) is responsible for leading the process. The metal complex in its higher state of oxidation captures the halogen from the initiator layer, forming an active organic radical (R^\bullet). The organic radical will react with the alkene monomer (A^+) growing polymer chains until the halogen is taken back, capping the growing chain (Wang and Matyjaszewski, 1995; Barbey *et al.*, 2009). This mechanism has been described in the Figure 1.12, and has been further detailed in various studies (Wang and Matyjaszewski, 1995; Patten and Matyjaszewski, 1998; Matyjaszewski and Xia, 2001).

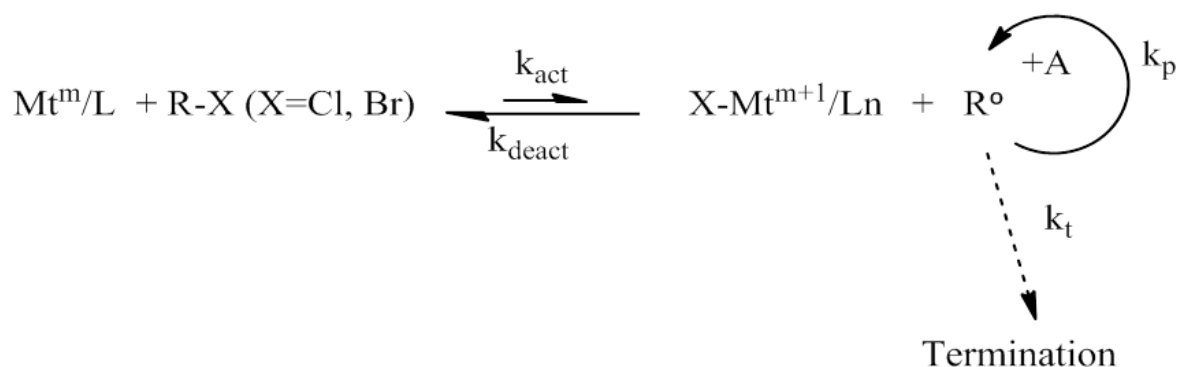


Figure 1.12. ATRP mechanism. A redox process generates active radicals that grow chains by reacting with monomers with the rate constant of propagation (k_{p}). As the polymerisation is a radical based procedure, the active radicals can also undergo termination with a rate constant (k_{t}) (Matyjaszewski and Xia, 2001).

One of the main factors to consider for ATRP process is the presence of the metal in its low oxidation state, which makes the reaction sensitive to oxygen. Thus, extreme care is needed to avoid oxidation before the reaction is carried out (Jakubowski and Matyjaszewski, 2005). An alternative process to avoid the oxidation step is ARGET ATRP. In this process, the presence of a reducing agent along with the metal in a higher state of oxidation is added and thus the metal is reduced *in situ*. In this manner, the reaction has a better tolerance for the oxygen or other radical traps (Jakubowski *et al.*, 2006) (see Figure 1.13). In this work, the synthesis of polymer brushes has been performed by the use of SI-ATRP and SI-ARGET ATRP. These methods are robust for surface coatings and have been used by various research groups to prepare surfaces for cell culture approaches (Mei *et al.*, 2005; Tugulu *et al.*, 2007; Chiang *et al.*, 2011).

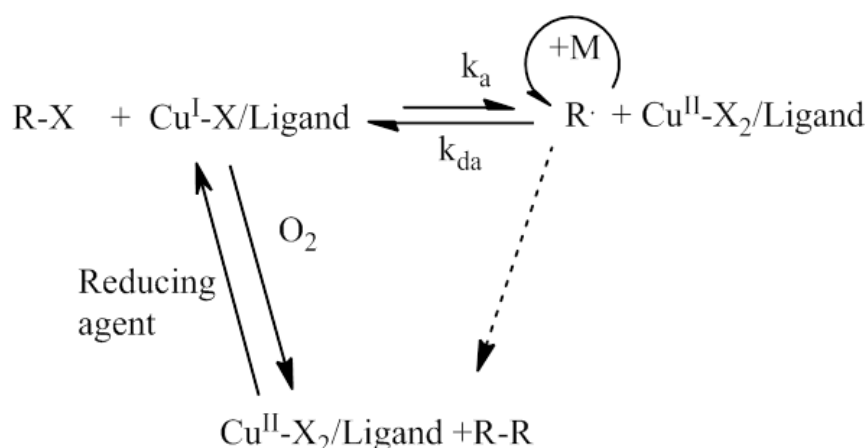


Figure 1.13. ARGET-ATRP mechanism. In ATRP, the metal in different states of oxidation (Cu(II) and Cu(I)) are added to the solution for the polymerisation. In ARGET-ATRP, only Cu(II) is added and a reducing agent is used to generate Cu(I) in the solution, minimising the amount of copper added to the solution (Jakubowski *et al.*, 2006).

To conclude, the synthesis of polymer brushes provides advantages such as its multifunctional character (Kumar *et al.*, 2007) and compatibility in a wide range of material chemistries, making them suitable for use as coatings for cell culture approaches (Moroni *et al.*, 2014).

1.3.3 Effect of chemical surface properties on cell behaviour

Chemical surface modification has emerged in cell culture approaches as an attempt to manipulate surface properties to enhance cell behaviour (Kim and Mooney, 1998; Rosso *et al.*, 2005; Thevenot *et al.*, 2008). Synthetically modified surfaces are popular due to their ease of design and manipulation, where surfaces can be finely manipulated to render different properties such as a change on surface wettability or charge. These are often cheaper than biological supports, and overall display reproducible and predictable properties that can be generated under controlled conditions (Dhandayuthapani *et al.*, 2011). As commented in Section 1.2.1, cells are very sensitive to the chemical cues presented at the surface material, suggesting a strong cross talk at the cell material interface. Thus, a subtle change in the chemical composition of the surface can elicit a change in cell response. There are various factors influencing the interaction of the cells with chemical layers such as its structure, wettability, charge interactions (Palyvoda *et al.*, 2008), chemical functionality (Faucheux *et al.*, 2004) and protein adsorption (Senaratne *et al.*, 2005). Studies have shown that the functionality of the end groups at the material surface influence cell growth and differentiation. Work reported by Lopez and Albers (1993) studied the interaction of mammalian cells (Rat Basophilic Leukaemia cells (RBL) and the embryonic carcinoma cell line, P19) on various SAMs alkanethiols on gold ($\text{HS}(\text{CH}_2)_n\text{R}$), where $\text{R} = \text{CH}_3$, COOH , $\text{N}(\text{CH}_3)_2$, and EG_6OH . Little cell attachment occurred in the hydrophobic monolayers ($-\text{CH}_3$ and EG_6OH) whilst cells attached to more hydrophilic layers ($-\text{COOH}$ and $\text{N}(\text{CH}_3)_2$). The same experiment was carried out in serum free medium and the authors found that attachment patterns changed, attaching this time to both hydrophobic and hydrophilic surfaces, with exception of $\text{EG}_6\text{-OH}$.

As such, surfaces with differing hydrophilic/hydrophobic properties can help to trigger divergent cell responses. Surface wettability influences hydrophobicity, hydrophilicity and surface free energy, all known to affect cell behaviour (Lee *et al.*, 2003; Arima and Iwata, 2007; Kobayashi *et al.*, 2012). Further research in self-assembled monolayers reported the effect of mixed SAMs on human umbilical vein endothelial cells (HUVEC) and epithelial HeLa cells (Arima and Iwata, 2007). CH_3/OH , CH_3/COOH and CH_3/NH_2 mixed SAMs were prepared at different ratios to display different wettability. When the composition of COOH

and NH_2 increased on CH_3/COOH and CH_3/NH_2 mixed SAMs, (which resulted in more hydrophilic surfaces, water contact angle $20\text{-}50^\circ$) HUVEC adhesion increased significantly. CH_3/OH showed cell adherence at a water contact angle of 40° , but as this value increased, cell adhesion decreased. HeLa cells (human cervical cancer cells) responded slightly different to the mixed SAMs, showing its maximum adhesion on CH_3/COOH at a water contact angle of 50° . These results suggested that there was an effect on cells depending on both the wettability and the end group. In addition, this study also highlighted the importance of different cell lineages responding differently to the same cues. In studies based on surface free energy, substrates containing low surface free energy substrata suppressed adhesion and spreading, whereas higher surface energy led to cell attachment (Comelles *et al.*, 2010). Similarly, surface potential has also been related with the ability to attract or repulse cells. Ishihara *et al.* (2015) used various polymer brushes to assess their responsiveness on HeLa cells. They found that the percentage of cell adhesion was correlated with the amount of the fibronectin adsorption, which was dependent on the surface potential of the surface coating. HeLa cells adhered to surfaces with a greater absolute value of surface z potential, whilst no attachment was found when surface had a potential near zero (see Figure 1.14).

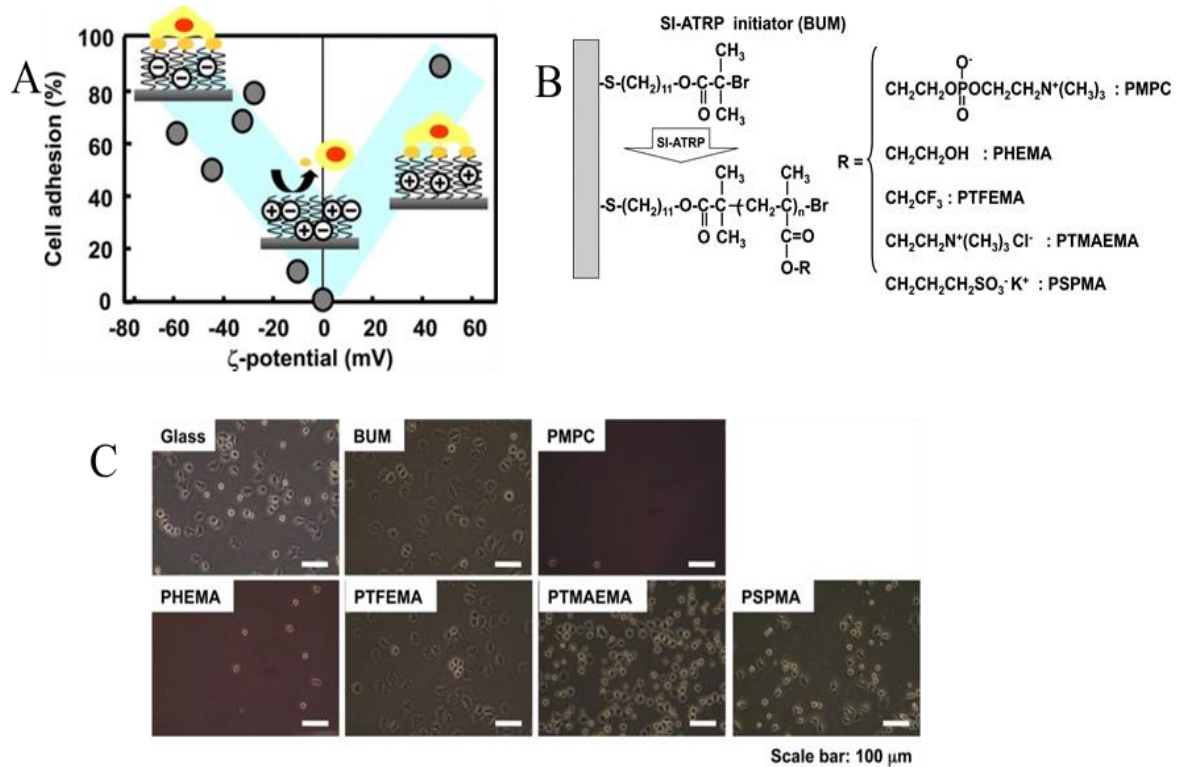


Figure 1.14. Effect of surface potential in cell culture. A) Schematic diagram of the effect of zeta potential on cell adhesion for surface coatings. B) Chemical structures carrying differing charges to obtain differing z potentials for their use in cell culture. C) HeLa cells cultured on coatings with different zeta potential. Adapted from Ishihara *et al.* (2015).

Due to its complex polymer architecture, more characteristics need to be considered when the surface coating is made of polymer brushes. Parameters related to the brush conformation such as the grafting density, thickness and side chain can be modified to elicit differing cell response (Gunkel *et al.*, 2011). Ren *et al.* (2013) formed poly(2-hydroxyethyl methacrylate) brushes (PHEMA) on glass/silicon wafers at different thickness for their use on vascular smooth muscle cells (VSMCs). The cells appeared to migrate to areas of lower thickness, avoiding the areas with thick brushes. The wide range of factors that can influence the success of these coatings is so vast that a single property cannot explain why an individual film is able to either attract or resist cell adhesion (Mendelsohn *et al.*, 2003; Thevenot *et al.*, 2008). What is certain is that all of these characteristics will play a role in the enhancement of cell behaviour under culture conditions.

1.3.3.1 Engineering approaches used to create surface chemical patterns

Chemical patterning has become an important method to achieve cellular organisation in fields such as tissue engineering or drug delivery (Kane *et al.*, 1999). The art of patterning allows the researcher to place the cells in specific locations at specific distances, depths or widths, ultimately achieving directionality and cell containment (Moroni *et al.*, 2014). By using chemical patterns, instructive chemical cues can be used to further guide cells into specific pathways, with the aim of reaching specific targets (Charest, 2007; Moroni *et al.*, 2014). The most common surface engineering technologies commented on Section 1.2.3 are frequently used for patterning chemical coatings such as SAMs and polymer brushes (Perez Roldan, 2011). Thus, the formation of chemical patterns includes the use of photolithography (see Section 2.2.1 to describe the principle). Takahashi *et al.* (2011) managed to pattern human dermal fibroblasts with photolithography using a block copolymer of poly(N-isopropylacrylamide)-b-poly(N-acryloylmorpholine) and poly(N-isopropylacrylamide) brushes (PIPAAm/PIPAAm-b-PAcMo). The copolymer was used as a cell repellent substrate while PIPAAm brushes were used as attractant surfaces. Patterned brushes led the spatial control of fibroblasts, where the copolymer proved to be a successful cell adhesion inhibitor (see Figure 1.15).

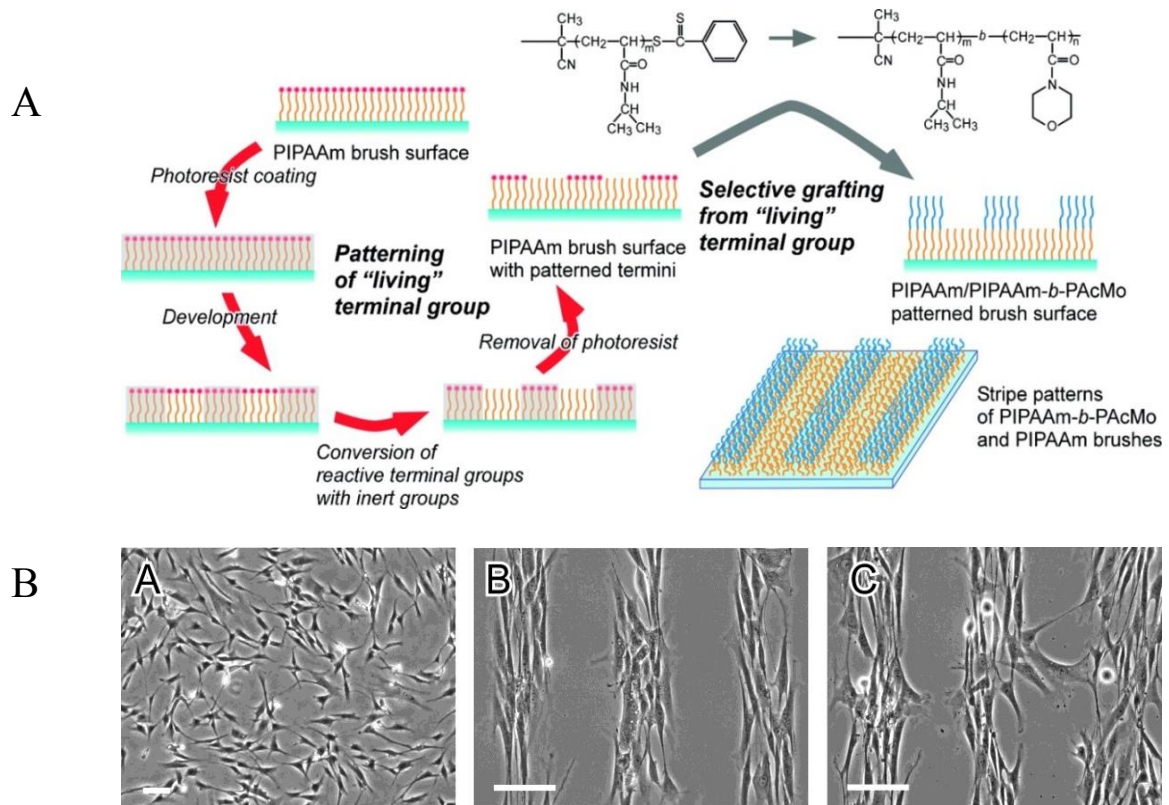


Figure 1.15. Use of photolithography for chemical patterning. A) Photolithographic procedure for the formation of PIPAAm/PIPAAm-b-PAAcMo brushes. B) Light micrographs of fibroblasts on PIPAAm/PIPAAm-b-PAAcMo patterned brush surfaces with stripe patterns of 25 μm (A) and 100 μm (B, C) in width. Scale bar= 100 μm . Adapted from Takahashi *et al.* (2011).

Other conventional approaches have been also used for patterning SAMs. Yamamoto *et al.* (2012) patterned 3-trimethoxysilylpropyl diethylenetriamine and n-octadecyltrimethoxysilane SAMs with electro-beam lithography to examine the role of neurite extension in the specification of the axon with primary hippocampal neurons. The authors used different pattern geometries consisting of long and short channels. Neurites that confined in short channels could not polarise, as the ability of the neurite to extend itself was constrained by the short shape of the pattern. However, a longer pattern shape allowed a single neurite to grow long enough to become an axon.

The use of soft lithography (microcontact printing, micromolding in capillaries, replica molding, etc.) has also been used to pattern proteins and chemical layers (Kane *et al.*, 1999). Cellular confinement in different island sizes created by microcontact printing resulted in the

commitment of human mesenchymal stem cells (hMSC) to different lineages (Figure 1.16A). When the island pattern was small ($1024 \mu\text{m}^2$), hMSC differentiated down the edipogenic lineage however, when the pattern became bigger ($10000 \mu\text{m}^2$) cells went down to an osteogenic lineage (McBeath *et al.*, 2004). This effect was also highlighted in a study reported by Ross *et al.*, (2012), where the formation of different titania nanodot patterns by anodisation allowed for enhancing osteoinduction in MSCs. When the nanodot patterns where 15 nm high, there was a production of osteocalcin deposits. With micromolding in capillaries technique (MIMIC), Shim and co-workers (2007) managed to pattern fibroblasts and bacteria. Polyethylene glycol (PEG) was used to inhibit cellular attachment, and a polyelectrolyte cationic polyallylamine hydrochloride (PAH) was utilised to promote cellular adherence (see Figure 1.16B). Fibroblasts managed to attach and grow in the in PAH zone whilst repelling PEG.

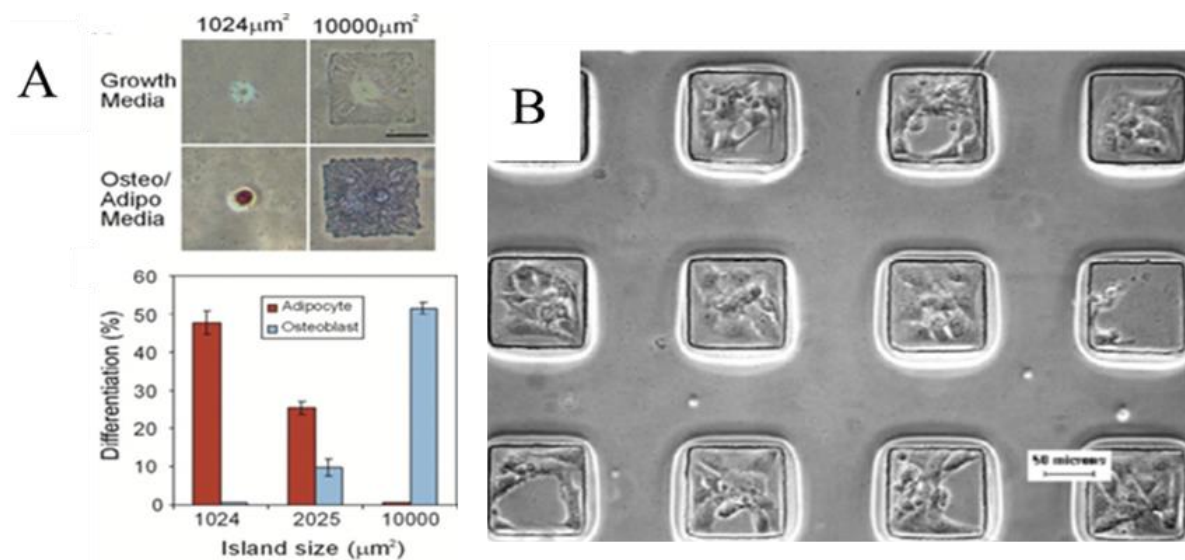


Figure 1.16. Effect of soft lithography patterns on cell culture. A) Cell images on the islands (red- lipid staining, blue- alkaline phosphatase). hMSC cells showed lineage commitment depending on adhesive island size. Adapted from McBeath *et al.* (2004). B) MIMIC pattern with PAH and PEG. The pattern was stable for at least a week. Adapted from Shim *et al.* (2007).

These studies clearly indicate that chemically modified surfaces have the ability to facilitate cell attachment and growth, and can be used to direct cell directionality and confinement. The most common techniques used for chemical patterns on cell culture approaches have been

briefly exemplified here, however other techniques that have been used to create chemical patterns for biological applications have been highlighted in the Table 1.2 for further interest of the reader.

Table 1.2. Selection of studies based on different patterning techniques for the immobilisation of cells and biomolecules. Adapted from Senaratne *et al.* (2005).

Patterning technique	Feature resolution	Applications	Substrate	Reference(s)
Photolithography	<10 μm	Alkyl- and amino-functionalised silanes for controlled neuronal cell growth, protein immobilisation and enzymatic assays	Silicon, fused silica glass	Kleinfield <i>et al.</i> (1998), Britland <i>et al.</i> (1992)
Soft lithography: Microcontact printing	50 μm	Astroglial cells attached selectively EDTA surfaces over OTS	Gold film on polyurethane	Craighead <i>et al.</i> (1998)
Direct evaporation	70 μm	R= NH ₂ , COOH and CH ₃ for adhesion of embryonic chick dorsal root ganglia (DRG) neurons and PC12 cells	SiOx	Naka <i>et al.</i> (2002)
Dip pen lithography	150 nm	Immobilisation of cysteine-labelled biomolecules through SAMs	Gold	Smith <i>et al.</i> (2003)
Low energy electron beam lithography	300 nm	Protein patterning OTS on silicon oxide and MHDA on gold and backfilled with amine-functionalised SAMs	SiO ₂ , gold	Harnett <i>et al.</i> (2001)
Electron beam lithography	~ 1 μm -< 30 nm	Virus detection using nanoelectromechanical devices	Silicon, glass gold	Ilic <i>et al.</i> (2004)
Focused ion beam	50 nm	Nanopipeting DNA/proteins for biological arrays	Gold	Bruckbauer <i>et al.</i> (2003)
Nanoimprinting	75 nm	APTES functionalised with biotin-succinimidyl esters used for streptavidin detection	Silicon	Hoff <i>et al.</i> (2004)

Although the use of topographical cues on neuronal cultures has been widely used over the years, the study of chemical modified surfaces on neurons has not been as thoroughly used. In addition, while various studies have used chemical patterns for neuronal guidance, not extensive research has been conducted whereby chemical patterned neuronal cells are engineered to grow towards specific targets to accomplish heterotypical communication.

1.4 Aim of the Thesis

The aim of this thesis is to utilise surface chemistry techniques to optimise conditions to control neuronal growth and directionality *in vitro*. Specifically, by generating multiple chemically modified surfaces with various properties and testing neuronal growth, viability and differentiation, modified surfaces that are both permissive and repulsive to neurons will be fabricated. These chemical modifications will then be coupled with suitable microfabrication techniques to generate chemical patterns that the neurons respond to in order to promote cell organisation and alignment. This will allow the use of directed interfaces with target cell types. In order to achieve these aims, the following objectives will need to be met:

- Prepare chemical cues with different properties to analyse differing cell behaviour, followed by surface characterisation techniques to obtain information about the chemical properties of the modified surface.
- Analyse cell behaviour on such surfaces, thus obtaining information about the viability, proliferation and differentiation depending on the surface properties of the modified material.
- Use surface engineering techniques to obtain a spatial control over cell behaviour, thus obtaining cell organisation.
- Attempt to achieve a biomimetic neuronal interface with other cell types in a co-culture system utilising chemical patterning.

2 General Methods

2.1 Methods for surface modification

The chemicals mentioned in this section were purchased from Sigma-Aldrich (unless otherwise stated) and used as received. Glass slides (1 mm-1.2 mm thick, Sigma Aldrich) and silicon wafers ($\langle 100 \rangle$ orientation, 1-100 $\Omega\cdot\text{cm}$, polished one side, Compart Technology, Peterborough, Cambridgeshire, UK) were cut $\sim 1\text{-}2\text{ cm}^2$ prior to modification with a diamond pen. The material was then treated to form thin polymer layers by chemical vapour deposition (CVD) and by the “grafting from” method described in Section 1.3.2. The cleaning (SIOH), silanisation (3-aminopropyltriethoxysilane, APTES), initiator attachment (α -bromoisobutyryl bromide, BIBB), poly(2-hydroxyethyl methacrylate) (PHEMA) and poly(methyl methacrylate) (PMMA) deposition processes have been previously described by Zhu (2012), whereas poly([2-(methacryloyloxy)ethyl]trimethylammonium chloride) (PMETAC) and 3-poly(3-sulfopropyl methacrylate) (PKSPMA) protocols have been described elsewhere and will be mentioned in their corresponding sections.

2.1.1 Surface cleaning

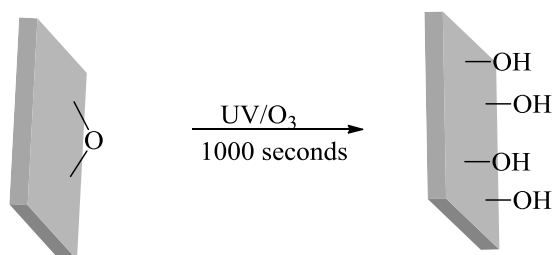


Figure 2.1. Surface cleaning under UV/ozone photo reactor.

Wafers and glass slides were cleaned with a UVP PR-100 UV/ozone photo reactor (Cambridge, Cambridgeshire, UK). Samples were placed at $< 1\text{ cm}$ from the UV light with the help of a metal stand and were treated in the photo reactor chamber for 17 minutes. Silicon wafers were set up directly into the UV/ozone chamber whereas glass slides were previously cleaned with detergent, acetone and rinsed with dH_2O . One of the samples was always exposed under water to observe whether they rendered hydrophilic as proof of the success of the cleaning process.

2.1.2 Formation of 3-aminopropyltriethoxysilane (APTES) by chemical vapour deposition (CVD)

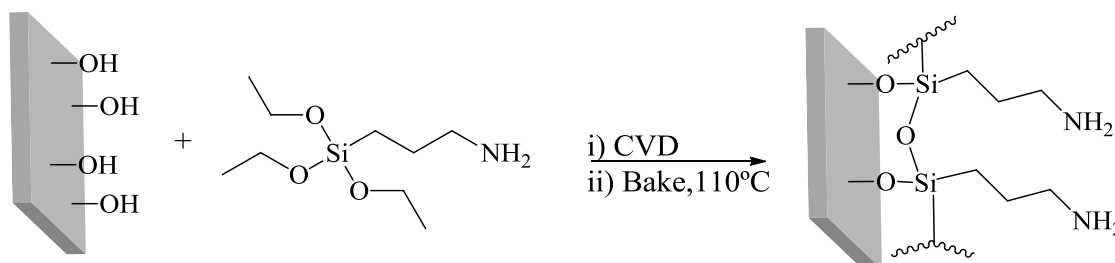


Figure 2.2. Deposition of 3-aminopropyltriethoxysilane (APTES) onto glass surfaces/silicon wafers.

Clean glass slides and wafers were placed in a vacuum oven along with 10 drops of 3-aminopropyltriethoxysilane (APTES, >98%, Sigma Aldrich) in aluminium foil. The vacuum was turned on and the glass slides were exposed to the APTES vapour for 30 minutes at room temperature (RT). Thereafter, the vacuum was removed and samples were annealed in an oven for 30 minutes at 110° C. The APTES functionalised samples were kept in a desiccator until further use.

2.1.3 Deposition of α -bromoisobutyryl bromide (BIBB) onto APTES-functionalised surfaces

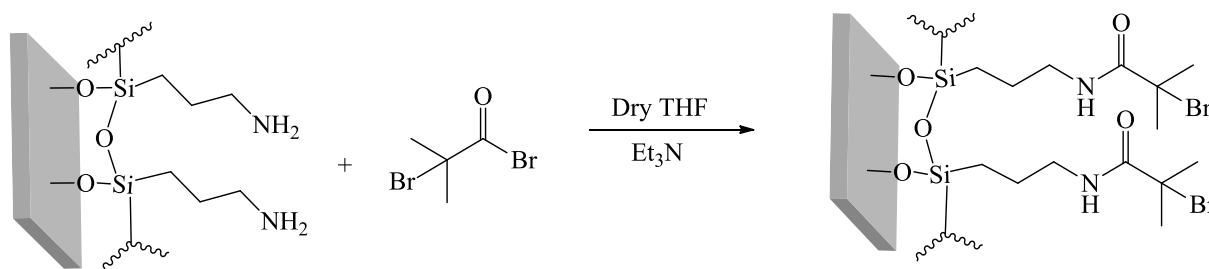


Figure 2.3. Deposition of α -bromoisobutyryl bromide (BIBB) onto APTES-functionalised glass surfaces/silicon wafers.

APTES-functionalised samples were placed in dry tubes or flasks and purged during 1-2 minutes with N₂. To form the amide-initiator, dry tetrahydrofuran (THF, Sigma Aldrich,

10 mL), dry triethylamine (>99.5%, 0.3 mL, 0.21 g, 2.1 mmol, Sigma Aldrich) and 2-bromoisobutyryl bromide (BIBB, >98%, 0.26 mL, 0.48 g, 2.10 mmol, Sigma Aldrich) were added into the tubes containing the APTES samples. After an hour, the samples were removed, rinsed with THF, methanol and dH₂O, and then dried under a flow of N₂.

2.1.4 Polymerisation of 2-hydroxyethyl methacrylate (HEMA) from BIBB-functionalised surfaces

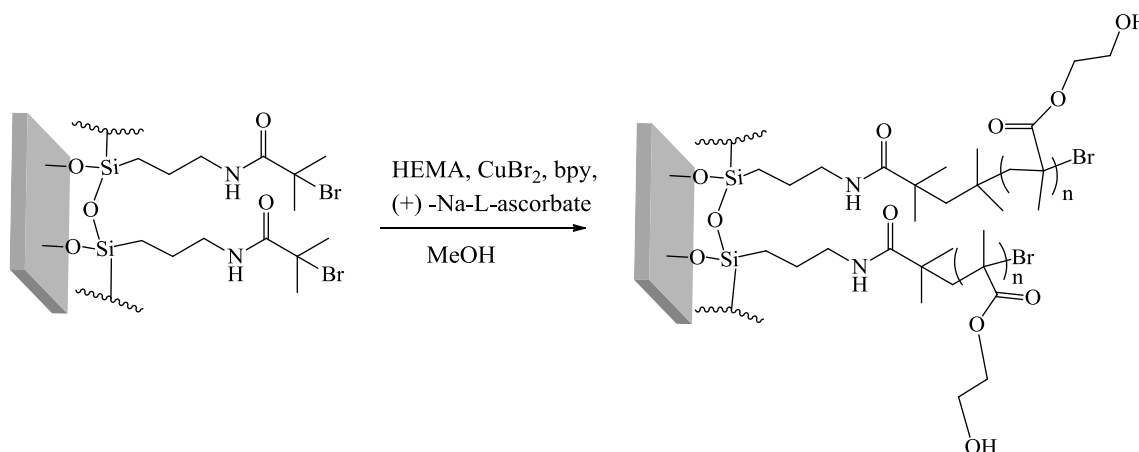


Figure 2.4. Polymerisation of 2-hydroxyethyl methacrylate (HEMA) from BIBB-functionalised glass surfaces/silicon wafers.

The monomer 2-hydroxyethyl methacrylate (HEMA, 98%, 20 mL, 20.74 g, 164.8 mmol, Sigma Aldrich) in methanol (20 mL) was stirred and degassed by bubbling through N₂ for 20 minutes in a 100 mL sealed three round bottom flask. To this solution, copper (II) bromide (CuBr₂, 98%, Sigma Aldrich, 0.0074 g, 0.033 mmol), (+)-sodium L-ascorbate (crystalline, ≥ 98%, Sigma Aldrich, 0.065 g, 0.33 mmol) and 2, 2'-bipyridine (bpy, 99%, Sigma Aldrich, 0.0515 g, 0.33 mmol) were added. The mixture was further stirred for 5 minutes whilst the initiator-coated samples prepared in Section 2.1.3 were placed in glass tubes that were sealed with a septum and degassed by purging N₂ through. Thereafter, the HEMA containing solution was used to fill these tubes *via* syringe until the BIBB initiator sample was completely covered. The sample was left in the solution under N₂ atmosphere for 24 hours, then washed sequentially with methanol and dH₂O. The washed samples were dried by blowing with N₂.

2.1.5 Polymerisation of methyl methacrylate (MMA) from BIBB-functionalised surfaces

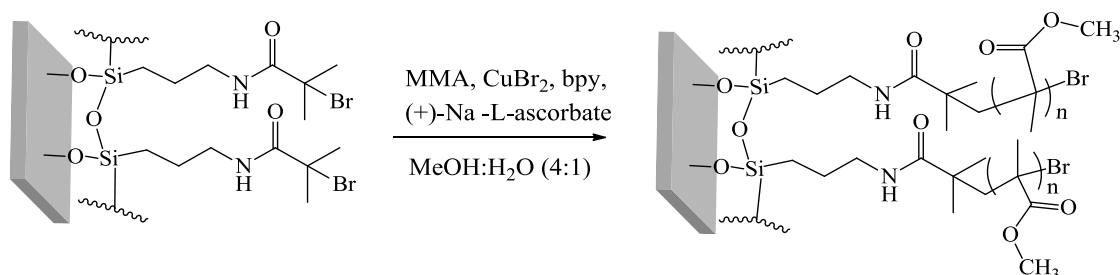


Figure 2.5. Polymerisation of methyl methacrylate (MMA) from BIBB functionalised glass surfaces/silicon wafers.

The polymerisation of methyl methacrylate (MMA, contains ≤ 30 ppm MEHQ as inhibitor, 99%, Sigma Aldrich) followed the same procedure as that of PHEMA (Section 2.1.4) with the following exceptions: the solvent mixture for poly(methyl methacrylate) (PMMA) was methanol:dH₂O (4:1 vol/vol) and the amount of monomer used was 20 mL (18.72 g, 187.0 mmol, Sigma Aldrich). Polymerisation time and washing process were also the same as PHEMA.

2.1.6 Polymerisation of 3-sulfopropyl methacrylate (KSPMA) from BIBB-functionalised surfaces

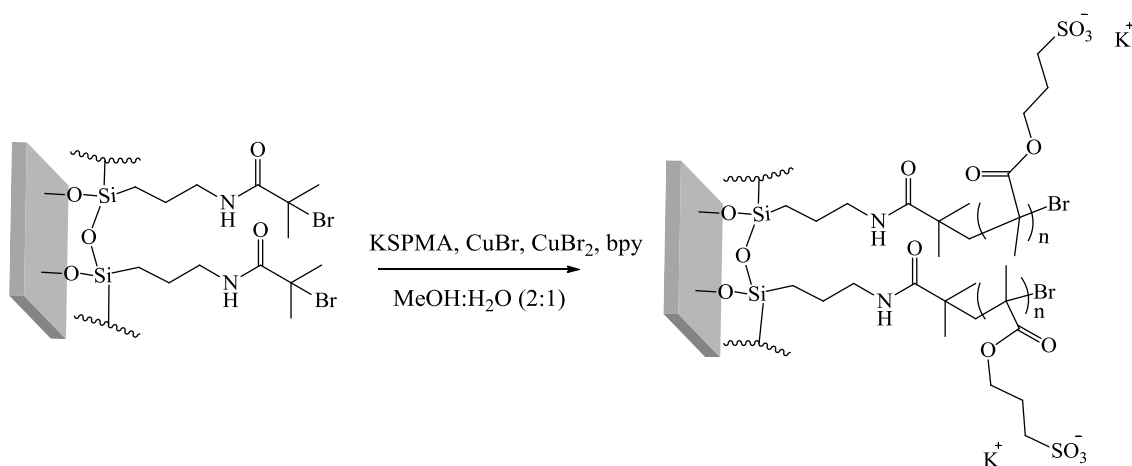


Figure 2.6. Polymerisation of 3-sulfopropyl methacrylate (KSPMA) from BIBB functionalised glass surfaces/silicon wafers.

The use of 3-sulfopropyl methacrylate potassium salt (KSPMA) for brush synthesis was previously described in the literature (Ramstedt *et al.*, 2007). Poly(potassium 3-sulfopropyl methacrylate) (PKSPMA) brushes were grown following a similar procedure as that of PHEMA (Section 2.1.4) with the following exceptions: 3-sulfopropyl methacrylate potassium salt (98%, 17.29 g, 70.2 mmol, Sigma Aldrich) was dissolved in methanol and dH₂O (2:1 vol/vol). After 10 minutes all the monomer was dissolved and 2, 2'-bipyridyne (bpy, 0.651 g, 4.17 mmol, Sigma Aldrich) and copper (II) bromide (CuBr₂, 0.0179 g, 0.08 mmol, Sigma Aldrich) were added. The mixture was stirred and degassed for an hour. Subsequently copper (I) bromide (CuBr, 99.9%, 0.230 g, 1.6 mmol, Sigma Aldrich) was added. As PMMA and PHEMA, polymerisation time and washing processes were carried out in the same manner.

2.1.7 Polymerisation of [2-(methacryloyloxy)ethyl]trimethylammonium chloride (METAC) from BIBB-functionalised surfaces

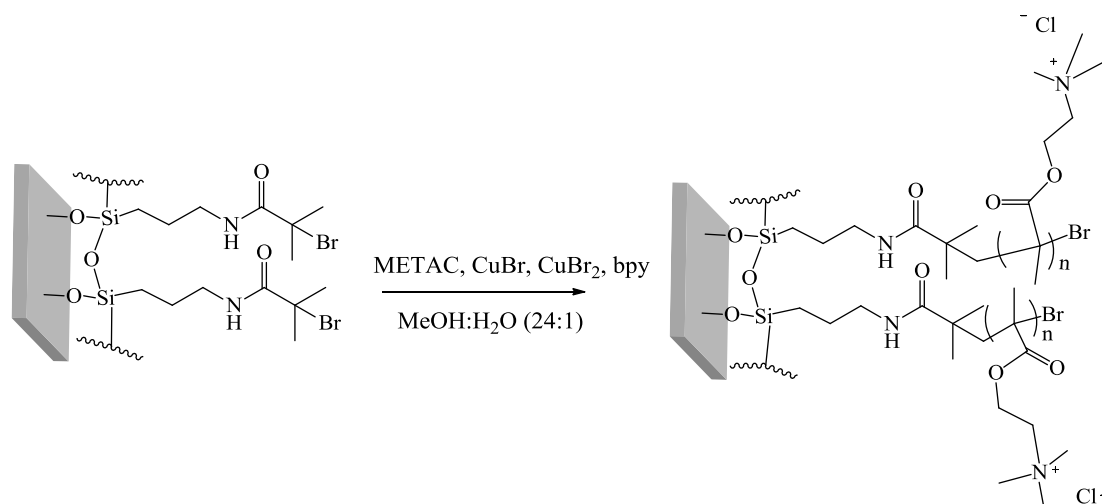


Figure 2.7. Polymerisation of [2-(methacryloyloxy)ethyl]trimethylammonium chloride (METAC) from BIBB-functionalised glass surfaces/silicon wafers.

The attachment of poly([2-(methacryloyloxy)ethyl]trimethylammonium chloride) brushes (PMETAC) was previously described in the literature (Wei and Ngai 2012). The monomer METAC (25 mL, 80 wt% solution in H₂O, Sigma Aldrich) was dissolved with methanol and dH₂O (24:1 vol/vol). The mixture was degassed and stirred to dissolve the monomer. After

30 minutes, 2,2'-bipyridine (bpy, 1 g, 6.4 mmol), copper (I) bromide (CuBr, 99.9%, 0.287g, 2 mmol) and copper (II) bromide (CuBr₂, 98%, 0.045 g, 2 mmol) were added into the solution which was stirred and degassed for at least 15 minutes. Thereafter, the process followed was the same as that of PHEMA.

2.2 Patterning methods

Various engineering techniques such as photolithography, scanning probe techniques and soft lithography among others, have been used in the literature to obtain chemical patterns for cellular guidance (Kane *et al.*, 1999; Staii *et al.*, 2009; Zhou *et al.*, 2013). This section has been dedicated to only cover the patterning techniques that have been used in this thesis.

2.2.1 Photolithography

Photolithography, also known as UV lithography, is a very high resolution technique utilised for microfabrication, especially in electronics (Kilby, 1964; Berkowski *et al.*, 2005). The principle behind this method resides on the use of a photoresist, UV irradiation and a photomask for transferring defined structures of any shape or geometry onto a flat surface. To carry out the process, a resist sensitive to UV light (photoresist) is placed uniformly onto the surface by lamination (dry film) or more commonly by spin coating (wet film) (Figure 2.8B) (Ito and Okazaki, 2000). Photoresists can be classified as negative or positive, depending on the effect that the UV light has on them. UV irradiation in positive photoresists results in the solubility of the UV exposed areas, whereas UV irradiation in negative resists leads to the crosslinking of the exposed areas, making them insoluble in the developing process. For photoresists that have been spin coated, an extra soft bake step may be necessary to eliminate the remainder of the solvent contained in the photoresist solution. Thereafter, the photoresist is covered by a photomask containing defined patterns, which are transferred to the surface when the UV light passes through (Figure 2.8A). Photomasks are commonly made of transparent sheets with an inked pattern or chromate glass. Once the structure within the mask is recorded in the resist, the pattern areas are developed by developing solutions. The patterned resist can be used afterwards for selective etching or a deposition process (Chen *et al.*, 2012).

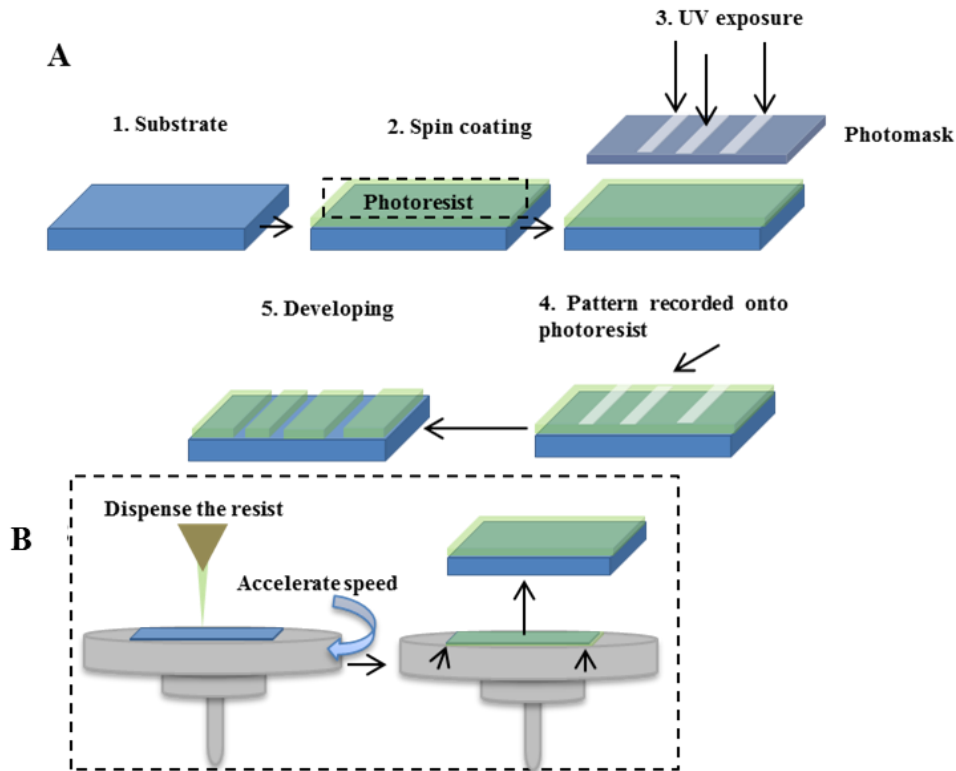


Figure 2.8. Schematic of photolithography principle. A) The photoresist is deposited onto the substrate for UV exposure through a photomask. The areas on the photoresist which have been exposed to the UV light are then removed by a developer solution, obtaining the patterned substrate. B) Photoresist deposition by spin coating. The sample is placed onto the spin coater stand and the resin is dispensed onto the surface. To create uniform layers, the stand will rotate at a specific speed to obtain a determined thickness of the photoresist layer.

2.2.2 Soft lithography: Micromolding in Capillaries (MIMIC)

Soft lithography has gained popularity as a tool for patterning cells into different geometries and sizes (Kane *et al.*, 1999). The term “soft” comes from the use of a soft, elastomeric material (normally polydimethylsiloxane (PDMS)) for fabricating relief structures containing the pattern of interest. The manner in which the elastomeric material is used (i.e. for stamping, as moulds, etc.) determines the type of soft lithography technique that is used. Soft lithography techniques include microcontact printing, microtransfer molding and micromolding in capillaries, among others (Xia and Whitesides, 1998; Lindquist *et al.*, 2012). In micromolding in capillaries (MIMIC), a PDMS mould with relief structures is positioned on the surface, making conformal contact and creating channels in the non-conformal contact areas. The channels are then filled with the polymer solution of interest and once the

polymerisation is complete, the mould is peeled off and the patterned structure is formed (see Figure 2.9).

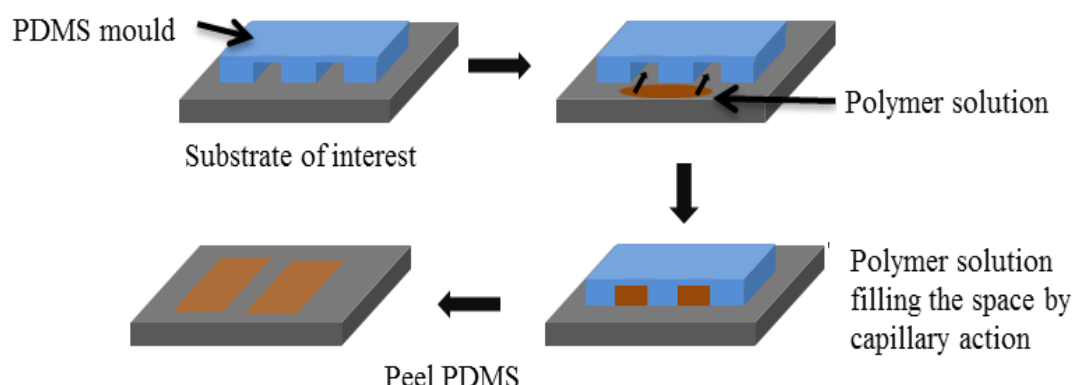


Figure 2.9. Micromolding in capillaries (MIMIC) principle. The PDMS mould is positioned on the surface and the polymer liquid is filled by capillary adsorption. Once polymerisation is complete, PDMS is removed.

2.3 Techniques for surface analysis

Surface characterisation techniques are essential to understand how a material surface has been modified after a treatment or deposition. The modified surfaces prepared in this thesis have been characterised by a combination of different methodologies to assess chemical changes on the surface (Fourier transform infrared spectroscopy (FTIR), x-ray photoelectron spectroscopy (XPS)), changes in surface wettability (water contact angle) and the thickness of the deposited layers (ellipsometry). The topographical changes after chemical patterning in Chapter 5 were also assessed by utilising atomic force microscopy (AFM). Such techniques have been used throughout this thesis and will be briefly described in the following sections.

2.3.1 Fourier transform infrared (FTIR)

FTIR is widely used to analyse the molecular structure of surfaces due to its ease of use and applicability to various materials (Gilmore, 2009). The principle of the technique relies on the ability of the chemical bonds within the sample to absorb IR radiation at different wavelengths. The IR, which is emitted by a light source, passes through the interferometer, which modulates the wavelength of light. The interferometer is composed of a beam splitter that reflects light off two mirrors, one fixed and one moving. The mirrors reflect the two light

beams back, recombining with each other at the beam splitter and creating a wave pattern known as the interferogram. Thereafter, the resulting beam reaches the sample and the IR is absorbed by the vibrations of the stretching, bending and rotation of chemical bonds within the sample. This induces changes in the interferogram, which are recorded by the detector. The interferogram can be then decoded to obtain the infrared spectrum. In the infrared spectrum, the IR absorbed gives rise to the different frequencies values (peaks or bands). These can be assigned to certain bonds within functional groups in the molecule to determine the main components of the samples, as certain bonds will produce characteristic bands, acting as a fingerprint (Förch *et al.*, 2009).

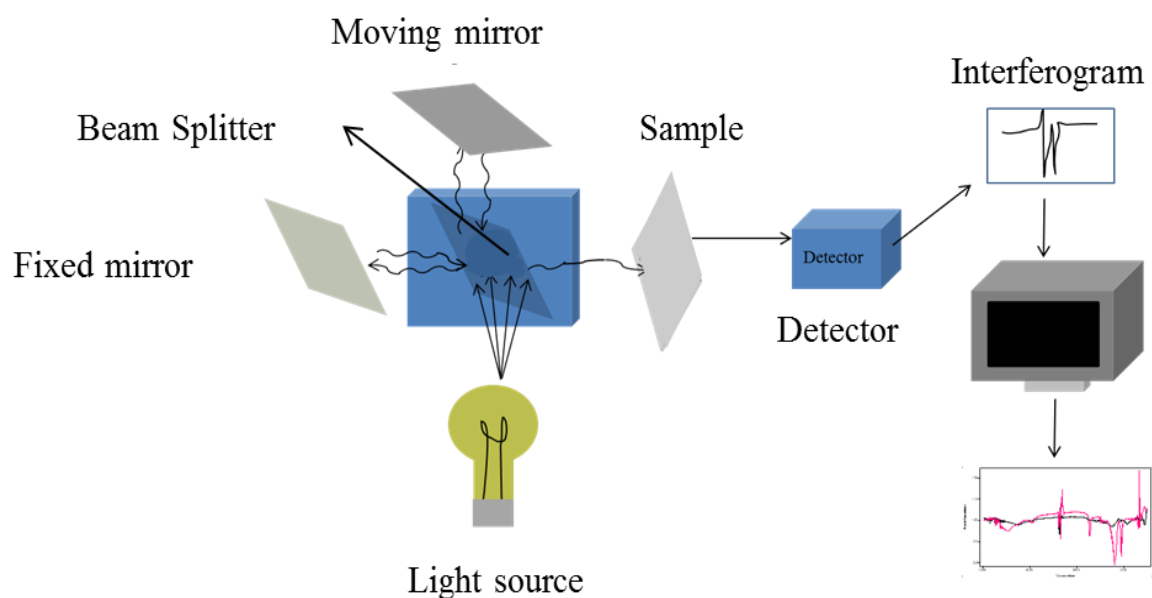


Figure 2.10. Schematic of FTIR principle. The source directs the IR radiation towards the beam splitter, which shines towards a fixed and a moving mirror. The recombined beam passes through the sample, absorbing IR at certain wavelengths and producing characteristics peaks in the intrared spectra.

Infrared analysis was conducted with a Perkin-Elmer Paragon 1000 FT-IR spectrophotometer. IR spectra were acquired on polymer brushes grown on silicon wafers using a clean polished silicon wafer for the background signal. Spectra were taken averaging a total of 128 scans per sample run.

2.3.2 Atomic force microscopy (AFM)

AFM is used to study the topographical surface features at the micro- and nano-scale. This technique makes use of a cantilever containing a sharp tip that interacts with the surface (Figure 2.11). The magnetic, electrostatic, attractive, repulsive and Van der Waals forces produced when the tip approaches the surface, creates a deflection of the cantilever, which is measured with a laser beam and recorded by an optical lever (Binnig and Quate, 1986; Takano *et al.*, 1999; Förch *et al.*, 2009; Albutt, 2013) (see Figure 2.11). The cantilever can be used in a non-contact, contact and tapping mode. In the non-contact mode, the tip is away from the surface, whilst the opposite occurs in the contact mode. For the tapping mode, the tip oscillates near its resonance frequency, contacting the sample for very little time (Jalili and Laxminarayana, 2004). Topographical images of the surface can be obtained by passing the scanning tip across the surface. The difference on the cantilever deflector in the raised and lowered areas will produce a topographical map (Jalili and Laxminarayana, 2004; Albutt, 2013).

For the AFM profiles shown in Chapter 5, Section 5.5.6.3, a Bruker Explorer AFM was used with SPMLab software in a tapping mode with a high resonance frequency (HRF) silicon probe.

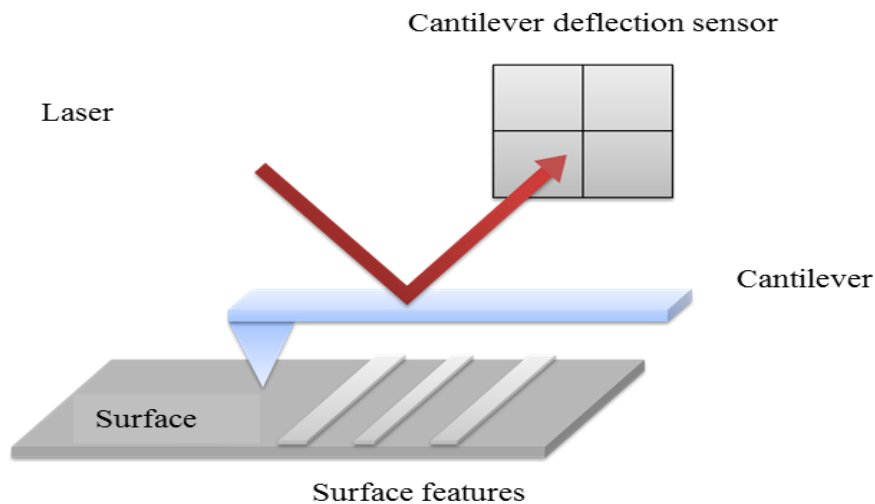


Figure 2.11. Schematic of AFM principle. The cantilever oscillates across the surface by the use of a piezoelectric component, imaging the surface topography.

2.3.3 Water contact angle (WCA)

The wettability of the surface is determined by the interactions at the interface of a liquid and a solid surface, and may suggest changes in the surface chemistry and topography of the surface. The degree of wettability can be determined by the surface tension (γ) between the interfaces involved (liquid-solid, solid-vapour and liquid-vapour), which can be measured by the water contact angle (WCA, see Figure 2.12). The WCA is defined as the angle (θ) formed at the solid-liquid and liquid-vapour interface, and can be calculated by drawing a tangent from the contact point to the limit of the drop (see Figure 2.12). The relationship between surface tension and contact angle for flat and smooth surfaces can be explained by the equation of Young Laplace, which correlates the interactions between the interface tensions and the water contact angle (Chau, 2009; Förch *et al.*, 2009; Yuan and T Randall Lee, 2013) (see Equation 2-1).

$$\gamma_{sv} - \gamma_{sl} = \gamma_{lv} \cos\theta \quad \text{Equation 2-1}$$

Where γ_{sv} is the surface tension at the solid vapour interface, γ_{sl} is the surface tension at the solid liquid interface and γ_{lv} is the surface tension at the liquid vapour interface. Depending on the interaction of water molecules between the surface and the liquid, the surface can be considered as hydrophilic (the angle is from 0 to 90°) or hydrophobic (the angle is beyond 90°) (Yuan and Lee, 2013).

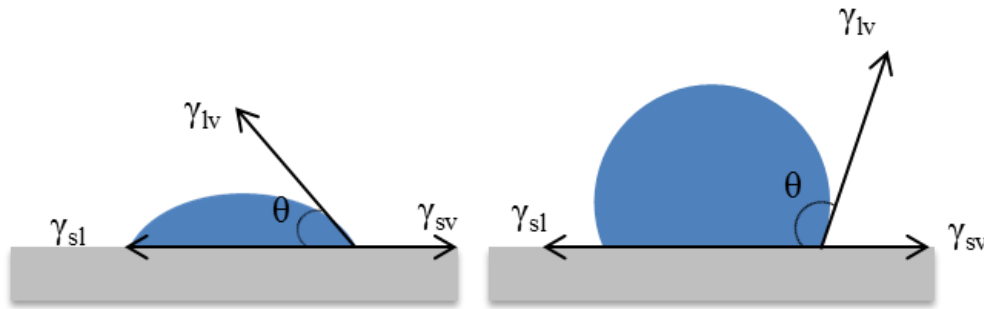


Figure 2.12. Water contact angle in a smooth surface. The tangent between the substrate and the drop determine the wettability of the surface. Surfaces with a water contact angle $<90^\circ$ are defined as less hydrophobic (left). Very hydrophobic surfaces are found when the angle is bigger than 90° (right).

The static sessile drop method is frequently used to measure the wettability of the new deposited films present on the surface (Lee *et al.*, 2004; Zeng *et al.*, 2011). In this technique, the measurements are obtained by depositing a drop of ultrapure water onto the surface. Once the drop is in contact with the surface, the shape of the droplet is captured by a high-resolution camera and analysed.

Water contact angle measurements were obtained using a DataPhysics OCA 20 and the measurement was conducted with SCA 20 software. A volume of 2 μL per drop of ultrapure water was used. Five values were taken from random parts of the samples.

2.3.4 Ellipsometry

This non-destructive technique has been used to determine film thickness in this thesis, as an indication of layer deposition onto the surface. In this method, a polarised light beam with known state of polarisation is directed onto the sample, producing a specular reflectance. From there, the sample measurement can be explained with various components (Figure 2.13) (Ohring, 2001; Förch *et al.*, 2009). The plane spanned by the incident and reflected light contains the component P and S (parallel and perpendicular to the plane, respectively). The state of polarisation is changed for both of them in a different manner, creating an elliptical polarisation of the light that is reflected. The change in the polarisation of the reflected light can be defined as the ratio of the reflection coefficients R_s and R_p . This ratio is related to the ellipsometer parameters Δ and Ψ (see Equation 2-2) (Förch *et al.*, 2009), where Δ indicates

the phase difference in the reflectance of both p and s- polarised light, and $\tan(\Psi)$ represents their reflectance magnitude. Ellipsometry is an indirect method and thus, the data produced by the different variation in the angle of incidence is based on a model which fits the data to obtain the value of the thickness (Ohring, 2001).

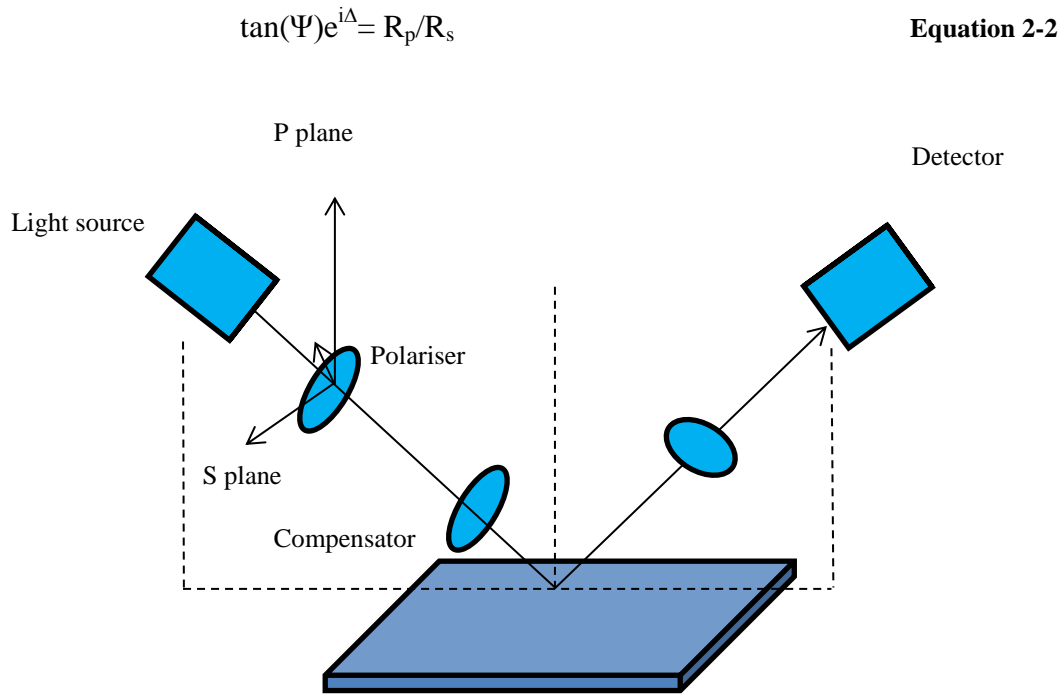


Figure 2.13. Schematic of ellipsometer principle. The figure indicates the different components as well as the incidence and reflected light planes. The measures recorded are provided by the change of polarisation as the incident light interacts with the sample. These changes are detected and interpreted by the ellipsometer giving the desired results.

Ellipsometry studies were conducted using a Gaertner Scientific L116-B rotating analyser ellipsometer, equipped with a 1 mW 632.8 nm helium-neon laser at an angle of incidence of 70° . For each measurement, the analyser of the ellipsometer was rotated from 0° to 180° in 10° increments. The voltage output of the detector measured at each angle of incidence was entered into a software designed by Dr Simon Martin (Loughborough University), which calculates the film thickness following the method reported by McCrackin *et. al.* (1963).

2.3.5 X-ray Photoelectron Spectroscopy (XPS)

XPS provides a detailed analysis regarding the elements presented on the surface (except H and He) (Briggs and Seah 1990; Förch *et al.*, 2009). The principle is focused on the electrons from the core level of the atoms. When a x-ray photon ($h\nu$) is irradiated onto the sample, the x-ray transfers enough energy to the electrons to leave the surface (Förch *et al.*, 2009; Briggs and Seah 1990; Gilmore, 2009) (Figure 2.14). These electrons are analysed according to the energy emitted, and the atom that they correspond to can be identified. The process can be described by the equation below:

$$KE = h\nu - BE$$

Equation 2-3

where $h\nu$ is the energy of the x-ray photon and KE is the kinetic energy of the photoelectron emitted when irradiated by the x-ray. The binding energy (BE) is characteristic for each atom and thus specific peaks for each corresponding atom appear in a photoelectron spectrum against binding energies, according to the energy of the x-ray and the respective kinetic energy of the photoelectrons (Förch *et al.*, 2009; Briggs and Seah 1990; Gilmore 2009).

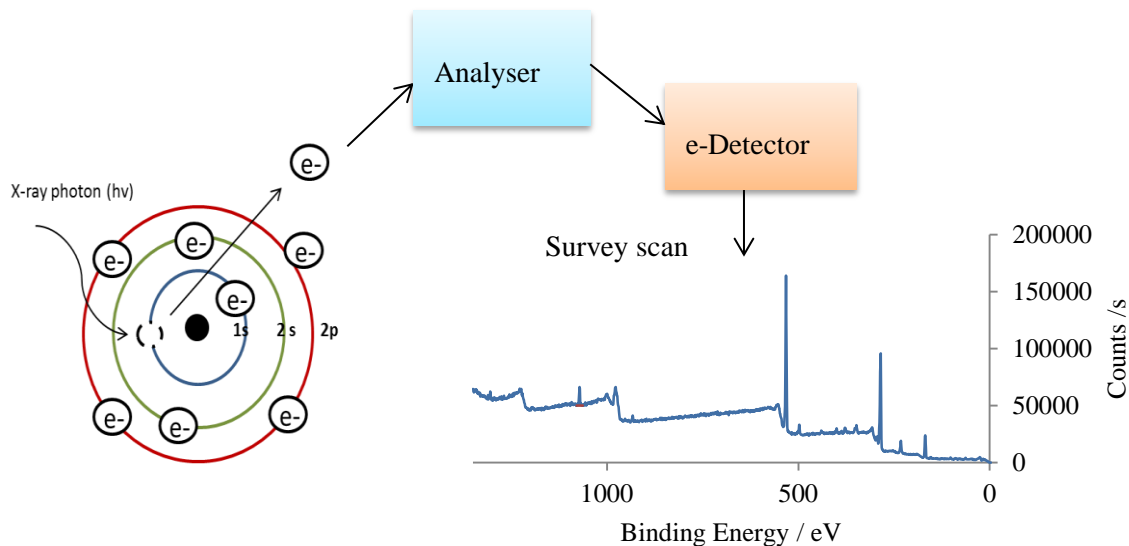


Figure 2.14. Schematic of XPS principle. Emission of a 1s photoelectron after being irradiated with enough energy from the x-ray to excite the electrons and leave the surface. The electrons are then collected by an analyser which measures the KE of the electrons. The KE is passed onto the detector for the generation of the spectra. Adapted from Gilmore (2009).

For XPS, a Thermo Advantage software in a Thermo Scientific K α with a monochromated Al K α x-ray source (1486.6 eV) was used. The peak was fitted using a Shirley background (Shirley, 1972). For survey scans, the parameters were 200 eV pass energy, 1 eV step size, 10 scans (to reduce noise) and 10 ms dwell time. For high resolution scans, 50 eV pass energy, 0.1 eV step size, 5 scans and 50 ms dwell time were used.

2.4 Cell culture methods

2.4.1 Cell culture: SH-SY5Y's

SH-SY5Y is a homogeneous neuroblast-like human subcloned cell line from SK-N-SH neuroblastoma cells, which has been widely used as an *in vitro* cell model in neurological studies (Joshi *et al.*, 2006; Xie *et al.*, 2010; Gunkel *et al.*, 2011). Due to the presence of the N-phenotype in these cells, their function, structure and electrophysiological properties can be of resemblance to dopaminergic or cholinergic neurons after differentiation. The process can be carried out by using different agents such as *all-trans* retinoic acid (ATRA) (Encinas *et al.*, 2000; Clagett-Dame *et al.*, 2006).

During the growth period, the SH-SY5Y neuroblastoma cell line (European collection of cell cultures) was incubated in growth media (GM) consisting of Dulbecco's Modified Eagle's medium GlutaMAX (DMEM GlutaMAX, Gibco, Invitrogen) supplemented with 10% of heat-inactivated foetal bovine serum (NFBS) (Gibco, Invitrogen) and 1% of Penicillin/Streptomycin (PenStrep: 100 units/mL penicillin and 100 μ g/mL streptomycin, Sigma Aldrich). Cells were maintained in a humidified 5% CO₂ atmosphere at 37° C and routinely passaged at confluence. Undifferentiated SH-SY5Y's were treated with differentiation media (DM) composed of GM with 10 μ M of *all-trans* retinoic acid (ATRA, Sigma Aldrich) in order to enable neuronal maturation and neurite outgrowth. During growth period, media was changed every 2 days. For experimentation on chemically modified surfaces, the samples were previously immersed in 70% IMS and dried in a sterile environment.

2.4.2 Cell culture: C2C12's

C2C12's murine myoblasts are a subclone of C2 myoblasts, derived from satellite cells (Burattini *et al.*, 2004). This myogenic cell line is well-established for research purposes as a reliable model in skeletal muscle studies mainly due to the spontaneous differentiation into myotubes on serum withdrawal (Yaffe and Saxel, 1977; Sharples *et al.*, 2012). Where C2C12's were used (Chapter 6), cells were grown in GM consisting of Dulbecco's Modified Eagle's Medium (DMEM), 20% Foetal Bovine Serum (MFBS) and 1% Penicillin/Streptomycin (PenStrep: 100 units/mL penicillin and 100 µg/mL streptomycin, Sigma Aldrich). In order to obtain the fusion of the myogenic cells into myotubes, differentiation media was used consisting of Dulbecco's Modified Eagle's Medium (DMEM), 2% Horse serum (HS) and 1% Penicillin/Streptomycin (P/S). In Chapter 6, the content of the differentiation media depended on the media compatibility experiments performed in Section 6.3; all of the different DM used in this thesis have been highlighted in Sections 6.2.2 and 6.2.3. During growth period, media was changed daily. For experimentation on chemically modified surfaces, the samples were previously immersed in 70% IMS and dried in a sterile environment.

2.4.3 Cell passaging

Cells typically grown in 75 cm² flasks (Nucn, Thermo Fisher, UK) were passaged when a confluence of 70-80% was attained. Subsequently, GM was removed and the flask was rinsed twice with 10 mL of Phosphate buffered saline buffer (PBS). Cells were trypsinised (trypsin/EDTA, SLS Scientific Laboratory supplies Ltd, Sigma Aldrich) by adding sufficient volume to cover the surface of the flask (normally 2 mL), and placed into the cell culture incubator for 5-10 minutes to allow for cellular detachment. Once cells were detached, GM was added into the flask in a greater volume than the enzyme to ensure its inhibition (3-4 mL). The solution was then transferred into a 15 mL tube for centrifugation and SH-SY5Y were spun at 300 g at 4° C for 7 minutes to secure the formation of the pellet. For C2C12's, the formation of the pellet was achieved by spinning the cells at 671 g for 5 minutes at 4° C. The supernatant was pipetted off and the pellet was re-suspended in 1 mL of GM. Cell counting was performed (see Section 2.4.4) for plating cells in experiments or re-plating into new 75 cm² flasks for further use.

2.4.4 Cell counting

Once cells were suspended in 1 mL of GM (see Section 2.4.3), 10 μ L of this solution was mixed with 90 μ L of trypan blue (1:10 vol/vol). Counting was performed using an improved Neubauer haemocytometer (Weber Scientific International Ltd., Teddington, U.K.). A coverslip was used to cover the counting zone so the solution could be transferred by capillary adsorption. Cells within the corner quadrants (see Figure 2.15A) were then counted under the microscope. The total number of cells counted within the 4 quadrants were divided by 4 to obtain the value of each individual quadrant. This was then multiplied by the dilution factor used (10 in this case) and by 10000 for the haemocytometer correction factor. The amount of media used to resuspend the cells was also multiplied to give an estimation of the number of cells in the solution (see Figure 2.15B).

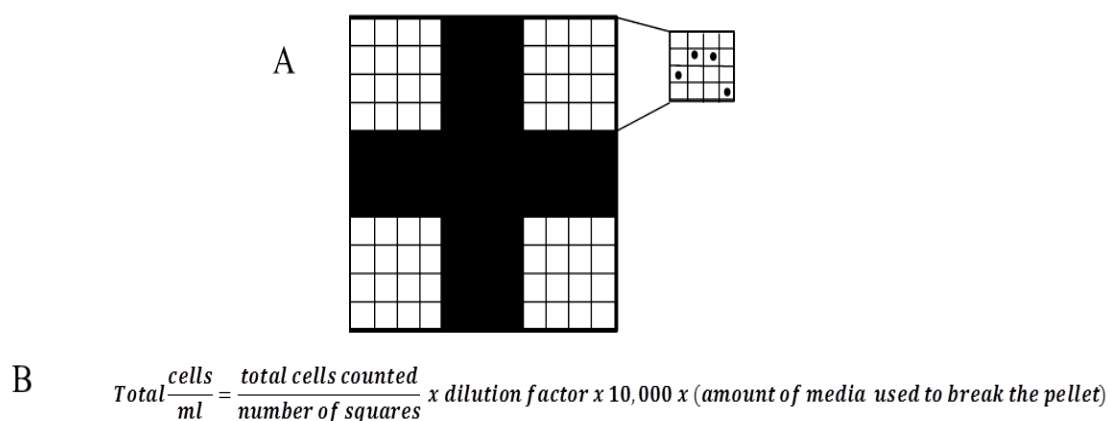


Figure 2.15. Hemocytomer grid used for cell counting. A) Cells in the Neubauer haemocytometer were counted in each quadrant corner and calculated from the equation described in the figure.

2.4.5 Cryopreservation of cells

Following cell number determination, excess cells were cryo-frozen by diluting the desired cell number with a solution containing GM and dimethyl sulfoxide (DMSO) (10:1, vol/vol respectively), and transferring the cell suspension to cryogenic tubes. Subsequently, tubes were placed in a Mr Frosty™ vessel and placed in a -80° C freezer to slowly freeze the cells overnight, prior to transfer to a liquid nitrogen dewar the following day.

2.4.6 Resurrection of cryopreserved cells

Vials stored as described in Section 2.4.5 were removed from the liquid nitrogen Dewar and defrosted in a water bath at 37° C. Cells in the vial were then transferred to a 75 cm² flask with 10 mL of GM and placed in the incubator at 37° C and 5% CO₂ for future use.

2.5 Techniques for biological analysis

The principle of the biological techniques used in this thesis have been highlighted in this section. These include:

- The use of LIVE/DEAD® Cell Viability staining to assess cell survival and biocompatibility on the various chemical modified surfaces
- AlamarBlue® assay to assess changes in cell metabolic activity on the different chemical modified surfaces
- Quant-iT™ PicoGreen® dsDNA assay to evaluate the degree of cell proliferation on the different chemical modified surfaces
- RT-qPCR to examine changes in gene expression on the different chemical modified surfaces
- Immunohistochemistry to investigate morphological changes after cells were grown on the different chemical modified surfaces

2.5.1 Principle LIVE/DEAD® Cell Viability staining

This method operates by identifying the cell population (live and dead cells) with the use of two different dyes: calcein AM and ethidium homodimer-1 (EthD-1). Calcein AM penetrates through the cell membrane of live cells due to its permeability. This compound is known to be very weak in fluorescence. However, once inside the cell, unspecific cytosolic esterases hydrolyse calcein AM by cleaving off an acetoxymethyl group, forming calcein (see Figure 2.16B). This compound emits a strong green fluorescence that is retained in the cytosol of the cells, due to its lack of membrane permeability (Stoddart, 2011; Tenopoulou *et al.*, 2007). EthD-1 is not permeable through cells thus will only enter to the cell when the membrane is damaged, intercalating with DNA to give a strong red fluorescence (see Figure 2.16A) (Stoddart, 2011; Haulang *et al.*, 1994).

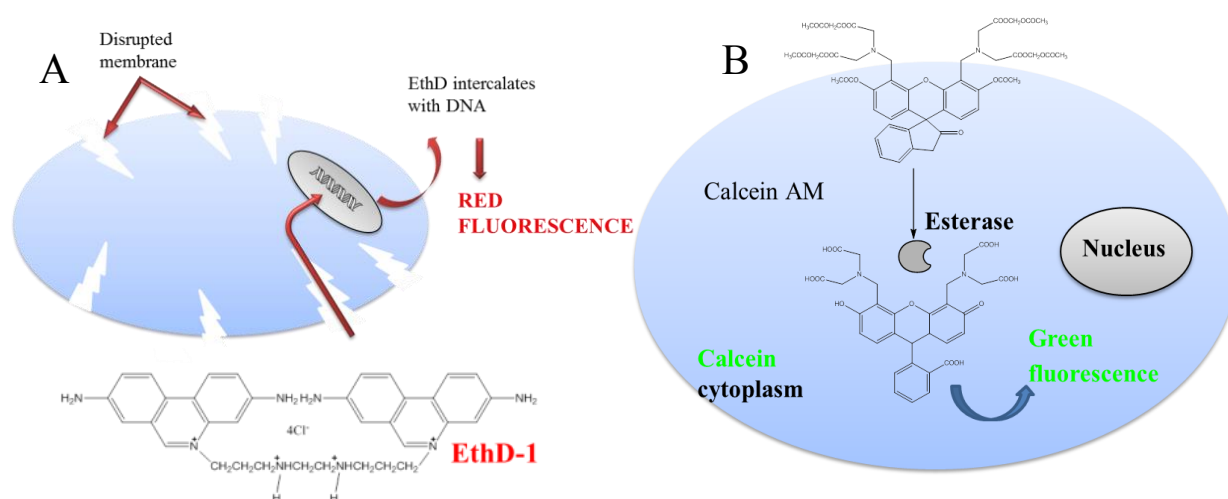


Figure 2.16. LIVE/DEAD® Cell Viability principle. A) EthD-1 penetrates the cells when the membrane is disrupted, intercalating with DNA and emitting a strong fluorescence. B) Calcein AM penetrates in the cells and is hydrolysed to form calcein, emitting green fluorescence.

2.5.2 Procedure LIVE/DEAD® Cell Viability staining

The optimisation for this staining has been illustrated in the Appendix 9.1 and the principle of the technique has been described in Section 2.5.1. Prior to cell culture, chemically modified samples were immersed in 70% IMS and dried in a sterile environment. SH-SY5Y's were passaged and counted as described in Sections 2.5.10, and seeded at 5000 cells/cm². Cells were cultured for a week and the growth media was changed every 2 days. Cell viability was then assessed by LIVE/DEAD® Viability/ Cytotoxicity Assay Kit (Invitrogen) after 1, 3, 5 and 7 days in culture. Samples were washed twice with PBS and incubated in a dye solution containing 0.5 μ M of calcein AM and 0.5 μ M of ethidium homodimer-1 in PBS (dye optimisation protocol can be found in Appendix 9.1). The samples were then incubated in the dark at RT for 45 minutes. Thereafter, the solution was pipetted off and the samples were mounted onto a glass coverslips by using Fluoromount™ Aqueous Mounting Medium. Five random images of each sample were imaged on both green and red channels and the number of live and dead cells were counted with the Image J counter plugin (1.50a).

EthD-1 has excitation and emission wavelengths of 528 nm and 617 nm (respectively) in the presence of DNA. Calcein has an excitation wavelength of 494 nm and an emission of 517 nm.

2.5.3 Principle AlamarBlue® assay

AlamarBlue® (also known as resazurin) has been used to assess proliferation, survival and metabolic activity (Vega-Avila and Pugsley, 2011). The reduced form of resazurin, known as resorufin, is the responsible for emitting fluorescence. Metabolically active cells let resazurin penetrate through the cell membrane into their cytosol, where mitochondrial enzymes reduce resazurin (blue, weakly fluorescent) into resorufin (pink, highly fluorescent, see Figure 2.17) (O'Brien *et al.*, 2000; Gonzalez and Tarloff, 2001; Gerhardt and Boccaccini, 2010; Vega-Avila and Pugsley, 2011). The assay has proved to be non-toxic, soluble in water and permeable through cells membranes.

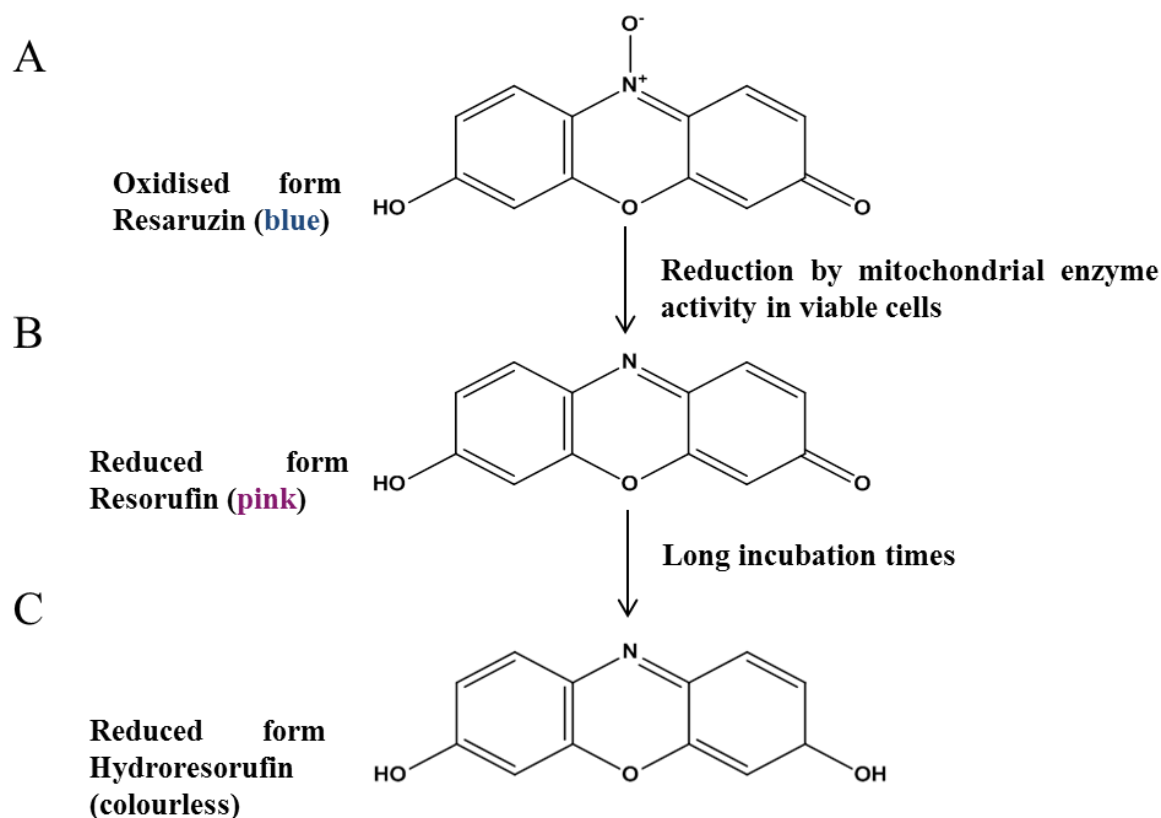


Figure 2.17. AlamarBlue® principle. A) The first chemical structure represents the oxidised form of AlamarBlue® (resazurin, weakly fluorescent). B) When reduced inside the cells, the reduced form of resazurin (resorufin) is the responsible for emitting fluorescence. C) Long incubation periods can lead to a colourless compound and therefore misleading results.

The fluorescence of the samples treated with alamarBlue® was measured in a Varioskan Flash plate reader (Thermo Scientific, UK). The reader filter was set up at 560 nm excitation wavelength and the emission at 590 nm. As the same cells were used sequentially for the differing time points, samples were washed at least twice with PBS and replenished with fresh GM. The reduced form of alamarBlue® was used as a positive control by autoclaving GM with 10% of alamarBlue® without cells for 15 minutes. The same solution prepared without autoclaving was used as a negative control.

2.5.4 Procedure AlamarBlue® assay

The basis of AlamarBlue® has been described above and the optimisation of this assay has been highlighted in the Appendix 9.2. AlamarBlue® (Invitrogen) was used to study the metabolic activity of SH-SY5Y's on chemically modified surfaces during the 1, 3, 5 and 7 days in cell culture. SH-SY5Y's were seeded at 10000 cells/cm² and cultured for a week. The growth media was changed every 2 days. After every time point, the medium from the samples was aspirated off and the substrates were washed with PBS twice. A solution of 10% alamarBlue® in serum free DMEM GlutaMAX was added into each well and incubated for 4 hours at 37° C. Thereafter, 100 µL of the supernatant was pipetted into a black opaque 96-well plate, which was maintained in the dark until fluorescence was measured. The fluorescence intensity obtained was correlated with the cell metabolic activity.

2.5.5 Principle Quant-iT™ PicoGreen® dsDNA Assay

PicoGreen® has been used as a selective manner to obtain DNA quantification and assess cell proliferation. This cyanine probe binds to double stranded DNA (dsDNA), giving a fluorescence proportional to the amount of DNA present (Cosa *et al.*, 2001; Dragan *et al.*, 2010).

2.5.6 Procedure Quant-iT™ PicoGreen®

The Quant-iT™ PicoGreen® dsDNA assay was used to assess cell proliferation at day 1, 3, 5 and 7 in culture. SH-SY5Y's were seeded at a density of 10000 cells/cm² and cultured for a week. After every time point, cells were lysed with 0.1% Triton-X100 in pure water and collected in nuclease-free vials. Vials were vortexed and 100 µL of lysate cells were pipetted into black flat-bottomed 96 well plates along with 100 µL of Quant-iT™ PicoGreen® working solution (1:200 vol/vol from 1x TE buffer). Plates were then incubated in the dark for 5 minutes at RT, and the fluorescence emitted by PicoGreen® was measured in a Thermo Scientific Varioskan Flash microplate reader, at excitation and emission wavelengths of 480 and 520 nm, respectively. Indirect quantification of DNA was calculated from the dsDNA standard curve shown in Figure 2.18.

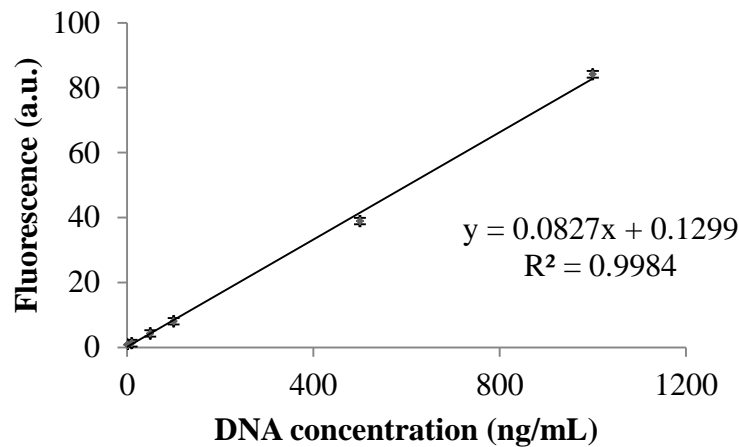


Figure 2.18. Standard curve used to determine [dsDNA] using the fluorescence of Quant-iT™ PicoGreen®. The standards were prepared from Lambda DNA standard (100 µg/mL) provided in the PicoGreen® kit with concentrations ranging from 0 ng/mL to 1000 ng/mL. Error bars correspond to the SD of the mean (n= 3).

2.5.7 Principle Reverse transcription polymerase chain reaction RT-qPCR

RT-qPCR has been utilised in molecular biology to measure mRNA levels within cells and tissues. The technique is based on the polymerase chain reaction (PCR) where small amounts of mRNA are reversed to complementary DNA (cDNA) and then amplified proportionally to estimate the amount of the target material in the sample (Mullis *et al.*, 1986). When comparing mRNA target sequences between treatments to obtain differences in gene expression, the RT-qPCR process begins by extraction of mRNA of the sample of interest (see Section 2.5.7.2 for extraction protocol). The mRNA is then converted into complementary DNA by reverse transcription and thereafter, the PCR process can be carried out by three main stages:

- **Denaturation.** The temperature is increased from 40-60° C (temperature for RT enzyme to work efficiently) to 90° C. This leads to the denaturation of the double stranded cDNA, separating both strands (Figure 2.19A).

- Annealing. Once the strands are separated, the temperature is reduced to meet the primer characteristics so the primer of interest will bind to the target sequence of DNA (Figure 2.19B).
- Extension. Once the primers are annealed to the DNA sequence, the temperature is raised again at the point where Taq polymerase (a thermo-stable DNA polymerase) works optimally. Then, the enzyme attaches to the initial site of the primers, using random dNTPs to synthesise new strands of the aimed DNA sequence (Figure 2.19C and D). This closes a cycle in the RT-qPCR process. In a PCR reaction, the cycle is repeated 30-40 times, accumulating a large amount of DNA copies.

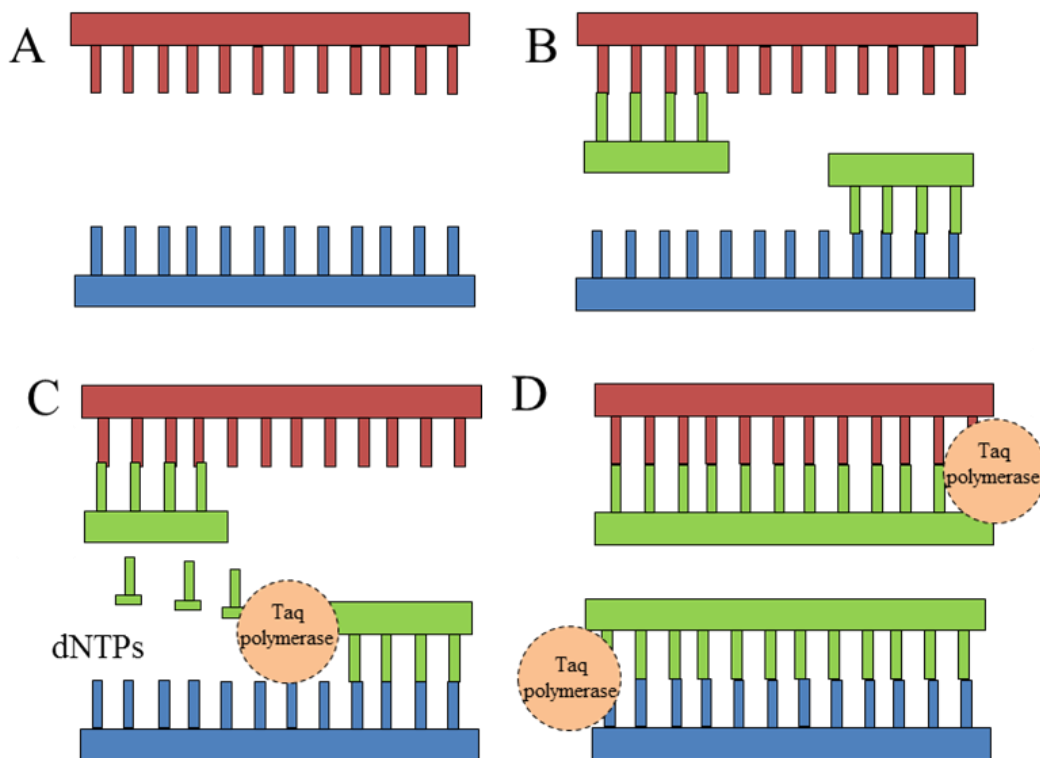


Figure 2.19. Three step process in RT-qPCR. A) Denaturation. B) Primer annealing. C and D) The DNA polymerase synthesises the newly double strand DNA.

The amplification of DNA is detected in RT-qPCR *via* fluorescence by the specific binding of the dye SYBR® green to the dsDNA. The fluorescence increases proportionally with the number of cycles, as DNA amplification occurs in every annealing step. When the fluorescence produced in the reactions surpasses the background fluorescence, the amount of target gene present in the DNA of the sample can be quantified. This point is known as the

threshold cycle (C_T). C_T values are inversely proportional to the amount of DNA target. Thus, high C_T values will indicate low amounts of the gene target, whereas lower C_T values will indicate greater amounts.

2.5.7.1 Primer design and specificity of the primers

Primers were purchased from Sigma Aldrich (UK) and were designed according to the properties specified in Table 2.1.

Table 2.1. Parameters used for primer design. The guanine-cytosine (GC) content, T_m and length of the primer must accomplish the requirements specified below. Further information can be found in Nolan *et al.* (2014) and Sigma-Aldrich Co. LLC. (2017).

Parameters to consider	Guidelines
GC content	~ 40-60%
Melting temperature (T_m)	Should be designed in a T_m higher than the T_m of possible subproducts (~60 °C) T_m designed so the annealing process is carried out optimally
Length (primer and products)	Primer longer than 17 bases (ideally 20-24) Product less than 200 bp long
Additional considerations	Avoid primers complementing themselves (primer/dimer formation) Gs and Cs longer than three bases should be avoided, otherwise this could lead to a polymerase slippage

Prior to using primer pairs, the efficiency and specificity of the reactions were verified. Primer specificity was assessed by running a melt analysis to examine the presence of a single product, confirming the purity of the primer. A single peak in the melting graph indicated the specificity of the primer (see Figure 2.20). The standard curve values for both primers defining data accuracy have been described in the Table 2.2.

Table 2.2. Primer sequences used in this thesis. The values obtained in the standard curve have been illustrated in the right column of this table. The amplification efficiency percentage indicates the rate at which an amplicon is generated. The slope is used to identify the amplification efficiency of the reaction, which means when the slope is ~ -3.3 , a 100% amplification efficiency can be generated. A high precision in the results can be assumed when the correlation coefficient is >0.99 (Biosystems, 2008).

Target mRNA	Sequence 5'-3'	Optimised values	Ref. Seq. Number
MAPT	F GAAAAATAGGCCTTGCCTTAG	$R^2 = 0.99$	NG_007398.1
	R CCTTGAGTTTCATCTCCTTTG	Scope= -3.3 Efficiency=100.3 %	
RPIIβ	F AAGGCTTGGTTAGACAACAG	$R^2 = 0.99$	NM_000938.2
	R TATCGTGGCGGTTCTTCA	Scope=-3.3 Efficiency= 100.6 %	

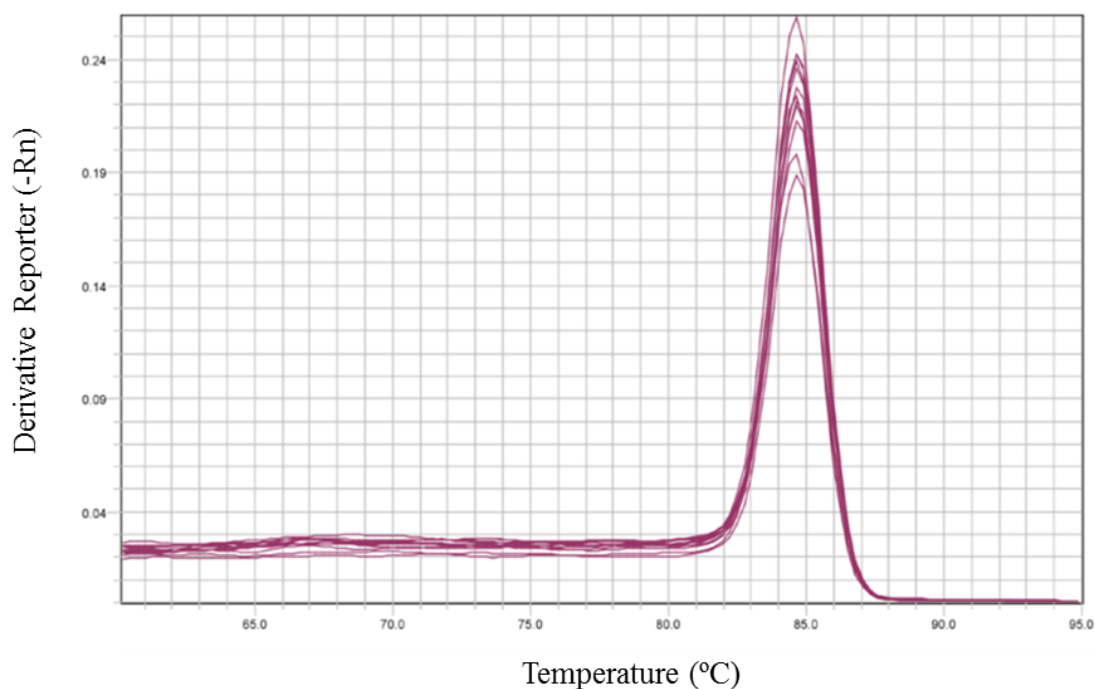


Figure 2.20. MAPT melt curve. Single peak presented in the melting curve, showing the presence of the desired product and therefore achieving specificity.

2.5.7.2 RNA extraction

RNA was extracted following the TRIzol® method as per the manufacturer instructions. Samples were washed with PBS and consequently treated with 500 µL of TRIzol® reagent (SLS Scientific Laboratory supplies Ltd, Sigma Aldrich). The surface was scraped with a pipette tip until a milky solution was obtained. This solution was transferred into a RNase free 1.5 mL tube. For RNA separation, 20% of chloroform was added, shaken for 15 seconds and incubated at room temperature (RT) for 5 minutes. Tubes were spun at 12000 g for 15 minutes at 4°C. The resultant aqueous RNA phase was extracted and transferred into a new tube, for subsequent precipitation of RNA with 250 µL of 2-propanol. The solution was incubated for 10 minutes at RT and spun at 12000 g for 10 minutes at 4°C. The RNA pellet at the bottom of the tube was washed with 75% ethanol and spun at 7500 g for 5 minutes at 4°C. Ethanol was removed and the pellet was left to air dry for 10-15 minutes. The RNA obtained was then dissolved in 50 µL of RNA storage solution (Ambion, UK) and stored at -80°C for

further analysis. RNA quantification (absorbance 260 nm) and purity (260/280 nm ratio) were determined spectrophotometrically using a NanoDrop 2000 (Thermo Scientific, UK).

2.5.7.3 Relative quantification PCR

Relative quantification of gene expression has been analysed in this thesis by the $2^{-\Delta\Delta C_T}$ method (Livak and Schmittgen, 2001). In this technique, a reference gene is used to normalise the data much like a loading control. Likewise, a reference sample in the experiment is used to relate the change of gene expression for the rest of the samples. An example of the method used to quantify gene expression in this thesis has been illustrated in Table 2.3, where the reference sample used has been “APTES 1” and the reference gene is RPII β .

Table 2.3. Example of data analysis carried out using the $2^{-\Delta\Delta C_T}$ method. Where $\Delta C_T 1 = C_T \text{ RPII}\beta \text{ average} - C_T \text{ MAPT average}$, $\Delta C_T 2 = \text{Calibrator MAPT} - \text{calibrator RPII}\beta$ and $\Delta\Delta C_T = \Delta C_T 2 - \Delta C_T 1$. Δ = Change, C_T = threshold cycle. MAPT refers to the gene of interest whereas RPII β is the house keeping gene.

Sample name	C_T MAPT average	C_T RPII β average	Calibrator MAPT	Calibrator RPII β	$\Delta C_T 1$	$\Delta C_T 2$	$\Delta\Delta C_T$	$2^{-\Delta\Delta C_T}$
APTES 1	28.38	20.14	28.38	20.14	-8.24	-8.24	0.00	1.00
APTES 2	27.83	20.44	28.38	20.14	-7.38	-8.24	-0.85	1.81
APTES 3	28.23	19.96	28.38	20.14	-8.26	-8.24	0.03	0.98
BIBB 1	28.34	21.46	28.38	20.14	-6.88	-8.24	-1.36	2.56
BIBB 2	25.91	19.79	28.38	20.14	-6.12	-8.24	-2.12	4.35
BIBB 3	27.83	20.80	28.38	20.14	-7.04	-8.24	-1.20	2.30

2.5.7.4 RT-qPCR procedure

The amplification of RT-qPCR was assessed by using QuantiFast® SYBR® Green one step kit (Qiagen) on ViiA™ 7 RUO Software. The principle of this technique has been described in Section 2.5.7. Reactions were prepared in 384 well plates and consisted of 20 ng of RNA in 5 µL, and 5 µL of master mix consisting of 4.7 µL SYBR® Green, 0.1 µL of both forward and reverse primer and 0.1 µL of quantifast reverse transcriptase kit. The reaction was carried out as follows: 50°C for 10 minutes and 95°C for 5 minutes, followed by 40 cycles of 95°C for 10 seconds and 60°C for 30 seconds.

2.5.8 Principle Immunocytochemistry

This common biological technique is used to identify certain cell proteins or antigens by the use of antibodies that binds to the protein of interest by specificity. Fluorescent compounds (fluorophores) are used to emit fluorescence when bound to the site of interest, thus allowing the visualisation of these cells under a fluorescence microscope.

Prior to the immunocyto-analysis, cells first need to undergo a fixation process to maintain the cell shape. This can be achieved by the use of organic solvents or cross-linking agents such as methanol or paraformaldehyde, respectively. A second step involves the permeabilisation of the membrane with detergents such as Triton X-100, allowing the staining components to enter the cell. Sometimes this step is not necessary, as some organic solvents allow cell permeabilisation and blocking solutions often incorporate the detergent. The blocking solution is used to avoid unspecific fluorescence binding by blocking the sites with serum. Thereafter, the primary antibody can be added to identify the site of interest.

The antibodies can be classified as polyclonal or monoclonal. Typically, antibodies are created by collecting the response produced in the animals when the antigen of interest is injected into their system. For polyclonal antibodies, the antigen of interest is injected into the animal system, and the multiple B-lymphocytes activate in order to generate the antibodies specific for that antigen. The antibodies are collected from the sera of the animal and purified for further use. For monoclonal antibodies, the antigen injection is performed similarly, with the exception that a single B-lymphocyte is isolated from the spleen of the animal, thus

achieving a higher specificity than in the polyclonal antibodies. The lymphocyte is then mixed with myeloma cells, forming hybridoma cells. This is because the limited life span of the B-cells would not allow to produce antibodies in large quantities. These cells produce only one antibody as it is produced by the mixture of myeloma cells and one B-cell and thus, the generated antibodies are more selective. With purification, the acquisition of a monoclonal antibody can be achieved. After the antibody selection, the use of direct or indirect fluorescence needs to be assessed to visualise the staining (Figure 2.21). When using direct fluorescence, the primary antibody is already conjugated with a fluorophore and the staining can be performed at once. For indirect fluorescence, a primary antibody is bound to the protein of interest and then a fluorophore-conjugated secondary antibody against the animal or IgG of the primary antibody is used. Alternatively, the use probe conjugated fluorescent dyes can also be used for direct fluorescence, where the staining process is carried out by simply incubate the sample with the probe-conjugated dye without the need of antibodies.

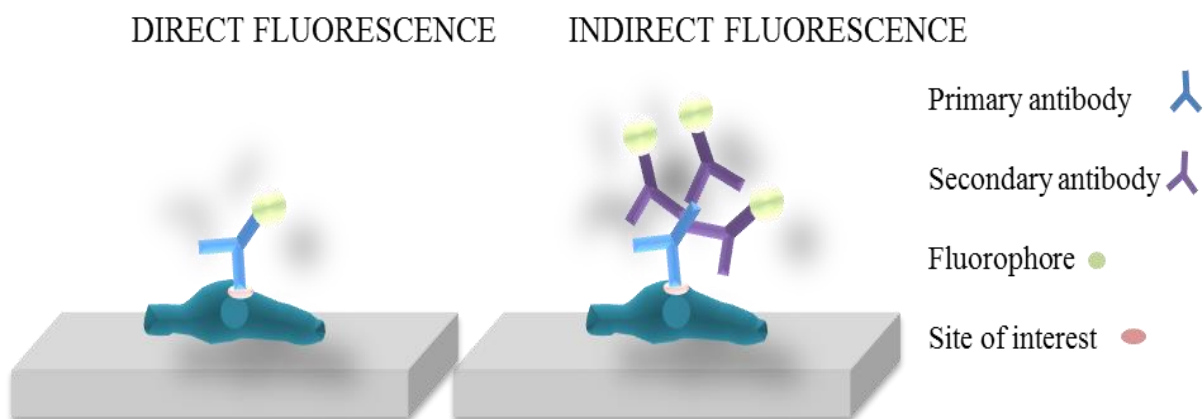


Figure 2.21. Immunocytochemistry principle for direct and indirect fluorescence.

2.5.9 Staining procedure

SH-SY5Y's were labelled with β tubulin III as a neuronal marker to assess neuronal morphology and neurite extension. Cells were fixed with methanol:acetone (1:1 vol/vol) or with 3.7% paraformaldehyde (Sigma Aldrich) in PBS. Once fixed, cells were permeabilised and blocked with a solution containing 5% goat serum (GS), 0.2% Triton-X100 and tris-buffered saline (TBS, pH= 8.5) for 30 minutes. Subsequently, samples were rinsed three

times with TBS and monoclonal mouse anti-human β tubulin III primary antibody was added (~2.0 mg/mL, SLS Scientific Laboratory supplies Ltd, Sigma Aldrich, 1:200 vol/vol in TBS) with 0.2% Triton-X100 and 2% goat serum in TBS. The sample was incubated in this solution for 2 hours and protected from light. Thereafter, samples were rinsed three times with TBS and then an Alexa Fluor® 488 goat anti-mouse IgG secondary antibody solution (~2 mg/mL, SLS Scientific Laboratory supplies Ltd, Sigma Aldrich, 1:200 vol/vol in TBS) with 0.2% Triton –X100 and 2% GS was added and incubated for an hour in the dark. At this stage, nuclear counterstain 4',6-diamidino-2-phenylindole (DAPI, Life technologies, Thermo scientific 1 mg/mL, 1:1000 vol/vol in TBS) was also added. The samples were then washed with TBS at least three times and mounted onto glass slides using Fluoromount™ mounting medium.

The staining of C2C12's to assess myotube formation and morphology was determined by actin staining. The cell membrane was permeabilised for 30 minutes with 0.2% Triton-X100 and samples were then incubated with rhodamine phalloidin (Sigma Aldrich, 1:200 vol/vol) in TBS for one hour. The samples were washed at least three times and nuclear counterstain DAPI was added (1:1000 vol/vol) for 10 minutes. At this point, samples were washed with TBS and mounted onto glass slides using Fluoromount™ mounting medium.

2.5.10 Image analysis

Fluorescence micrographs were taken with a Leica DM2500 fluorescence microscope and a Leica DMIL-LED microscope was used for phase contrast micrographs.

For neurite measurement described in Chapter 4 and 5, neurite extension was traced with “freehand” segmented lines and measured in a Fiji (Java 1.6.0_24) image analysis software (Image J 1.50a) (Figure 2.22). Neuron protrusions were considered neurites when these were \geq than 10 μ m. Measurement was applied when neurites crossed from neuron to neuron, from cell body to branches and from cell body to the end of the neurite. Neurites overlapping each other but not interacting (one above, other below) were measured as separate neurites, otherwise (e.g. connecting and forming one) measurement was performed until the point they met. Cells in bulks, clumped or forming networks where neurite measurement was unfeasible were not measured due to difficulties in the visualisation and multiple neurite crossing. To

calculate cell viability data in Chapter 4 as well as the percentage of the generating neurites and cell confinement in Chapter 5, a cell counter macro plugin on Fiji software was used (Java 1.6.0_24). For the viability data, the number of live cells divided by the total number of live and dead cells displayed as a percentage was defined as the fractional viability. For the data in Chapter 5, the number of cells extending neurites divided by the total number of cells counted (within the channels) was displayed as a percentage. Likewise, the numbers of cells within the channels divided by the total number of cells presented in the image was also displayed as a percentage for cell confinement.

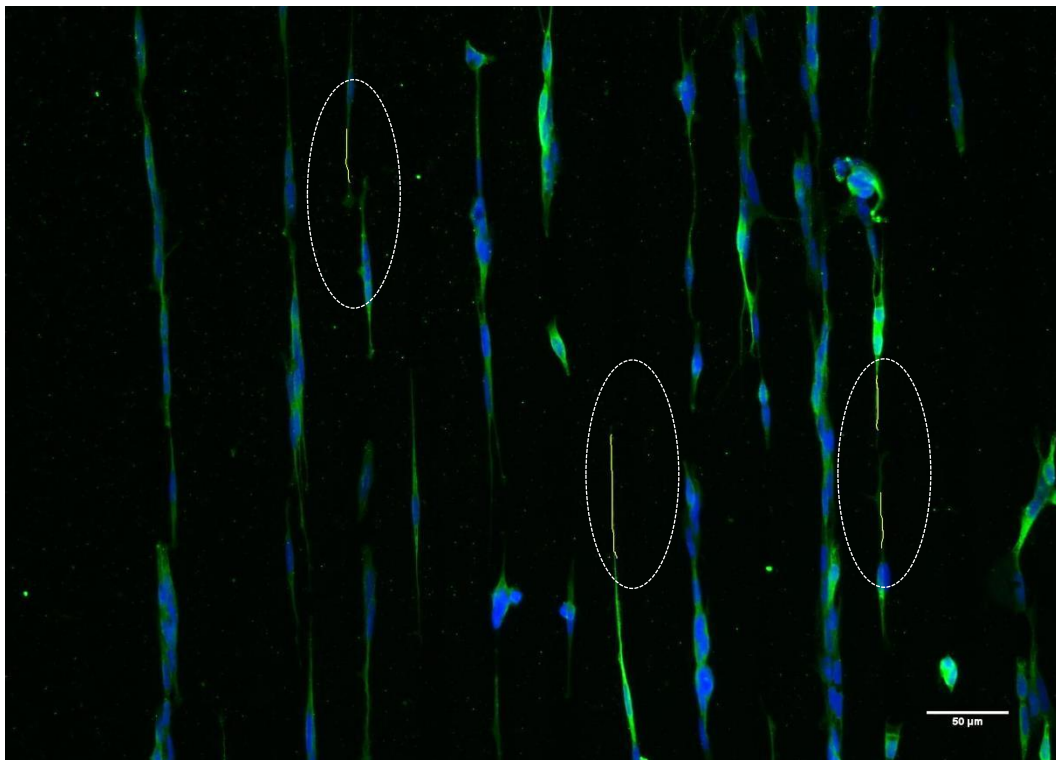


Figure 2.22. Analysis of neurite length. Representation of neurite measurement by tracing a line across the neurite with Image J Fiji software. Scale bar= 50 μm .

In Chapter 5, nuclei alignment was obtained from DAPI images using a customised Fiji (Java 1.6.0_24) image analysis software macro (Image J 1.50a, Figure 2.23), where the angle of the nuclei was obtained by using the channels as the reference point. Vertical lines parallel to the channels were considered as the point at which cells were perfectly aligned (0 degrees). The

nuclei alignment was calculated by interquartile ranges. Measures were considered when at least three cells were in the image.

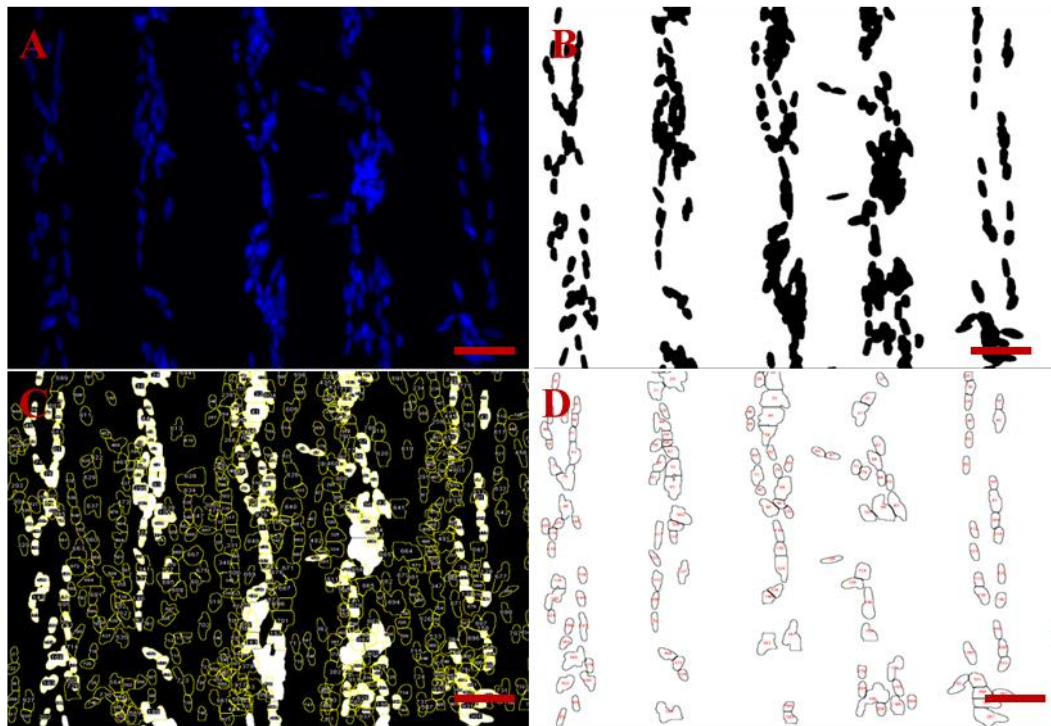


Figure 2.23. Analysis nuclei alignment. A) Fluorescence micrographs with nuclei DAPI counterstain at 20x magnification for nuclei analysis. B) Auto threshold by running macro analysis. C) Application of watershed and identification of nuclei area from all the image sequences (white lines are for the cells of interest). D) Final result after analysing particles with defined parameters. Scale bar= 100 μ m.

In Chapter 6, fibres were considered myotubes when cells had three or more nuclei and presented an elongated morphology. For myotube width, the measurement was carried out by drawing a line perpendicularly to the axis of the myotube in a representative area with Image J Fiji software.

2.5.11 Statistical analysis

GraphPad Prism 6.0 software was used for statistical data analysis. Specific statistical analyses performed in this thesis have been highlighted in the methods section of each chapter, as each experiment had specific analytical requirements.

3 Generation of chemically modified surfaces

3.1 Introduction

When cells attach to a surface material, various physical and chemical interactions occur *a priori* between the cell environment and the surface, including water layer formation, surface-molecule bonding, etc. (Roach *et al.*, 2007). Such interactions can facilitate protein adsorption from cell culture media and thus support possible mediation of cell attachment and behaviour. In this regard, surface properties are known to be partially responsible for the degree of protein adsorption and denaturation. This in turn determines the degree of affinity of the cells by the material and therefore the consequential cell response (Roach *et al.*, 2007; Ventre *et al.*, 2012; Thevenot *et al.*, 2008).

Surface properties such as surface chemistry and physical cues have been shown to significantly influence cell behaviour *in vitro* (Thevenot *et al.*, 2008; Chang and Wang, 2011). The term ‘surface chemistry’ includes several parameters such as wettability, surface energy, surface charge and chemical functionality. Some of these surface characteristics have shown to trigger various cell responses, suggesting that each parameter could contribute to the differing cell responses observed (Wei *et al.*, 2009; Zhao *et al.*, 2010; Wan *et al.*, 2012). Consequently, modifying surface parameters has become a valuable tool *in vitro* to regulate cell behaviour and promote a greater understanding of the cell-material cross-talk (Ventre *et al.*, 2012). By inducing small changes on the surface chemistry, cell processes such as adhesion, proliferation and differentiation could be regulated (Chang and Wang, 2011; Shah *et al.*, 2016). For example, a decrease in osteoblast adhesion was observed when the wettability of the surface was altered towards hydrophobicity in the work performed by Wei *et al.* (2009). In a similar study by Tamada and Ikada (1993), fibroblasts showed optimum cell adhesion with a moderate wettability (water contact angle was 60-80°). Surface charge has also been observed to influence cell behaviour, as discussed in 1.3.3 of Chapter 1 (Thevenot *et al.*, 2008; Tan *et al.*, 2013). The surface chemical functionality is another parameter that has been related to changes in cell behaviour (Ren *et al.*, 2009; Kuzmyn *et al.*, 2014). For example, Faucheux and co-workers (2004) used coated glass and silicon wafers with layers containing various functional end groups -CH₃, -CH=CH₂, -NH₂, -COOH and polyethylene glycol (-PEG), to test the effect on human fibroblasts. Strong attachment and spreading was found in the coatings with -NH₂ and -COOH terminating groups, whilst poor

adhesion was observed for the hydrophobic layers containing $-\text{CH}_3$ and PEG (see Figure 3.1). The success of the $-\text{NH}_2$ and $-\text{COOH}$ layers was correlated in this study with the different hydrophilicity rendered by the different end groups, as well as the greater ability of these surfaces to adsorb certain proteins.

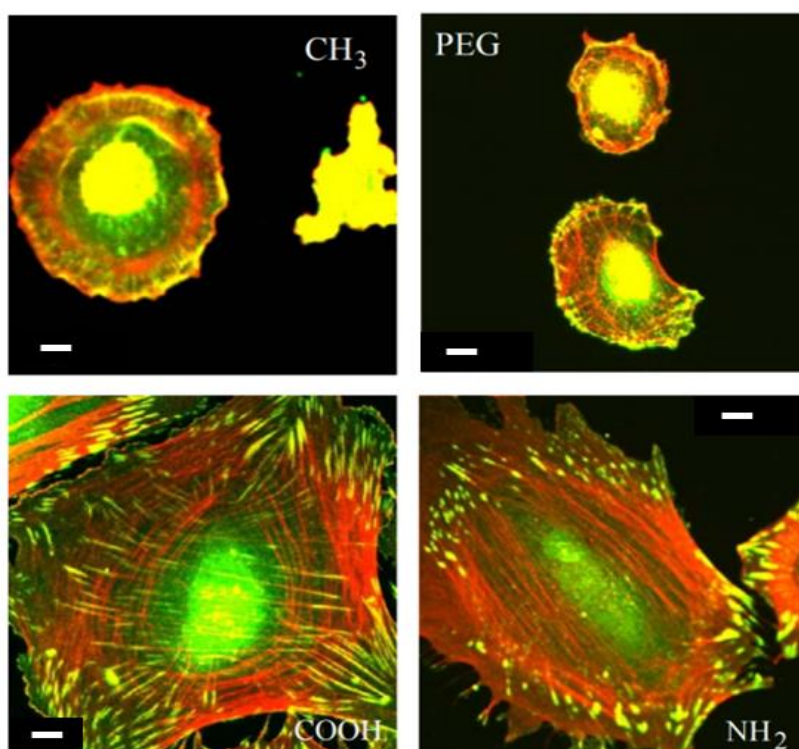


Figure 3.1. Effect of surface chemical functionalities in cell culture. Confocal images of human fibroblasts attached on SAMs with different end groups ($-\text{CH}_3$, $-\text{PEG}$, $-\text{COOH}$ and $-\text{NH}_2$) after 2 hours of cell seeding. Cells were immunolabelled for vinculin (green) and F actin (red). Adapted from Faucheux *et al.* (2004). Scale bar= 10 μm .

Moreover, when various surface properties have been studied under culture (see Table 3.1), various cell responses in terms of adhesion, proliferation and differentiation have been observed, suggesting that responses are a consequence of a combination of factors rather than parameters in isolation (Arima and Iwata, 2007). Although a diverse range of research has been conducted to assess and control cell behaviour in response to different surface properties, it is important to mention that the response between cell lineages is variable among the same surface parameters, and therefore the mechanisms underpinning the cellular response to

specific chemical and physical cues is not fully understood (Senaratne *et al.*, 2005; Krishnamoorthy *et al.*, 2014).

Table 3.1. Effect of surface charge and wettability on various cell types. Adapted from Thevenot. *et al.* (2008).

Functional end group	Characteristics	Cell effect
-CH ₃	Neutral charge, hydrophobic	Promoted leukocyte adhesion
-OH	Neutral charge, hydrophilic	Osteoblast differentiation
-COOH	Negative charge, hydrophilic	Osteoblast attachment
-NH ₂	Positive charge, hydrophilic	Myoblast and endothelial proliferation
-CH ₂ NH ₂	Neutral charge, hydrophilic	Promoted CHO cells adhesion

Therefore, the use of well-defined modified surfaces is necessary to determine the main factors that regulate the behaviour of specific cell types. Over many years, surface modification techniques have been developed in order to create homogeneous and consistent modified surfaces (Zhu *et al.*, 2001; Thevenot *et al.*, 2008; Raynor *et al.*, 2009). Various studies have made use of self-assembled monolayers (SAMs) and polymer brushes as a robust tool to manipulate surface properties (Senaratne *et al.*, 2005; Raynor *et al.*, 2009). Both methods have been described in Section 1.3 of Chapter 1 and thus, only their main characteristics and the differences between them have been highlighted in Table 3.2.

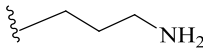
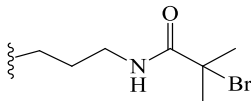
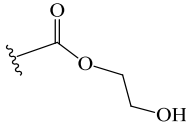
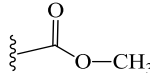
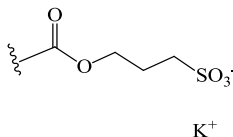
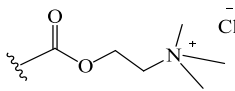
Table 3.2. Main considerations when comparing SAMs and polymer brushes for thin film formation.Adapted from Raynor *et al.* (2009).

	SAMs	Polymer brushes
Advantages	Molecularly well-defined layers	Long-term stability
	Simple protocols for their formation	Various methods can be used for their preparation (“grafting from” and “grafting to”) and also variety in polymerisation methods
	End groups used to tailor surface properties can be used as an anchor point for biological ligands	Tunability through the use of a wide range of monomers Greater film thickness which might provide self-healing of defects
Disadvantages	Thin layer increasing the presence of pinholes and defects	More complex preparation
	Limited long term stability	More complex structure: more features to be considered

3.1.1 Objectives of the chapter

The aim of this chapter was to chemically modify glass slides and silicon wafers by using various SAMs and polymer brushes, which were chosen to display different surface properties (functional group variation, different surface charge, surface wettability, etc.; Table 3.3). To ensure the coatings were being deposited, the surfaces were analysed by XPS, FTIR, WCA and ellipsometry. The ethos behind using surfaces with differing parameters was that these surfaces would be consequently used in neuronal cell culture to obtain an optimum control over neuronal growth. Thus, a range of surface parameters that had been associated with changes in cell behaviour were used. The outcome of these surfaces on cell culture could have an impact on future work regarding the control over cell behaviour and hence, obtaining information regarding the general structure of the coatings was essential.

Table 3.3. Chemically modified surfaces used highlighting their functional group and surface wettability.

Abbreviated name for the chemical structures used in this thesis	Main characteristics	Chemical structure (functional end group)
APTES	-NH ₂ , hydrophilic	
BIBB	-Br, hydrophobic	
PHEMA	-OH, hydrophilic	
PMMA	-CH ₃ , hydrophobic	
PKSPMA	-SO ₃ ⁻ , hydrophilic	
PMETAC	N ₃ ⁺ , hydrophilic	

3.2 Methods

The principle of the techniques used for surface characterisation, as well as the chemical reactions for the differing polymerisations have been described in Chapter 2, Sections 2.3 and 2.1, respectively.

3.3 Results

XPS was used along with FTIR to analyse the chemical surface composition of the films, whereas ellipsometry and WCA were used to determine the film thickness and surface

hydrophilicity, respectively. Surface modification began with the oxidation of the glass surface *via* UV/ozone treatment, which was used to remove the organic contaminants as well as promoting the formation of a hydroxyl (–OH) layer on the surface (indicated as SIOH). Thereafter, APTES deposition was carried out by the formation of Si-O-Si bonds on the surface, followed by the anchoring of a BIBB initiator, which would in turn allow the synthesis of the polymer brushes (PHEMA, PMMA, PKSPMA and PMETAC) by surface initiated polymerisation.

3.3.1 X-ray Spectroscopy (XPS)

XPS analysis of the Si-OH layer (SIOH) showed the silicon (Si2p) and oxygen (O1s) peaks as the most predominant elements on the surface. This was anticipated, as these two atoms are the characteristic elements of glass surfaces (Table 3.4). The analysis also showed the presence of carbon (C1s) in the clean glass slide, which was probably due to hydrocarbon contamination (Ma *et al.*, 2007; Dworak *et al.*, 2013).

Table 3.4. Percentage composition of Si2p, C1s, O1s, N1s and Br3d after the cleaning, silanisation and initiator deposition. The presence of groups such as N1s and Br3d after the deposition of APTES and BIBB as well as an increase in C1s content, led to the conclusion that new polymer layers were being deposited on the surface.

Modification step	Atomic composition (%)				
	Si2p	C1s	O1s	N1s	Br3d
Clean glass (Si-OH, named as SiOH)	28.1	4.6	56.4	-	-
Silanisation (Si-NH₂)	26.4	20.0	47.2	1.6	-
Initiator (Si-Br)	27.9	10.9	54.2	0.9	0.1

APTES attachment showed an increase in the carbon percentage (C1s), along with the presence of a new nitrogen peak ~400 eV containing 1.6% nitrogen content (N1s), which had not been observed in the clean glass slide (Figure 3.2). This suggested the successful addition of amine and propyl groups onto the surface.

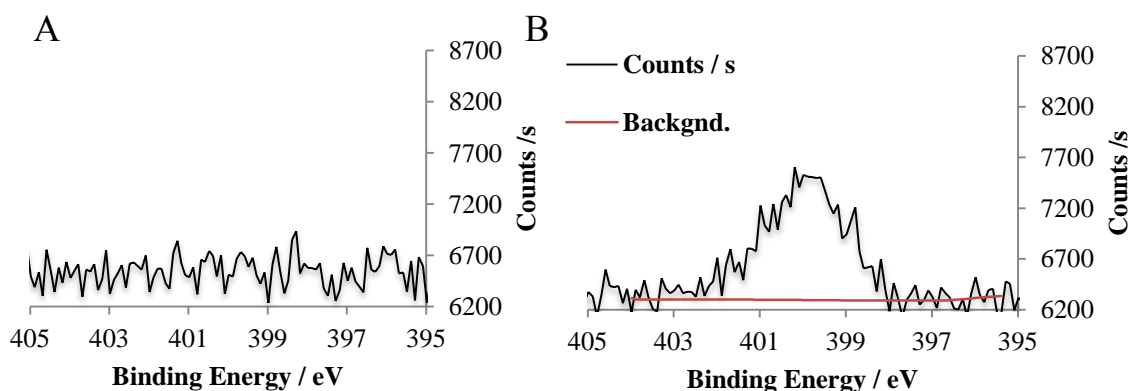


Figure 3.2. N1s high resolution spectra of A) UV/ozone glass slide and B) APTES functionalised surface. The spectra indicated that nitrogen components had been incorporated on the glass surface, confirming APTES deposition.

The introduction of BIBB onto the APTES surface was confirmed by the presence of a Br3d peak (Br3d₅ and Br3d₃, see Table 3.4 and Figure 3.3), along with an increase in C1s content.

There was an increase in oxygen content (O1s) compared to APTES, perhaps due to the introduction of C=O groups in this structure.

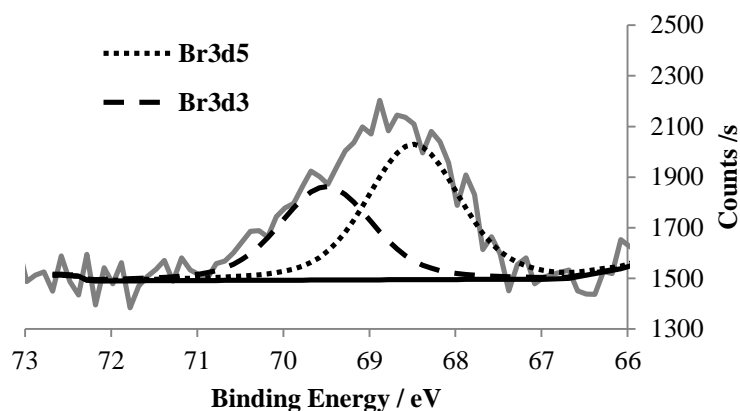


Figure 3.3. Curve-fitted XPS spectrum of Br3d core-line recorded for BIBB functionalised glass slide. The different lines correspond to Br3d5 and Br3d3.

After the attachment of a BIBB initiator, the grafting of the brushes was carried out to obtain PMETAC, PKSPMA, PHEMA and PMMA layers. XPS analysis of the brushes indicated a drastic reduction in the Si2p signal when compared with the percentage of Si2p showed in the clean glass slides (SiOH). This suggested that the glass surface was being covered by a new polymer layer, resulting in the attenuation of the main surface signal (see Table 3.4 and Table 3.5).

Table 3.5. Percentage of Si2p, C1s and O1s atomic composition after the polymerisation of the brushes.

The attenuation of the Si2p percentage after polymer brush formation indicated that the glass layer was covered by a new brush layer.

Polymer brushes	Atomic composition (%)		
	Si2p	C1s	O1s
PHEMA	9.5	57.3	32.7
PMMA	1.6	72.3	26.0
PKSPMA	0.6	61.8	27.2
PMETAC	4.1	65.7	18.9

The XPS survey spectra and C1s high-resolution spectra for the brushes have been highlighted in Figure 3.4, Figure 3.5, Figure 3.6 and Figure 3.7. For PHEMA, the survey spectrum (Figure 3.4A) showed the O1s, C1s and a small peak for Si2p from the main surface. The C1s core-level spectrum (Figure 3.4B) was fitted with three main components at 284.6, 286.5 and 288.9 eV (Figure 3.4) instead of five (Briggs and Seah, 1990) for simplicity. The peak at 284.63 eV was attributed to $\underline{\text{C}}\text{-H}/\underline{\text{C}}\text{-C}$, the 286.5 eV peak to $\underline{\text{C}}\text{-O}$, and the peak at 288.9 eV was assigned to $\text{O}-\underline{\text{C}}=\text{O}$ (Figure 3.4B). The peak assignment has been highlighted in the chemical structure within the figure for clarity (Figure 3.4B).

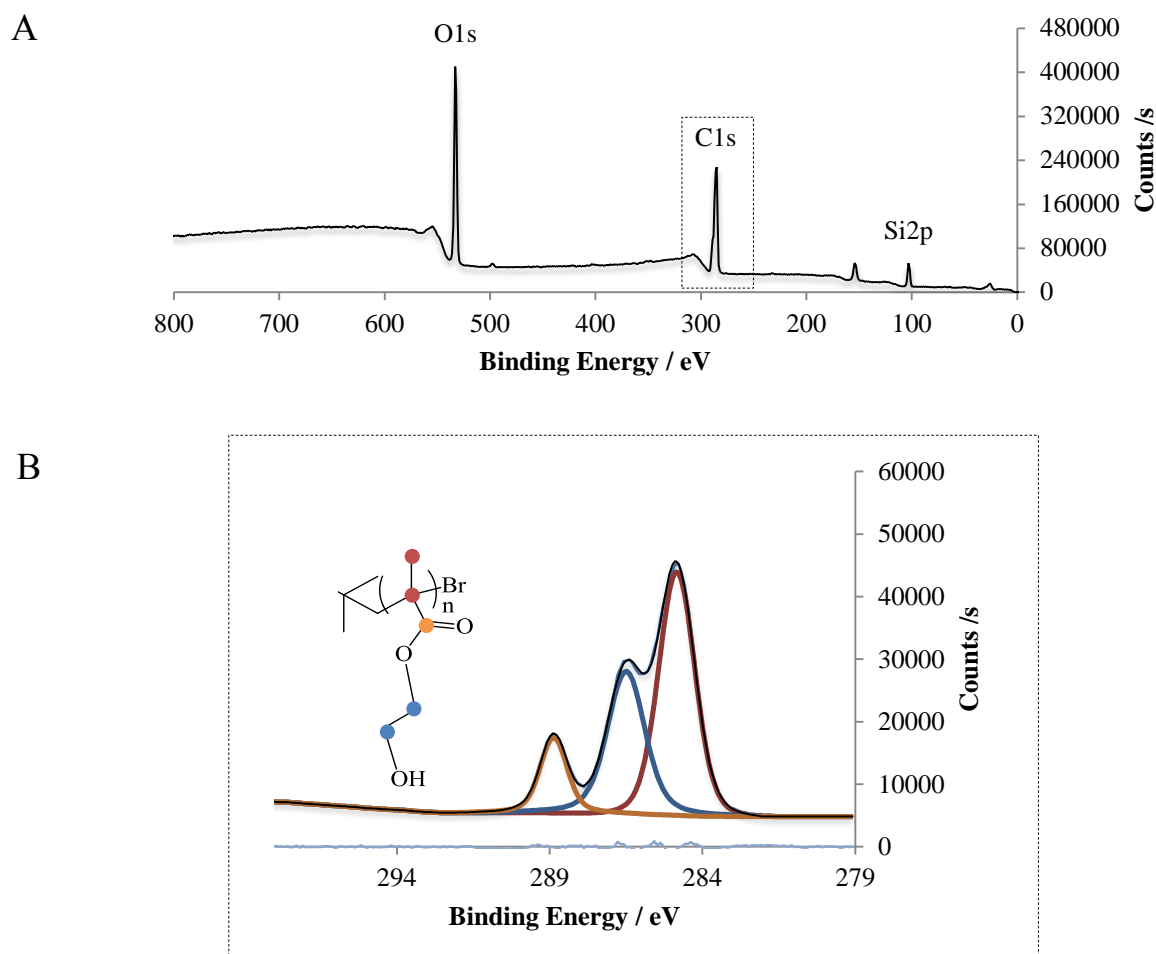


Figure 3.4. XPS analysis of PHEMA brushes. A) Survey spectrum of functionalised PHEMA brushes. B) High-resolution C1s XPS spectrum of functionalised PHEMA brushes. The coloured carbons (red, blue and yellow) represented in the chemical structure correspond to the coloured peaks in the C1s spectra.

For PMMA, XPS spectrum showed the main components presented in its structure (Figure 3.5A). The high resolution spectra of C1s of PMMA (see Figure 3.5B) was fitted to 3 peaks at 284.7, 286.5 and 288.8 eV. The last two corresponded to $\text{C}-\text{O}$ and $\text{O}-\text{C}=\text{O}$ respectively, whilst the peak at 284.7 was attributed to $\text{C}-\text{C}$ and $\text{C}-\text{H}$. The peak assignment has been highlighted in the PMMA chemical structure within the figure for clarity.

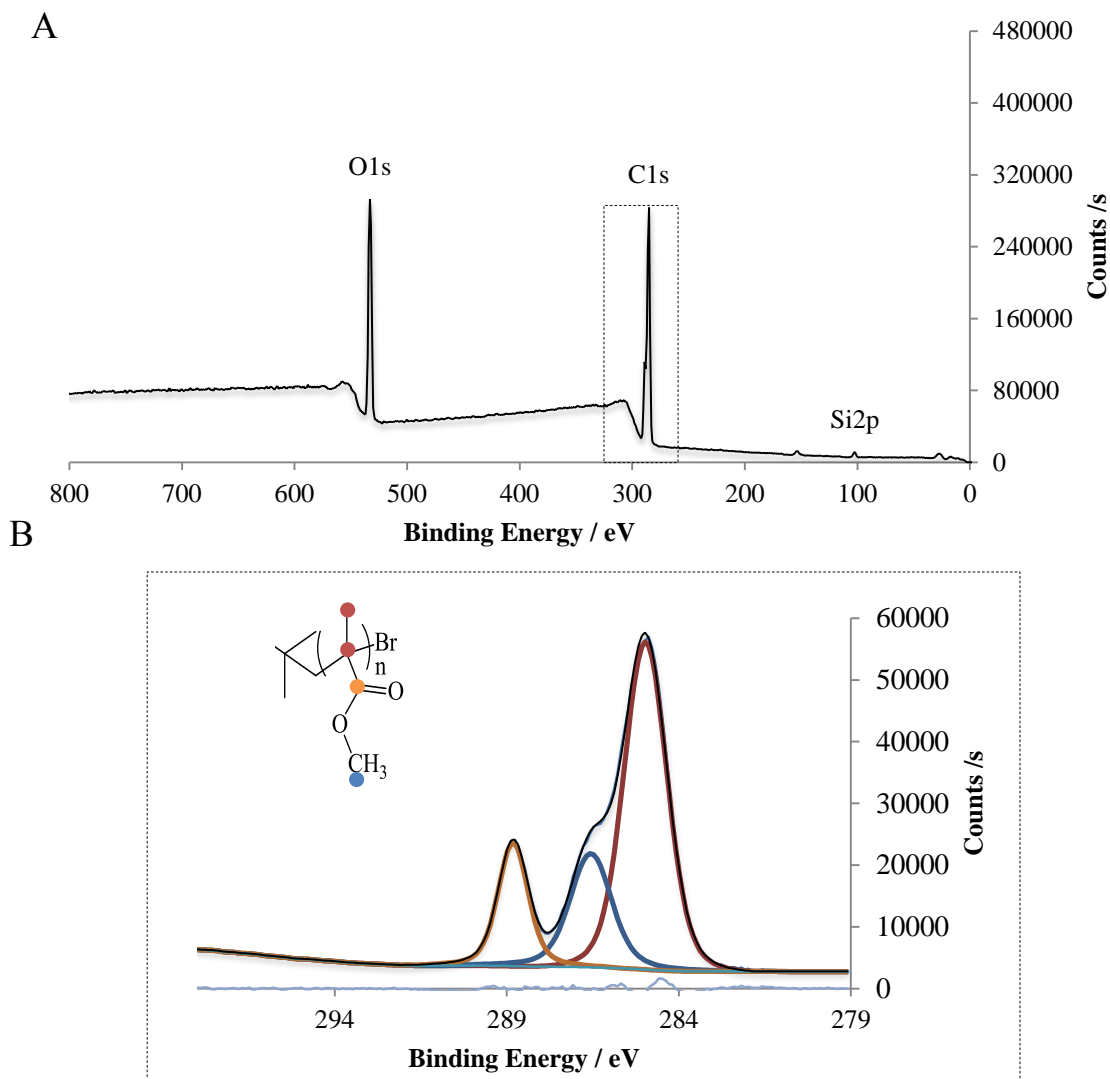


Figure 3.5. XPS analysis of PMMA brushes. A) Survey spectrum of functionalised PMMA brushes. B) High-resolution C1s XPS spectrum of functionalised PMMA brushes. The coloured carbons (red, blue and yellow) represented in the chemical structure correspond to the coloured peaks in the C1s spectra.

In the PMETAC brush, the presence of a prominent peak N1s at 402.4 eV in the XPS spectrum corroborated the successful grafting of the quaternised amine brush (Figure 3.6A). The broad spectrum also showed C12p peaks, thus further confirming the presence of the PMETAC layer. The high resolution C1s spectrum showed the different chemical environment for the carbon, containing peaks at 284.7, 286.2 and 288.8 eV attributable to $\underline{\text{C}}\text{-H/C}$, $\underline{\text{C}}\text{-N/ C-O}$, and $\text{O}=\underline{\text{C}}\text{-O}$ species, respectively (Figure 3.6B).

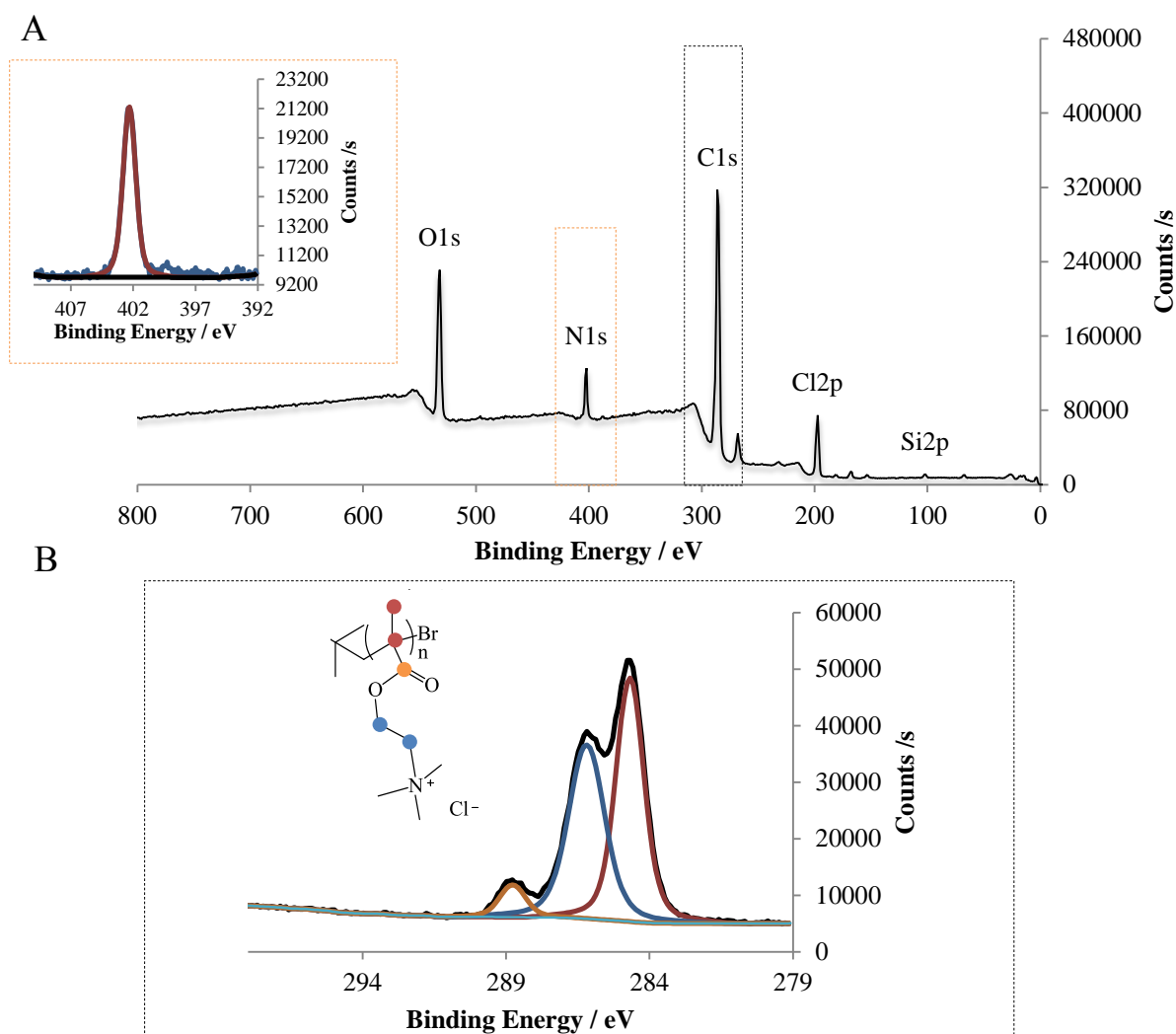


Figure 3.6. XPS analysis of PMETAC brushes. A) Survey spectrum of functionalised PMETAC brushes. The orange dashed square represents the N1s high resolution spectra with the N1s peak ~402 eV. B) High-resolution C1s XPS spectrum of glass functionalised PMETAC brushes. The coloured carbons (red, blue and yellow) represented in the chemical structure correspond to the coloured peaks in the C1s spectra.

For PKSPMA, the broad spectrum showed the strong S2p peaks at 167.5 eV and 168.7 eV, corresponding to the sulphonate groups presented on PKSPMA (see Figure 3.7A). The C1s high resolution spectrum was analysed and fitted with 3 peaks at 284.8, 286.5 and 288.9 eV corresponding to C-C/C-H , O-C and O-C=O respectively (see Figure 3.7B). The additional peaks in the C1s spectrum at 293-294 eV arise from potassium (Figure 3.7B).

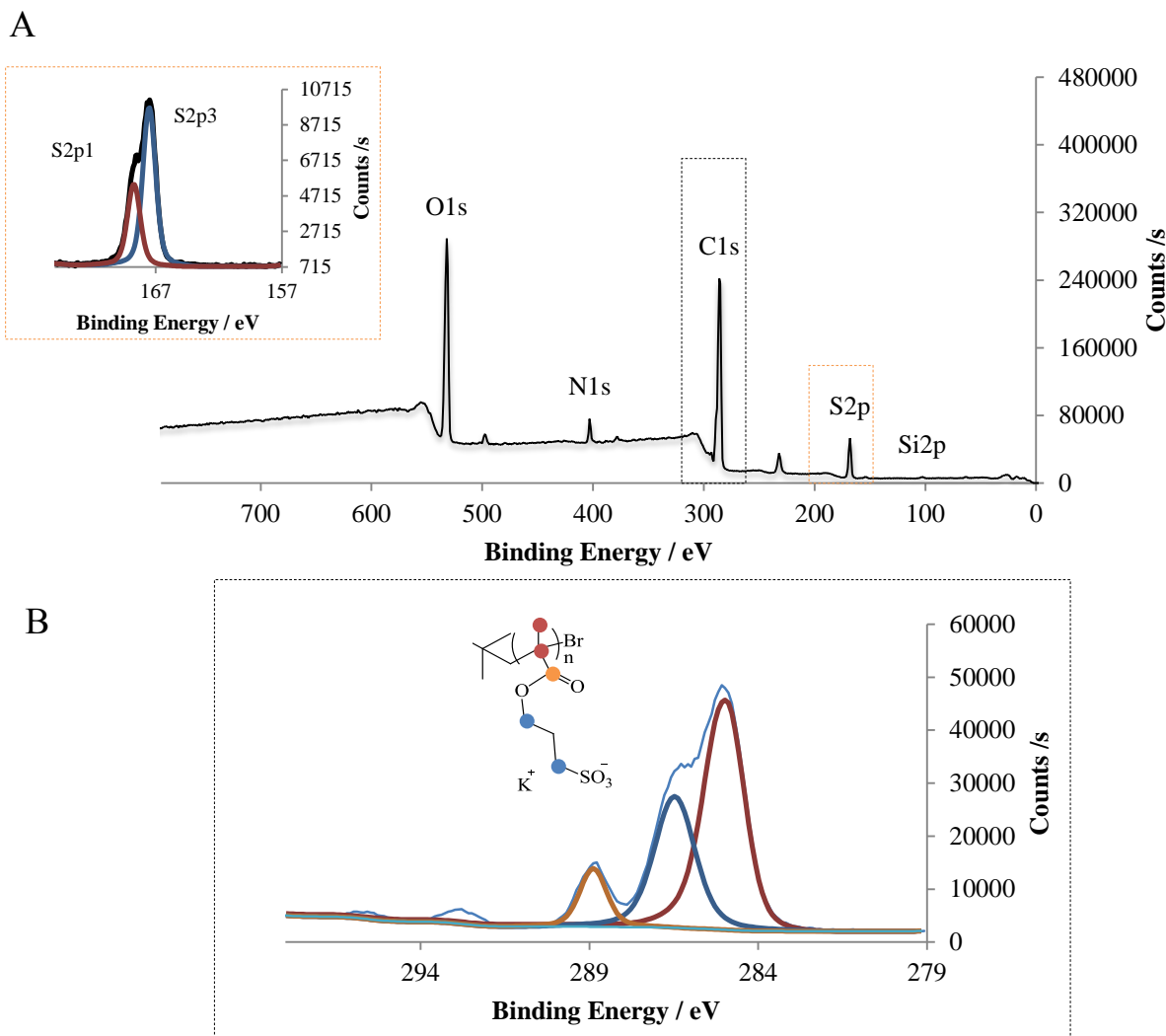


Figure 3.7. XPS analysis of PKSPMA brushes. A) Survey spectrum of functionalised PKSPMA brushes. The S2p core level spectrum of the brush in the orange dashed square was peak fitted to S2p1 and S2p3. B) High-resolution C1s XPS spectrum of functionalised PKSPMA brushes. The coloured carbons (red, blue and yellow) represented in the chemical structure correspond to the coloured peaks in the C1s spectra.

Together, the XPS data suggests that new functional groups are being incorporated on the surface as well as new layers being deposited on the surface by the attenuation of the main surface signal. This analysis provided essential information regarding the chemical composition of the new layers on the surface.

3.3.2 Fourier transform infrared spectroscopy (FTIR)

Surface chemical analysis of the polymer brushes by FTIR was illustrated in Figure 3.8. The spectra showed various peaks found around $3000\text{--}2800\text{ cm}^{-1}$ for PKSPMA (green), PHEMA (red), PMMA (blue) and PMETAC (purple), attributed to the stretching of C-H groups. Furthermore, the characteristic C=O stretching peak of acrylate polymers appeared at $\sim 1780\text{--}1720\text{ cm}^{-1}$ for all the brushes, suggesting that the polymerisation was successful (see Figure 3.8). In PHEMA, peaks $\sim 1080\text{ cm}^{-1}$ and $\sim 1159\text{ cm}^{-1}$ corresponded to C-O-C bands from the hydroxyl group and from the ester, respectively. In PKSPMA samples, strong peaks were found at a similar range of $\sim 1050\text{ cm}^{-1}$ and $\sim 1190\text{ cm}^{-1}$. These corresponded to the asymmetric and symmetric stretching of the S=O bonds. In PMMA, the peak $\sim 1150\text{ cm}^{-1}$ was assigned to the C-O of the ester. In PMETAC, peaks were arising around 1200 cm^{-1} which could also be assigned to the C-O ester groups. The black spectrum corresponded to the non-coated silicon wafer, which main peak corresponds to the Si-O asymmetric stretching mode of the silicon.

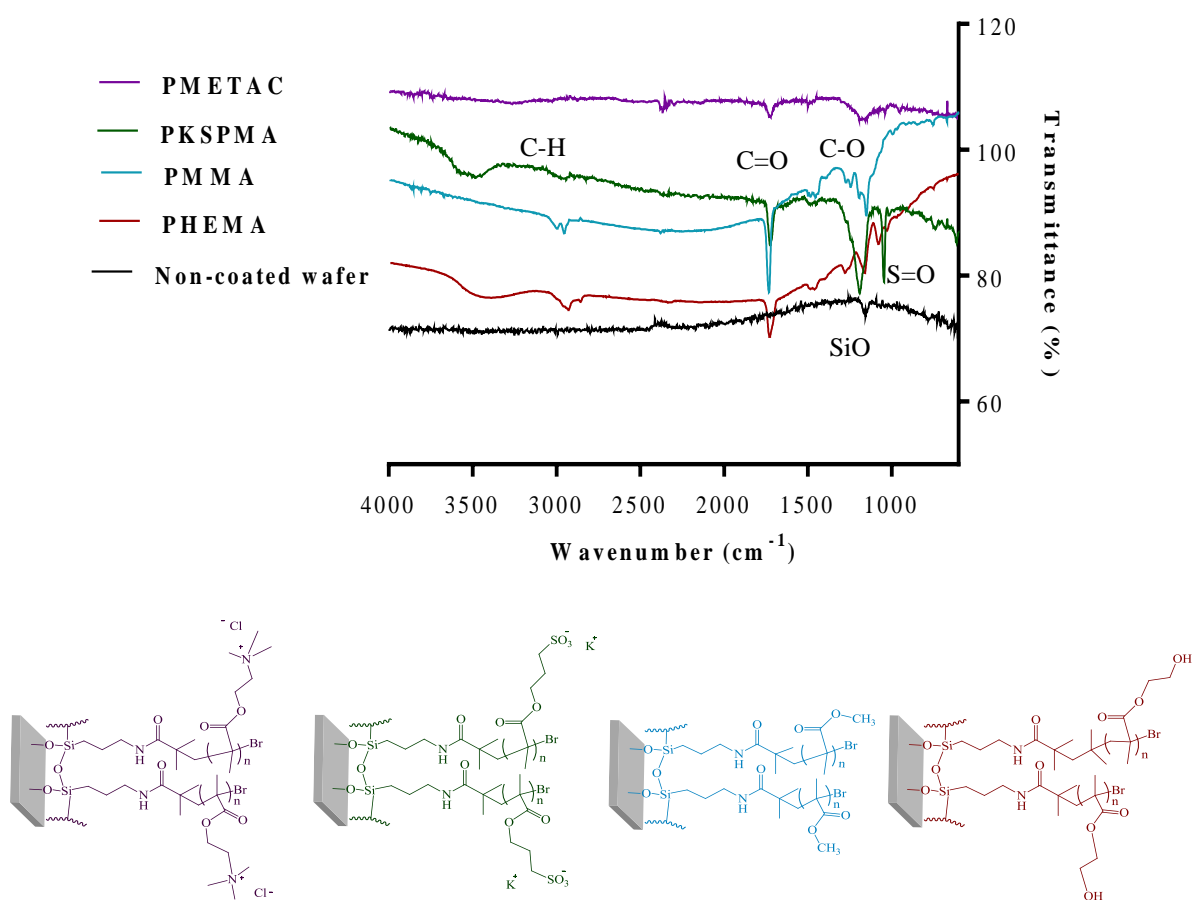


Figure 3.8. FTIR characterisation of polymer brushes. The main functional groups have been highlighted in the spectrum, and the chemical structure of each brush has been illustrated according to the colour of each spectrum. PMETAC, purple; PKSPMA, green; PMMA, blue; PHEMA, red; non-coated wafer, black.

3.3.3 Water contact angle (WCA)

Wettability of the different polymers can determine important changes on the surface chemistry and thus, this parameter was analysed by static water contact angle. The principle of this technique has been described in Chapter 2, Section 2.3.3. Measures performed on the control samples (non-coated glass) showed a moderate hydrophilicity (see Figure 3.9) of $\sim 30\text{--}40^\circ$. Once glass slides were treated with UV/ozone, the new presence of --OH groups led to a reduction in water contact angle, rendering a more hydrophilic surface (Figure 3.9 and Table 3.6).

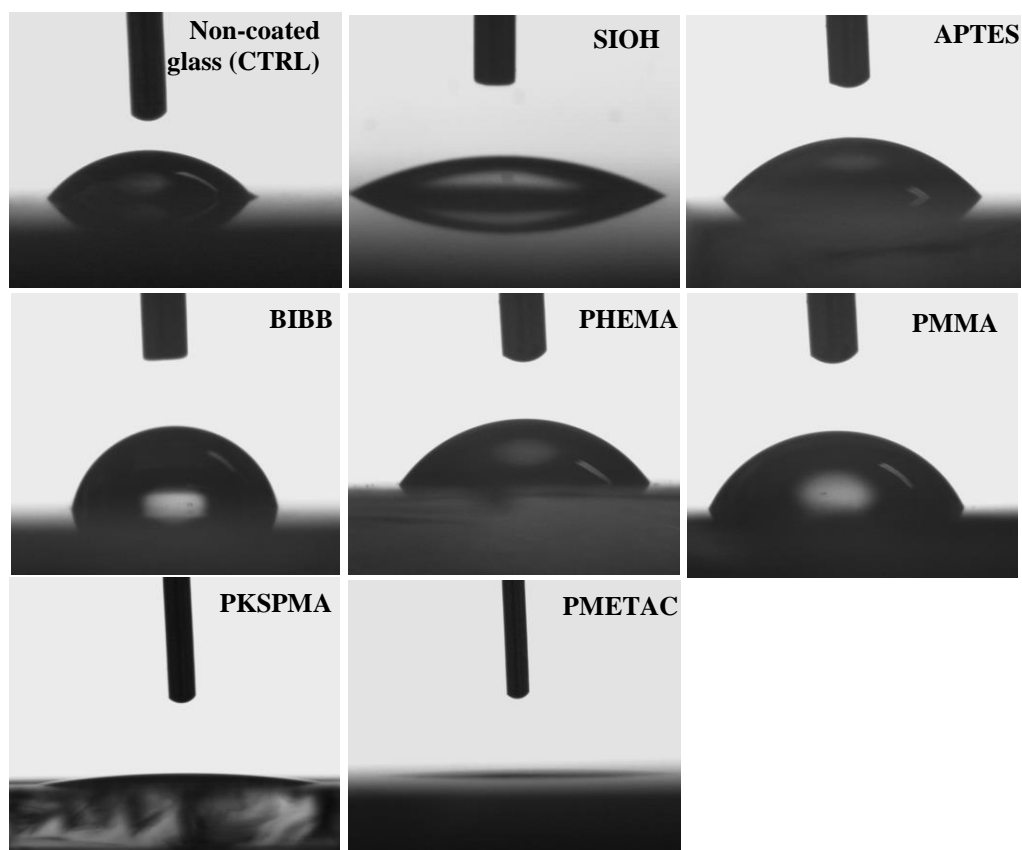


Figure 3.9. Images of water droplets (2 μL) during water contact angle measurements for CTRL (non-coated glass), SIOH, APTES, BIBB, PHEMA, PMMA, PKSPMA and PMETAC. The images were taken immediately after the droplet got in contact with the surface.

The water contact angle is influenced by the nature of the monolayer and therefore, the incorporation of amine and propyl groups on APTES attachment led to an increase in WCA when compared to the clean UV/ozoned glass (SIOH). Thereafter, the attachment of BIBB initiator and PMMA brushes containing moderate hydrophobic end groups ($-\text{Br}$ and $-\text{CH}_3$, respectively) led to an increase in water contact angle indicating the presence of hydrophobic surfaces. In contrast, wet surfaces with a contact angle of $<20^\circ$ were found for PMETAC and PKSPMA brushes. The presence of $-\text{OH}$ groups in PHEMA rendered a moderate wettability on the surface, obtaining similar values to APTES (see Figure 3.9 and Table 3.6).

Table 3.6. Average water contact angle for each surface. The values indicate $n = 4 \pm$ the SD of the mean. Water contact angle could not be assessed when surfaces were completely wet, thus the angle was assumed to be $<5^\circ$ (*).

Surface deposition	Water contact angle ($^\circ$)
Non-coated glass	49.6 ± 14.8
SIOH clean slide	15.1 ± 2.4
APTES	43.4 ± 3.9
BIBB	80 ± 4.8
PHEMA	53.9 ± 8.6
PMMA	81.2 ± 16.6
PKSPMA	17.2 ± 5.8
PMETAC	* <5

3.3.4 Brush thickness

When polymer brushes are synthesised on silicon wafers, one of the first signals that indicate the procedure has been successful is the presence of different colours on the surface formed by optical interference, which is created by the combination of different wavelengths from the interfaces of the film. The colour variation on the silicon wafer was therefore considered as a preliminary indication of successful polymerisation (see Section 9.3 and Figure 3.10) (Pliskin and Conrad, 1964; Henrie *et al.*, 2004). Ellipsometry was then used to obtain a quantitative measure of the thickness of brushes.



Figure 3.10. PKSPMA brushes deposited on silicon wafers. The change of colour on the silicon surface (in this case from grey to blue) can be an indication of the presence of new layers on the surface. The colour chart in the Appendix 9.3 was used as a guidance to estimate the brush thickness. Scale bar= 0.5 cm.

The ellipsometric values of the films showed thick layers for PKSPMA (118.8 ± 9.8 nm, $n= 3$) and PHEMA (98.9 ± 25.6 nm, $n= 3$), albeit the latter with greater variations between repeats. Thinner films were found in the synthesis of PMMA brushes (59.68 ± 9.2 nm, $n= 3$) and PMETAC brushes (33.6 ± 8.6 nm, $n=3$) with the latter being the thinnest of the synthesised brushes.

It is noteworthy that the thickness measures reported are greater than the sampling depth of XPS (see Section 3.3.1), meaning that no signal of silicon should have appeared in the XPS spectrum of the brushes. This could be due to small defects in the coating, exposing the underlying glass slide or wafer and therefore showing a small amount of silicon from the surface.

3.4 Discussion

Parameters involved in cell-substrate interactions such as film architecture (Ren *et al.*, 2013), surface charge (Palyvoda *et al.*, 2008), wettability (Arima and Iwata, 2007), chemical functionality (Faucheux *et al.*, 2004) and protein adsorption (Senaratne *et al.*, 2005) have been known to alter cell response. Thus, the use of chemically modified materials has grown in popularity in the biomaterial field as the modified surfaces can display reproducible and

predictable properties that can be generated under controlled conditions (Dhandayuthapani *et al.*, 2011). Polymer brushes and SAMs have been utilised in this work, as these contain different properties that can be used to promote or even inhibit cellular differentiation, proliferation and survival (Olivier *et al.*, 2012). It is of great importance that the properties of these surfaces are assessed before their use in cell culture, since the generated surfaces can differ significantly depending on the way they are produced or the nature of the layer. In this manner, the differing cell response obtained among the modified surfaces could then be associated with the parameters analysed previously.

3.4.1 Surface preparation

The surface treatment began with a preliminary cleaning step by UV/ozoning the surface. This treatment is a safe and effective method for cleaning surfaces (Lim *et al.*, 2008), where glass slides and silicon wafers acquire a layer of OH groups, activating the surface for the next group to anchor (Barbey *et al.*, 2009). A second step involved the attachment of APTES by vapour deposition. This created Si-O-Si bonds by the hydrolysis of one of the ethoxy groups with the consequent condensation reaction, anchoring this component onto the substrate (Howarter and Youngblood, 2006; Acres *et al.*, 2012). An annealing step was carried out for the formation of Si-O-Si bonds between the APTES neighbours chains to promote a dense film (Scallan, 2007; Pasternack *et al.*, 2008; Zhu, 2012). A third step involved the use of α -bromo isobutyryl bromide (BIBB) to create the initiator layer for the attachment of PKSPMA, PHEMA, PMMA and PMETAC brushes by SI-ATRP and SI-ARGET ATRP.

3.4.2 Surface characterisation

Various techniques have been utilised in this work to assess the surface characteristics of the coatings. XPS data in Section 3.3.1 showed the different chemical surface composition for each surface. In APTES, the 1.6 % N1s content indicated the presence of this coating on the surface, with a ratio N1s:Si2p of 0.06, which is in good agreement with the 0.07 N1s:Si2p value found in the literature for APTES deposited by chemical vapour deposition (Zhang *et al.*, 2010). The presence of a new Br3d peak when BIBB was deposited showed Br3d5/2 and Br3d3/2 with a ratio of 1.4:1, respectively, corresponding to the ratio found in the literature

(1.4:1) and thus suggesting the presence of the successful initiator on the surface (Alswieleh *et al.*, 2014). The content of N1s in this layer was bigger than the bromine peak. It has been suggested that this can occur due to the instability of the Br-C bond, which leads to a decrease in Br3d signals (Zhang *et al.*, 2006; Wasserman *et al.*, 1989; Wu *et al.*, 2015). In relation to the brushes, PKSPMA showed strong peaks of S2p3 and S2p1 corresponding to the sulphonate groups (Ramstedt *et al.*, 2007; Tan *et al.*, 2013). Likewise, PMETAC showed the characteristic N1s peak from the quaternary ammonium cation shown in the literature (Yameen, 2008; Zhou *et al.*, 2013; Tan *et al.*, 2013), altogether indicating the presence of both coatings. There was an unexpected nitrogen peak present on the PKSPMA spectra that was also observed in the work carried out by Ramstedt *et al.*, (2007). The authors suggested that the presence of N1s could be due to traces of bpy trapped within the brush from the SI-ATRP reaction. For PHEMA and PMMA, the XPS analysis of the C1s signal revealed the presence of different chemical environments for carbon, which was expected for these substrates. In addition, the theoretical [O]:[C] ratio of the homopolymers MMA (0.4) and HEMA (0.5) is in agreement with the PMMA and PHEMA [O]:[C] ratio found in this report (0.36 and 0.57 respectively) (Chen *et al.*, 2009).

FTIR was used to determine the chemical composition of the brushes. The main C=O peak observed in all the polymer brushes gave a further indication of the chemical environment present in these brushes along with the XPS results. This data aligns with previous reports assessing the composition of such brushes (Anderson, 1964; Ramstedt *et al.*, 2007; Bach *et al.*, 2012; Zhu, 2012; Borozenko *et al.*, 2014).

Brush thickness was determined by ellipsometry and showed polymer layers containing ≥ 30 nm layers deposited on the surface. This did not correspond with the results obtained in XPS for the brushes, as such thick layers should have covered the small Si2p peaks observed in the spectrum of the brushes. This could be due to defects on the surface either during the attachment (SAMs are known to have limited robustness, and perhaps defects on the initiator layer led to further defects on the polymer brush) or simply by manual handling (e.g. using tweezers), forming scratches and thus defects on the surface (Ma *et al.*, 2004). It is important to consider that ellipsometric measures were performed on silicon wafers whilst XPS analysis was performed on glass slides. Although the procedure was performed in exactly the same

manner, the polished silicon wafer would likely lead to less surface defects than glass. Due to this, perhaps glass slides were more susceptible to defects on the surface, leading to imperfections on the coating and the results in the XPS data.

In terms of wettability, an increase in water contact angle after the deposition of APTES was an indication of a successful coating. The presence of carbon chains along with the amine groups led to an increase in the water contact angle up to $\sim 45^\circ$. This result is in agreement with the literature (Kim *et al.*, 2009; Acres *et al.*, 2012), where the APTES WCA has been reported to have values between $45\text{--}50^\circ$. Tailoring the initiator onto APTES introduced the presence of hydrophobic groups resulting on a surface towards hydrophobicity with a WCA $70\text{--}80^\circ$, consistent with previous literature (Li *et al.*, 2011). Likewise, PMMA had a water contact angle $\sim 70^\circ$, possibly due to the hydrophobic $-\text{CH}_3$ end groups of the polymer chain (Kobayashi *et al.*, 2012). In the literature, water contact angle values in PMMA are $\sim 68^\circ\text{--}75^\circ$ (Ma *et al.*, 2007; Luzinov and Minko, 2012). The different values could be due to the differences in brush synthesis across the studies, which resulted in different brush thicknesses and ultimately induced variations in the surface wettability (Wei and Ngai, 2012). Contrary to PMMA, very hydrophilic surfaces such as PKSPMA and PMETAC showed a water contact angle $\sim 17^\circ$ and $< 5^\circ$. The wetting properties of these polyelectrolyte brushes depend greatly on the ions and their interactions. Effects such as the presence of the ions and charge repulsion of the chains can contribute to the wet properties on these polyelectrolyte films (Azzaroni, 2012).

As described above, every SAM and polymer brush is provided with a vast range of specific characteristics and therefore, the need to examine such surfaces to provide an insight about their characteristics is essential to avoid an unexpected cell response (Tong and Shoichet, 2001; Jans *et al.*, 2009). This will allow the accurate responsiveness of neuronal cells in the following chapters, aiding neuronal guidance and improving current *in vitro* neural systems.

3.5 Chapter summary

This chapter has highlighted the formation and characterisation of the modified surfaces by using polymer thin films, such as polymer brushes and SAMs. The success of film deposition

had to be assessed so these coatings could be further used in this thesis for cell testing. To this end, the differing coatings were analysed by XPS, FTIR, WCA and ellipsometry. This chapter has shown that these properties differ greatly amongst the generated surfaces and therefore, each modified surface should be examined in culture as they are likely to trigger different neuronal response. The differing behaviour provided by these surfaces could be key when using them as a potential tool to generate neuronal guidance.

4 Neurons cultured on chemically modified surfaces

4.1 Introduction

Cell behaviours such as adhesion, proliferation and differentiation are dependent on the multiple chemical and physical cues present in their microenvironment (Gomez *et al.*, 2007; Teixeira *et al.*, 2009; Belkaid *et al.*, 2013) (Figure 4.1). For neurons, the surrounding cues are particularly important, as such signals are sensed by the growth cone, encouraging axonal outgrowth and thus aiding neuronal development and regeneration (Gomez *et al.*, 2007; Yamamoto *et al.*, 2012). In light of this, advances in the biomaterial field have led the development of surface modification methods for cell culture approaches, where surface properties (physical, chemical, etc.) can be finely modified to enhance differing cell responses. For instance, Brunetti *et al.* (2010) investigated the response of SH-SY5Y's on nanorough surfaces, suggesting a decrease in cell adhesion when surface roughness increased, highlighting the importance of surface changes on cell response. In another study, neurospheres cultured on chemically modified substrates containing $-NH_2$, $-COOH$ and $-SH$ groups were shown to extend long protrusions and interact with the neighbouring neurospheres. This suggests that surface chemistry influenced the communication between neurospheres (Ren *et al.*, 2009). As such, modifying surfaces to alter neuronal functionality within *in vitro* systems could contribute to obtain a greater understanding of the functionality underpinning neuronal growth and regeneration (Gordon *et al.*, 2013).

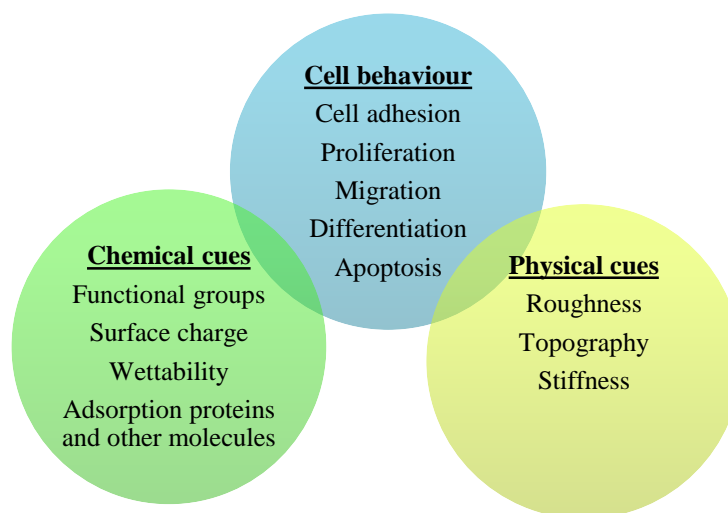


Figure 4.1. Main factors affecting cell behaviour. In isolation or combined, these characteristics have an impact on cell response.

Strategies for chemical surface modification allow the incorporation or modification of various chemical surface cues (by grafting methods, plasma or chemical vapour deposition, among others) (Govindarajan and Shandas, 2014) to induce cell response, and ultimately contributing to specific cell behaviours and function. Polymer brushes and self-assembled monolayers (SAMs) are commonly used as a robust technique for surface modification (Palyvoda *et al.*, 2008; Raynor *et al.*, 2009; Moroni, Gunnewiek and Benetti, 2014), as they can be manipulated to display a wide range of functionalities that can be reproduced in a controllable manner (Zhao *et al.*, 2011a; Zhou *et al.*, 2013; Kuzmyn *et al.*, 2014) (Chapter 1, Section 1.3 and Chapter 3, Section 3.1). Furthermore, SAMs and polymer brushes have been successfully utilised in neuronal cell culture (see Chapter 1, Section 1.3.3). Palyvoda *et al.* (2008) found an improvement in neuronal adhesion when amino-terminated alkanethiol SAMs were used. Likewise, methacrylate polymer brushes containing tethered neurotransmitter acetylcholine functionalities were used to control neuronal growth by combination of these brushes with microfabrication (Zhou *et al.*, 2013). When considering the results from these studies, as well as others in the literature, neuronal adhesion is frequently facilitated by amino-containing surfaces (Khan and Newaz, 2010). In addition, changes in the wettability of the surface also contributes to neuronal behaviour, suggesting that hydrophilic surfaces are prone to neuronal cell adhesion (Lee *et al.*, 2003). Although visible trends can be extracted from previous studies, every SAM and polymer brush has a vast range of specific characteristics that can differ from the technique used or the parameters used during synthesis. In addition, the disparity in the response between different cell types also contributes to the need to examine such modified surfaces in cell culture to avoid potential unexpected cell responses (Tong and Shoichet, 2001; Jans *et al.*, 2009).

4.1.1 SH-SY5Y cells as a neuronal model on chemical modified substrates

Primary and neuronal cell lines have been used on modified surfaces (see Table 1.1. for a selection of studies regarding the modification of surface properties and the consequent effect on neuronal cells) (Palyvoda *et al.*, 2008; Dong *et al.*, 2010; Zhou *et al.*, 2013; Buttiglione *et al.*, 2007; R  he *et al.*, 1999; Ruardij *et al.*, 2000). Neuronal cell lines are often utilised in this area, as they provide indefinite cell numbers, reduced variability between cultures and are simpler to implement in culture conditions (Kovalevich and Langford, 2013). Thus, all the

inconveniences related with primary cultures such as the high cost, complex surgeries and ethical issues are avoided (Podrygajlo, 2009). SH-SY5Y is a human neuroblastoma cell line that has been extensively used as a neuronal *in vitro* model (Klein *et al.*, 1999; Xie *et al.*, 2010). The parental cell line contained at least two morphologically and biochemically distinct phenotypes: neuroblast-like (N-type) and epithelial-like cells (S-type) (Ross *et al.*, 1983; Encinas *et al.*, 2000). SH-SY5Y's were derived from a neuroblastic subclone, thus the population can be considered as neuroblast-like cells (Encinas *et al.*, 2000). The development of these cells into a more mature phenotype can be achieved by using differentiating agents such as *all trans* retinoic acid (ATRA) (Encinas *et al.*, 2000; Clagett-Dame, McNeill and Muley, 2006). The use of ATRA allows the expression of mature neuronal markers and a morphology with long and extended neurites, similar to primary cultures (Encinas *et al.*, 2000; Clagett-Dame *et al.*, 2006).

SH-SY5Y's have been reported to alter levels of adhesion and differentiation when cultured on modified surfaces however, a considerable percentage of these studies have only been reported on physical modifications. Nevertheless, in a study based on chemical modification by Buttiglione *et al.* (2007), SH-SY5Y's were cultured in plasma modified surfaces containing carboxylic and nitrogen groups. The presence of carboxylic groups influenced the expression of a differentiation marker (NF-H), whereas amine-surfaces aided cell adhesion. This study supported the tendency regarding the use of amine coatings for neuronal cell adhesion however, only two chemical functionalities were examined in this study and certain properties were very similar among them (i.e. similar wettability). Furthermore, the type of technique used to modify the surface could lead to changes in the structure of the film and thus, changes in cell response could occur on the same type of coating prepared by different methodologies (Ren *et al.*, 2013).

Chemically functionalised surfaces allow the possibility to specifically design biological patterns of different size and geometry, which could be used to study more closely cell-cell communication, organogenesis and cellular alignment. Particularly for neuronal cells, their guidance in these patterns could potentially contribute to the study of the wiring network *in vitro* in a more simplistic and controllable manner (Senaratne *et al.*, 2005; Lee *et al.*, 2007).

4.1.2 Objectives of the chapter

This chapter aimed to use the characterised modified surfaces described in Chapter 3 to examine the growth and development of SH-SY5Y's. To this end, the viability, proliferation rate, metabolic activity, mRNA expression of MAPT and level of morphological differentiation of SH-SY5Y's for the modified surfaces, were analysed. The outcome of these experiments would allow for the identification of the surfaces that promote or inhibit neuronal cell response for their consequent use on cell patterning. Thus, the possibility to combine various coatings for creating a cell-attractive/repulsive pattern for neuronal guidance could be achieved (Senaratne *et al.*, 2005; Lee *et al.*, 2007).

4.2 Methods

4.2.1 General procedure for LIVE/DEAD® staining of mammalian cells

The principle and procedure for LIVE/DEAD® staining has been described in Chapter 2, Section 2.5.1. Dye optimisation and consequent results have been included in the Appendix 9.1.

4.2.2 Assessment of metabolic activity: General procedure for alamarBlue®

The principle and the procedure for alamarBlue® staining has been described in Chapter 2, Section 2.5.3. alamarBlue® optimisation and consequent results have been highlighted in the Appendix 9.2.

4.2.3 Proliferation assay: Quant-iT™ PicoGreen® dsDNA assay

The principle, the procedure, and the standard curve for DNA quantification for this assay have been described in Chapter 2, Section 2.5.6.

4.2.4 Morphological and biochemical assessment of neuronal differentiation

4.2.4.1 Neurite length general procedure

For differentiation experiments, 5000 cells/cm² were seeded onto the chemically modified surfaces and cultured in GM until 50% confluency was reached. Thereafter, cells were treated with DM (consisting of GM with 10 µM of *all-trans* retinoic acid (ATRA)) for 5 days.

Neurite length was measured for each condition before DM was added (preATRA time point) and then after 1, 3 and 5 days in DM (labelled as DM1, DM3 and DM5). Image J software was used to measure the length of individual neurites by tracing a “freehand” line across the neurite, as illustrated in Figure 2.22. GM and DM were changed every 2 days.

4.2.4.2 RT-qPCR

RT-qPCR analysis was performed for the mRNA expression of MAPT and RPII β . The sequences for these primers, the protocol and the principle of RT-qPCR are outlined within the methods (Sections 2.5.7 and 2.5.7.4).

4.2.4.2.1 MAPT gene expression

For gene expression experiments, 5000 cells/cm² were seeded on APTES, BIBB and non-coated glass. SH-SH5Y's were cultured in GM until 50% confluency was reached, and then treated with DM for 3 days. RNA was extracted using TRIzol® as described in Section 2.5.7.2 and quantified spectrophotometrically using a NanoDrop 2000 (Thermo Scientific, UK). Data was analysed using the 2^{- $\Delta\Delta C_T$} method (Livak and Schmittgen, 2001) described in Chapter 2, Section 2.5.7.3. Data was normalised to RPII β and relative to a single APTES sample.

4.2.5 Effect of PHEMA brush thicknesses on cell behaviour

Due to the large variability in the cell response found on PHEMA surfaces, an experiment to assess the effect of PHEMA film thickness on SH-SY5Y's was conducted. PHEMA brushes were prepared as described in Section 2.1.4 by using various polymerisation times (1, 3, 6 and 24 hours), given that the thickness of the brush was proportional to the time of the sample exposed to the polymer solution. For cell experimentation, 5000 cells/cm² were seeded on these samples, cultured in GM for 5 days and stained according to the Section 2.5.9.

4.2.6 Statistical analyses

For all the data analysis, GraphPad commercial software 6.0 was utilised for statistical analysis. Differences were considered statistically significant when $p \leq 0.05$.

A one-way ANOVA was used to analyse statistical differences in cell viability data, with a Bonferroni post-hoc test to compare the main surface effects on neuronal behaviour.

A repeated measures two-way ANOVA was used to analyse the proliferation and metabolic activity determined by Quant-iT™ PicoGreen® and alamarBlue®, respectively. A Bonferroni post-hoc test was used for multiple comparison tests to determine differences among the different surfaces over time.

For neurite length data, a repeated measures two-way ANOVA with a Bonferroni post-hoc test was used for multiple comparisons, to determine differences in neurite length among the different surfaces over time. Differences in MAPT gene expression between control, APTES and BIBB were analysed using a one-way ANOVA. Gene expression of BIBB and APTES was determined by an unpaired t-test. Lastly, Pearson linear regression (two tailed) was used to analyse the relationship in neuronal behaviour (neurite length) as a function of water contact angle.

4.3 Results

4.3.1 Effect of chemical surface modifications on cellular viability

Cellular viability was examined on chemically modified surfaces (as generated in Chapter 3) at days 1, 3, 5 and 7 (see Figure 4.2) with the optimised parameters found in the Appendix 9.1 (see Figure 9.1). Whilst cell viability was high on the majority of chemical surfaces through all the culture period, neurons cultured on PMETAC showed a reduced viability across all the time points (Figure 4.3). The results suggested that PMETAC coating may have a degree of toxicity, an effect that became more pronounced over time ($p < 0.001$ after 3 days in culture, Figure 4.3). Although cell viability was similar for the majority of the coatings with the exception of PMETAC, the amount of cells that adhered to these substrates appeared different (see Figure 4.5).

In the first day of culture, all the coatings had a relatively similar amount of cells adhered on the surface, presumably reflecting the time it takes for cells to attach as well as proliferate. However, in the following time points, SH-SY5Y's were able to grow and proliferate on all

coatings except for PMETAC and PKSPMA. For the latter, cell viability percentage seemed as high as in the other coatings however, SH-SY5Y's had not predilection for this surface, avoiding attachment. Cell number on PKSPMA and PMETAC substrates appeared continuously low throughout the course of the experiment, whilst APTES, BIBB, SIOH, PMMA and control substrate (non-coated glass) seemed to proliferate over time, albeit with non-significant differences between the substrates ($p > 0.05$) except for APTES at day 3 ($p < 0.05$, see Figure 4.5). For PHEMA samples, cell responses on these cells were highly variable, from several adherent cells on the surface to a completely lack of them in some cases.

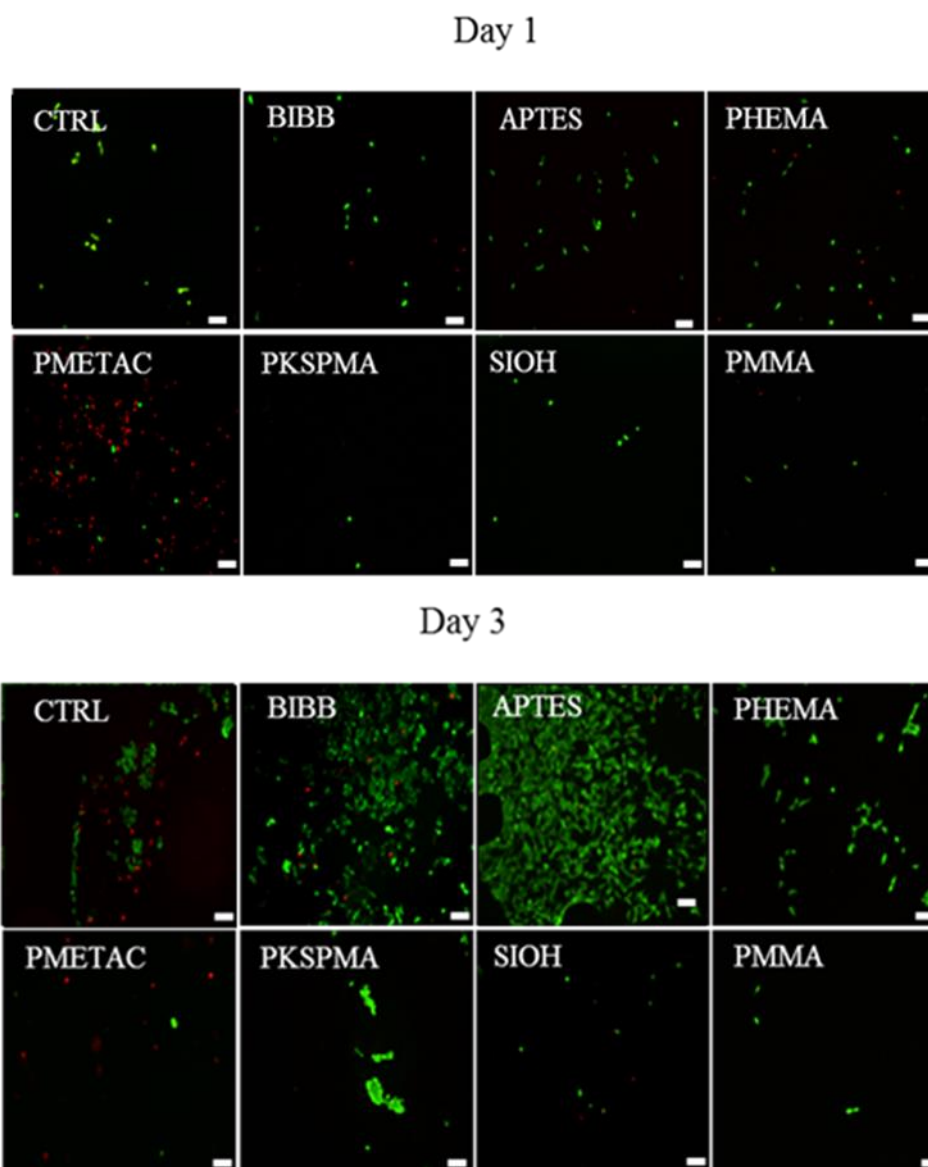


Figure 4.2. Representative fluorescence micrographs LIVE/DEAD® staining of SH-SY5Y after 1 and 3 days cultured on the different chemical surfaces. Calcein AM for live cells (green) and ethidium homodimer (EthD-1) for dead cells (red). CTRL is non-coated glass. Scale bar= 100 μ m.

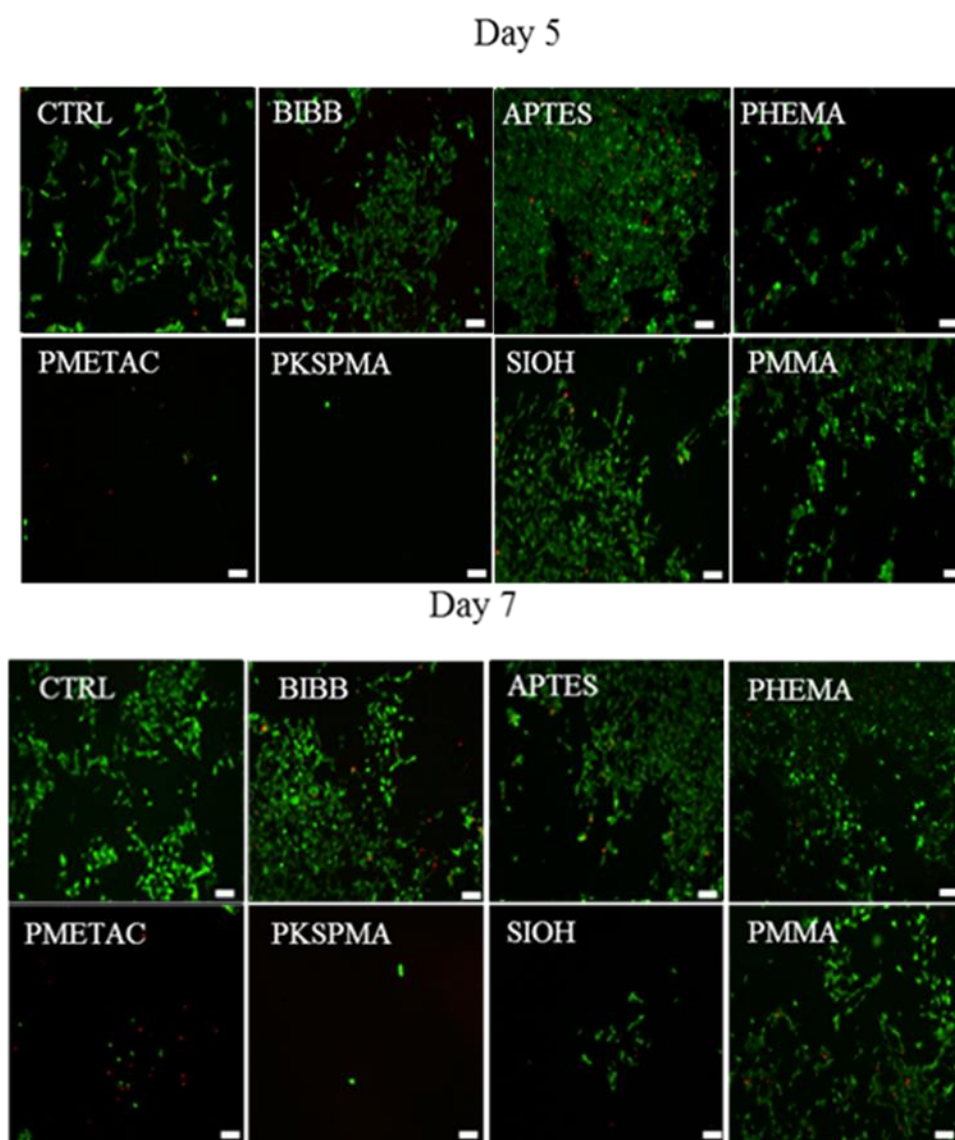


Figure 4.3. Representative fluorescence micrographs LIVE/DEAD® staining of SH-SY5Y after 5 and 7 days cultured on the different chemical surfaces. Calcein AM for live cells (green) and ethidium homodimer (EthD-1) for dead cells (red). CTRL is non-coated glass. Scale bar= 100 μm..

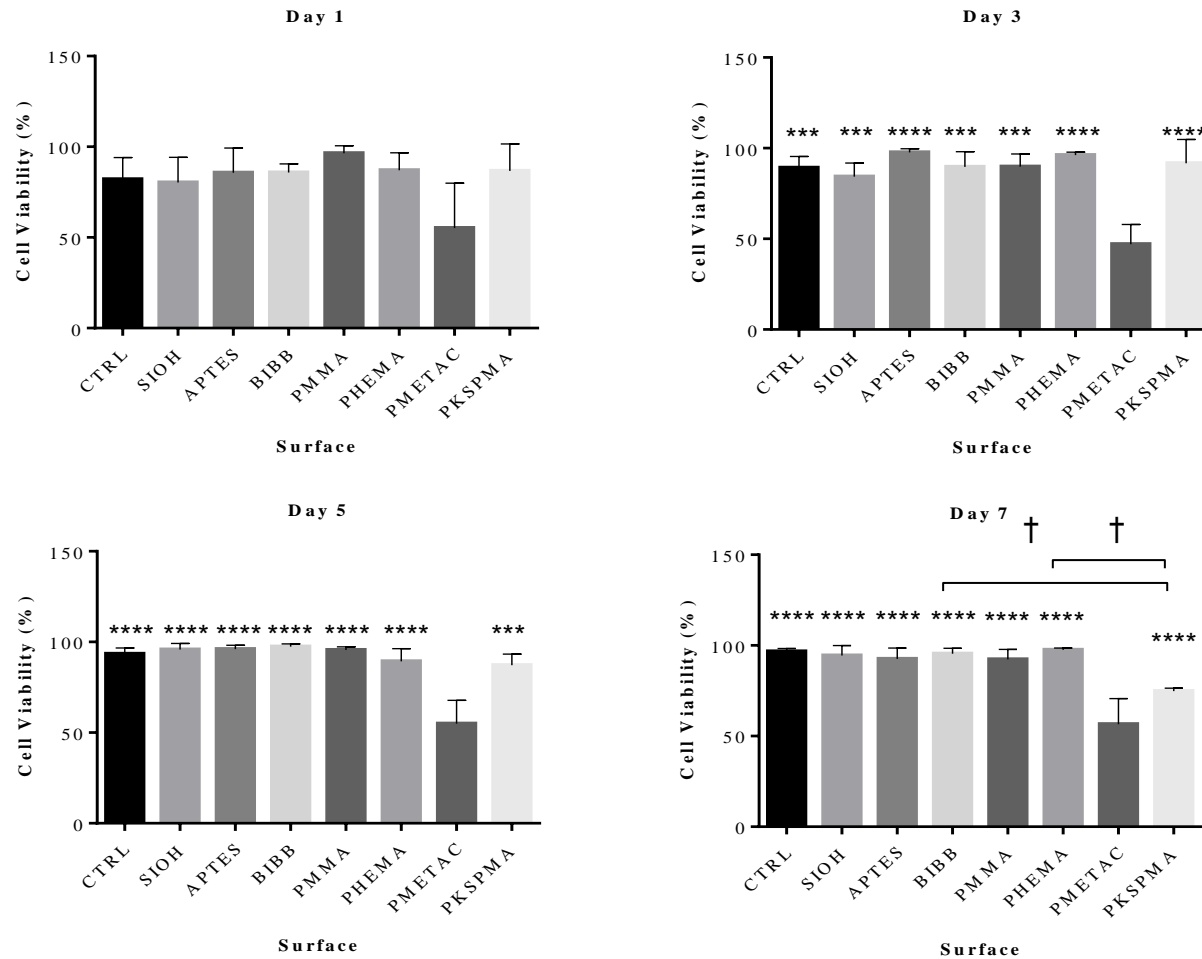


Figure 4.4. SH-SY5Y's cell viability (%) on the different chemical coatings at days 1, 3, 5 and 7. High cell viability was presented in all the coatings throughout the time course when compared to non-coated glass (CTRL) except for PMETAC. Statistical analyses were assessed by one-way ANOVA, followed by a Bonferroni post-hoc test. Data are presented as the mean, with error bars as SD. Asterisks indicate statistical differences between the substrates vs. PMETAC, whilst the crosses indicate differences vs. PKSPMA (* $p < 0.05$, ** $p < 0.01$, *** $p < 0.005$, **** $p < 0.001$, $n = 3$).

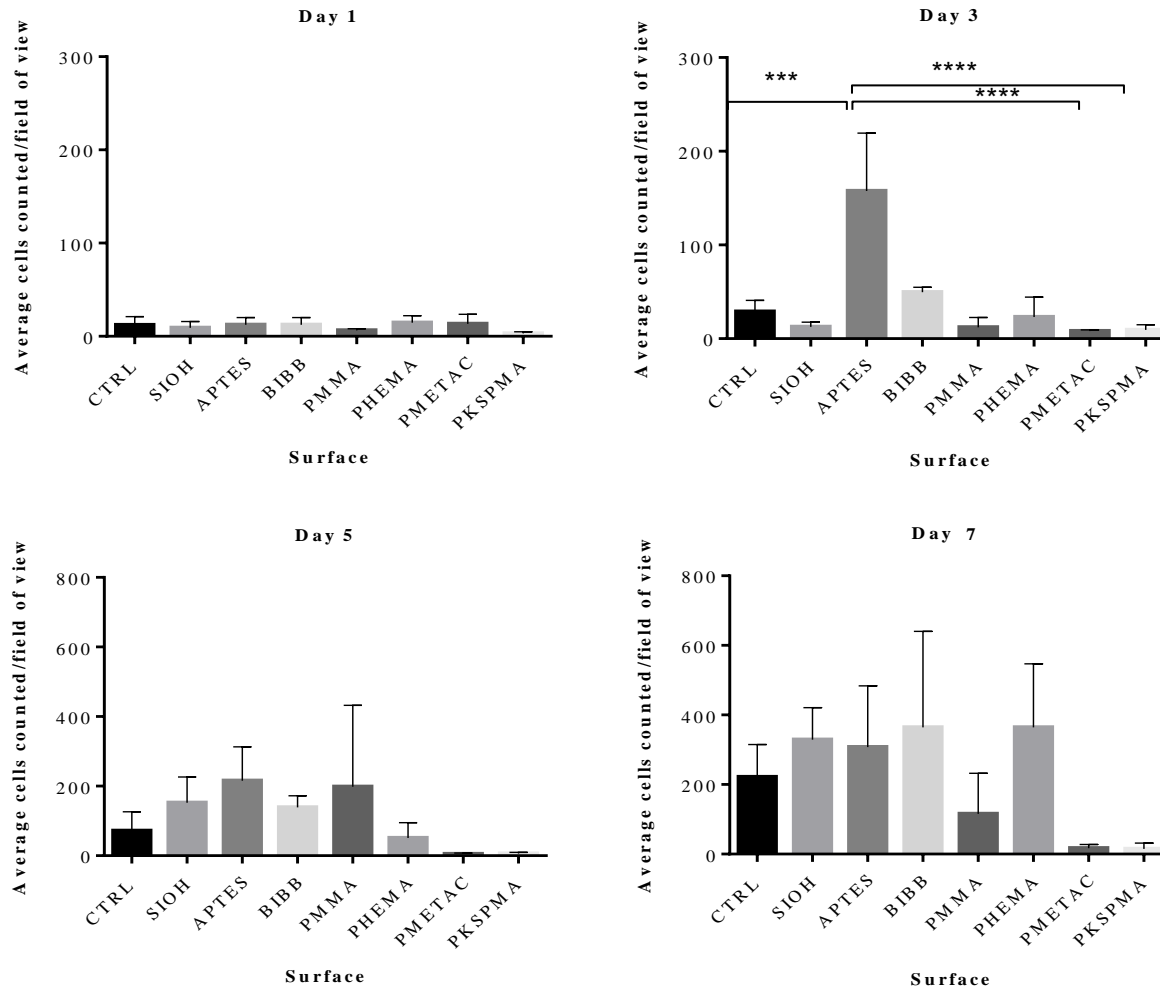


Figure 4.5. Average number of SH-SY5Y's counted per field of view on the different chemical surfaces at days 1, 3, 5 and 7. The figures illustrate that although cell viability could be high on the substrates, the number of cells adhered was different. Statistical analyses were assessed by one-way ANOVA followed by a Bonferroni post-hoc test. Data are presented as the mean, with error bars as SD. Asterisks indicate statistical differences between the substrates vs. PMETAC (*p<0.05, **p<0.01, *** p<0.005, **** p<0.001, n= 3).

4.4 Cellular metabolism and proliferation

To further explore the effect of the coatings on cell behaviour, the quantification of metabolic activity (AlamarBlue®) and cellular proliferation (PicoGreen®) on each of the surfaces was investigated.

4.4.1 Assessment of metabolic activity on chemically modified surfaces

The different chemically modified substrates were examined using AlamarBlue® at day 1, 3, 5 and 7, according to the optimisation data obtained in Appendix 9.2. After 24 hours in culture, the fluorescence intensity was similar among the coatings, with the exception for PKSPMA and PMETAC, which showed a lower fluorescence intensity (although non-significant) suggesting that cellular activity in these coatings was reduced ($p > 0.05$, see Figure 4.7). Phase contrast microscopy (see Figure 4.6) illustrated a similar area covered by cells in CTRL (non-coated glass), APTES, BIBB and to a lesser extent in SIOH, PMMA and PHEMA. In contrast, detached cells and clumps were observed in PKSPMA and PMETAC samples indicating cells had not attached onto these surfaces. After 72 hours, APTES fluorescent intensity showed the most profound increase among all of the coatings, followed by BIBB and non-coated glass, thus suggesting a higher metabolic activity compared to the other modified surfaces (see Figure 4.7, $p > 0.05$). At day 5, the fluorescence of non-coated glass and BIBB increased, suggesting that metabolic activity continued to rise. A plateau in the fluorescence of APTES samples was observed from day 3-5, a phenomenon that could be related to a spontaneous differentiation of these cells on the APTES surface, due to a reduction in proliferation because of contact inhibition. The metabolic activity of SH-SY5Y's cultured on PMMA and SIOH samples did not increase significantly during the course of the experiment. Likewise, a low metabolic activity was observed on PHEMA samples, where only a slight increase in fluorescence was observed at day 7. A noticeable decrease in fluorescence from cells cultured on PKSPMA and PMETAC surfaces was shown at day 7, indicating that there were very few cells on these coatings. Overall, APTES, BIBB and non-coated glass increased in fluorescence intensity at the end of the culture period, whilst PMMA, SIOH, PHEMA, PKSPMA and PMETAC fluorescence levels remained significantly lower ($p < 0.05$, see Figure 4.7).

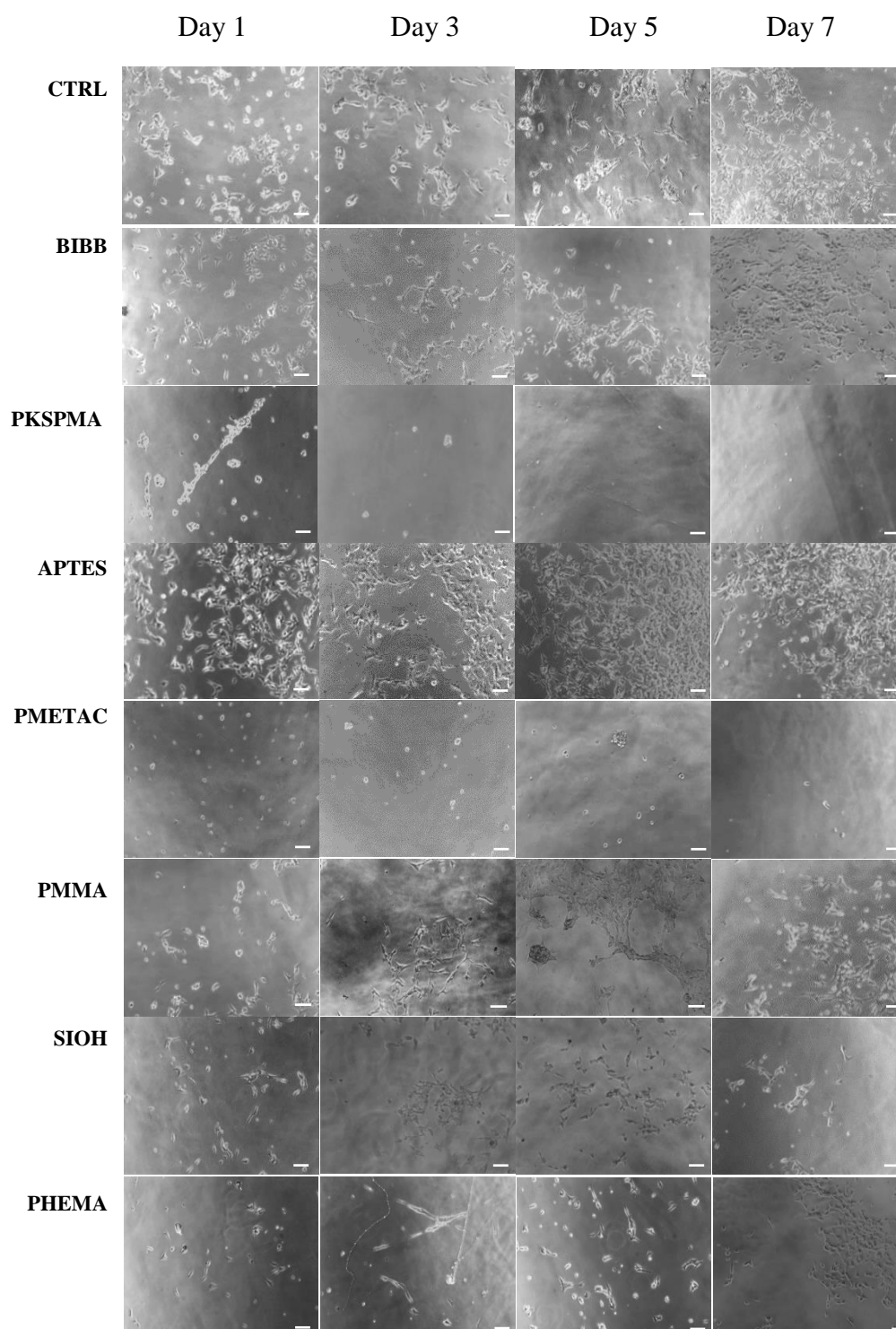


Figure 4.6. Comparative light micrographs illustrating the proliferation rate prior performing the alamarblue® assay on the different chemical surfaces. SH-SY5Y's were seeded (10000 cell/cm²) on the different chemical substrates and cultured for 1, 3, 5 and 7 days. The media with 10% alamarBlue® was incubated and measured at 560 and 590 nm. Scale bar= 100 µm.

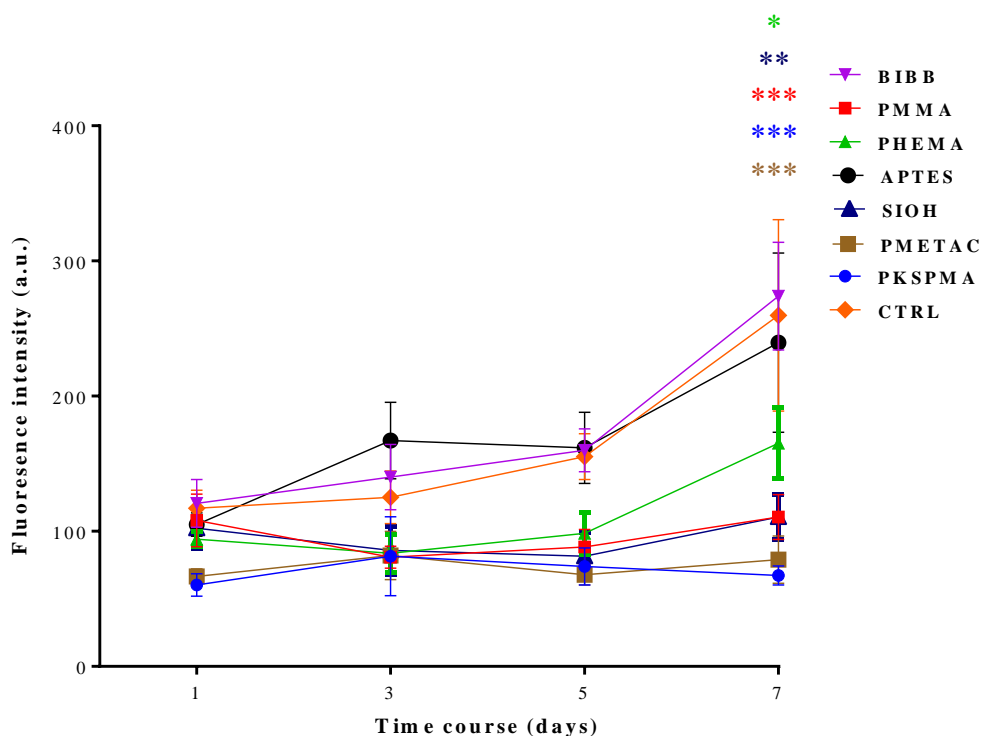


Figure 4.7. Metabolic activity assessed by alamarBlue® fluorescence on SH-SY5Y's. Cells were treated with 10% of alamarBlue® at days 1, 3, 5 and 7 for BIBB, PMMA, APTES, PMETAC, PKSPMA, SIOH, PHEMA and CTRL (non-coated glass). Error bars represent S.E.M. of the mean. Asterisks indicate statistical differences between the substrates vs. non-coated glass (CTRL, * $p < 0.05$, ** $p < 0.01$, *** $p < 0.005$, $n = 4$).

4.4.2 Assessment of cell proliferation on chemically modified surfaces

Quant-iT™ PicoGreen® was used for DNA quantification in order to provide a more accurate idea of the proliferation activity of SH-SY5Y's on these chemical coatings. Similar to alamarBlue®, certain trends were observed when using the PicoGreen® assay. APTES, BIBB and non-coated glass exhibited the highest proliferation rates over the 7 day culture period, increasing from day 1 until the end of the experiment (see Figure 4.8, $p < 0.05$ for day 7 when compared to PKSPMA and PMETAC).

In contrast to the metabolic activity data (Figure 4.7), there was an increase in proliferation on cells cultured on PMETAC and PKSPMA, however the rates remained low compared to non-coated glass ($p < 0.05$ from day 3 to day 7, Figure 4.8). The degree of proliferation on PMMA and SIOH samples increased exponentially until day 5 and then reached a plateau at

day 7. In addition, PHEMA obtained lower levels of DNA when compared to PMMA and SIOH, showing an increase at day 7 and thus suggesting variability in cell behaviour for this coating. Although cells seemed to grow and attach favourably on PHEMA, the lack of cell response was also observed on certain samples, thus obtaining changeable results. All together, these results indicate that APTES and BIBB were comparable to non-coated glass (CTRL) in terms of cellular proliferation and metabolic activity, whilst substrates such as PKSPMA and PMETAC were not able to obtain viable cells to adhere and proliferate.

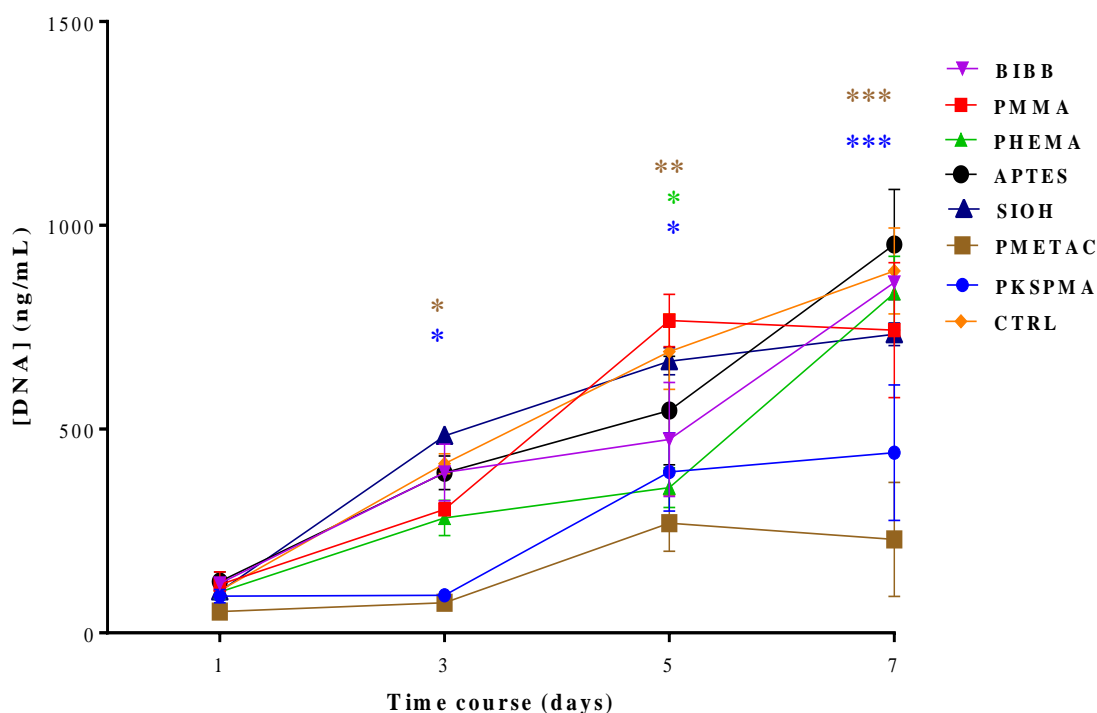


Figure 4.8. Proliferation rates assessed by DNA quantification from Quant-iT™ PicoGreen® fluorescence of SH-SY5Y's. Cells were lysed at day 1, 3, 5 and 7 for BIBB, PMMA, APTES, PMETAC, PKSPMA, SIOH, PHEMA and CTRL (non-coated glass). Error bars represent S.E.M. of the mean. Asterisks (which have been coloured in accordance with the colour legend) indicate statistical differences between the substrates vs. non-coated glass (CTRL, * $p < 0.05$, ** $p < 0.01$, *** $p < 0.005$, $n = 3$).

4.5 Effect of PHEMA brush thicknesses on cell behaviour

SH-SY5Y's triggered a very variable response when experiments were performed on PHEMA brushes, thus leading to investigate the reason for such inconsistency. Properties

such as the grafting density and thickness of the polymer brush have been related to the ability of the cells to attach to polymer brushes. In this study, an inconsistency of cell behaviour on PHEMA brushes was often observed and thus, experiments were conducted to analyse whether a reduction or increase on film thickness during brush preparation caused such variability. To this end, a range of different thicknesses were tested for SH-SY5Y's to determine whether thickness was causing the unpredictable cell behaviour. PHEMA brushes were prepared using various polymerisation times (1, 3, 6 and 24 hours) given that the thickness of the polymer is proportional to the time of the sample exposed to the polymer solution, thus obtaining a range of various thicknesses.

The growth of the PHEMA brushes over time has been illustrated in Figure 4.10. An increase in brush thickness occurred when the samples were exposed to the polymer solution for longer periods ($p < 0.05$ for 1 hour vs. 24 hours polymerisation time, Figure 4.9A). SH-SY5Y's were then cultured on these samples and the differing behaviour has been illustrated in Figure 4.9. When cells were cultured on samples with thinner brushes (1 hour polymerisation time, Figure 4.9A) cells adhered and grew on these surfaces, exhibiting short extensions. As the brush thickness increased (3, 6 and 24 hours, Figure 4.9B, C and D, respectively) the number of cells decreased on the surfaces, indicating a lack of cell predilection for this surface when brush thickness increased. As there was a certain degree of variation in the thicknesses of the samples between repeats, the ability to assess a specific thickness value at which cells were attaching and proliferating was unfeasible. Nevertheless, there was a clear difference in cell behaviour when the polymer thickness was altered. Brushes with a thickness of 90-100 nm resulted in a decreased cell attachment, whereas an increased cell attachment was shown when polymer thickness was thinner (20-40 nm) (see Figure 4.10B). The standard polymerisation time used in this thesis for PHEMA was 24 hours, thus according to this data there should be a lack of cells attached on this surface. As predicted, a clear variability in the formation of the brush when prepared probably led to a reduction of thickness, which finally resulted in cells attaching onto this surface. However, this study aimed to identify the reason for the variation, rather than determine an optimum thickness for this brush. As more reliable coatings were available (APTES, BIBB, see Section 4.6), PHEMA brushes were discarded for further experimentation since the process of

making the brush appeared to have inherent variability and the cellular response was not predictable.

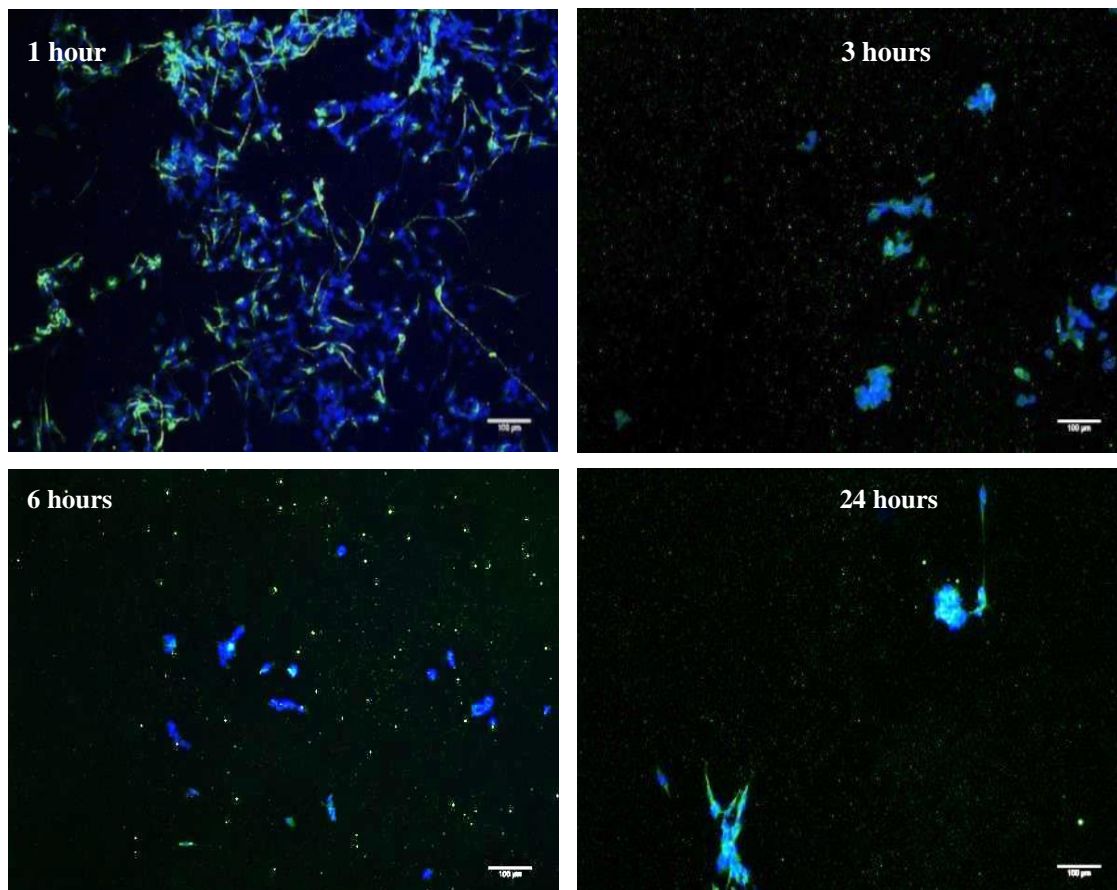


Figure 4.9. SH-SY5Y's cultured on PHEMA samples generated at different polymerisation times. Cells were grown in GM and stained after 5 days. Fixed cells were labelled with β tubulin III (green) and the nuclei was labelled with DAPI (blue). Scale bar= 100 μ m.

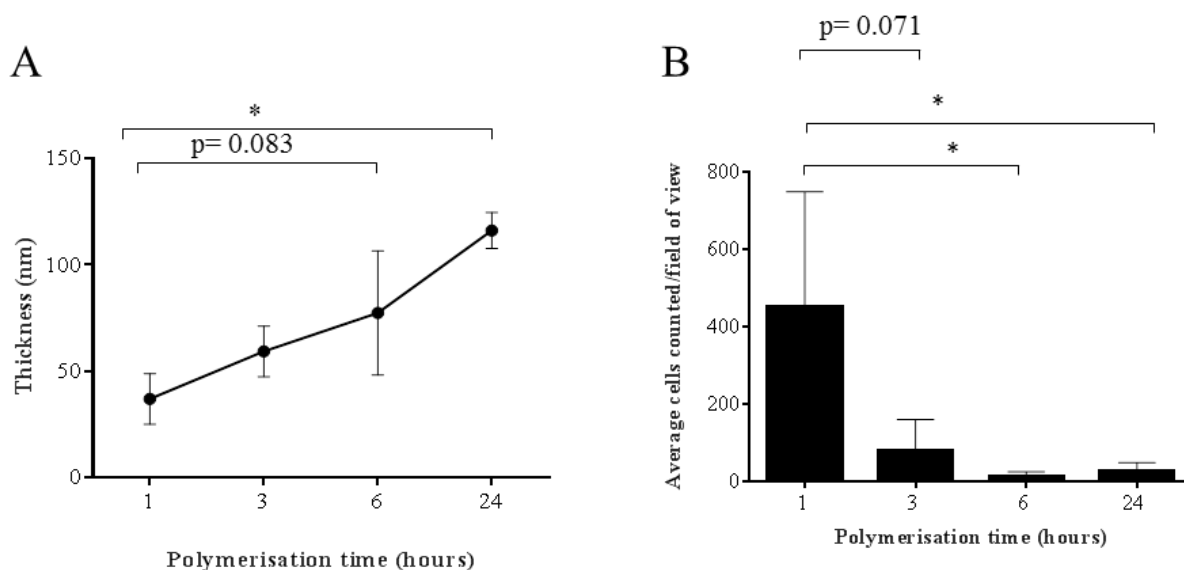


Figure 4.10. Effect of PHEMA film thicknesses on cell behaviour. A) PHEMA brush thickness during SI-ATRP reaction over a 24 hours period. B) Average number of cells per field of view presented on the samples at different brush thicknesses. Error bars correspond to the SD of the mean ($n=3$).

4.6 Effect of surface coatings on neurite outgrowth and differentiation of SH-SY5Y cells

Neurite outgrowth provides a good indication of morphological changes into a more mature, differentiated phenotype. This parameter was measured in cells cultured on the previously mentioned surface coatings to study whether their presence could trigger intracellular signals leading to neurite extension. Neurite length was measured before the differentiating agent (*all trans* retinoic acid, ATRA) was added and then after 1, 3 and 5 days in DM. When comparing main surface-time effects, average neurite length was greater on APTES and BIBB ($p<0.05$) compared to control (non-coated glass) before ATRA was added. This may suggest a major level of neuronal differentiation on these modified substrates even prior to the addition of the differentiating agent (Figure 4.11 and Figure 4.12). After 24 hours of adding retinoic acid (DM1), an overall increase in neurite length on all modified surfaces could be observed, with the largest neurite outgrowth in neurons cultured on APTES and BIBB ($p<0.05$ for BIBB). In contrast, the measures on PKSPMA and PMETAC samples could not be assessed due to the lack of cell adhesion and therefore differentiation. PMMA remained similar to non-coated

glass, whilst a slight reduction in neurite length was observed in SIOH, with no significant differences before and after the addition of retinoic acid ($p>0.05$). After 3 and 5 days in ATRA, the ability to accurately measure neurite outgrowth was compromised due to the slower but continued proliferation and neurite extension. Thus, a plateau and even a reduction in neurite length was observed in the final time point (5 days) for all the coatings presented.

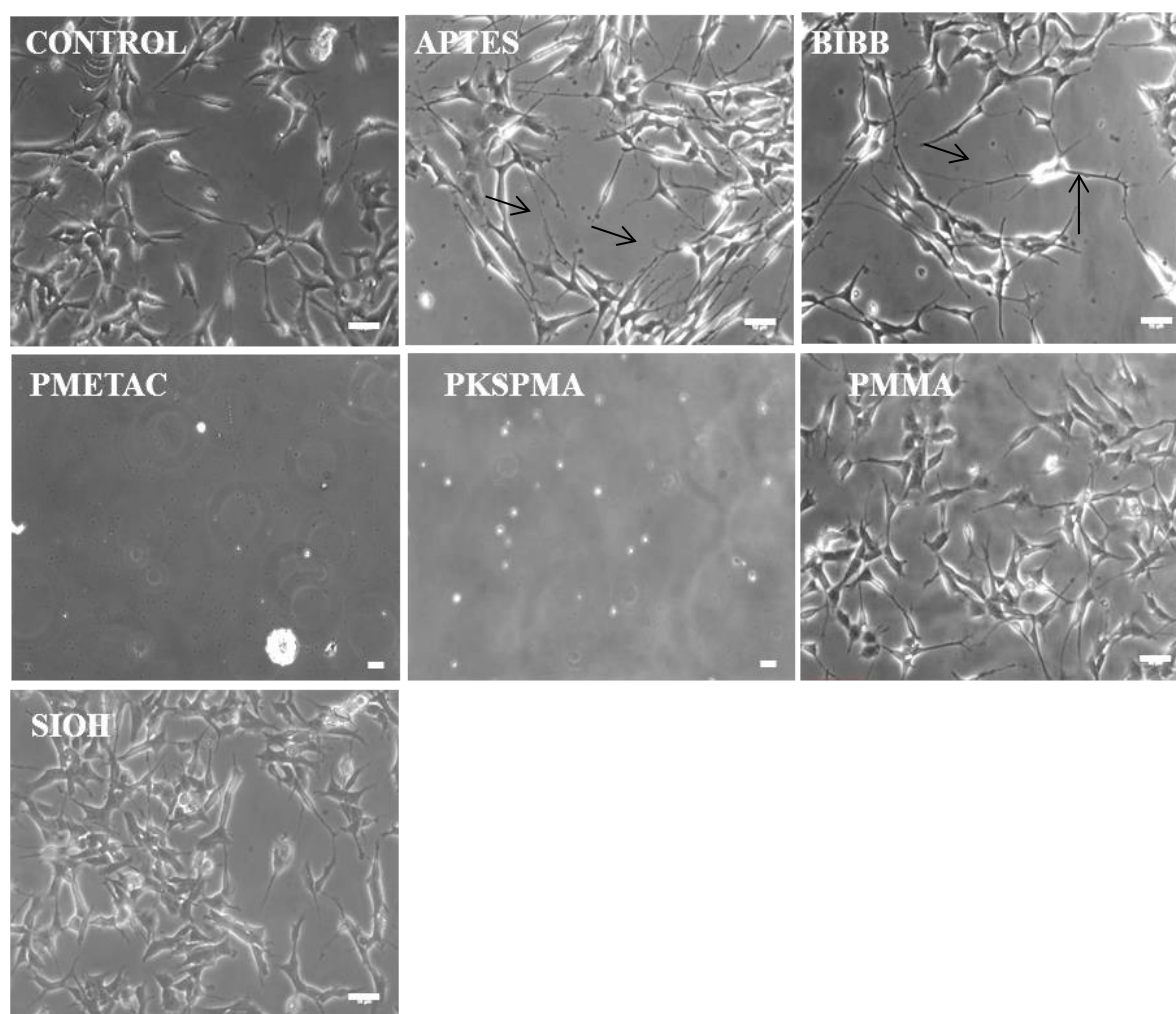


Figure 4.11. Representative phase contrast micrographs illustrating neurite outgrowth. Images represent the different chemical coatings after 1 day in ATRA (DM1) for all the substrates except for PMETAC and PKSPMA, where micrographs show SH-SY5Y's on these substrates after 10 days in culture. White arrows indicate neurite outgrowth. Scale bar= 50 μ m.

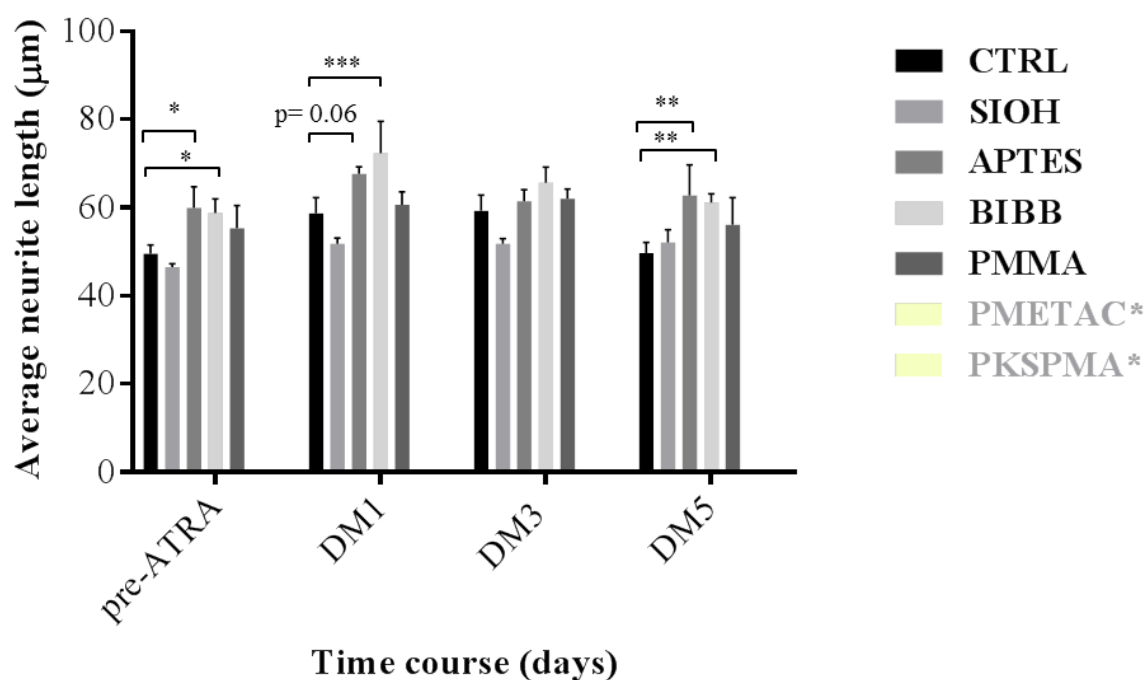


Figure 4.12. Average neurite length measured on BIBB, APTES, PMMA, SIOH and the control (non-coated glass). The measurements were taken with phase contrast images. Error bars correspond to SD of the mean. Asterisks represent the significant differences found when compared with non-coated glass (* $p < 0.05$, ** $p < 0.01$, *** $p < 0.005$, $n = 3$). *PMETAC and PKSPMA appear in the legend to highlight that these coatings could not be measured due to the lack of cell attachment.

Microtubule associated protein-tau (MAPT) was used to obtain further information about which coating promoted neuronal maturation to the greatest extent. Neurons were examined on non-coated glass, APTES and BIBB samples as these coatings showed the greatest neurite outgrowth. There was an increase in MAPT expression for control (non-coated glass) compared to APTES and BIBB, although the differences did not reach significance. This may be due to the large variability in the control surface. MAPT mRNA expression was higher in neurons cultured on BIBB compared to APTES (Figure 4.13, $p = 0.06$), which may indicate a greater presence of neuronal maturation in neurites presented on BIBB vs. APTES, although with non-significant differences (Figure 4.13).

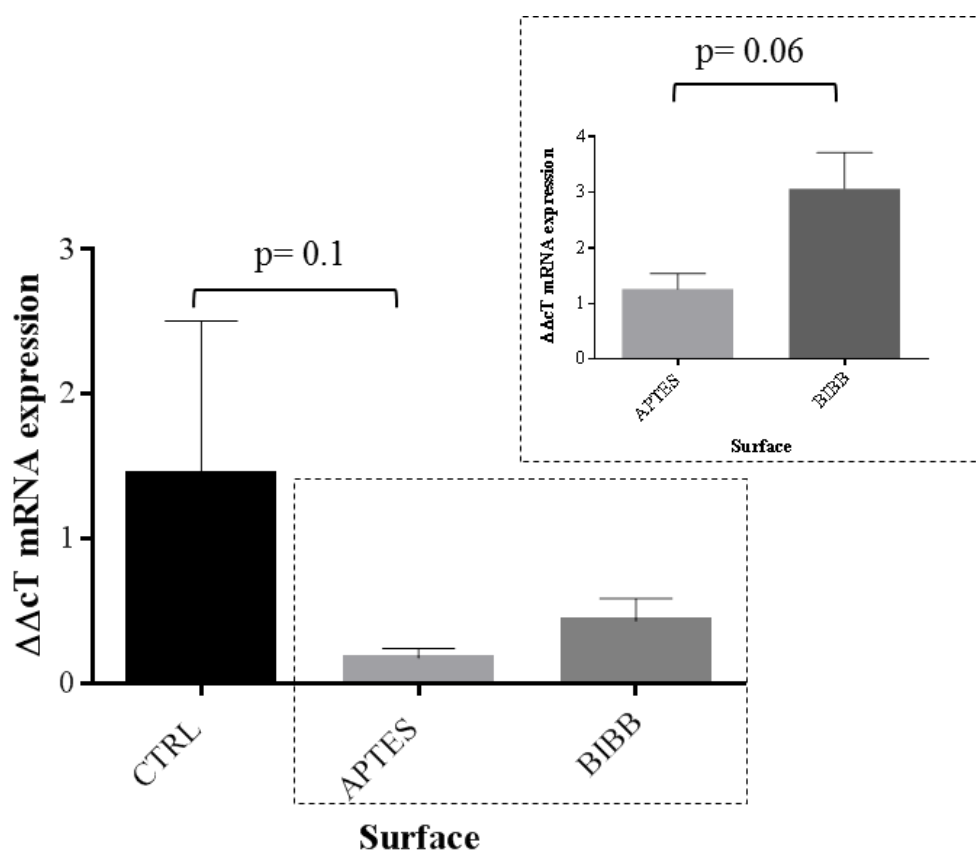


Figure 4.13. Expression of MAPT gene on modified surfaces. MAPT codes for tau protein involved in microtubule stabilisation. SH-SH5Y's were cultured on CTRL (non-coated glass), APTES and BIBB substrates. Error bars correspond to SD of the mean (n= 3).

4.7 Correlation between neurite length and water contact angle

The relationship between wettability and neurite outgrowth was analysed to determine whether this sole characteristic had a greater effect on neurite extension than any other material property, as previous reports have highlighted its influence in cell culture applications. Average neurite length was greater on surfaces with a wettability between 40-60°, however, overall wettability had very small influence on neurite outgrowth (Figure 4.14, $R^2= 0.58$ for DM1, and $R^2= 0.56$ for pre-ATRA).

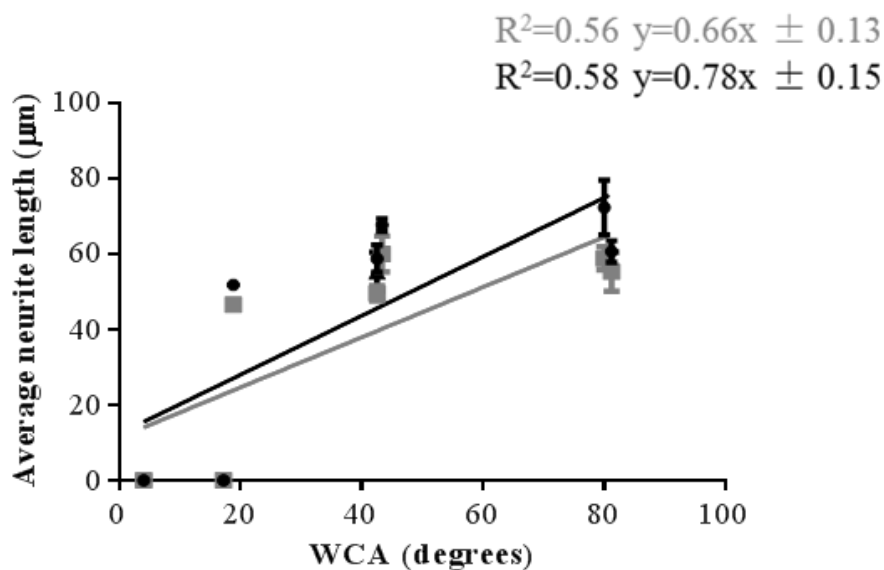


Figure 4.14. Relationship between WCA vs. average neurite length. Error bars represented the SD of the mean. PreATRA has been plotted in grey colour whilst DM1 is represented as black.

4.8 Discussion

Manipulating surface characteristics to enhance precise neuronal behaviour, such as attachment, proliferation and differentiation is fundamental to obtain a reliable neuronal *in vitro* system (Greco *et al.*, 2013; Tonazzini *et al.*, 2014). Chemically modified surfaces have been known to affect cell attachment and growth (Raynor *et al.*, 2009) and therefore, these have been extensively used to manipulate cell behaviour. Due to the ease of design and ability to coat a wide range of materials, the chemically modified surfaces can be a useful tool in neuroscience (Kim and Mooney, 1998; Rosso *et al.*, 2005; Krishnamoorthy *et al.*, 2014).

4.8.1 Effect of surface chemistry on cell behaviour

The first response when a material is under cell culture conditions is the arrival of water molecules on the surface, forming a water shell. Following this, the adsorption of proteins and other molecules occurs so when cells reach the surface, they interact with the surface through the protein layer, forming cell-surface interactions (Roach *et al.*, 2007; Ventre *et al.*, 2012). The interaction between the surface material and the water layer depends on the

material surface properties, which in turn are responsible for the degree of protein adsorption and ultimately for cell fate (Roach *et al.*, 2007). In order to determine whether surface chemistry could promote or aggravate such interactions, the behaviour of SH-SY5Y's on different SAMs and polymer brushes was examined. The mainly neuroblast-like nature of SH-SY5Y's offer biochemical and functional properties that are similar to primary neurons. For that reason, this cell line has been used as a useful neuronal cell line model (Xie *et al.*, 2010).

Neurite length data demonstrated that there was at least a morphological indication of neurite elongation for BIBB and APTES substrates, suggesting the level of differentiation was greater when compared to non-coated glass. A non-morphological criterion was also necessary to determine whether a morphological change was responsible for an internal biochemical change. Thus, the expression of MAPT was analysed on cells cultured on CTRL, APTES and BIBB, as the surfaces promoted the greatest neurite outgrowth (see Figure 4.12). Non-significant differences across the different surfaces were found in terms of MAPT mRNA expression. When comparing MAPT mRNA regulation between APTES and BIBB, a higher expression of MAPT in cells cultured on BIBB was found. Once cells become polarised, MAPT is mainly found in the axons (Yamamoto *et al.*, 2012), however MAPT is also found in the cell body and neurites before polarisation takes place. Thus, although neurite outgrowth was achieved, perhaps neurites were not specified to become an axon, resulting in an equal expression of MAPT among the different surfaces (Yamamoto *et al.*, 2012).

Lee *et al.* (2003) showed that a continuous increase of surface wettability on polyethylene surfaces contributed to an increase and subsequent decrease of neuronal adhesion. A greater formation of neurites towards hydrophilicity was also shown in this study, indicating a strong adhesion and neurite extension on surfaces with moderate hydrophilicity. This data is similar to the trends shown for APTES substrate, which was also suitable in this thesis for neurite outgrowth. The requirement of a moderate hydrophilic surface to obtain a positive neuronal response could explain why very hydrophilic surfaces, such as PMETAC and PKSPMA, did not succeed in obtaining neuronal adhesion and proliferation. This requirement is however, not related to BIBB as its water contact angle was $\sim 80^\circ$ and despite

that, BIBB was shown to be favourable for SH-SY5Y's in terms of proliferation, viability and neurite outgrowth. The lack of cell predilection for PMMA could be due to its hydrophobic nature however, its levels of hydrophobicity are similar to BIBB. Different wettability has also been related to the ability of the surface to adsorb proteins from the serum media (Arima and Iwata, 2007; Wei *et al.*, 2009) in turn facilitating cell adhesion. Therefore, this parameter is another factor to consider when assessing why different substrates inhibit or favour neuronal behaviour, and may explain the different behaviour among the surfaces (Lee *et al.*, 2003). Electrostatic interactions, not only between these adsorbed proteins and the coatings, but also between the coatings and the cell membrane likely contribute as well to the different cell behaviour (Zhang *et al.*, 2006; Jiang and Cao, 2010). This could indicate why the charged surfaces of PKSPMA and PMETAC inhibited cell adhesion. Particularly for PMETAC, the highly positive charge presented on this brush has been shown to induce toxicity by interaction with charges in the cell membrane (Wan *et al.*, 2012; Zhou *et al.*, 2012).

The chemical functionality of different substrates has been investigated as one of the main factors responsible for different cell behaviour (Faucheux *et al.*, 2004; Arima and Iwata, 2007; Palyvoda *et al.*, 2008; Roach *et al.*, 2010). Substrates containing amine groups, such as APTES, have been shown to be favourable for neuronal behaviour (Kleinfeld *et al.*, 1988; Palyvoda *et al.*, 2008; Dong *et al.*, 2010; Khan and Newaz, 2010). For substrates such as BIBB, various research groups demonstrated that substrates containing bromide groups obtained a positive cell response (Rühe *et al.*, 1999), leading to the hypothesis that wettability is not the main factor to consider and that other parameters could promote an equally favourable response in SH-SY5Y's (Ren *et al.*, 2009). It is not clear which exact mechanisms control the interactions between neurons and chemical substrates (mainly due to the complex number of factors involved). However, the attractive and inhibitory cell responses that these surfaces can achieve could be of great importance for the development of novel bio devices with a controlled neuronal organisation (Ren *et al.*, 2009; Tan *et al.*, 2013)

4.8.1.1 Different thicknesses for PHEMA in cell culture

Brush structure is considered an important factor involved in cell behaviour (Mei *et al.*, 2005; Mrabet *et al.*, 2009; Zhao *et al.*, 2011; Ren *et al.*, 2013). The variable behaviour of SH-SY5Y's in PHEMA samples across different analyses led to the hypothesis that a brush thickness variation may be responsible for the altered cell behaviour. Different thicknesses were examined in cell culture, but the lack of thickness reproducibility made it difficult to obtain reliable results. It was observed that even polymerisations for an identical period of time resulted in variable brush length (see Figure 4.10). There was a greater cell response when PHEMA brushes were thinner, however the amount of cells attached was still low and it was not possible to obtain an optimum range of brush thickness for cell adhesion. Various studies have shown that there is a correlation between cell adhesion and film thickness. Deng *et al.* (2014) found that smooth muscle cells had decreased adhesion on PHEMA as the coating grew thicker. Ren *et al.* (2013) explored a gradient of different thicknesses of PHEMA, and found that vascular smooth muscle cells remained in the zones where the PHEMA polymer was thinner (3-10 nm). In addition, there are various parameters that could influence a change in brush conformation, thus a change on brush thickness could have affected brush conformation, leading to variability in the sample, and therefore, the behaviour of the cells (Krishnamoorthy *et al.*, 2014).

4.8.2 Chapter summary

In this chapter, the influence of different polymer coatings on neuronal survival, differentiation, metabolic activity and proliferation was examined. It was found that neuronal behaviour *in vitro* is partially dependent on the interaction between the cell and the attachment surface. Cells cultured on APTES and BIBB displayed a greater neurite outgrowth, cell proliferation and survival, whereas a lack of cell adhesion and impaired growth was observed on PKSPMA and PMETAC brushes. Non-apparent toxic effects were shown on PKSPMA however, a certain degree of toxicity was observed on PMETAC. The “permissive” and “non-permissive” cell coatings identified in these results could be incorporated into a more complex structure by using appropriate engineering techniques. Cells could be placed in patterned areas to be of more resemblance to the neuronal circuit. This could result in a more accurate study of different cell interactions for systems such as

neurons and astrocytes in the brain, and also neurons and their interaction with innervating targets.

5 Creating chemical patterns for neurite guidance

5.1 Introduction

Highly organised structures containing geometrical patterns are known to be part of the complex neuronal network present in the nervous system, arranging numerous neuronal connections and ultimately giving rise to critical physiological functions (Peyrin *et al.*, 2011; Shah *et al.*, 2016). Examples of this type of architecture can be found in the dorsal retina of chicken and mice, where defined canals are packed with axons (Silver and Sidman, 1980; Rajnicek *et al.*, 1997), or in the dorsal column of frogs, which provides tracks that guide dorsal root ganglion (DRG) axons after their entry into the spinal cord (Clark *et al.*, 1993). Indeed, neuronal organisation is essential for development, but also for neural functionality. The loss of the complex neuronal wiring is responsible for the vast majority of neurogenerative diseases and some central and/or peripheral nerve injuries, leading to severe damage of various motor and cognitive functions (Klein *et al.*, 1999; In *et al.*, 2005; Shah *et al.*, 2016). The ability to re-direct these connections in order to understand the underlying mechanisms of such diseases and also to succeed at enhancing neural regeneration is pivotal for neural engineering applications (In *et al.*, 2005; Gomez *et al.*, 2007).

Neuronal directionality seems crucial for neural development and function, however, its presence in *in vitro* systems is limited. Conventional neuronal cultures are commonly presented in very simplistic homogeneous surfaces, leading to a disorganised environment where neuronal guidance is not apparent (Khan and Newaz, 2010; Ventre *et al.*, 2012; Poudel *et al.*, 2013). Fortunately, several groups have demonstrated that neurons are extremely influenced by their surroundings, indicating a strong crosstalk at the cell-material interface and thus a high sensitivity to changes in their external environment (Tong and Shoichet, 2001; Fan *et al.*, 2002; Teixeira *et al.*, 2009; Khan and Newaz, 2010). As a result, changes in the surface parameters combined with the current advances in microfabrication have allowed the specific manipulation of surface cues in cell culture. Such manipulations could provide new platforms and approaches for cellular studies, whilst generating simpler and refined models to study complex neuronal interactions.

5.1.1 Micropatterning surfaces and the ability for cell confinement

Advances in engineering patterning methods at the nano- and micro-scales have made the manipulation of surface cues possible, in a manner where cells can represent the native environment more closely (Tan *et al.*, 2013; Krishnamoorthy *et al.*, 2014). The cues of interest (topographical, chemical, mechanical, etc.) can be specifically designed depending on the purpose of the experiment so that cells can be placed in specific locations at specific distances, depths or widths, guiding them into restricted pathways with the aim of reaching particular targets (Moroni *et al.*, 2014). For chemical pattern formation, the use of chemical gradients, surfaces coatings or ECM proteins can be combined with engineering patterning methods in order to attain a spatial control over cell growth (In *et al.*, 2005; Roach *et al.*, 2010).

There are several engineering techniques available for chemical patterning and these include colloidal lithography, nanoimprint lithography, nanografting, nanoshaving, soft lithography, etc. (Ogaki *et al.*, 2010). The most common methods for micro-patterning chemical functionalities are soft lithography techniques (microcontact printing, microtransfer molding, etc.), (Kane *et al.*, 1999; Falconnet *et al.*, 2006) and conventional photolithography (Falconnet *et al.*, 2006; Molnar *et al.*, 2007; Zhou *et al.*, 2013). In *et al.* (2005) created chemical patterns by microcontact printing in order to pattern SH-SY5Y's in channel sizes of 10-30 μm width. The study illustrated that single, elongated cells appeared in the 10 and 20 μm wide lines, whilst multiple cells occupied the width of 30 μm line patterns. Likewise, Klein *et al.* (1999) used microcontact printing to obtain a control over SH-SY5Y's, however, various cells were observed to fill the 20 μm wide line, forming small aggregates. The use of microcontact printing is widely used in microfabrication due its simplicity and the convenient reuse of the stamps. However, the ink mobility during the patterning process (causing ink spreading towards unwanted areas) as well as the possible stamp deformation (swelling/shrinking can lead to changes in the original channel sizes) can cause defects on the pattern, thus contributing to variable results in cell response. The use of a more refined patterning technique for neuronal guidance, such as photolithography could perhaps improve this part of the process, due to its high efficiency on the control of size and shape geometries (Molnar *et al.*, 2007; Takahashi *et al.*, 2011; Zhou *et al.*, 2013).

The type of technique used is not the only parameter to consider when patterning cells, since the type of cue to pattern, the amount of cells seeded and the pattern design will all have an effect on cell response. Regarding the pattern design, axons are typically directed towards specific targets by preformed canals or paths (as exemplified in the previous section). For this reason, using channels as the pattern geometry would not only allow for neuronal alignment and directionality but would also appear to bear a closer resemblance to the *in vivo* environment when compared to conventional culture techniques. A positive outcome on this process could lead to the localisation of defined neural-neural connections when attempting to create more representative neuronal culture models or even the improvement of co-culture systems by directing heterotypical communication.

5.1.2 Objectives of the chapter

The importance of manipulating neuronal directionality *in vitro* has been highlighted above and consequently, the aim of this chapter was to obtain a reliable procedure to pattern SH-SY5Y's by the use of chemical patterning so neuronal organisation and directionality could be performed. To achieve this, a new approach to pattern SH-SY5Y's by chemical patterning the anionic cell repulsive actuator poly(potassium 3-sulfopropyl methacrylate) (PKSPMA) brush was used. Furthermore, the use of different pattern sizes were utilised to achieve neurite directionality. The use of this “non-cell friendly” coating could facilitate a spatial control over cell growth without the need for extra cell attractive coatings (e.g. ECM proteins), resulting in a simple and reproducible method.

5.2 Methods

The methods carried out throughout this section to optimise the chemical patterning include:

- Binary coating formation PKSPMA/BIBB.
- Pattern formation and PDMS mould fabrication by dry film photolithography. The use of PDMS moulds for MIMIC soft lithography and direct photolithography for chemical patterning.
- Pattern formation and PDMS mould fabrication by wet film photolithography. The use of PDMS moulds for MIMIC and direct photolithography for chemical patterning.

5.2.1 Binary coating formation (Binary sample)

The differentiation, viability and proliferation data commented in Chapter 4 demonstrated that APTES and BIBB coatings promoted a positive cell response on SH-SY5Y's, whilst PKSPMA appeared to inhibit cell adhesion without inducing any toxic effect. As such, it was investigated whether fabricating a binary-coated slide (half BIBB/half PKSPMA) would lead to a spatial control on cell growth without any visible negative effects. To this end, a binary-coated sample was prepared by submerging half of a BIBB initiator sample (prepared as indicated in Section 2.1.3) into the KSPMA monomer solution for 24 hours under N₂. To carry out the process, the BIBB sample was placed in a tube sealed under N₂ and the KSPMA solution was injected *via* syringe until half the BIBB sample was covered (~1 cm). In this manner, only half of the sample would be covered by PKSPMA polymer solution, whilst the other half would remain as BIBB.

5.2.2 Binary sample under cell culture conditions

The binary sample was sterilised with 70% of industrial methylated spirit (IMS) (Fisher Scientific) and left to dry under sterile conditions. SH-SY5Y's were evenly seeded at a density of 5000 cells/cm² and cultured for a week in GM, to examine whether the binary pattern led to cell confinement. Thereafter, cells were fixed and stained as described in Section 2.5.9. Growth media was changed every 2 days.

5.2.3 Photolithography *via* dry film photoresist: fabrication of masters for MIMIC and direct patterning

The photolithography process has been divided in two different sections due to the different equipment used and the different nature of the photoresists. For photolithography performed with dry film photoresist, silicon wafers/coated glass slides were cleaned with seneo 4010 universal solvent and subsequently, a negative tone dry film photoresist Ordyl alpha 940 (~40 µm film thick, see Table 5.1), was laminated onto the substrate using an Albyco Photopro33 laminator heated to 115°C. A photomask containing ink printed channels (100-600 µm width) on a transparent sheet (Figure 5.1, left) was placed on top of the laminated substrate and UV exposed in a Parker unit for 3 seconds. Thereafter, the samples were developed in an

ultrasonic bath using 1% of potassium carbonate solution, and used either to add a second coating (procedure was explained in Section 5.5.2) or as a master for soft lithography.

Table 5.1. Main characteristics of the Ordyl dry film photoresist. Adapted from Srl (2003).

Ordyl dry film ALPHA 940	Main characteristics
Thickness	40 μm
Optimum lamination temperature	Range of 105-125° C
Resolution (lines and spaces, respectively)	40 μm , 50 μm

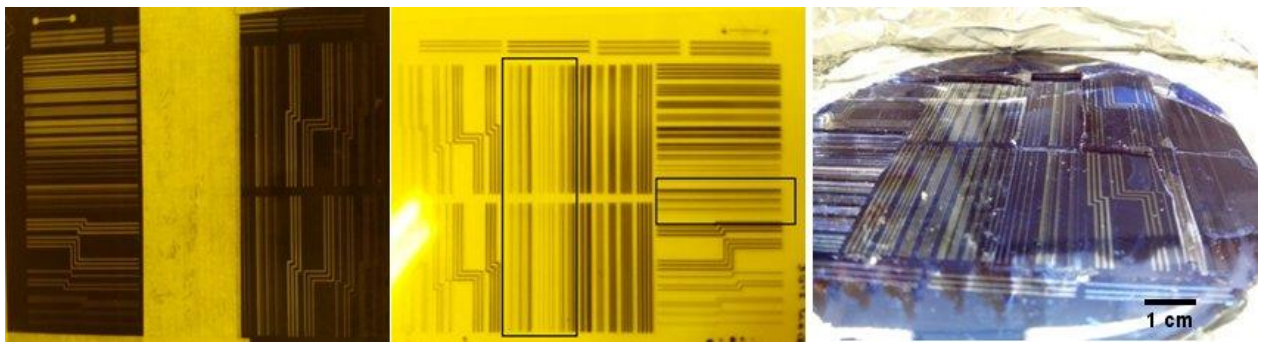


Figure 5.1. Macroscopic images of the photomasks used and the master fabricated with PDMS cast on top. PDMS moulds were cut from the master with a scalpel and used for MIMIC technique. Scale bar= 1 cm.

5.2.4 Fabrication of PDMS moulds for MIMIC technique

PDMS moulds were prepared using Sylgard® 184 silicone elastomer kit (Dow Corning), consisting of sylgard-184 elastomer and curing agent prepared in a 10:1 ratio. The mixture was weighed and stirred for ~5 minutes. Thereafter, the mix was degassed for 20 minutes in a vacuum desiccator to eliminate any air bubbles. The PDMS mixture was then poured onto a petri dish containing the master produced by photolithography (Section 5.2.3) and placed in an oven at 50-60° C to cure the PDMS. Once the PDMS was cured, moulds were cut with a scalpel in such a manner that it formed a network with open ends. The trimmed PDMS mould

was placed on a sample to make conformal contact and then, MIMIC process was carried out (see Figure 5.2A).

5.2.5 Creating BIBB/PKSPMA patterns by MIMIC technique

The fabricated PDMS moulds prepared in Section 5.2.4 were placed in contact (patterns down) with a BIBB-coated sample. Gentle pressure was applied with tweezers to ensure good contact between the mould and the sample. The conformal contact between the BIBB sample and the PDMS formed a channel network where PKSPMA polymer solution was syringed through, filling the channels by capillary action (see Figure 5.2A and B). The PDMS was removed from the surface after 24 hours, and the surface was thoroughly washed with methanol and dH₂O. A change in water contact angle across the sample after rinsing with dH₂O suggested the formation of a binary coating.

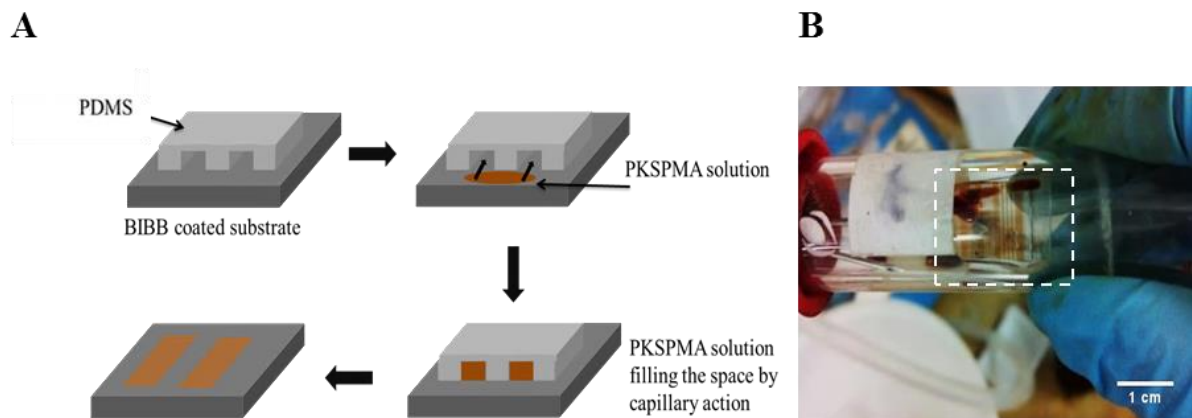


Figure 5.2. MIMIC process. A) A PDMS mould was placed onto a BIBB sample by conformal contact. Thereafter, PKSPMA solution was flowed through the channels by capillary action, and the PDMS mould was removed after the polymerisation was completed. B) Macroscopic image of MIMIC process when the PKSPMA solution (brown lines) occupied the channels between the BIBB sample and the PDMS mould. Scale bar= 1 cm.

5.2.5.1 BIBB/PKSPMA patterns formed by MIMIC technique under cell culture conditions

Samples containing MIMIC micropatterns were sterilised with 70% IMS and left to dry under sterile conditions. SH-SY5Y's were evenly seeded across the pattern at a density of 5000 cells/cm². Due to the differences in channel width, the period in growth media was

determined when channels were at least 50% confluent with cells. Thereafter, differentiation was induced by using DM for 3 days to promote neurite outgrowth. Cells were then fixed and stained with β tubulin III and DAPI, as described in Section 2.5.9.

5.2.6 Photolithography *via* wet film photoresist

5.2.6.1 Mask design

The mask (JD Photo-Tools, Manchester, UK) was designed by Dr. Paul Roach (Loughborough University, previously at Keele University when experiments were conducted) using AutoCAD 2014 software. The template consisted of parallel lines of various widths (3, 5, 10, 20, 50, 75 and 100 μm and gaps of 40, 40, 30, 20, 40, 80 and 100 μm , respectively) and 0.8 cm length, to test the effect of channel size on neuronal culture.

5.2.6.2 Photolithography process *via* wet film photoresist

The principle of conventional photolithography has been described in Chapter 2. The details of soft baking, UV exposure and developing are different depending on the photoresist used and thus, the protocols for the different photoresists used have been highlighted in the Sections 5.2.6.3 and 5.2.6.4. The general procedure consists on spin coating the photoresist, soft baking to evaporate the remainder of the solvent on the photoresist, UV exposure and developing. To perform soft lithography, a SU-8 10 photoresist was used. When samples were utilised directly in photolithography, a S1813 photoresist was used.

5.2.6.3 SU-8 10 photoresist

SU-8 10 (MicroChem, Chestech Ltd, Warwickshire) was spin coated (Laurell WS-650-23B) at 4400 rpm for 1 minute to obtain a thickness of $\sim 5 \mu\text{m}$. Thereafter, samples were prebaked at 95° C for 1 minute and exposed under UV by 55 light integra through a glass photomask. Various steps for post baking included baking at 65° C for 1 minute, 95° C for 1 minute, 125° C for an extra minute and then slowly cooling down to RT. For photoresist developing, the sample was developed in 2-(methoxy 1-methylethyl acetate) and washed with isopropanol. The resulting sample was dried with an air gun and used as a master to obtain PDMS moulds for MIMIC technique.

5.2.6.4 S1813 photoresist

The photoresist S1813 (MicroChem, Chestech Ltd, Warwickshire) was spin coated (Laurell WS-650-23B) at 3000 rpm for 1 minute to obtain a thickness around $\sim 1.5 \mu\text{m}$. The spin-coated sample was prebaked upside down at 115°C for 1 minute until solvent was completely evaporated. Samples were then placed in the mask aligner for UV exposure through a glass photomask at 50 light integra ($\sim 18.2 \text{ s}$ exposure time). Exposed areas were developed by rinsing the sample in a developer solution of dH_2O and NaOH (1:1 vol/vol) and then washing with dH_2O . The resulting sample was dried with an air gun and used under different strategies described in Sections 5.2.7.1, 5.2.7.2 and 5.2.7.3.

5.2.7 Chemical pattern *via* wet film photoresist

Photolithography *via* wet film photoresist was performed on non-coated glass slides, PKSPMA and BIBB coated samples. Each of these strategies contains different steps that have been highlighted in the Sections 5.2.7.1, 5.2.7.2 and 5.2.7.3.

5.2.7.1 PKSPMA as the starting surface

PKSPMA brushes were spin coated, soft baked, UV exposed and developed as described in Section 5.2.6.4. After the photolithography process, samples were plasma etched to eliminate the exposed PKSPMA areas followed by APTES deposition (Section 2.1.2). The non-exposed photoresist was removed by rinsing the sample with acetone (Figure 5.3). Samples were consequently dried with a flow of N_2 .

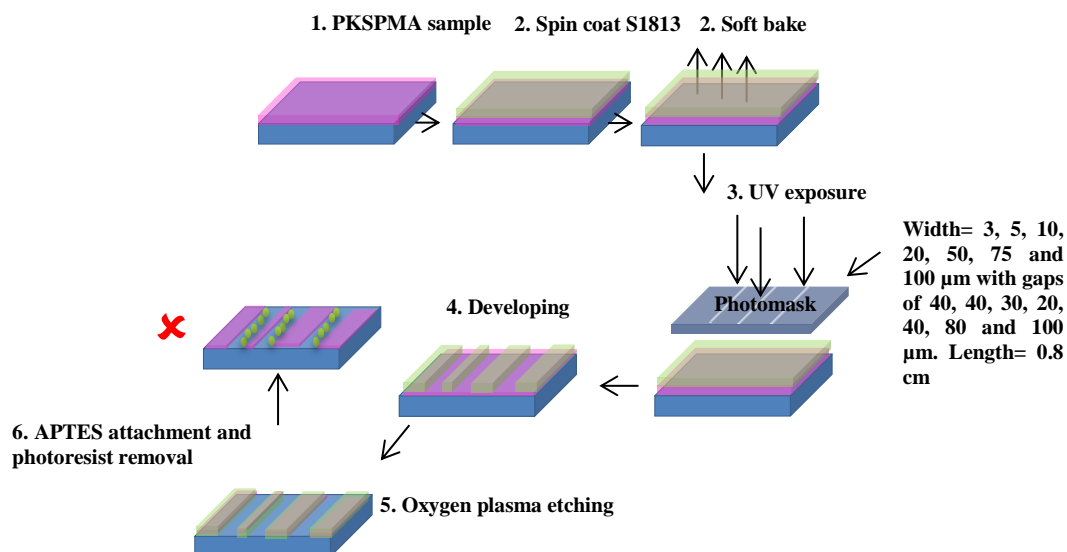


Figure 5.3. Schematic describing the photolithographic process for obtaining a PKSPMA/APTES pattern.

After removing PKSPMA from the exposed areas, these were used to attach APTES by chemical vapour deposition. The remainder of the photoresist was then removed by acetone washing.

5.2.7.2 BIBB as the starting surface

The procedure described for BIBB contains the same steps as the previous section up to the developing process (Figure 5.4). The BIBB exposed areas were used to grow PKSPMA brushes by SI-ARGET ATRP, as described in Section 2.1.6. After PKSPMA deposition, samples were washed thoroughly with methanol and dH_2O , and the remainder of the photoresist was removed with additional washes of acetone. Samples were consequently dried with a flow of N_2 . In another attempt, this procedure was repeated with a hard baking step, as similarly described in the following section. The results have been detailed in Section 5.2.7.2.

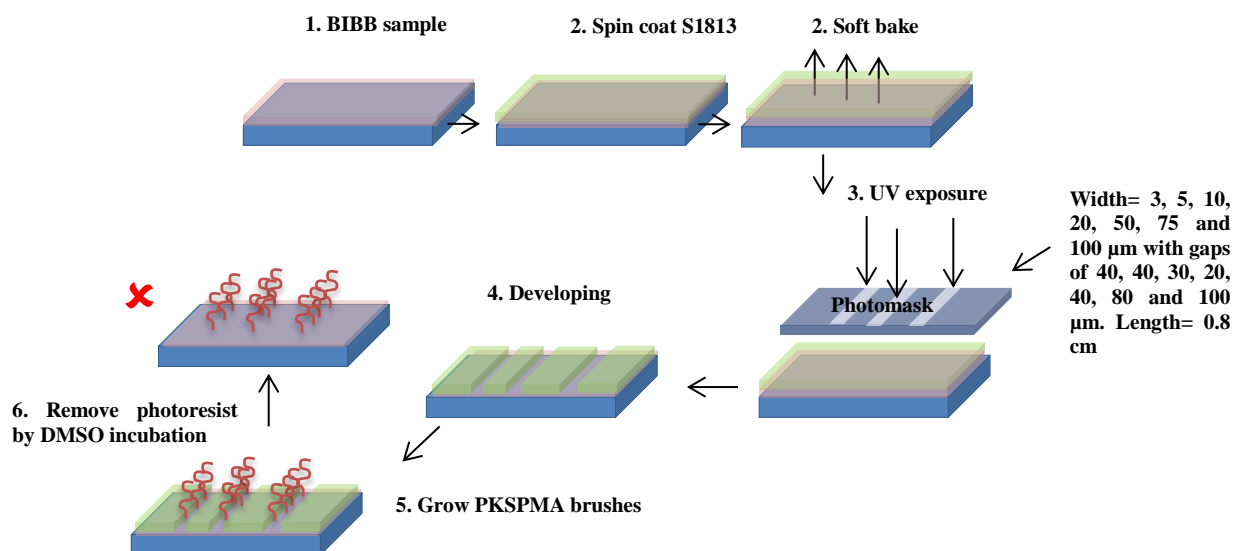


Figure 5.4. Schematic describing the photolithographic process for obtaining a PKSPMA/BIBB pattern.

The exposed areas that resulted from developing were used to grow PKSPMA brushes, whilst the areas where S1813 remained contained BIBB stripes.

5.2.7.3 Non-coated glass slide as the starting surface

The steps until developing were performed on a non-coated glass slide as described in previous strategies above (Sections 5.2.7.1 and 5.2.7.2). The developed samples were hard baked at $\sim 200^\circ\text{C}$ for at least 15 minutes and left to slowly cool to RT. The exposed areas were used to grow PKSPMA by the routinely procedure of UV/ozone cleaning, APTES and BIBB attachment that was described in Sections 2.1.2, 2.1.3 and 2.1.6. The photoresist on the non-exposed areas was present during the polymerisation steps. Once PKSPMA was formed, the photoresist was removed by incubating the samples in DMSO and confirming its complete removal under the microscope (Figure 5.5).

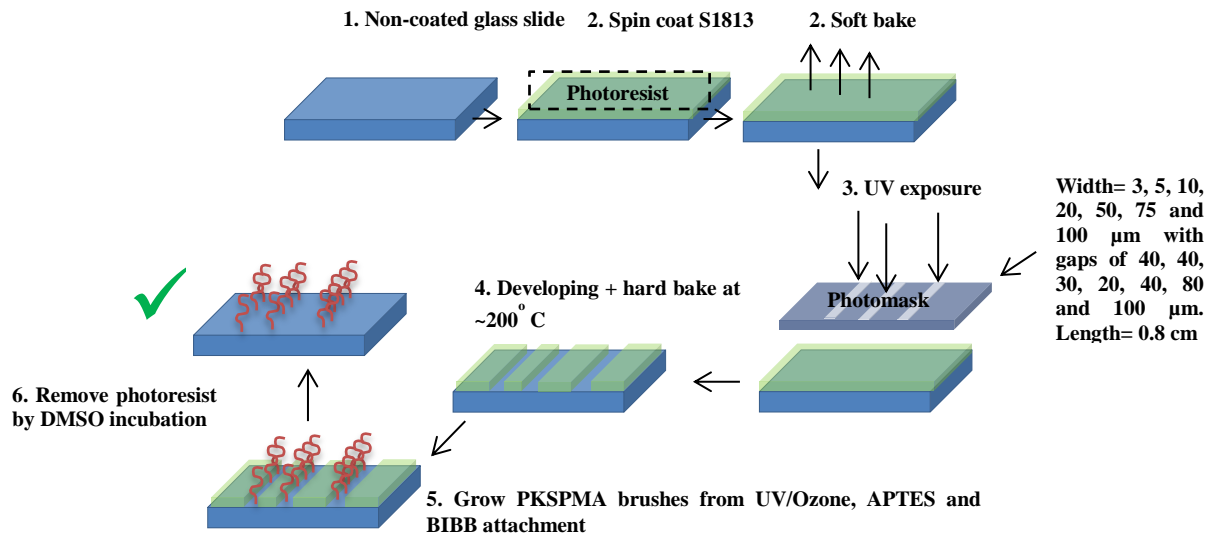


Figure 5.5. Schematic describing the photolithographic process for obtaining a PKSPMA/glass pattern. Samples were hard baked after developing to maintain the photoresist in place during the polymer growth process.

5.3 Experimental set up of SH-SY5Y on different channel widths

As the procedure displayed in Figure 5.5 was successful, SH-SY5Y's were grown, trypsinised and counted as described in Section 2.4. To identify how cell density could influence cell confinement in the patterned channels, SH-SY5Y's were seeded evenly at 5000, 10000 and 15000 cells/ cm^2 on the patterned samples, and cultured in GM for a period of 3 days. Neuronal differentiation was induced at this point by incubating cells in DM containing ATRA differentiating agent for an additional 3 days. Patterned samples were then fixed and used for immunocytochemistry (Section 2.5.9). Fluorescence micrographs were taken with a 20x magnification objective and five random images were captured at the end of the experiment for every channel size. The measurements performed have been described in Chapter 2, Section 2.5.10. GM and DM were changed every 2 days.

5.4 Statistical analysis

All data is presented as mean (\pm SD). A two-way ANOVA was used to analyse the channel data followed by a Bonferroni post-hoc test to determine the effect of the channels sizes over the different cell densities. Differences were considered statistically significant when $p \leq 0.05$.

5.5 Results

5.5.1 First attempts in cell spatial constraining: binary sample

Chemically modified coatings were analysed to obtain a permissive and repulsive cell coating, therefore when engineering techniques were used, patterning of these two coatings would allow the spatial constraining of cells into desired zones. Before using such techniques, an attempt to put both coatings together in the same sample was conducted. As a BIBB-initiator was necessary for the formation of polymer brushes (and it was shown to promote viability and proliferation, see Section 4.4.2), the formation of a binary coating was performed by dipping half a BIBB initiator sample into a PKSPMA containing solution (shown to promote a very poor cell attachment, see Section 4.3.1). As a result, half of the sample was covered by PKSPMA, whilst the other half remained coated with BIBB.

The chemical composition of the binary sample was analysed by FTIR and XPS. FTIR analysis illustrated the main C=O peak around 1720 cm^{-1} in the PKSPMA spectrum, as well as the peaks corresponding to the asymmetric and symmetric stretching of the S=O bonds. These peaks did not appear on the spectrum represented by BIBB (Figure 5.6).

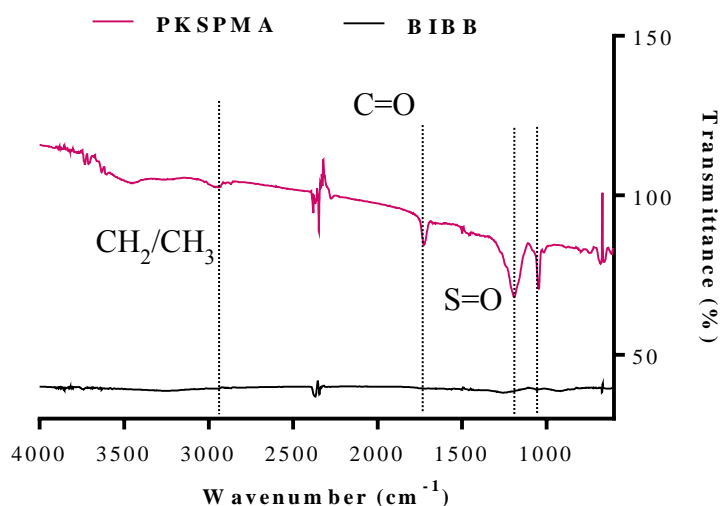


Figure 5.6. FTIR spectrum of PKSPMA (pink) and BIBB (black) binary sample. The C=O stretching ($\sim 1720\text{ cm}^{-1}$) as well as the stretching of the S=O bonds ($\sim 1000\text{--}1200\text{ cm}^{-1}$) confirmed the presence of the brush in that part of the sample only.

For the XPS data, the results have been highlighted in Table 5.2 and Figure 5.7. In the table, the percentage composition of Si2p between BIBB and PKSPMA suggested that PKSPMA had been successfully coated on that side of the sample, as Si2p signal from the glass surface was attenuated compared with BIBB, indicating the presence of a thicker layer on that side of the sample. The PKSPMA zone had a $\sim 27\%$ more C1s content than BIBB, which was comprehensible due to the presence of more C-C, C-O and C=O bonds in the polymer brush. In addition, the characteristic peak of S2p presented on PKSPMA brushes was only found on the side where the brush had been intentionally grown (Figure 5.7). Furthermore, the peak of Br3d was only present in BIBB zone (Figure 5.7) indicating that the initiator was covering that zone of the sample. These results together indicated that PKSPMA was present on the desired part of the sample, whilst the remaining part contained the functionalised BIBB initiator.

Table 5.2. Atomic composition of Si2p, C1s and O1s was determined by XPS on both sides of the binary sample (half BIBB and half PKSPMA).

Atomic composition (%)		
Element	HALF BIBB	HALF PKSPMA
Si2p	25.1	1.0
C1s	27.5	51.7
O1s	44.5	31.0

The different hydrophilicity of the sample after polymerisation showed a change in the wettability of the surface in the PKSPMA area, suggesting that a change on the chemical environment of the sample could have occurred. PKSPMA area rendered very hydrophilic behaviour whereas BIBB showed a hydrophobic tendency (Figure 5.7).

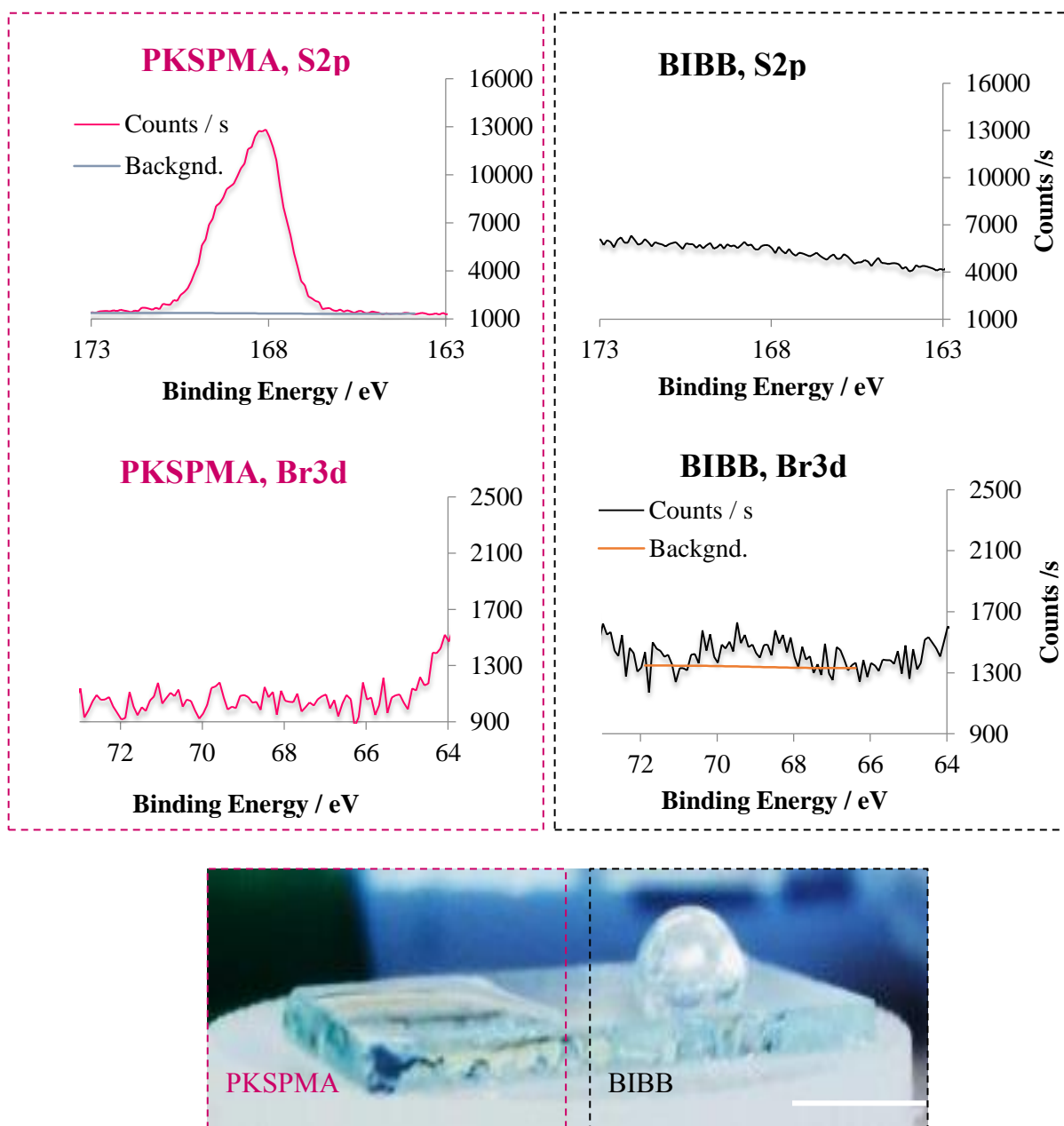


Figure 5.7. XPS analysis of S2p and Br3d core level spectra of PKSPMA (pink) and BIBB (black). The presence of the S2p peak in the PKSPMA zone (pink) suggested the presence of the polymer brush. In the lower part of the figure, a macroscopic image shows a glass slide functionalised with PKSPMA and BIBB at different parts of the sample. The different areas can be identified by the different hydrophilicity on the sample. Scale bar= 1 cm.

SH-SY5Y's were then evenly seeded across the binary coating for 7 days to demonstrate that both substrates could co-habit together, without altering the cell behaviour that had

previously been observed when these coatings were presented on independent samples. After a week in GM, the cells in the BIBB zone were confluent, whereas no cells were observed in the multiple focal planes examined in the PKSPMA region (Figure 5.8). The presence of a PKSPMA region did not appear to negatively affect the cells allocated in the BIBB region, further supporting the previous results indicating that PSKPMA restricts cell growth without any toxic side effects (Section 4.3.1). Surprisingly, cells appeared to form a “wall” once they reached the point where PKSPMA started (Figure 5.8).



Figure 5.8. Interface of BIBB/PKSPMA binary sample. Montage of light micrographs that illustrate the “wall” formed by the cells at the interface between both coatings after 5 days in GM (10x magnification). Scale bar= 100 μm .

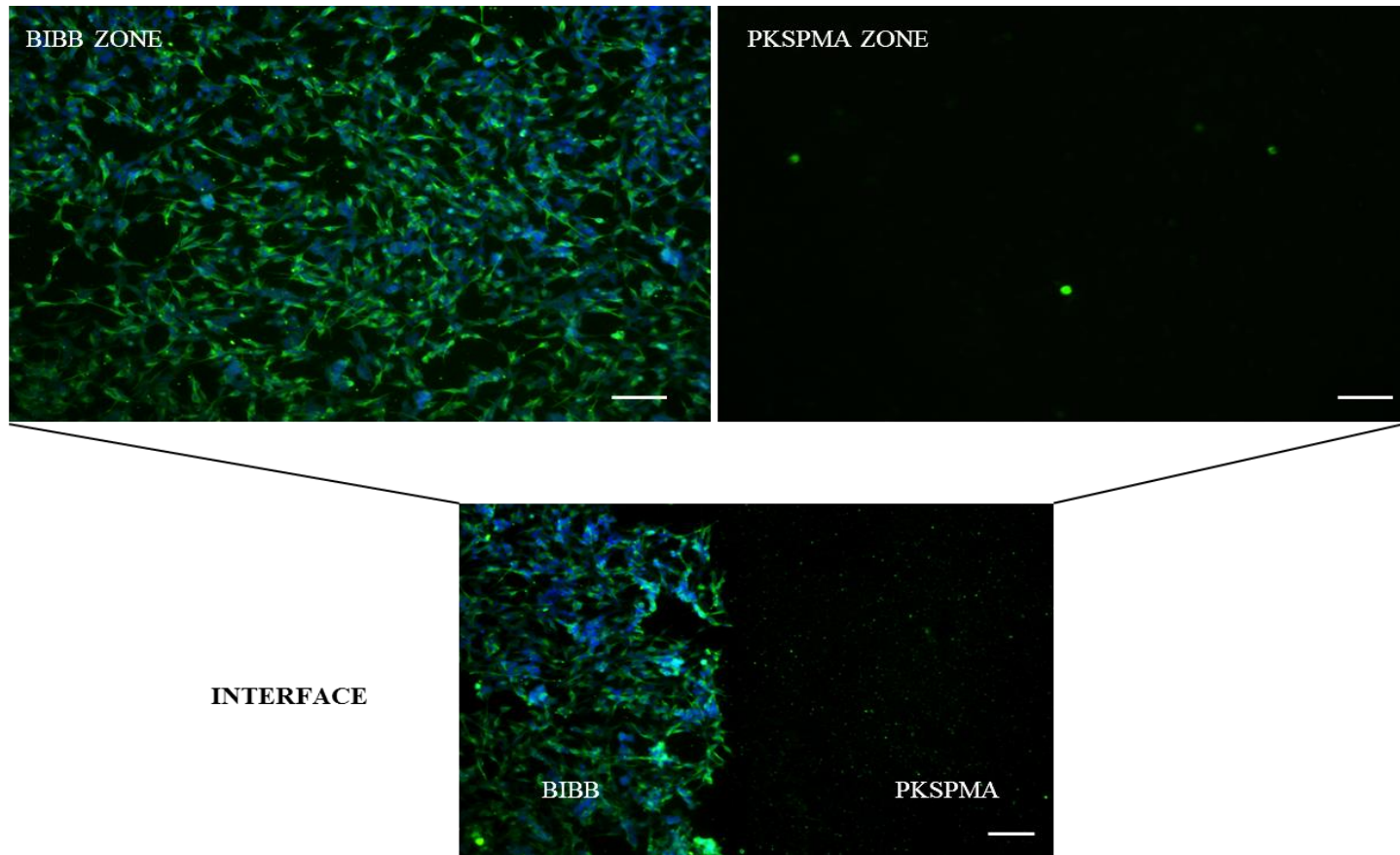


Figure 5.9. SH-SY5Y cells were grown on the binary sample and stained after a week in GM. Fixed cells were labelled with β tubulin III (green) and nuclei were labelled with DAPI (blue). Scale bar= 100 μ m.

5.5.2 Photolithography *via* dry film photoresist

The binary coating proved successful and thus, the next step was to obtain a more defined pattern structure. To achieve this, photolithography was utilised. A dry film photoresist was laminated on the different chemically modified surfaces (BIBB, PKSPMA and APTES) to carry out the UV exposure, development and formation of the binary pattern. When the photoresist was attached onto APTES or BIBB, the subsequent steps for growing PKSPMA in the exposed areas resulted in photoresist detachment thus, preventing the formation of a binary pattern (Figure 5.10). The sensitivity of the photoresist against solvents was primarily responsible for its removal. The reduction of steps to avoid photoresist damage was essential during the process and therefore, several attempts with PKSPMA samples were conducted. The process with PKSPMA would only involve UV/ozone to etch the PKSPMA exposed areas and would avoid the brush growth process. Unfortunately, when PKSPMA brushes were used as the starting sample for photolithography, the attachment of the photoresist to this surface was weak, resulting in an unsuccessful process. By optimising various parameters (UV exposure, type of photoresist), this technique had a great potential in terms of resolution and consequently, attempts with different procedures were accomplished in the following sections with higher resolution equipment. In addition, the use of soft lithography (MIMIC) was also carried out as an alternative route for cell patterning.

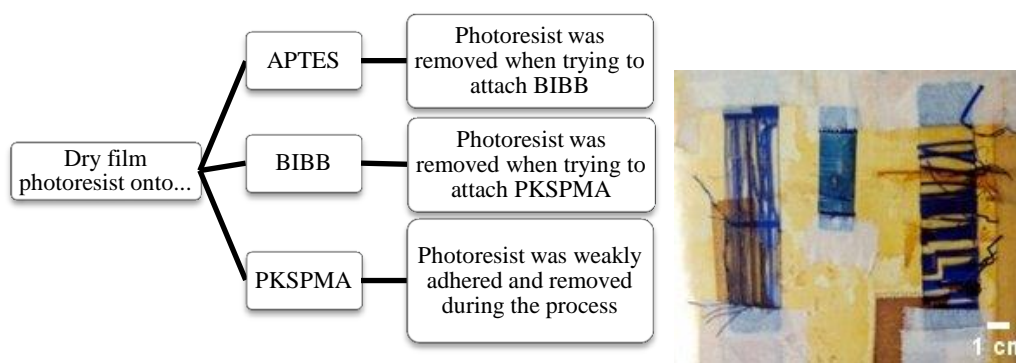


Figure 5.10. Photolithography with dry film photoresist. Left) Attempts performed by starting from different chemical layers in order to obtain the chemical pattern. Right) Functionalised PKSPMA samples during photolithography process. The photoresist did not adhere properly, slowly detaching from the substrate and making the pattern process void. Scale bar= 1 cm.

5.5.3 Patterning SH-SY5Ys using soft lithography MIMIC technique

Due to the lack of success using photolithography *via* dry film photoresist directly onto modified surfaces, this method was then only used to produce the masters for the micromolding in capillaries technique (MIMIC, see Section 2.2.2). After undergoing MIMIC (Section 5.2.5 for the protocol), the areas where PKSPMA polymer solution was injected had a dark brown/grey colour, whilst the areas where the PDMS was, remained with the colour of the wafer (Figure 5.11). When polymer brushes are produced on silicon wafers, these generate characteristic colours on the silicon material (Henrie *et al.*, 2004). The presence of newer films on silicon wafers can be observed by the recombination of different wavelengths when light is reflected off the interfaces of the film (Yom *et al.*, 2012), resulting in colours on the surface. Thus, a change in the surface colour could indicate the presence of new films on the surface.

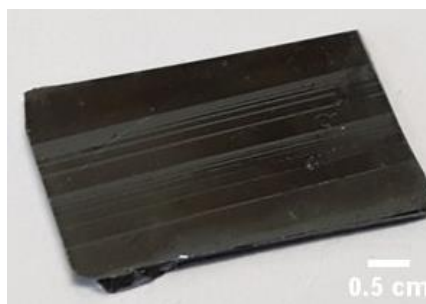


Figure 5.11. Macroscopic image of a MIMIC patterned sample with BIBB/PKSPMA. The different colour on the surface suggests the presence of various environments on the surface. Scale bar= 0.5 cm.

The chemical composition of the MIMIC pattern was analysed by XPS (Figure 5.12). For the main surface atoms (C1s, Si2p and O1s), an increase in C1s content in PKSPMA indicated the presence of a thicker layer compared to BIBB C1s percentage (50.4% and 38.5%, respectively). Furthermore, the attenuation of the Si2p peak in PKSPMA area (12.4% and 31% for PKSPMA and BIBB, respectively) indicated the presence of new layers on the surface, thus suggesting the presence of the brush. XPS analysis also showed the presence of a small percentage of S2s in the BIBB area (see Figure 5.12). This could however be due to contamination after removing the mould, along with the numerous washes across the entire sample to remove remnants of the KSPMA solution.

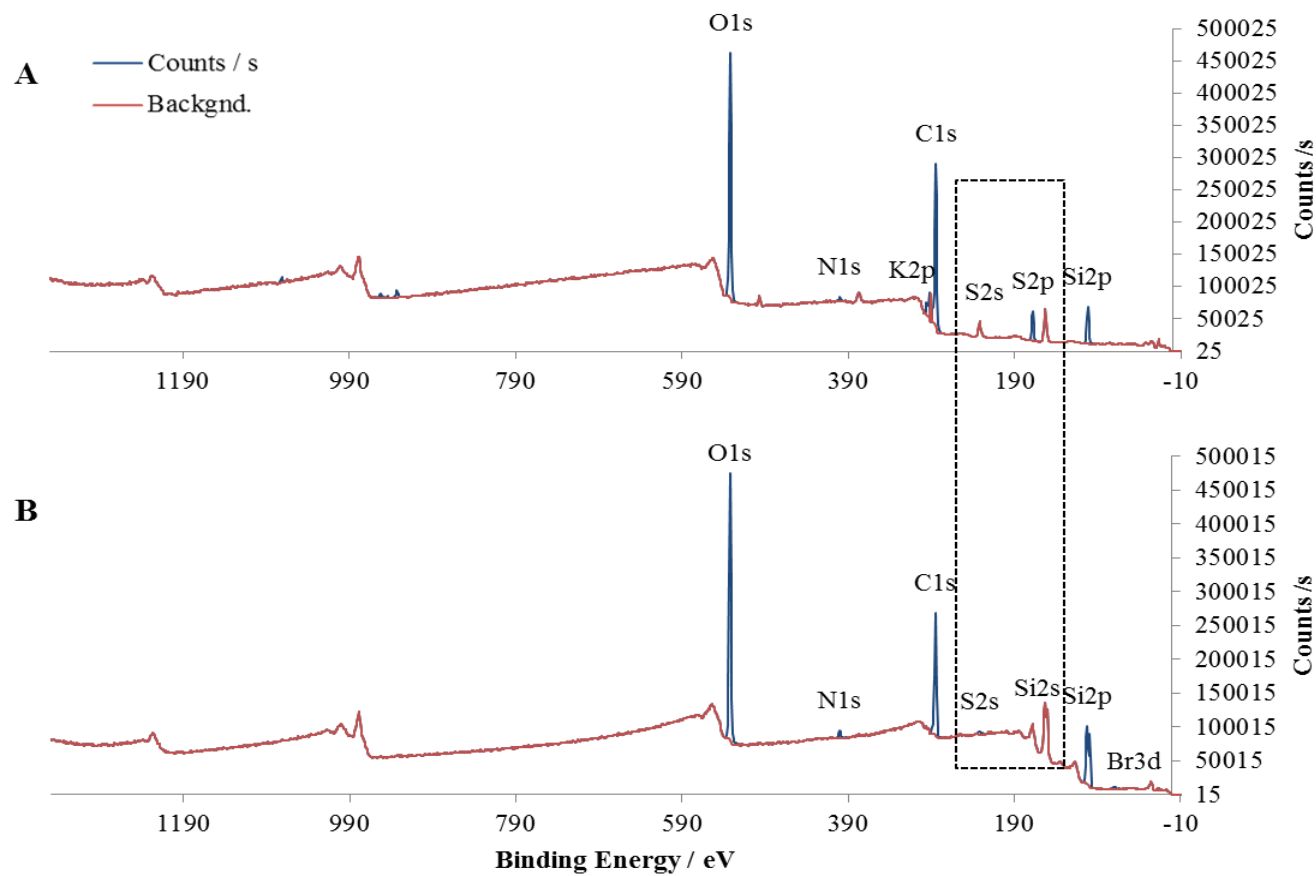


Figure 5.12. XPS spectrum of A) PKSPMA area and B) BIBB area. For PKSPMA, the S2p and S2s peaks appeared in the spectrum. In BIBB, Br3d can be appreciated in the spectra.

The SH-SY5Y's were cultured on MIMIC patterned samples according to Section 5.2.5.1. The presence of cells constraining in the channels suggested that MIMIC had been carried out successfully (Figure 5.13). It is important to note that cells constrained themselves into the channels as soon as they were seeded, proliferating and filling the whole pattern. If BIBB areas would have been covered with PKSPMA brushes (as suggested by the S2s peaks shown in Figure 5.12), no attachment would have taken place initially, or as an alternative, a gradient of cells would have been formed from BIBB towards PKSPMA surface.

Various patterns of different widths and shapes were attempted using the MIMIC method, ranging from 100- 600 μm width. As illustrated in Figure 5.13, cells occupied the spaces available to them, constraining themselves to these structures. Interestingly, SH-SY5Y's tended to grow towards the periphery of the lines first (Figure 5.13D), perhaps sensing the edges of the cell repulsive PKSPMA brushes, since these maintained a height of $\sim 40\text{-}60\text{ nm}$. Subsequently cells proliferated, occupying in the entire line pattern.

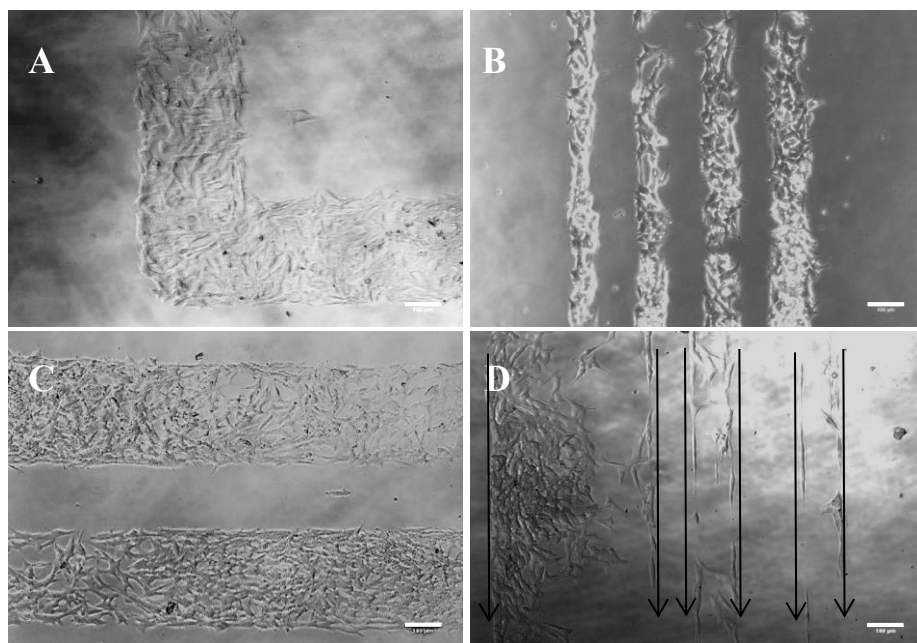


Figure 5.13. MIMIC patterns under neuronal cell culture. A) L pattern with a width of $\sim 300\text{ }\mu\text{m}$ after 4 days in culture. B) Line patterns with a width of $\sim 100\text{ }\mu\text{m}$ after 5 days in culture. C) Line patterns with a width of $\sim 300\text{ }\mu\text{m}$ after 5 days in culture. D) Representation of neuronal cells in the edges of the channels when first seeded on the patterned samples. Light micrographs at $\times 10$ magnification. Scale bar= $100\text{ }\mu\text{m}$.

5.5.4 Photolithography *via* wet film photoresist

Using the MIMIC technique, cell confinement was achieved, and the chemical coatings proved successful for cell growth restriction in specific areas. However, the resolution obtained using dry film photolithography was not enough to constrain single neuronal cell bodies and thus, guide isolated neurite extension. Through collaboration with external researchers (Dr. Paul Roach, Keele University), it was possible to attempt photolithography using more advanced equipment than was previously available. To this end, the different strategies attempted with dry film photoresist were performed again with wet film photoresists and new equipment. The detailed processes have been described in Sections 5.2.6, 5.5.5 and 5.5.6.

5.5.5 MIMIC with wet film photolithography masters

PDMS casting was performed on various masters. Firstly, a master was created with a ready available mask containing 5 μm channels and thereafter, the mask with different channel sizes described in Section 5.2.6.1 was used for creating a master for MIMIC. The PDMS moulds with 5 μm channels were created with a master containing the SU-8 10 photoresist (Section 5.2.6.3). Albeit KSPMA monomer solution seemed to flow through the channels straight after its injection (Figure 5.14A), the PDMS mould eventually detached from the surface, causing the PKSPMA coverage of the entire surface pattern. When did this not occur, pattern lines could be observed after rinsing the sample with dH_2O , due to the different hydrophilicity between BIBB and PKSPMA (see Figure 5.14B). However, the lines were often incomplete or appeared to have several defects. The premature detachment of the mould before polymerisation was complete was probably the main reason for these defects. Such a phenomenon did not occur when MIMIC was carried out with the PDMS moulds created with dry film photolithography. This could be due to the different height: width ratio on the PDMS moulds, compared to the previous masters created with dry film photolithography. Due to the lack of success in producing a reliable and reproducible pattern for cell culture, this technique was discarded.

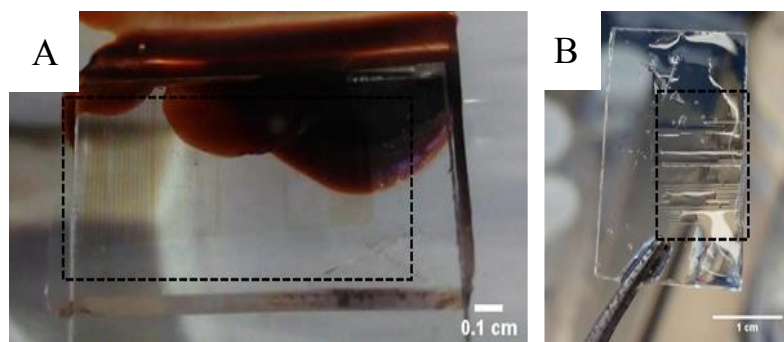


Figure 5.14. MIMIC patterns with high resolution features. A) Macroscopic images illustrating the MIMIC process carried out with the customised master made of SU-8 10 photoresist. Although initially PKSPMA solution seemed to flow only through the channels and the procedure appeared successful, early PDMS detachment or eventual leakage led to the null or incomplete formation of the pattern. B) The different hydrophilicity of BIBB/PKPSMA is shown in the sample. The defects in the pattern could be observed after the washes with dH₂O. Scale bar= 0.1 cm on the left and 1 cm on the right.

5.5.6 Conventional photolithography

5.5.6.1 PSKPMA as the starting surface

Similar to when dry film photoresist was used, starting with PKSPMA brushes would involve fewer steps and therefore, this was the first strategy attempted with wet film photoresist. PKSPMA patterning would involve the exposure of PKSPMA areas and its consequent removal with oxygen plasma treatment. Thereafter, APTES would be deposited in these areas to obtain a cell attractant coating. Although it seemed like a simple method, this process proved unviable as S1813 photoresist did not attach properly to the PKSPMA surface and when it did attach, several imperfections in the pattern were observed (Figure 5.15).

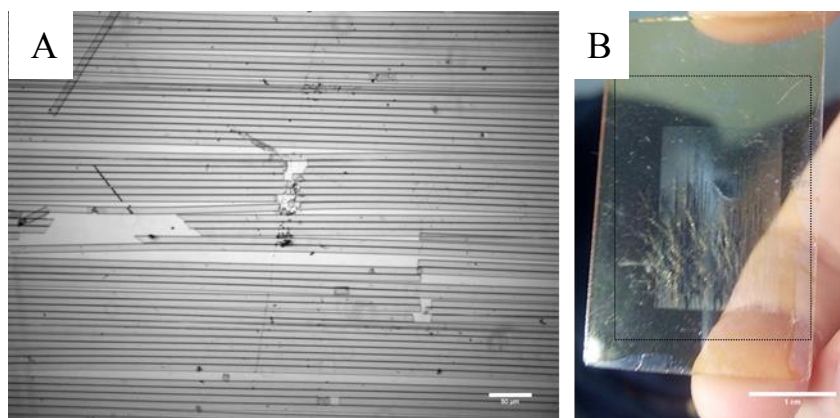


Figure 5.15. PKSPMA/APTES patterns. A) Microscopic and B) macroscopic images of S1813 photoresist on a PKSPMA glass coated sample. The lack of affinity between S1813 photoresist and the brush contributed to defects in the pattern. Scale bar= 50 μm on the left and 1 cm on the right.

When the S1813 photoresist was able to appropriately coat the PKSPMA surface, the pattern strategy was carried out as described in Section 5.2.7.1. Thereafter, SH-SY5Y's were seeded onto these samples. Although some cells were able to attach and align across the channels (see Figure 5.16), the rate of success for this process was low and thus, this strategy was discarded and other avenues were explored to obtain reliable patterns.

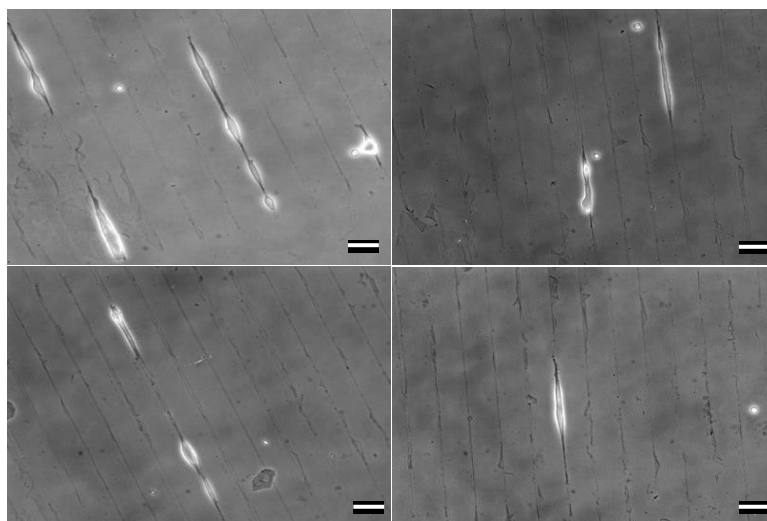


Figure 5.16. APTES/PKSPMA patterns under cell culture. Although some cells managed to attach and align towards the pattern lines, the difficulties facing the attachment of S1813 photoresist onto PKSPMA led to continuous imperfections in the pattern. Scale bar= 50 μm .

5.5.6.2 BIBB as the starting surface

An attempt to pattern BIBB/PKSPMA was also carried out as detailed in Section 5.2.7.2. Although the process resulted in the adequate attachment of S1813 photoresist, the procedure proved challenging when PKSPMA brushes were formed on the patterned areas. The responsiveness of S1813 photoresists under solvents interfered in the polymerisation steps and as a consequence, the photoresist used to cover the BIBB areas detached. As a result, the entire area was covered by PKSPMA, and the cell attractant surface was lost in the process. Thus, cells did not have a preference towards any part of the sample and cell attachment was null (Figure 5.17).



Figure 5.17. BIBB/PKSPMA patterns under culture. Due to the continuous photoresist removal during PKSPMA growth, the patterning strategy was incomplete, leading to the lack of cell response. Scale bar= 50 μm .

Due to the photoresist removal, a hard bake step was added to the photolithography process in order to maintain the photoresist in its position until the end of the chemical modification. The process followed was the same as described in Section 5.2.7.2, with the exception of the sample being hard baked for at least 15 minutes at $\sim 200^\circ\text{C}$ after developing. Contrary to previous attempts, the photoresist remained on the sample during the consequent growth of the brush. When the photoresist was no longer necessary, the sample was incubated in DMSO until its removal. Unfortunately, the strong attachment of the photoresist towards BIBB samples after hard baking, made its removal arduous and most of the photoresist remained intact even after days in DMSO (see Figure 5.18A). Nevertheless, SH-SY5Y cells were

seeded on samples where the photoresist had been partially removed. The process was successful as cells were found confined in the channels covered by BIBB and avoiding PKSPMA areas (see Figure 5.18B, white arrows). However, the complete removal of the photoresist was unfeasible and thus, this process was discarded.

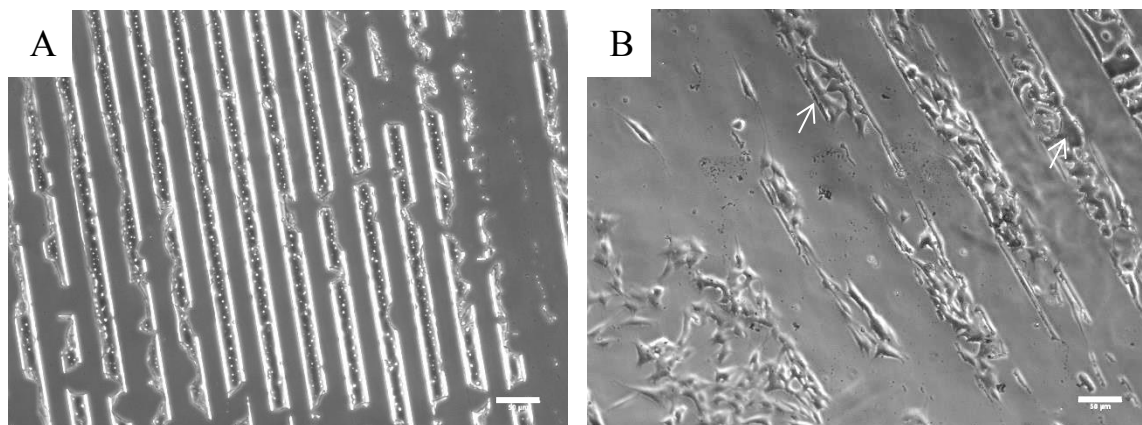


Figure 5.18. BIBB/PKSPMA patterns in cell culture after hard baking. A) BIBB/PKSPMA samples after DMSO treatment. The S1813 photoresist remained on the sample after several washes. B) BIBB/PKSPMA samples in cell culture. Although the cells attached and proliferated across the channels, traces of photoresist remained (white arrows). Scale bar= 50 μm .

5.5.6.3 Non-coated glass slide as the starting surface

Conventional photolithography was performed on non-coated glass as a starting point, following the steps described in Section 5.2.7.3. To avoid photoresist removal due to solvents in the steps involving the brush growth (APTES, BIBB and PKSPMA), the S1813 photoresist was hard baked at $\sim 200^{\circ}\text{C}$ for 15-20 minutes to ensure the photoresist was firmly baked. UV/ozone treatment, APTES, BIBB and PKSPMA steps were carried out with non-visible indication of photoresist removal in the non-coated glass areas intended for cell growth. After the polymerisation process, the sample was incubated in DMSO for photoresist removal. Unlike what happened previously (Figure 5.18), the photoresist appeared completely removed from the surface. Since this procedure (Figure 5.19) seemed successful, the possible pattern formation was analysed by AFM.

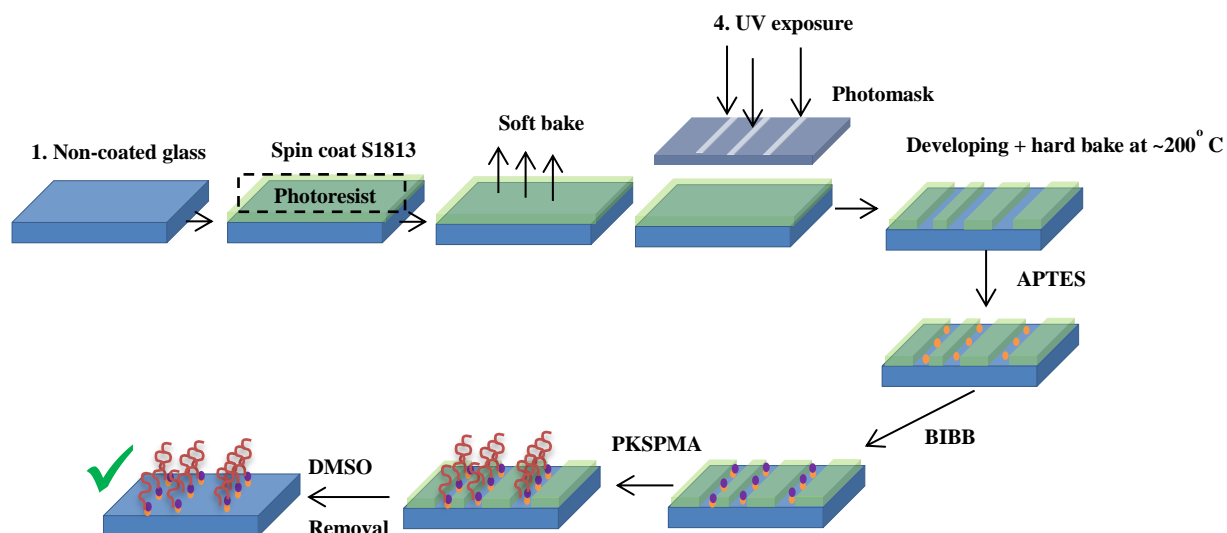


Figure 5.19. Schematic of the photolithographic procedure to obtain PKSPMA/glass patterns.

The height profile extracted from AFM analysis showed the presence of various channel widths (Figure 5.20 and Figure 5.22). The channels with the smallest width (3 μm) were not finely formed through the photolithography process, due to limitations in the equipment resolution. However, the next channel widths (5, 10 μm width) were observed by AFM analysis (Figure 5.20), showing the gaps containing the brush with a height of ~20-30 nm. The channels can be observed by a drop on the height, presenting the non-coated glass areas with the corresponding width. SH-SY5Y's also responded to these channel sizes, arranging their cell body to fit inside them (Figure 5.20). Although these channel widths were achieved under this procedure, the reproducibility of these sizes on the samples was poor and thus, the smallest channel width used for further cell experimentation was 20 μm .

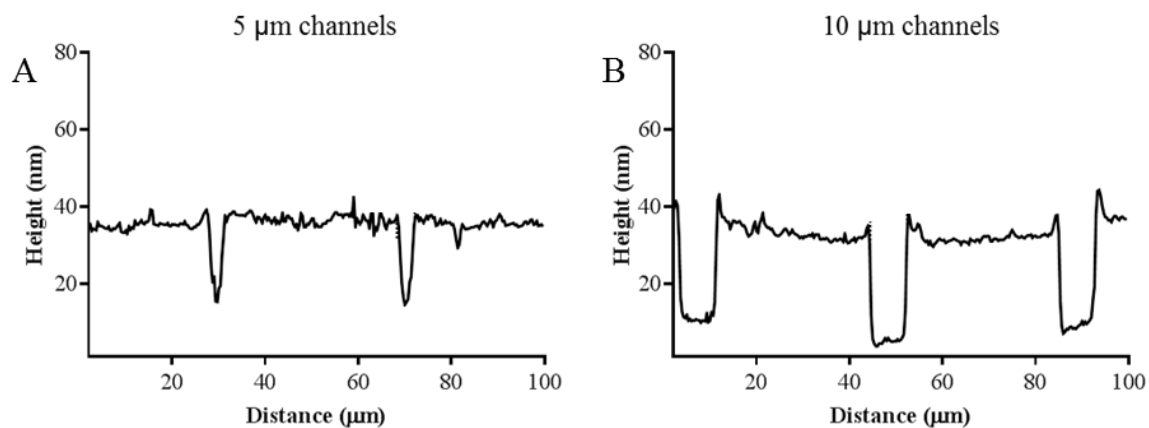


Figure 5.20. AFM height profiles showing the patterned PKSPMA polymer brush samples on glass for A) 5 μm and B) 10 channel widths. The PKSPMA brush was not present in 5 and 10 μm , but was in the gaps of 40 and 30 μm widths, respectively.

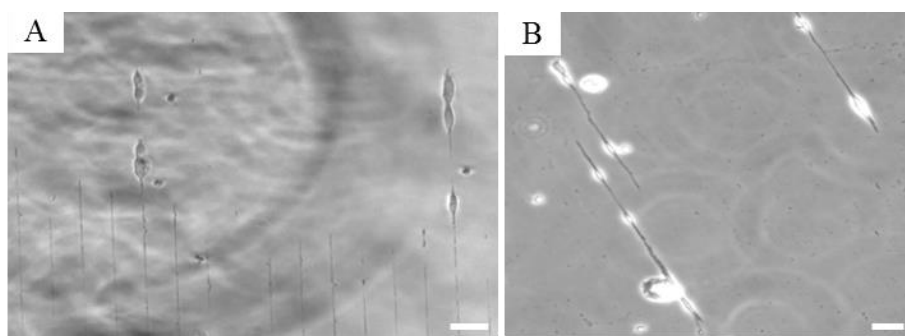


Figure 5.21. Patterns with 5 and 10 μm channel width under cell culture. Light micrographs illustrate the SH-SY5Y's response in 5 μm (A) and 10 μm (B) channel width after 3 days in growth media. Scale bar=100 μm .

Similarly, AFM profiles for the 20, 50, 75 and 100 μm channels widths were illustrated in Figure 5.22. The profiles highlight the difference in height between the PKSPMA brush (pillars) and the non-coated glass areas, as well as indicating the formation of the different channel widths.

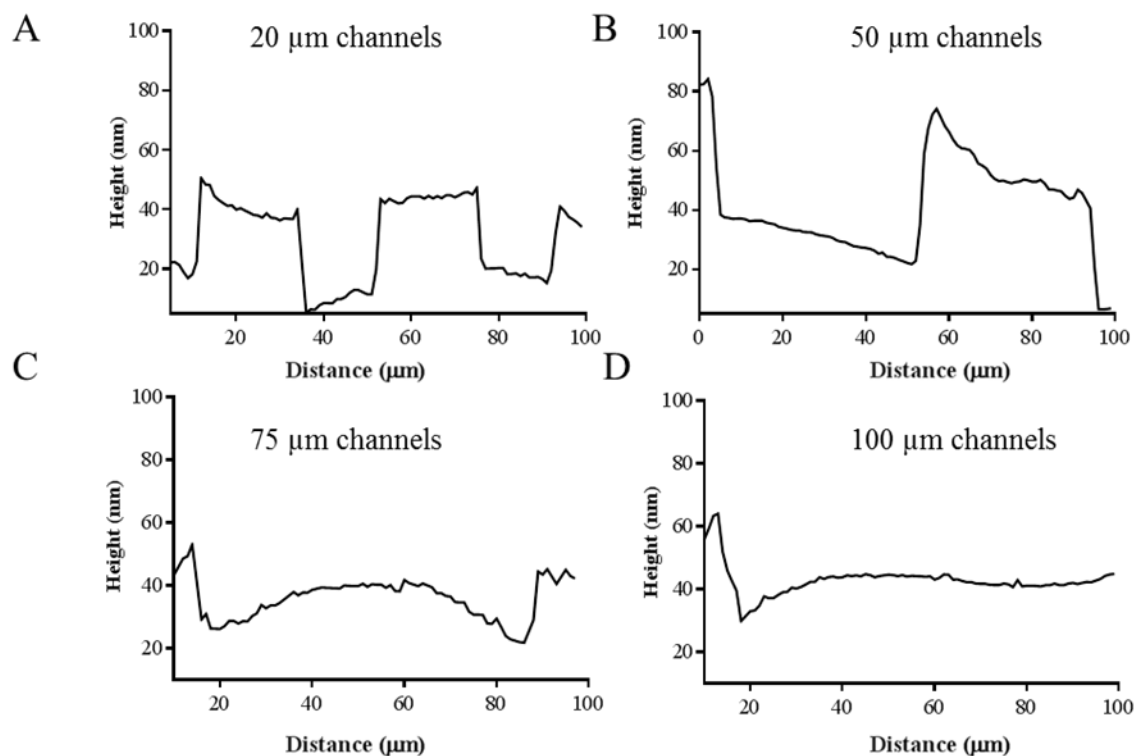


Figure 5.22. AFM height profiles showing the patterned PKSPMA polymer brush samples on glass containing approximately A) 20, B) 50, C) 75 and D) 100 μm channel widths for cell growth. The PKSPMA brush was grown in the gaps of approximately 20, 40, 80 and 100 μm widths, respectively.

The efficacy of the PKSPMA brush as a repulsive coating was illustrated in Section 5.5.3, when the brush was patterned with soft lithography. However, the geometrical constraints did not show neuronal alignment due to the wide pattern sizes. Nevertheless, the new strategy described above provided defined patterns with smaller channel sizes and thus, this methodology was utilised to show the effect of channel size (20, 50, 75 and 100 μm channel widths) on different SH-SY5Ys cell densities (5000, 10000 and 15000 cells/cm²).

Variations in the channel width showed a significant effect on neurite length, neurite number and neurite alignment. However, channel width did not affect cell confinement within the pattern (Figure 5.25). The longest neurites were observed when the channel size was 20 μm , in which cells were seen to rearrange their cytoskeleton in order to fit in the channel, exhibiting an elongated shape and extending neurites (see Figure 5.23).

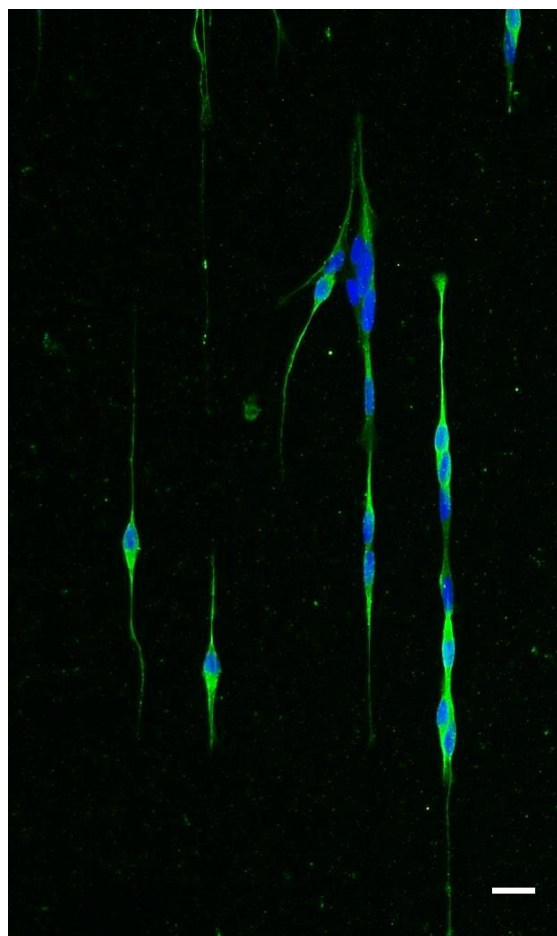


Figure 5.23. SH-SY5Ys patterned in channels of 20 μm width. Cells were seeded evenly and cultured in growth media for 3 days. To promote neurite extension, cells were consequently culture for 3 days in DM. Green= β tubulin III (neuronal cell body), blue= DAPI (nuclei). Scale bar= 50 μm .

A reduction in neurite length was observed as the channel size increased. This was likely due to an increase in cells per channel, which led to cell-cell communication rather than neurite extension (see Figure 5.24 and Figure 5.25, $p < 0.05$ between 20 vs. 100 μm for 5000 and 10000 cells/ cm^2 and 20 vs. 75 μm channel width for 5000 and 15000 cells/ cm^2). This trend was also reflected in the amount of cells generating neurites, where 50, 75 and 100 μm wide channels had fewer cells containing neurites, although this was non-significant (see Figure 5.25, $p > 0.05$ except for 20 vs. 50 μm channel width for 10000 cells/ cm^2).

Nuclei were considered perfectly aligned within the line pattern when the interquartile range value was ~ 0 . Considering this, cells were more aligned when channel size was 20 μm width,

where cells extended themselves across the line pattern, showing a certain degree of neuronal directionality. There was a clear trend towards smaller channels sizes, obtaining more aligned nuclei when compared to the bigger channel sizes (see Figure 5.25, $p < 0.05$ for 20 vs. 100 μm channel width for 5000, 10000 and 15000 cells/ cm^2 and 20 vs. 75 μm channel width for 5000 cells/ cm^2). Cell confinement, which was referred to as the efficiency of the pattern to contain the cells within the channels, showed no trends regarding the different channel sizes. This was a further indication that PKSPMA brushes were effective as a cell repulsive coating.

Further analysis was focused on whether the position of the cell within the pattern would be defined by the amount of cells used. Hence, various cell densities (5000, 10000 and 15000 cells/ cm^2) were examined for the various channels widths (Figure 5.24 and Figure 5.25). For the channel widths presented, the cell densities used showed little difference towards the parameters measured (neurite length, the percentage of cells generating neurites, nuclei alignment and cell confinement). However, some non-significant tendencies could be observed regarding the cell density used, such as the greater spreading of neurons and their neurites through the channel width for the lowest cell densities (5000 cells/ cm^2), or the less aligned and spread neurons due to overcrowding of the channels in the highest cell density (15000 cells/ cm^2). Alternatively, the medium cell density (10000 cells/ cm^2) seemed more consistent among the different parameters used and thus this cell density was used for further experimentation. It is important to mention that the seeding density used may not exactly correspond to the cells attached on the substrate. This is primarily due to cells potentially attaching to the plastic around the edge of the glass ‘sliding’ and/or ‘slipping’ below the glass slide and attaching to the tissue culture plastic. Nevertheless, the amount of pattern filled with the small, medium and high cell density used seemed consistent throughout the different samples examined.

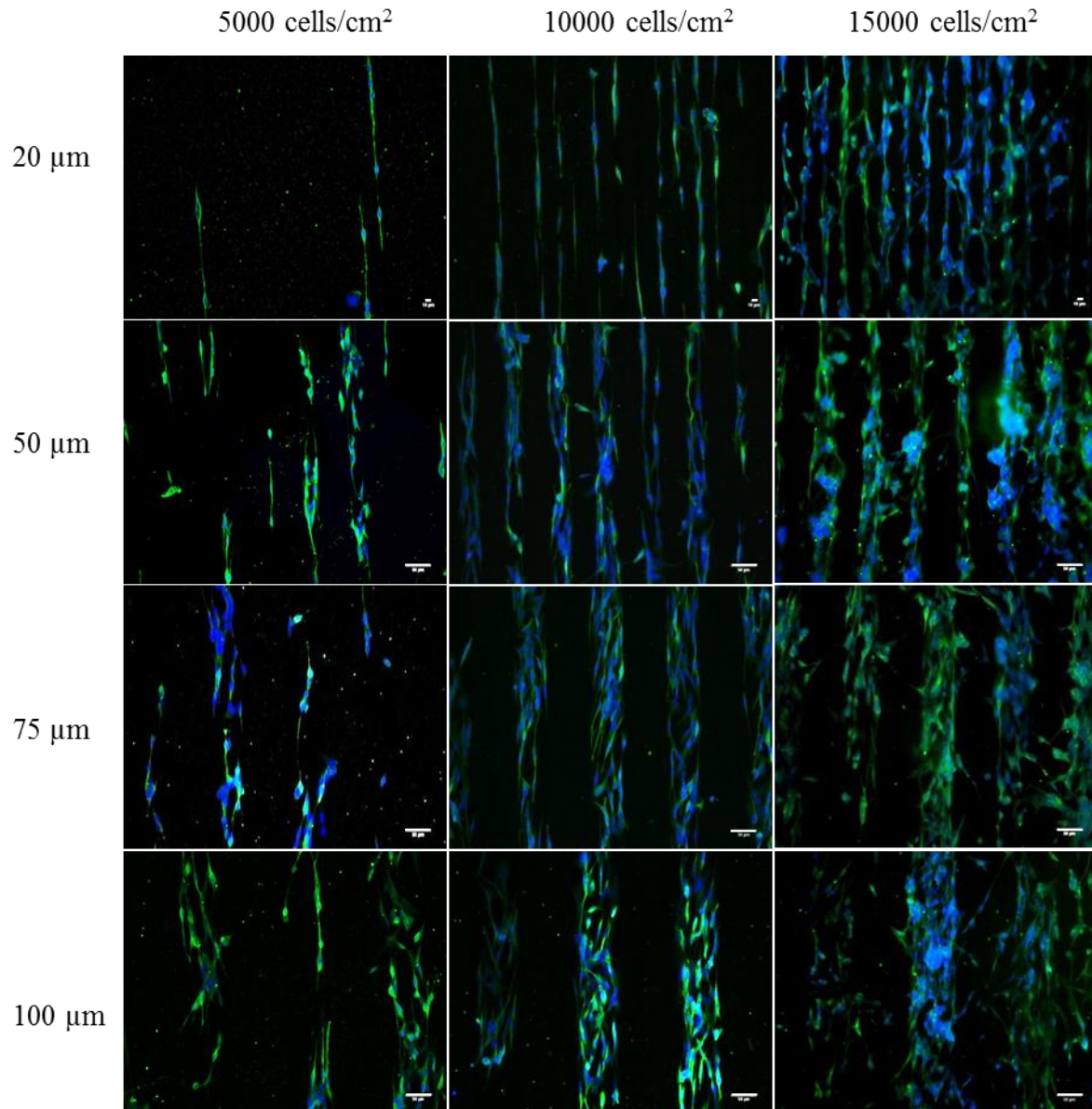


Figure 5.24. SH-SY5Y cells seeded at 5000, 10000 and 150000 cells/cm² in 20 µm, 50 µm, 75 µm and 100 µm wide channels. SH-SY5Y's were seeded evenly and cultured in growth media for 3 days. To promote neurite extension, cells were consequently culture for 3 days in DM. Scale bars are 10 µm for the 20 µm channels, and 50 µm for the remainder of the images. Green= β tubulin III (microtubules, neuronal cell body), blue= DAPI (nuclei).

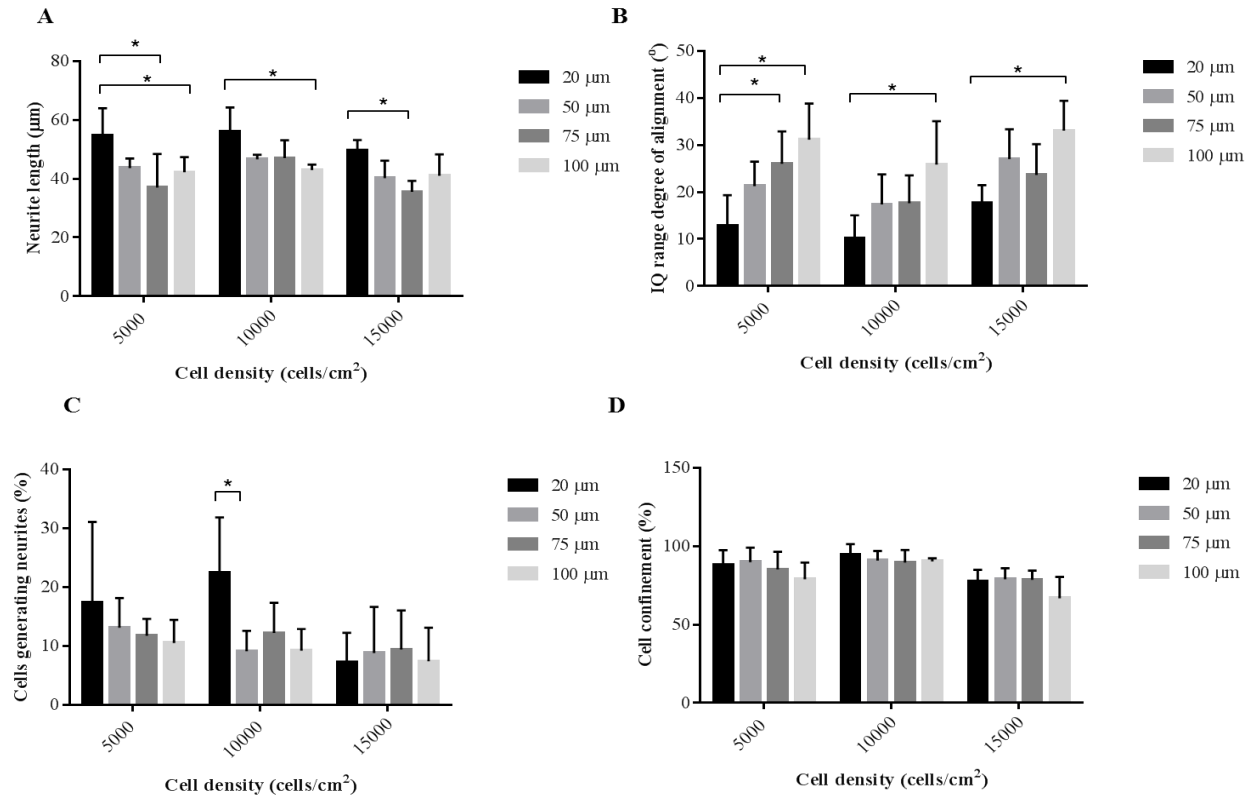


Figure 5.25. Analysis of SH-SY5Y's patterns at different cell densities (5000, 10000 and 15000 cells/cm²) and channel widths (20, 50, 75 and 100 μm). A) Average neurite length. B) Analysis of nuclei alignment within the channel. C) Percentage of cells that generated neurites within the channels. D) Cell confinement highlighted the pattern efficiency of PKSPMA to constrain cells within the channels. Error bars represent the SD of the mean. Significant differences have been highlighted with asterisks. Statistical analyses were assessed by a two-way ANOVA followed by a post-hoc Bonferroni test (* $p < 0.05$, $n = 4$).

The width of the channels also appeared to affect neurite directionality and the formation of neuronal connections. The smaller the channel size, the more directed the neurite was towards the y-axis of the channel. With the adequate cell density, neurite elongation occurred along the line pattern direction, achieving neurite directionality (Figure 5.26).

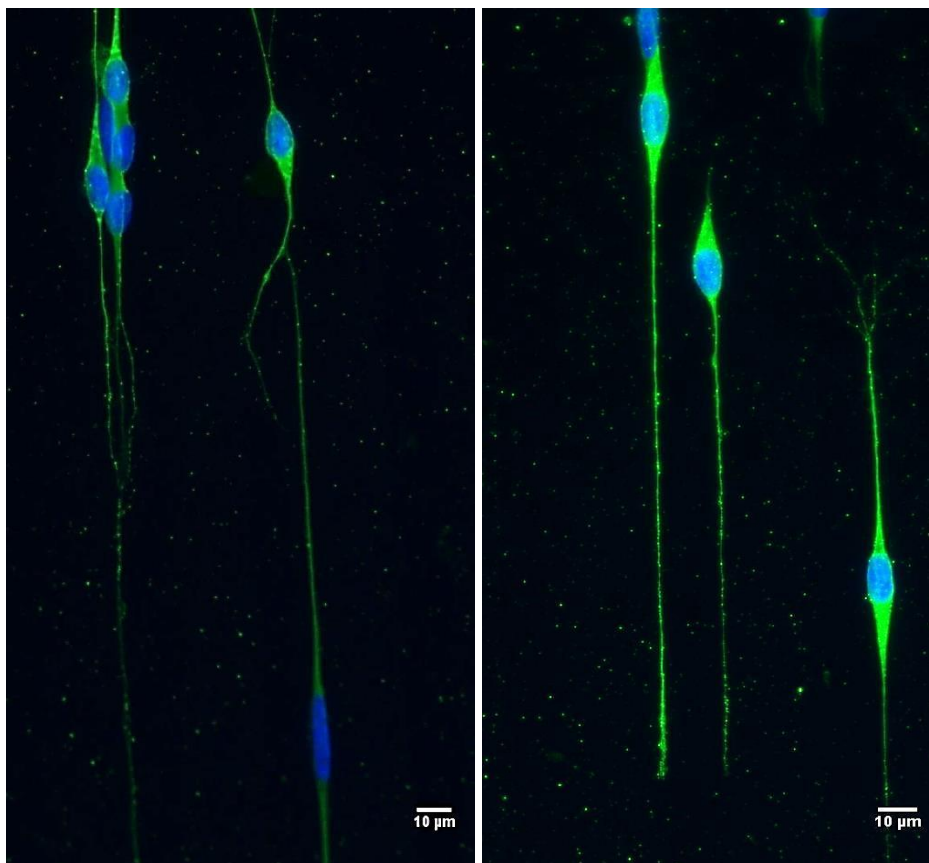


Figure 5.26. Patterned SH-SY5Y cells seeded at 10000 cells/cm² in 20 µm wide channels. When appropriate channel width and cell density was attained, neurite directionality and long extension was achieved. Green= β tubulin III (microtubules, neuronal cell body), blue= DAPI (nuclei). Scale bar= 10 µm.

Overall, these results indicated that 20 µm channel width showed the constraint of elongated cells and was suitable for obtaining neurite directionality.

5.6 Discussion

Highly organised structures with defined tracks are known to be present in the nervous system (Shah *et al.*, 2016). Neurons in the ventricular zone during development of the

forebrain follow an ordered path previously created by glial cells, suggesting the presence of guiding cues in biological systems (Lee *et al.*, 2007). Consequently, the random and uncontrolled neurite spreading in conventional cell culture conditions is not a suitable illustration of neuronal behaviour (Yamamoto *et al.*, 2012). Controlling neuronal directionality by patterning surface characteristics could overcome this issue, resulting in a great improvement for neuronal tissue engineering.

5.6.1 Controlling cell confinement from cm to μm sizes

Obtaining control over cell growth by generating a sample containing both attractive and repulsive coatings was successfully achieved (Section 5.5.1). Although the area where cells could adhere to was at least 1 cm, and there was no sign of cytoskeleton rearrangement, the wall created by the neurons at the interface of the coatings resulted in the successful control on cell confinement. XPS data confirmed the presence of both coatings within the same sample, with similar values to these coatings in individual samples (see Chapter 3). In addition, FTIR spectra showed the C=O and S=O peaks presented in PKSPMA area, which is in agreement with the literature (Ramstedt *et al.*, 2007) and with the results shown in Chapter 3.

MIMIC technique was successfully used to confine cells into more defined structures, confirming this technique can be suitable for cell patterning (Shim *et al.*, 2007). Neurons were effectively constrained within the channels, recreating the structures made of PKSPMA/BIBB patterns. By analysing the chemical environment of PKSPMA and BIBB areas, XPS data revealed the presence of sulphur traces in BIBB lines. Researchers have reported the successful inhibition of cell growth for this coating with thicknesses as small as 15 nm (Letsche *et al.*, 2009; Tan *et al.*, 2013). Thus, the presence of a small amount of S2s was likely due to contamination after sample washing rather than brush formation in the BIBB area. The patterns created by MIMIC allowed the containment of cells in specific locations. However, the channels were too wide to guide neuronal alignment (Nam *et al.*, 2014) and thus to guide possible neurite extension. In addition, the chances of finding defects on the surfaces due to imperfections from soft lithography methods (Kane *et al.*, 1999) such

as air bubbles trapped between the mould and the surface or the possible leakage that occurred when using smaller features, led the direction of this work towards other techniques.

Photolithography has been widely used due to its high resolution patterns (Senaratne *et al.*, 2005). When dry film photoresists were used, several problems made this procedure inadequate for surface patterning. Firstly, the process of lamination could damage the surface coating. Furthermore, with ink printed sheet masks and dry film photoresists, the resolution achieved was never less than 50 μm . Thus, an alternative method to place the photoresist on the sample had to be utilised. The use of wet film photoresists, chromate glass masks and a more potent UV aligner, allowed the formation of a higher pattern resolution and more reliable patterns for neuronal guidance. With the adequate parameters, this technique has great potential in cell culture applications (Falconnet *et al.*, 2006; Molnar *et al.*, 2007), allowing the development of defined patterns that permit the study of cell behaviour.

5.6.2 Does cell density and channel width affect cell rearrangement within the pattern?

Geometrical constraints are known to influence neuronal morphology (In *et al.*, 2005; Junkin and Wong, 2011). In a study performed by Nam *et al.* (2014), SH-SY5Y's were seeded on PDMS substrates containing various channel sizes (20, 40, 60 and 100 μm). The study showed that in 20 μm width patterns, only two neurites were observed and these were confined along the pattern direction. Neurites appeared highly aligned when measured in 20 μm channels, whilst a low percentage of neurites were aligned on 100 μm width channels. In addition, mean neurite length was small in wide channels such as 100 μm , but as the channel width reduced, neurite length increased. Smaller channels widths were utilised in a study performed by Klein *et al.* (1999). This group showed the patterning of SH-SY5Y's by microcontact printing in 5, 8, 10 and 20 μm wide channels. Elongated single cells could be observed in this study for 5, 8 and 10 μm width, whereas double lines of neurons were observed in the 20 μm width. This contradicts the study presented by Ino *et al.* (2005) where 20 μm wide lines were shown to give single lines of SH-SY5Y's. As observed in this current work, the amount of cells seeded could lead either to the free outward spreading of a single line of cells towards the 20 μm channels or to the presence of various cells overlapping across the width of the channel. Ino *et al.* (2005) also used two different cell densities

showing that cell spreading was reduced when cell density increased. In Klein *et al.* (1999), the cell density used was even greater than the highest cell density used in this thesis (20000 cells/cm²). The disparity between the studies could be that at high cell densities, multiple cells can position themselves across the channel at the beginning of the culture, meaning that the space to migrate across the channel becomes very limited. Other factors such as the method of seeding, the surface area occupied by the cells, etc. could influence the result. These results suggest that constraints in cell shape are greatly affected by geometrical constraints, but other factors such as the cell density could influence neuronal arrangement.

In terms of using smaller channel sizes (<20 µm), Chelli *et al.* (2014) used microcontact printing for the patterning of SH-SY5Y cells, using channel sizes ranging from 15-45 µm. The study showed single elongated cells for the smallest channel size (~15 µm). This study along with the ones described earlier in this section suggest that efforts to decrease channel widths to 1- 5 µm may not be worthwhile for cell patterning, as single elongated cells can be achieved with widths of 10-20 µm. The studies discussed above regarding ≥20 µm channels width align with the observations presented in this work, where a greater neurite length and a higher degree of alignment was observed in the small channel sizes (20 µm). Furthermore, in the present work, neurites also appeared to be aligned in 20 µm channels (see Figure 5.26), overall suggesting that geometrical constraints regulate the directionality of neurite outgrowth.

5.6.3 Chapter summary

This chapter details the optimisation of a reliable and reproducible pattern using different engineering strategies and chemical processes. The biological characterisation of the coatings in Chapter 4 was successfully reproduced in this section, where the previously described “cell repulsive” substrate was successfully adapted for cell patterning. Although smaller resolution lines (5 and 10 µm) appeared to constrain single cells and promote neurite outgrowth, these sizes were not examined here due to the lack of reproducibility in these features. Nevertheless, 20 µm wide channels were shown to promote neurite directionality when cultured under adequate parameters, obtaining a high degree of neuronal alignment and an increase in neurite length.

Chapter 5: Creating chemical patterns for neurite guidance

The micro-patterns resulted from this study could be designed so that cell-cell communication, single cell differentiation or polarisation could be monitored.

6 Interactions between neurons and myotubes in a chemically patterned co-culture

6.1 Introduction

In vitro mammalian cultures have been well established to study the complexities underpinning cell physiology. There has been a growing interest to integrate heterotypic cells within the same *in vitro* model in order to mimic functional interactions between different cell types (Grey, 2011; Smith *et al.*, 2016). Some tissues depend on the input from other biological components to mature and achieve an adult phenotype. Thus, the presence of different cell populations *in vitro* could potentially alter growth and differentiation patterns of certain cell types. This may in turn generate more mature cellular phenotypes, thus obtaining a closer resemblance to the *in vivo* microenvironment (Larkin *et al.*, 2007; Guo *et al.*, 2010; Ostrovidov *et al.*, 2014). In the case of skeletal muscle, the integration of multiple cell populations within the same culture system could be advantageous for studies regarding skeletal muscle development, functionality and pathophysiology (Martin *et al.*, 2015; Smith *et al.*, 2016). *In vivo*, this tissue connects with neural, vascular and myotendinous interfaces. Therefore, when cultures are based on a single cell type, the lack of cell-heterotypic communication can be seen as a limitation (Larkin *et al.*, 2007; Ostrovidov *et al.*, 2014).

Skeletal muscle has been studied in cell culture systems due to its great potential in regenerative medicine and cell based assays, using cell lines such as the C2C12 myoblast cell line (Cooper *et al.*, 2004; Larkin *et al.*, 2007; Ostrovidov *et al.*, 2014). The C2C12's have the ability to recreate functional skeletal muscle *in vitro* due to its capability to differentiate into mature myotubes (Sharples *et al.*, 2012; Ostrovidov *et al.*, 2014). Various studies noted the difference in cell functionality when systems integrate heterotypic cells within the same culture (Martin *et al.*, 2015). Cooper *et al.* (2004) showed a higher degree of myotube formation and survival when C2C12's were co-cultured with fibroblasts. Likewise, Cairns *et al.* (2010) co-cultured chondrocytes with C2C12's, and found that co-culturing muscle and cartilage resulted in an increase in cartilage matrix production.

It is important to develop systems whereby neurons are co-cultured with skeletal muscle cells to aid the study of the mechanisms underpinning the neuron-muscle interface, known as the neuromuscular junction (Larkin *et al.*, 2007; Martin *et al.*, 2015). Larkin *et al.* (2007) showed that by adding neurons into skeletal muscle constructs, an improvement in muscle contractile

force and functionality was observed. Similarly, a greater myotube formation was observed in nerve-muscle co-cultures of C2C12's and PC12 neurons when these were compared to aneural cultures (Ostrovidov *et al.*, 2014). There is evidently a positive interaction regarding neuronal-muscle co-cultures. However, the lack of control on the growth and position of both cell types makes the specific study of extra and intra-cellular communication challenging, preventing the formation of accurate *in vitro* models (Zahavi *et al.*, 2015).

Systems aimed to separate neuronal and skeletal muscle cells to control directionality and synapses are becoming a very useful tool in research, where the control of the different cell microenvironments allows for a better understanding of NMJ processes and neuron-fibre interactions (Zahavi *et al.*, 2015). Compartmentalised microfluidic devices have been widely used in this area, however, the use of PDMS in these devices has several disadvantages (permeability of PDMS, adsorption of small molecules, low implantation possibilities, etc.) (Halldorsson *et al.*, 2005) preventing the creation of unbiased results. Alternatively, the use of patterned chemical surface cues could potentially be developed on a wide range of materials (Raynor *et al.*, 2008; Wan *et al.*, 2013; Sheng *et al.*, 2015), providing a tool to constrain the differing cell types to specific areas of any biodevice.

6.1.1 The effect of retinoic acid on skeletal muscle

For systems with various cell populations, improving the culture conditions to attain the successful growth of both cell types is essential. Commonly, every cell type contain their own growth and differentiation conditions and thus, optimisation needs to be carried out to ascertain the most suitable conditions for co-culturing (Goers *et al.*, 2014). The use of retinoic acid in neuronal cell culture has been widely used due to its effect in various biological processes, such as cell differentiation (Encinas *et al.*, 2000; Clagett-Dame *et al.* 2006; Joshi *et al.*, 2006; Grey, 2011). The mechanism of action is related to the family of nuclear receptors retinoic acid and retinoic X (RARs and RXRs, respectively) (Clagett-Dame *et al.*, 2006; Xie *et al.* 2010). Retinoic acid binds to both of these receptors forming a heterodimer. This in turn binds to promoter regions on DNA coding for target genes, inducing their transcription and triggering effects within the cell (Clagett-Dame *et al.*, 2006; Joshi *et al.*, 2006; Xie *et al.*, 2010; Grey, 2011). The role of retinoic acid in neurogenesis is

well recognised *in vitro* and thus, *all trans* retinoic acid (ATRA) has been utilised as a potential differentiating agent (Clagett-Dame *et al.*, 2006; Kovalevich and Langford, 2013). In terms of the effect of retinoic acid in muscle, different studies have found conflicting results, since it has been shown to both inhibit and promote muscle development. Xiao *et al.* (1995) showed that retinoic acid in primary cultures (neonatal limbs, limb buds, embryonic somites) inhibited myogenic differentiation depending on the dose used. Furthermore, it was found that there was a repressed accumulation of myosin heavy chain protein and a decrease in myotube formation when ATRA was added to the culture. The use of ATRA in a C2C12's culture study performed by Zhu *et al.* (2009) showed improved fusion of myoblasts along with a greater expression of myogenic markers. The different concentration of retinoic acid as well as the different cell sources used between these studies varied significantly, which might be the cause of such disparity.

6.1.2 Objectives of the chapter

Directing neuronal cells towards specific targets, such as skeletal muscle, is essential to induce defined and localised heterotypic cell communication. Therefore, the aim of this chapter was to use the chemical patterned surfaces created in Chapter 5 to direct the patterned neurons towards the C2C12 skeletal muscle cell line. The culture of both cell types required media and experimental set up optimisation and thus, this part of the thesis highlights the different attempts used to assess such difficulties. The organised neuron muscle co-culture developed in this work could contribute to the continuous development of *in vitro* neuromuscular models, providing a step forward in the accurate use of these models in the future.

6.2 Methods

C2C12 murine myoblasts and SH-SY5Y neuroblastoma cells were routinely cultured, passaged and plated according to Section 2.4.2. The standard growth and differentiation conditions for the mono-culture of each cell type has been described in Sections 2.4.1 and 2.4.2. Likewise, the procedure used for the immunostaining process of both cells lines has also been previously described (Section 2.5.9). For co-culture experimentation, the GM used consisted of Dulbecco's modified Eagle's medium GlutaMAX supplemented with 10% of

heat –inactivated foetal bovine serum (NFBS) and 1% of Penicillin/Streptomycin (P/S). For co-culture differentiation, the DM utilised was optimised (see Sections 6.3.2 and 6.3.3). This DM consisted of Dulbecco's modified Eagle's medium GlutaMAX, supplemented with 2% NFBS, 1% P/S and 1 μ M of ATRA.

6.2.1 Effect of repulsive and attractive coatings on C2C12's

C2C12 murine myoblasts were cultured at 10000 cells/cm² on PKSPMA, BIBB and control samples for 3 days in GM. Thereafter, cells were cultured for 3 days in standard DM for muscle differentiation consisting of DMEM, 2% Horse serum (HS) and 1% Penicillin/Streptomycin (P/S). The samples were fixed and stained according to Section 2.5.9. The half-and-half sample (binary sample, BIBB/PKSPMA) described in Section 5.2.1 for neurons was also attempted with myoblasts. A cell density of 10000 cells/cm² were seeded and maintained in the half-and-half sample for 7 days to examine whether the effect of PKSPMA on C2C12's was the same as for SH-SY5Y's. GM was changed daily and DM was changed every 2 days.

6.2.2 Differentiation media optimisation for C2C12's and SH-SY5Y's: reduction in serum percentage

The differentiation media used in mono-cultures for C2C12's and SH-SY5Y's was different in terms of the serum and its percentage. Therefore, optimisation experiments were carried out to obtain a differentiation media for co-culture experiments that promoted neurite outgrowth and myotube formation. Consequently, three coverslips were placed in 6-well plates and C2C12's were seeded at a density of 10000 cells/cm². Cells were cultured in GM consisting of DMEM, 20% foetal bovine serum (MFBS, Gibco) and 1% Penicillin/Streptomycin (PenStrep: 100 units/mL penicillin and 100 μ g/mL streptomycin, Sigma Aldrich) for 3 days. For SH-SY5Y's, cells were seeded at 10000 cells/cm² and maintained in GM consisting of Dulbecco's modified Eagle's medium GlutaMAX (Gibco, Invitrogen) supplemented with 10% heat –inactivated foetal bovine serum (NFBS) (Gibco, Invitrogen) and 1% Penicillin/Streptomycin. To find a suitable differentiation media where both C2C12's and SH-SY5Y's could differentiate, various differentiation media (see Table 6.1) were utilised after a 3 day GM period and these were maintained for 3 further days to

observe cell morphology. Five random images were taken per coverslip, obtaining 15 images per repeat. DM was changed every 2 days.

Table 6.1. Composition of different media used for the co-culture of SH-SY5Y's and C2C12's. Foetal bovine serum (MFBS), heat –inactivated foetal bovine serum (NFBS) and horse serum (HS) were utilised to find the optimum differentiation media for both cell types.

Differentiation media	Components
DM1	GlutaMAX + 2% HS + 1% P/S
DM2	GlutaMAX + 2% HS + 10 μ M ATRA + 1% P/S
DM3	GlutaMAX + 2% NFBS + 10 μ M ATRA + 1% P/S
DM4	GlutaMAX + 2% MFBS + 10 μ M ATRA + 1% P/S
DM5	GlutaMAX + 5% NFBS + 10 μ M ATRA + 1% P/S
DM6	GlutaMAX + 5% MFBS + 10 μ M ATRA + 1% P/S

6.2.3 Differentiation media optimisation for C2C12's and SH-SY5Y's: ATRA dose effect

The observations performed in experiments regarding DM optimisation indicated variations in myotube morphology when the neuronal differentiating component (*all trans* retinoic acid, ATRA) was used on C2C12's (Section 6.3.3). Thus, 10000 cells/cm² of C2C12's were plated and grown for 3 days in GM and thereafter, C2C12's were differentiated with GlutaMAX, 2% NFBS (according to results obtained, see Section 6.3.1) and differing concentrations of ATRA (see Table 6.2). The same procedure was also carried out on SH-SY5Y's as these DM differed from the routine neuronal DM.

Table 6.2. Composition of different media used with differing concentration of *all-trans* retinoic acid (ATRA) for the co-culture of SH-SY5Y's and C2C12's.

Differentiation media	Components
DM7	GlutaMAX + 2% NFBS + 10 μ M ATRA + 1% P/S
DM8	GlutaMAX + 2% NFBS + 5 μ M ATRA + 1% P/S
DM9	GlutaMAX + 2% NFBS + 1 μ M ATRA + 1% P/S
DM10	GlutaMAX + 2% NFBS + 0.5 μ M ATRA + 1% P/S
DM11	GlutaMAX + 2% NFBS + 0.1 μ M ATRA + 1% P/S

6.2.4 Co-culture experimentation with SH-SY5Y's and C2C12's using chemical patterning and physical barrier

C2C12's and SH-SY5Y's were both cultured at a density of 10000 cells/cm² on a sample with two different areas: one made of non-coated/PKSPMA patterns (as the ones utilised in Chapter 5, see Figure 6.1) and other containing unpatterned non-coated glass. In order to separate both cells in their corresponding area, each cell type was seeded by drop culture on one side of the sample (neurons= patterned area, muscle= non-patterned area) and were allowed to attach. After 30 minutes, the well containing the sample was filled with GM. In the middle of the sample, either a 0.2 mm coverslip or a rectangular PDMS wall of ~0.2-0.3 cm was placed to avoid cell migration from one area to the other, until differentiation was induced. The routine protocol was 3 days in GM and once both cell populations were proximate to each other, differentiation was induced for a further 3 days. Depending on the level of proximity of the respective cell populations or difficulties during experimentation, the time course either was extended or shortened as appropriate (see Section 6.3).

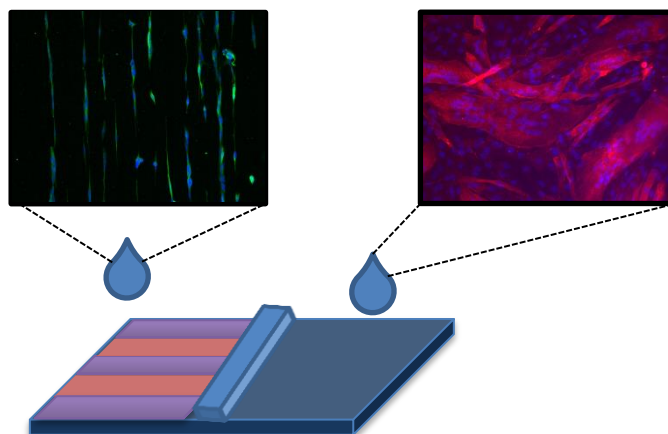


Figure 6.1. Experimental set-up for co-culture. A patterned region made of PKSPMA/glass was created for the neurons. On the other side, non-coated glass was prepared for the C2C12's to adhere. A barrier was set up at the interface to avoid the undesired mixing of both cell types before differentiation.

6.2.4.1 Co-culture experimentation with SH-SY5Y's and C2C12's without a physical barrier

This experimental set-up was similar to that described in Section 6.2.4. A sample with a patterned and a non-patterned area was used for each cell type (neurons= patterned area, muscle= non-patterned area, Figure 6.2). As no barrier was used to separate both cell types, different seeding methods were applied to ensure the connection of both cells types. In the first approach, both cell types were seeded by drop culture at the same time (10000 cells/cm^2) and allowed to attach in each corresponding region. On the second approach, 10000 cells/cm^2 of SH-SY5Y's were added onto the pattern, allowed to adhere and maintained in GM for 2 days. Thereafter, C2C12's were added on the other side, allowed to grow until confluency, and then both were differentiated for 3 days. In the final approach, C2C12's were seeded first at a cell density of 10000 cells/cm^2 , grown until confluency, and then differentiated to induce myotube formation. Thereafter, SH-SY5Y's were seeded on the patterned area, allowed to attach and maintained in differentiation media until neurons reached the C2C12's area.

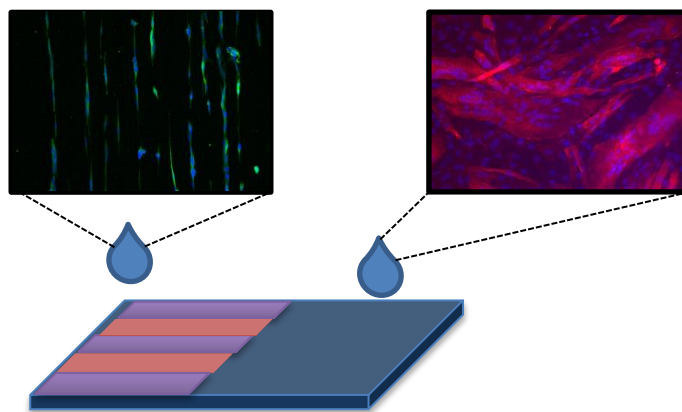


Figure 6.2. Experimental set-up for co-culture with no barrier at the interface. A patterned region made of PKSPMA/glass was created for the neurons. On the other side, non-coated glass was used for the culture of C2C12's. Droplets of cells were seeded on both sides to allow heterotypical cell communication.

6.2.5 Statistical analysis

All results are presented as mean \pm SD, unless otherwise stated. Media compatibility data was analysed with Prisma GraphPad 6.0 software. A standard one-way ANOVA with multiple comparison Bonferroni post-hoc test was used to determine differences in neurite length, myotube width, myotube number and nuclei per myotube. Image analysis regarding myotube and neuron morphology has been described in Chapter 2, Section 2.5.10. Differences were considered statistically significant when $p \leq 0.05$.

6.3 Results

6.3.1 Repulsive and attractive coatings on C2C12's

The main purpose of this chapter was to co-culture muscle and neuronal cells on semi-patterned areas to obtain an organised co-culture system. To this end, C2C12's were analysed to assess whether the “cell repulsive” coating for SH-SY5Y's (PKSPMA; see Chapter 5) had the same inhibiting effect on C2C12's (Figure 6.3). By finding a similar response for C2C12's, the patterning of different areas with the same principle as for SH-SY5Y's could be used. Consequently, C2C12's were cultured for a week in the binary coating samples prepared in Section 5.2.2 for neurons. Likewise, these cells were also cultured on independent samples of PKSPMA, BIBB and non-coated glass for 3 days in GM, followed by

3 days in DM to enhance myoblast fusion into multi-nucleated myotubes (see Figure 6.3A). As observed in Figure 6.3A, C2C12's successfully grew and differentiated on independent non-coated glass (CTRL) and BIBB surfaces, whilst a very low cell attachment was found on PKSPMA samples. The use of the binary coating sample (Figure 6.3B) resulted in the growth and proliferation of C2C12's in the BIBB region until they reached the BIBB-PKSPMA interface, where cells stopped migrating. Once in the PKSPMA area, attachment and consequential growth of myoblasts was inhibited, as previously observed with SH-SY5Y's (Section 5.5.1). Therefore, the PKSPMA brush acted as an efficient "cell repulsive" coating for C2C12's, in the independent samples and in the samples composed of BIBB and PKSPMA.

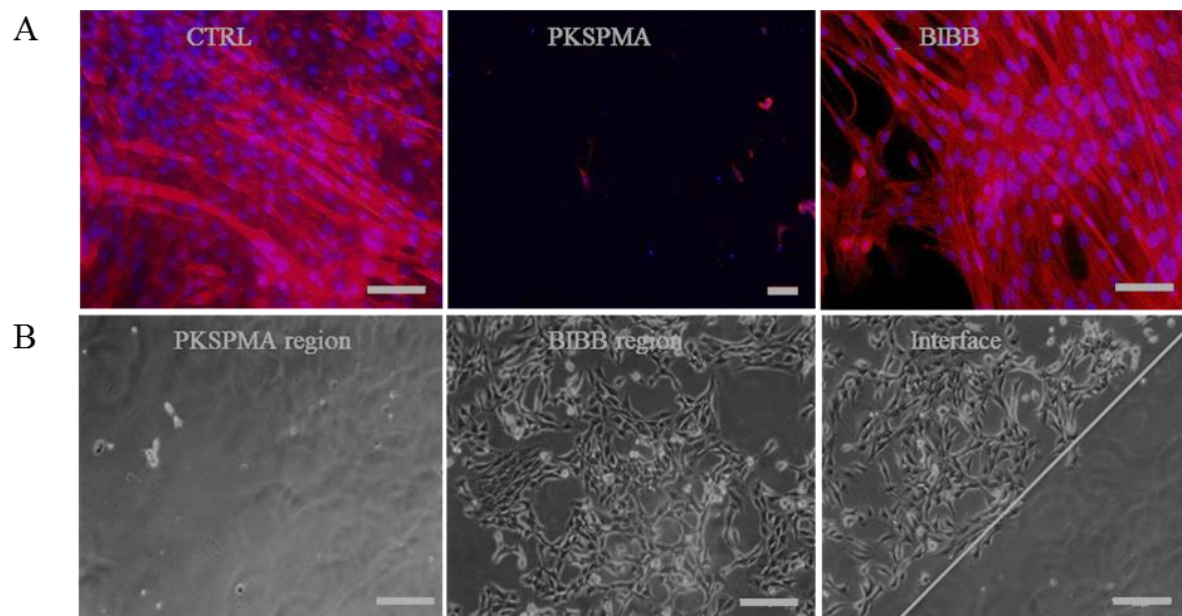


Figure 6.3. Effect of BIBB and PKSPMA surfaces in C2C12's. A) Fluorescence micrographs illustrating the culture of C2C12's on non-coated glass slides (CTRL), PKSPMA and BIBB samples. B) Light micrographs representing BIBB and PKSPMA areas after 3 days in GM. The white line drawn across the right micrograph highlights the area where BIBB finishes and PKSPMA starts. Red= rhodamine phalloidin to define F-actin filaments and blue= DAPI as a nuclear counterstain. Scale bar= 100 μ m.

6.3.2 Differentiation media optimisation for C2C12's and SH-SY5Y's: reduction in serum percentage

Once the main surface coatings were examined under both cell types, the next step was to generate a media environment where both neurons and muscle cells could differentiate together. As each cell line typically requires their own differentiation media, various combinations were used to optimise differentiation conditions for both cell types. To this end, C2C12's and SH-SY5Y's were treated with four different combinations of DM (see Figure 6.4 and Table 6.1). The C2C12's were firstly treated with the differentiation media components for the neurons containing 10% of heat-inactivated foetal bovine serum (NFBS) and 10 μ M of ATRA. After 3 days in this media, no sign of myotube formation was observed (Figure 6.4A). Consequently, the next condition consisting of 10% of the serum used for C2C12's growth (MFBS) containing 10 μ M of ATRA was examined. Similar to the first treatment, myotube formation was not accomplished and cells continued proliferating across the wells (Figure 6.4B). The third combination consisted of a mixture of both DM for neuron and muscle (2% HS + 10 μ M ATRA). In this case, morphological indication of myotube formation was observed (see Figure 6.4C). The established DM for C2C12's was also used as the control for comparison (GlutaMAX + 2% HS, D) and as expected, myoblasts fused to form myotubes. It is important to mention that the myotubes seen in condition C were somewhat thinner than in the control samples. Nevertheless, myotube formation was achieved with condition C and D, which was necessary for further neuronal-muscle co-cultures.

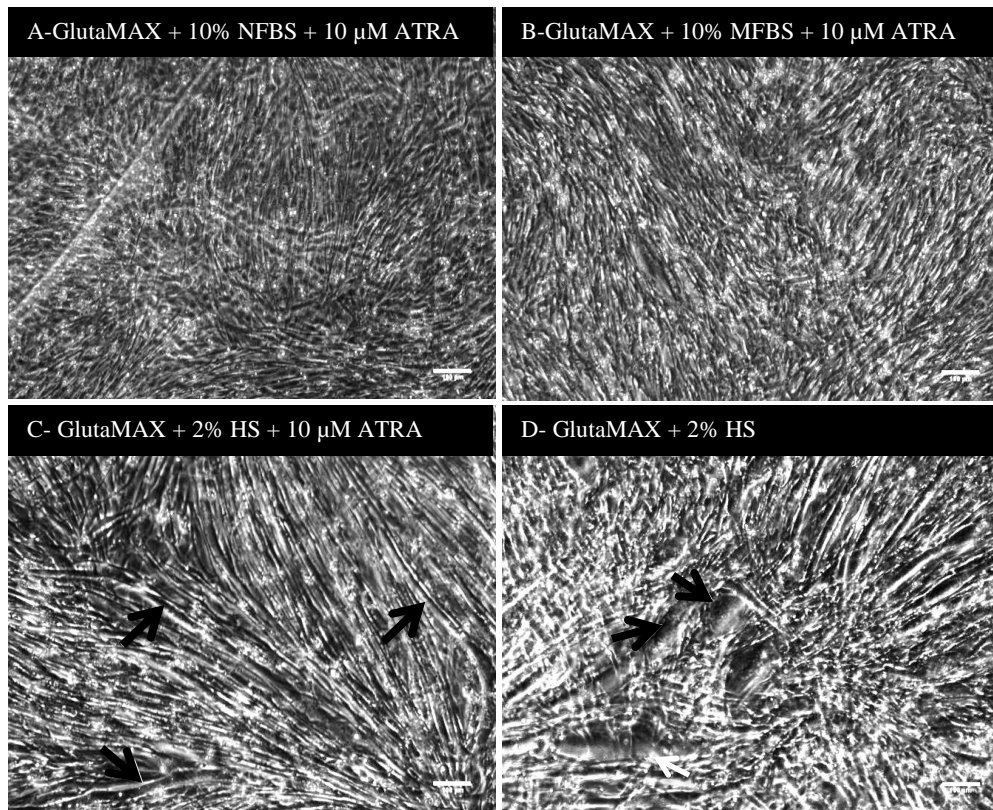


Figure 6.4. Phase contrast micrographs of C2C12's after 3 days in various DM. The different DM have been labelled on the images for clarity. A) CTRL DM for neurons containing GlutaMAX, 10% NFBS and 10 μ M ATRA. B) DM containing GlutaMAX, 10% MFBS and 10 μ M ATRA. C) Combination of both neuronal and muscle DM containing GlutaMAX, 2% HS and 10 μ M ATRA. D) CTRL DM for C2C12's containing GlutaMAX and 2% HS. The white arrows indicate the presence of myotubes within the culture. Scale bar= 100 μ m.

The same media conditions were utilised for the culture of SH-SY5Y's. As expected, the standard DM for the neurons promoted the formation of neurites along with an elongated cell shape (Figure 6.5A). Similar morphology was observed for the condition B, where elongated cells and neurite extensions were shown (Figure 6.5B). In contrast, the change from MFBS and NFBS to HS, with or without ATRA, resulted in detached or clustered structures forming clumps and thus, presenting a lack of neurite extension (see Figure 6.5C and D).

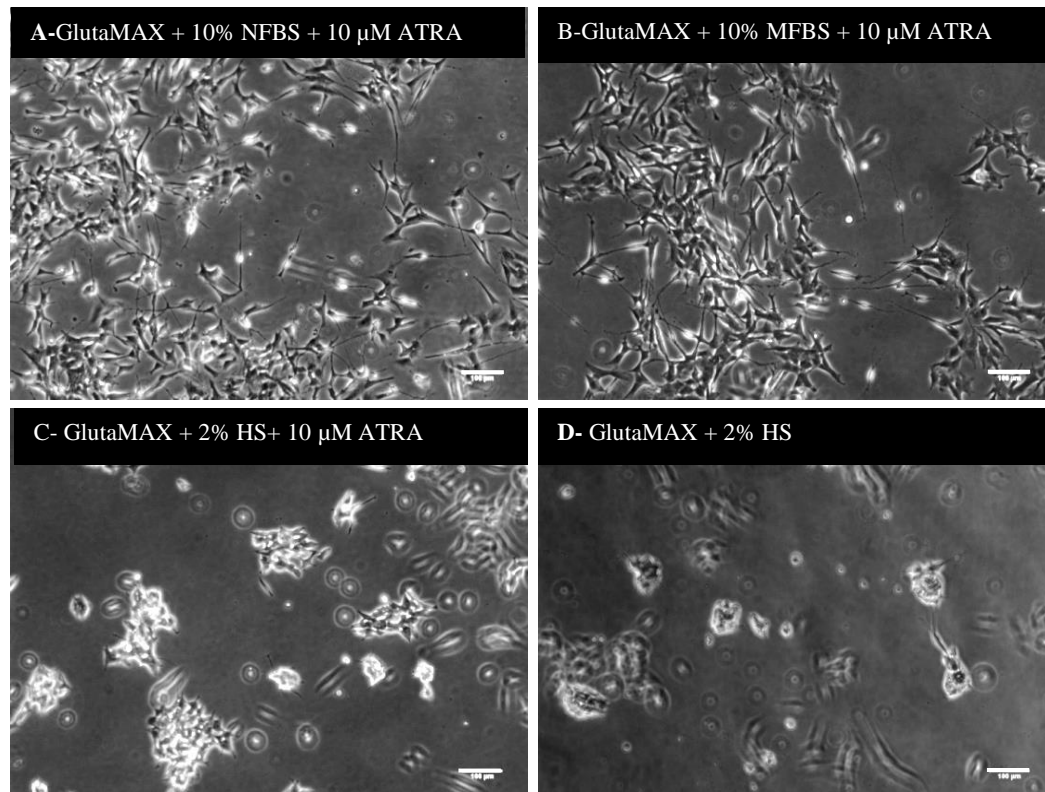


Figure 6.5. Phase contrast micrographs of SH-SY5Y's after 3 days in various DM. The different DM have been labelled on the images for clarity. A) CTRL DM for neurons containing GlutaMAX, 10% NFBS and 10 μ M ATRA. B) DM containing GlutaMAX, 10% MFBS and 10 μ M ATRA. C) Combination of both neuronal and muscle containing GlutaMAX, 2% HS and 10 μ M ATRA. D) CTRL DM for C2C12's containing GlutaMAX and 2% HS. Scale bar= 100 μ m.

It was clear after these experiments that the conditions that promoted myotube formation (C and D) were not suitable for neuron differentiation, due to neuronal detachment and clump formation. Likewise, the differentiation media conditions that promoted neurite extension were lacking myotube formation. Thus, alternative media conditions were used, consisting of different percentages of both MFBS and NFBS (2% and 5%) along with 10 μ M of ATRA. For the conditions with a reduction in serum percentage, C2C12's showed myotube formation, with non-statistical differences in the number of myotubes across the different conditions when compared with the control condition (2% HS, $p > 0.05$, Figure 6.6). In terms of myotube width, myotubes were thinner in the media with different serum percentages than in the control samples (2% HS, $p < 0.05$, Figure 6.6). The main difference among the control condition vs. the conditions with a reduced serum percentage was the presence of ATRA in

the culture, leading to the supposition that the concentration of retinoic acid could be promoting such morphological changes. Nevertheless, the DM consisting of 2% NFBS and ATRA was the most adequate, given that the number of myotubes was consistent and the width of the myotube was the most similar to the control samples.

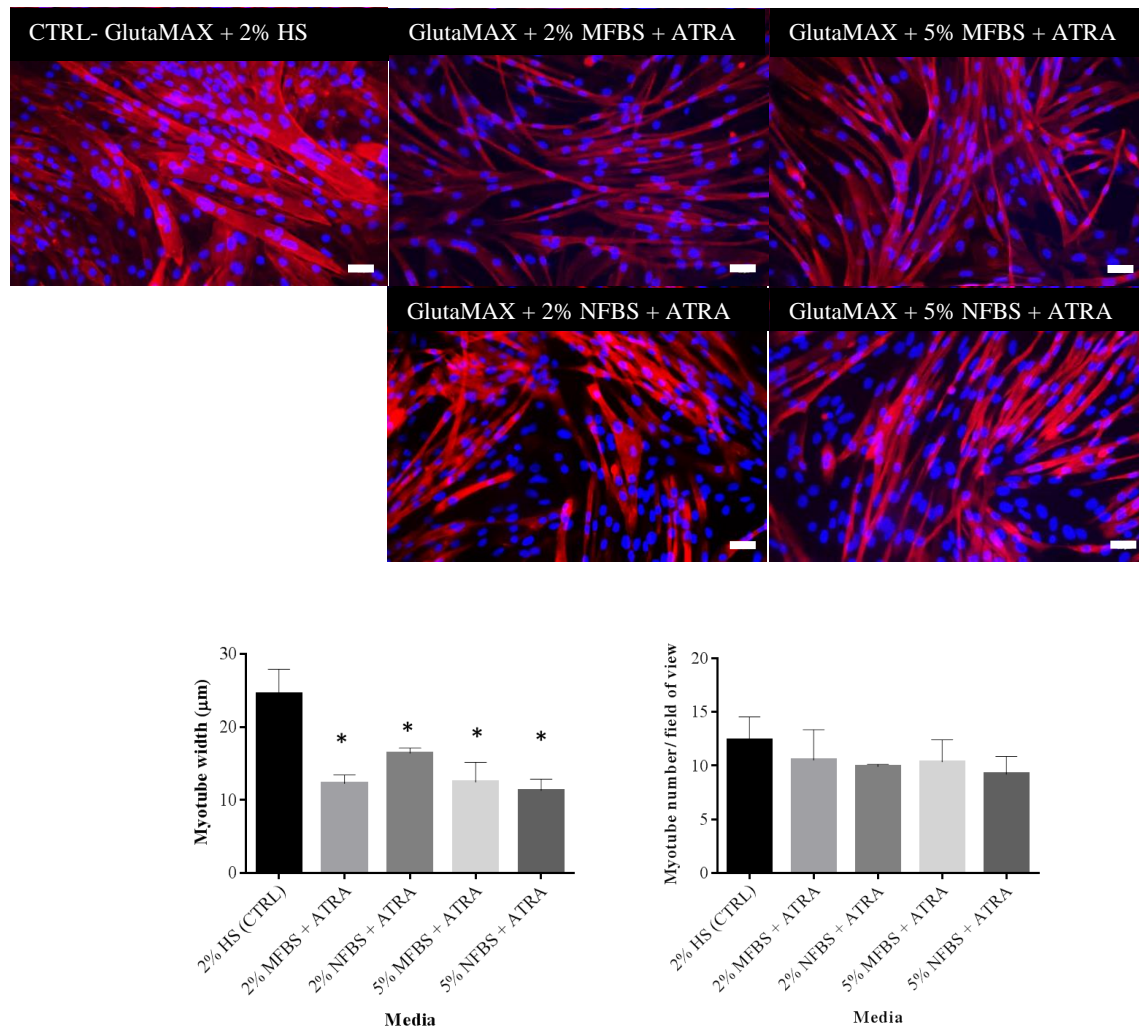


Figure 6.6. Fluorescence micrographs of C2C12's myoblasts and myotube morphology analysis after 3 days in various DM. The different DM have been labelled on the images for clarity. Myotube width and the number of myotubes were analysed to discern differences among the conditions. Error bars correspond to SD of the mean (n= 4). Images have been stained with rhodamine phalloidin to define F-actin filaments and DAPI as nuclear counterstain. A one-way ANOVA with a multiple comparison Bonferroni post-hoc test was used to analyse differences among the different conditions. Asterisks indicate significant differences when compared to 2% HS ($p < 0.05$). Scale bar= 40 μm.

The same culture conditions were consequently used on SH-SY5Y's. The different serum and percentage used did not seem to inhibit neurite extension. On the contrary, there was a slight increase in neurite length for all of the conditions when compared with the control DM used for neuronal differentiation, although it was not significant ($p > 0.05$, Figure 6.7). To conclude, 2% NFBS with ATRA was chosen as the DM for the co-culture, since neurite length and myotube formation were enhanced with this condition. Furthermore, the effect on myotube width was least detrimental in this condition when compared to the other differentiation media used, and thus this condition was consequently used for further experimentation.

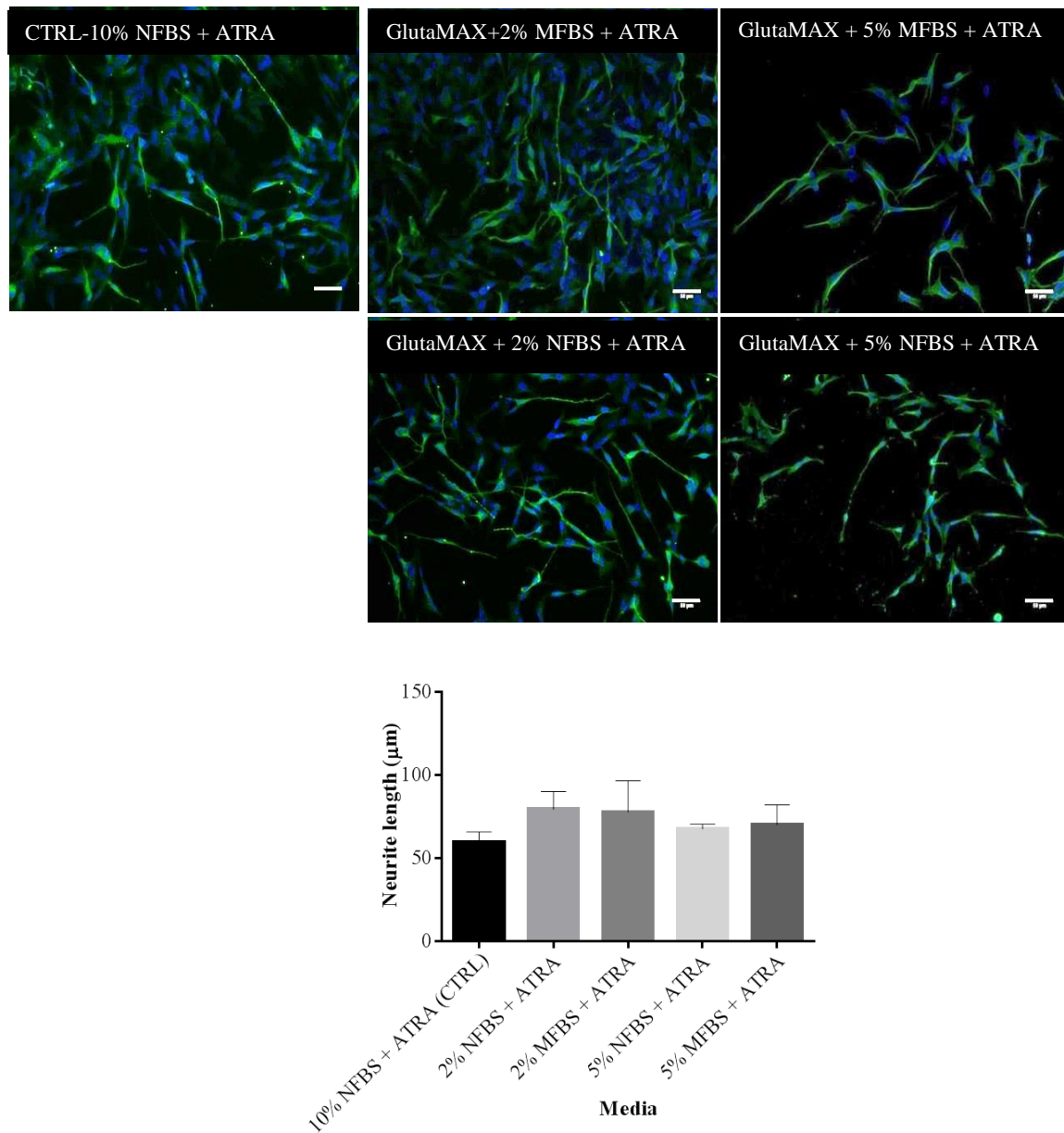


Figure 6.7. Fluorescence micrographs of SH-SY5Y's and neurite length analysis after 3 days in various DM. The different DM have been labelled on the images for clarity. Neurite length was measured and a standard one-way ANOVA with multiple comparison Bonferroni post-hoc test was used to analyse differences among conditions. Error bars correspond to SD of the mean (n= 4). Green represents the neurons stained with β tubulin III and blue represents the nuclei stained with DAPI. Asterisks indicate differences when $p < 0.05$. Scale bar= 50 μ m.

6.3.3 Differentiation media optimisation for C2C12's and SH-SY5Y's: ATRA dose effect

Morphological variations in myotube width have been observed in cultures where ATRA was added (see Figure 6.6). Therefore, differing ATRA concentrations were used to analyse whether this differentiating agent had any relation to the changes in myotube width. Thus, a concentration of ATRA ranging from 0.1-10 μM was used for experimentation (see Figure 6.8). After using different doses of ATRA, the number of myotubes and the degree of maturation (nuclei per myotube) were similar among the different doses used. A slight increase in myotube number was produced when ATRA was present, although no significant differences were reported ($p>0.05$). There was a large difference in myotube width when the concentration of ATRA increased. In the control samples (no ATRA), the widest myotubes were $\sim 25 \mu\text{m}$. However, when small doses of ATRA were added, myotubes appeared thinner, obtaining an exponential reduction in myotube width from the lowest to the highest concentrations of ATRA with significant differences for all of the doses used when compared to the control samples ($p<0.05$, see Figure 6.8). The reduction in myotube width became particularly drastic when 5 μM and 10 μM of ATRA were used. At the highest concentration (10 μM), the myotube width was reduced by nearly half that of the control (no ATRA, see Figure 6.8). This data demonstrate that high concentrations of ATRA can lead to morphological impairment of myotubes and thus, lower doses of ATRA were used for further experimentation.

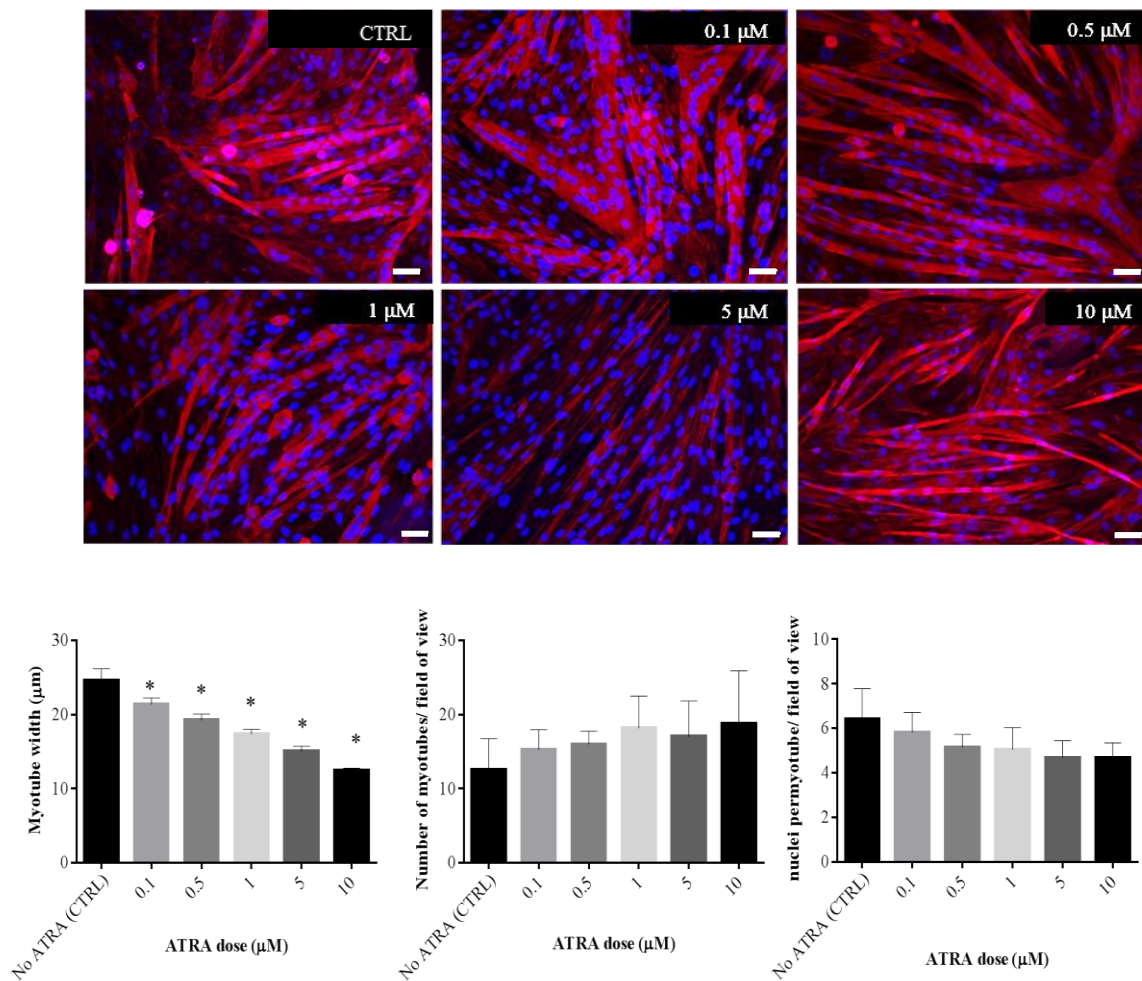


Figure 6.8. Fluorescence micrographs of C2C12's myoblasts and myotube morphology analysis at different ATRA concentrations after 3 days in DM. The different doses have been labelled on the images for clarity (CTRL refers to 2% NFBS with no ATRA). Myotube width (diameter), number of myotube and nuclei per myotube were analysed. A standard one-way ANOVA with a multiple comparison Bonferroni post-hoc test was used to analyse differences in the dose effect. Error bars correspond to SD of the mean ($n = 4$). Images have been stained in red with rhodamine phalloidin to define F-actin filaments and blue with DAPI for the nuclei. Asterisks indicate differences vs. CTRL when $p < 0.05$. Scale bar = 50 μm .

The standard dose of retinoic acid used for neuronal differentiation was 10 μM and thus, the different doses were analysed on SH-SY5Y's to avoid changes in neuronal differentiation. For this cell line, reducing the ATRA concentration resulted in a slight decrease in neurite elongation (Figure 6.9). The control condition promoted the shortest neurites, since this culture was not provided with ATRA. However, as the dose increased, neurite length increased proportionally, with a more pronounced effect when concentrations $\geq 1 \mu\text{M}$ were

used (Figure 6.9, $p < 0.05$ for $\geq 1 \mu\text{M}$ ATRA when compared to control). Altogether, the optimum media chosen for co-cultures was 2% NFBS with $1 \mu\text{M}$ of ATRA, since myotube width was not as reduced with this concentration and significant differences in neurite length were not evident between 1-10 μM of ATRA.

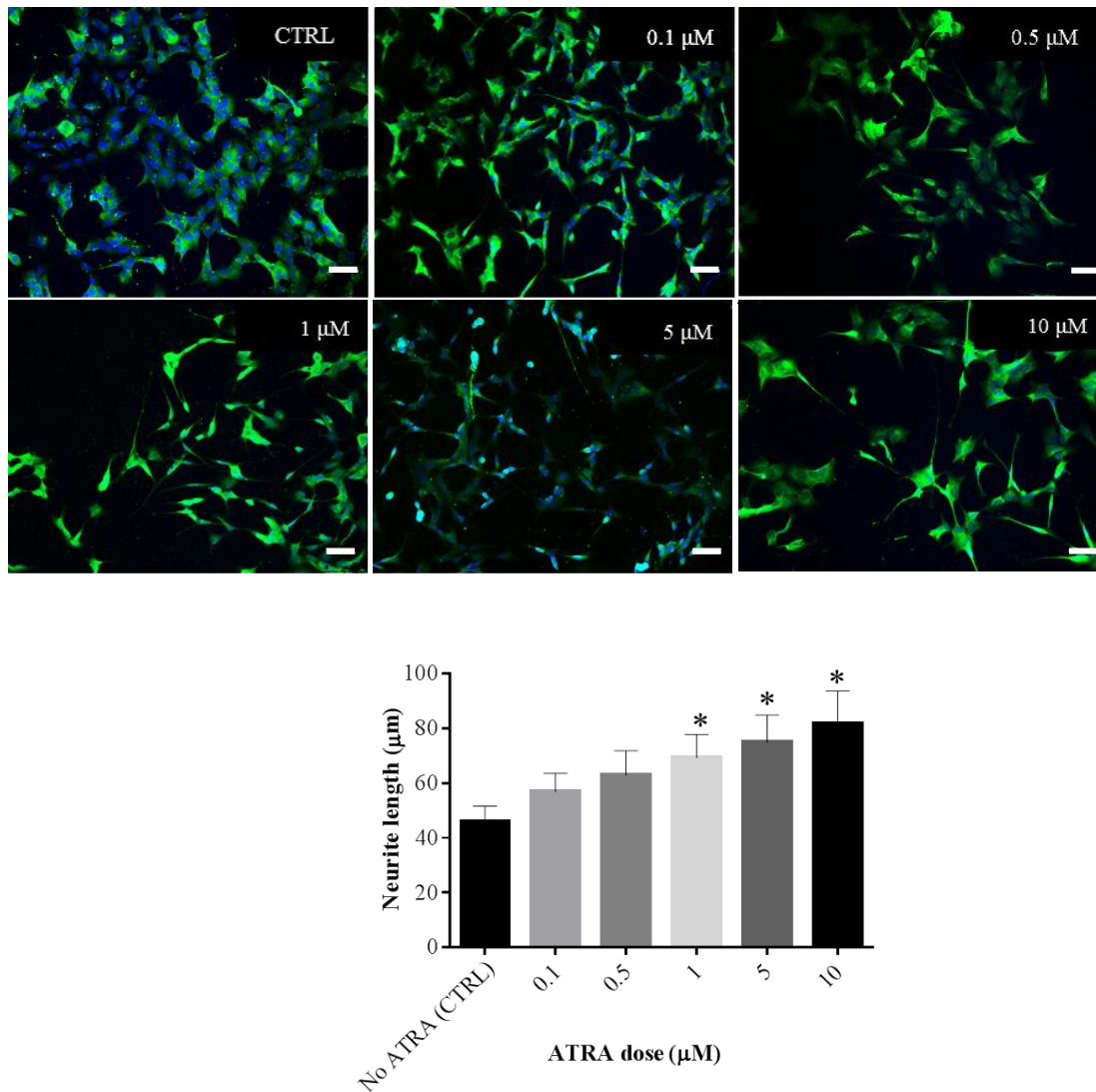


Figure 6.9. Fluorescence micrographs of SH-SY5Y's and neurite length at different ATRA concentrations after 3 days in DM. The different doses have been labelled on the images for clarity (CTRL refers to 2% NFBS with no ATRA). A standard one-way ANOVA with a multiple comparison Bonferroni post-hoc test was used to analyse differences in the dose effect. Error bars correspond to SD of the mean ($n = 4$). Images have been stained with β tubulin III to define neural microtubules in green and blue with DAPI for the nuclei. Asterisks indicate differences when $p < 0.05$ vs. CTRL. Scale bar = $50 \mu\text{m}$.

6.3.4 Co-culture experimentation with SH-SY5Y's and C2C12's

Once media optimisation was complete, the co-culture of both cell types was tested. For this purpose, the samples were made of a patterned side with the patterned lines used in Chapter 5 for neuronal directionality, and a non-patterned area for muscle cells to remain isolated until these were reached by the patterned neurons. As these two areas were not compartmentalised, it was necessary to use a “stopper” or “wall” to constrain both cells within their own areas until differentiation was carried out. To this end, a 0.2 mm coverslip was initially used as a “wall” to separate both cell types (Figure 6.10) and then SH-SY5Y's and C2C12's were seeded on each side of the wall. Both cell types were constrained when they reached the coverslip barrier, cohabiting under both growth and differentiation media with no apparent negative effects. However, undifferentiated C2C12's entered into the SH-SY5Y's patterned area after a few days in culture (2-3 days), resulting in the mixing of both cell types prior to myoblast fusion or neurite extension (Figure 6.10).

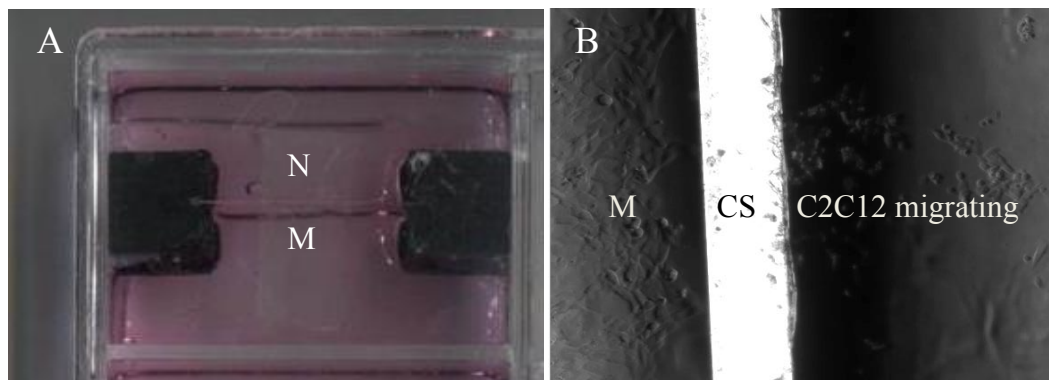


Figure 6.10. Co-culture of C2C12's and SH-SY5Y's with a physical barrier to separate cell populations. A) SH-SY5Y's were cultured on the top of the slide with patterned channels (N) and on the other side, unpatterned C2C12's were seeded (M). The sample was glued at the bottom of the chamber with aquarium glue to avoid floating within the medium. B) The entering of undifferentiated C2C12's towards the neuronal area can be observed (M= C2C12's area, CS= coverslip).

To avoid the C2C12's migrating towards the SH-SY5Y's area, the wall material was changed to a thin “wall” of PDMS to make direct contact with the glass sample (Figure 6.11). The main issue with the PDMS wall was that it had to be thick enough to hold itself upright. This unfortunately led to the formation of a large gap between neurons and muscle cells when the

wall was removed (Figure 6.11). Neurons moved towards the muscle area to initiate contact with C2C12's, by extending long protrusions (Figure 6.12A), however, it was rare that the neurons reached the myotubes before detaching from the surface. Even when myoblasts were fused into myotubes, undesired proliferation of undifferentiated myoblasts continued migrating, invading the neuronal area (Figure 6.12B). Albeit neurons and myoblasts seemed to interact with each other (Figure 6.12C), the invasive nature of C2C12's led to a lack of directionality or control over both populations. Using a blocking technique to separate both cell populations did not further benefit the neuronal-muscle co-culture and therefore, this option was discarded. Instead, various plating conditions were used to address a guided neuron-muscle interaction without the need of physical barriers. To this end, different strategies were utilised consisting of manipulating the seeding time of both cell populations. The first strategy consisted of seeding both cell populations in droplets at the same time, and allowed them to attach. In the second strategy, neurons were seeded first, allowed to attach and proliferate, and then myoblasts were seeded in the other region. In the last approach, myoblasts were added and differentiated, and thereafter neurons were seeded onto the patterned areas.

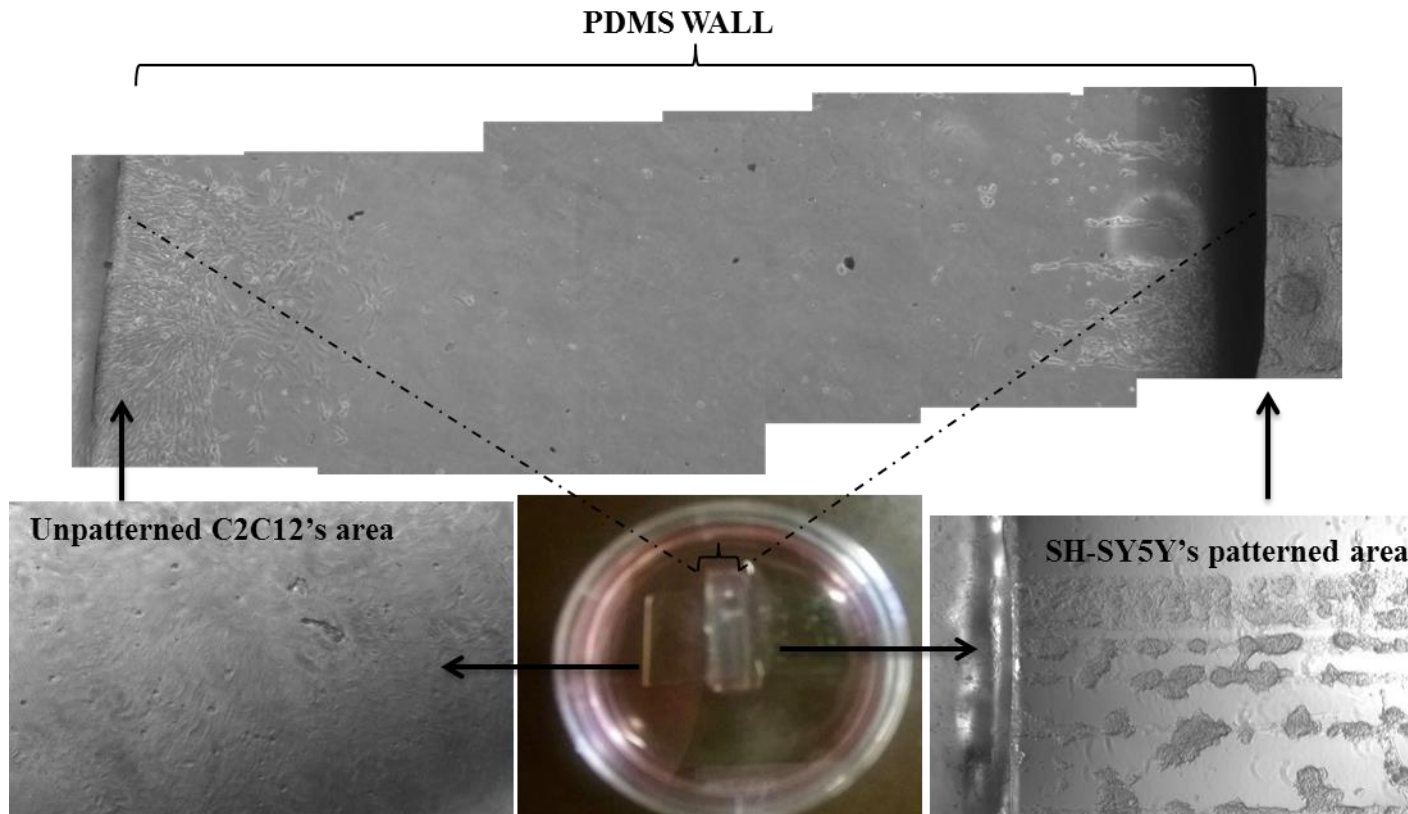


Figure 6.11. Co-culture with a PDMS barrier at the co-culture interface. A PDMS “wall” was used to stop the C2C12’s (left) and SH-SY5Y’s (right) from mixing. At the top, both SH-SY5Y’s and C2C12’s were migrating towards each other under the PDMS wall.

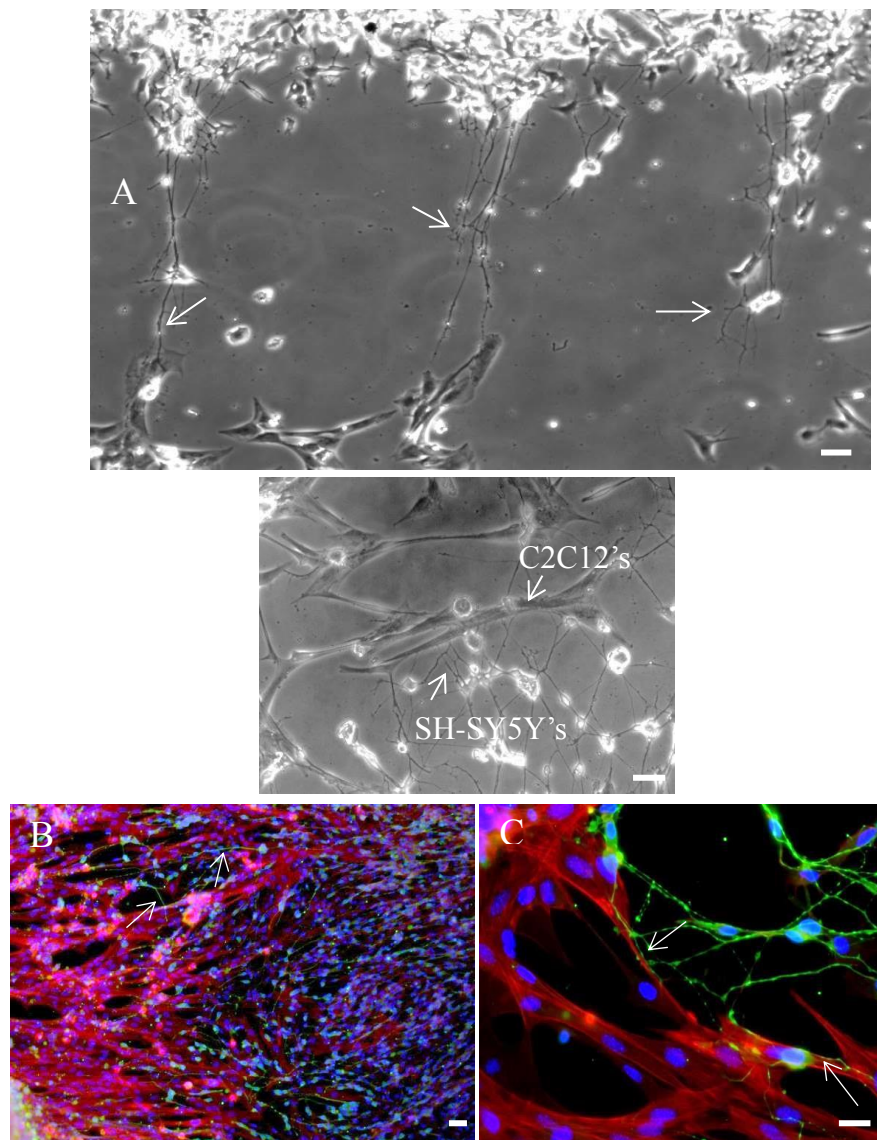


Figure 6.12. Attempts to create a neuron-muscle interface when culturing with a PDMS wall. A) Light micrographs after 8 days in culture show neurons extending long processes to initiate contact with C2C12's myoblasts (white arrows). B) Fluorescence micrographs illustrate neurons migrating towards the non-patterned area and merging with C2C12's. C) Interaction between SH-SY5Y's and C2C12's where long neurites are wrapping the C2C12's (white arrows). Red stain represents F-actin filaments of C2C12's stained with rhodamine phalloidin and blue represents the nuclei stained with DAPI. Neurons were stained with β tubulin III (green). Scale bar= 50 μ m.

For the first strategy, both cell types were seeded into their corresponding areas and were allowed to attach closely. The greater growth rate of C2C12's in comparison to SH-SY5Y's prevented the separation of both cell types. Although neurons began occupying the channels

and extending neurites, undifferentiated C2C12's emerged into the patterned area, obtaining the patterning of both C2C12's and SH-SY5Y's (see Figure 6.13). It is important to note that even though directionality towards muscle was not clear, both cell types made contact with each other within the pattern, co-habiting with no negative effects.

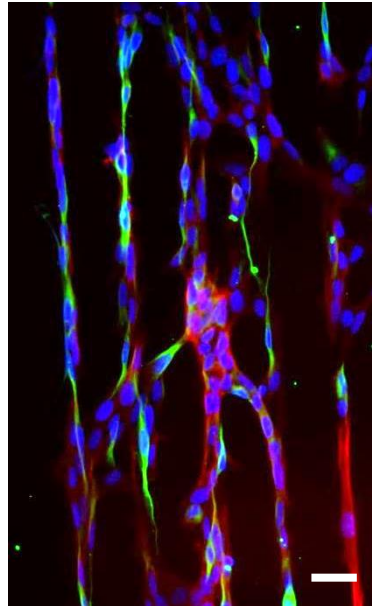


Figure 6.13. Attempts to create a neuron- muscle interface by seeding cell droplets on different sides of the sample. Although neurons seemed to grow in the pattern towards the muscle area, undifferentiated C2C12's migrated towards the channels, occupying the spaces and avoiding neuronal guidance. Red stain represents F-actin filaments of C2C12's stained with rhodamine phalloidin. Blue represents the nuclei stained with DAPI. Neurons were stained with β tubulin III (green). Scale= 100 μ m.

In the second strategy, neurons were seeded on the patterned area and allowed to grow to fill the patterned channels. Myoblasts were seeded later, so they would have less space to migrate towards the channels. Unfortunately, this approach proved unsuccessful due to the continuous merging of undifferentiated cells towards the neuronal patterns, regardless of whether the channels were already occupied by neurons. This in turn prevented the neuronal packing of the channels and thus, the directed neuronal-muscle interaction (Figure 6.14).

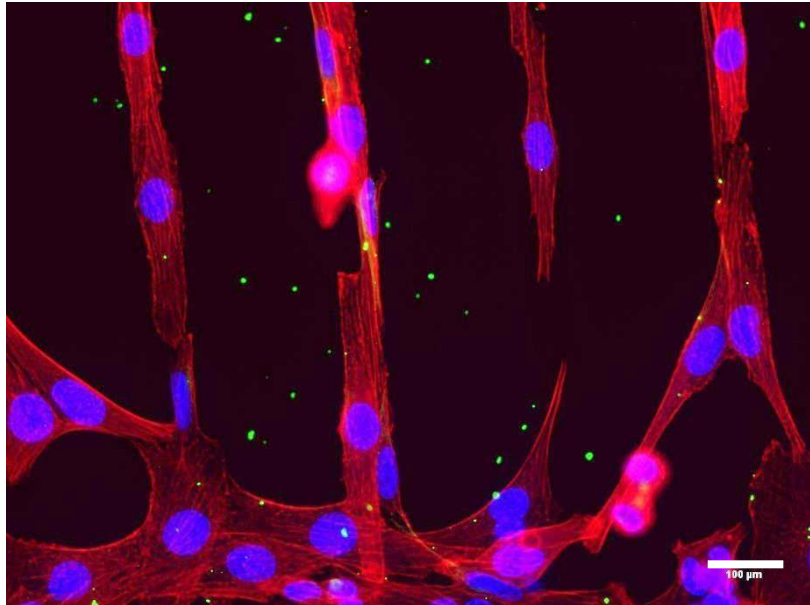


Figure 6.14. Attempts to create a neuron- muscle interface by seeding cells at different time points. Neurons were seeded first on the patterned areas and then C2C12's were placed on the other side of the sample. C2C12's colonised the patterns created for neuronal guidance, preventing the formation of a organised co-culture. Red stain represents F-actin filaments of C2C12's stained with rhodamine-phalloidin and blue represents the nuclei stained with DAPI. Neurons were stained with β tubulin III (green). Scale= 100 μ m.

In the third approach, there was a need to assess the colonisation of C2C12's towards the patterned area and therefore, C2C12's were seeded first, allowed to attach, proliferate and differentiate to form myotubes. Thereafter, neurons were seeded in the patterned areas to create the directed interface. This strategy proved the most successful among the three, as myoblasts fused into myotubes after 3 days in differentiation media (Figure 6.15C) whilst neurons were shown to be patterned towards the muscle area after 2 days of cell seeding. Most importantly, SH-SY5Y's showed a different morphology when compared to single neuronal cultures. In mono-culture, elongated shapes in the cell body with various neurites can be observed after differentiation. However, when cultured with C2C12's, several neurite extensions were formed, presenting a mature morphology with more and longer neurite processes than in mono-culture (Figure 6.15A). This behaviour could be an attempt to establish contact with the myoblasts, indicating the possibility of a positive interaction between SH-SY5Y's and C2C12's. Interestingly, clump of neurons with several extensions were also formed (see Figure 6.15B).

Various drawbacks were found when different seeding points were used for both cell populations. Since the surface had been covered with media during the culture of the first cell population, the positioning of the second cell type in a specific area was problematic due to the wettability of the surface. This resulted in the continuous undesired mixing of both populations. Thus, although the vast majority of both cell populations remained in their own areas (especially in the last approach), there was typically some undesired combining of both cell types in both the unpatterned and patterned areas (see Figure 6.15A and Figure 6.16A, B and C). In addition, as the droplets were concentrated in one spot, some neurons tended to form clumps in those areas and did not appear to spread and migrate as they would do in normal mono-culture conditions, creating some undesired clumps within the channels. Although the creation of an interface where patterned neurons could be directed towards a myotube area was attempted, the invasive nature of C2C12's created issues with the separation of the cell types. This was due to the continuous migration and proliferation of C2C12's before neurons were allowed to differentiate and reach the muscle area (Figure 6.16A, B and C).

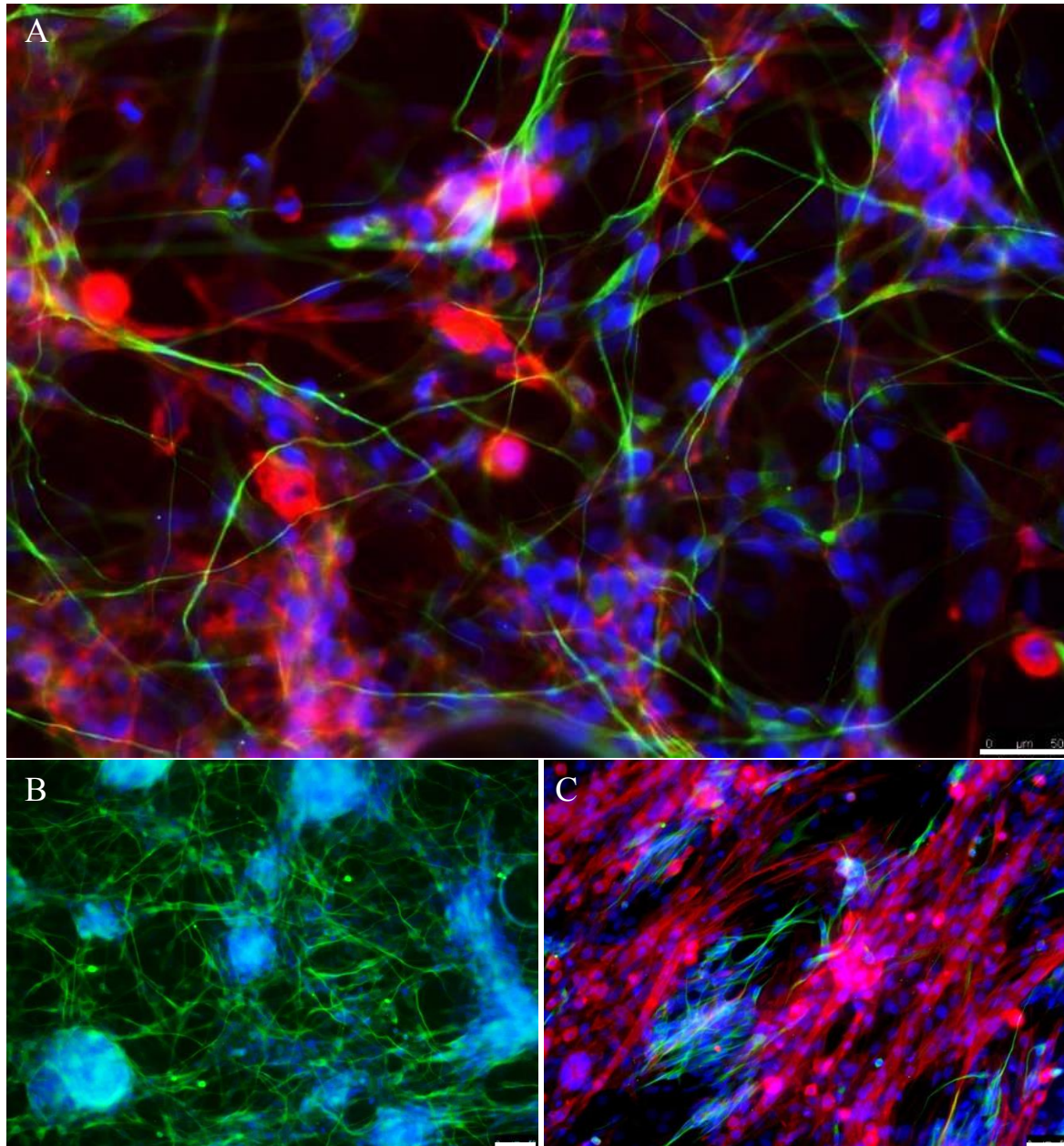


Figure 6.15. Unpatterned areas covered by C2C12's and SH-SY5Y's. A) In the unpatterned C2C12's area, SH-SY5Y's and C2C12's are mixed together. B) In a neuronal area near the pattern, long neurite processes were extended. C) Myotubes could be visualised in the muscle region, however, some neurons were also found in this area. C2C12's were stained with rhodamine-phalloidin (red), neurons were stained with β tubulin III (green) and blue represents the nuclei stained with DAPI. Scale= 50 μ m.

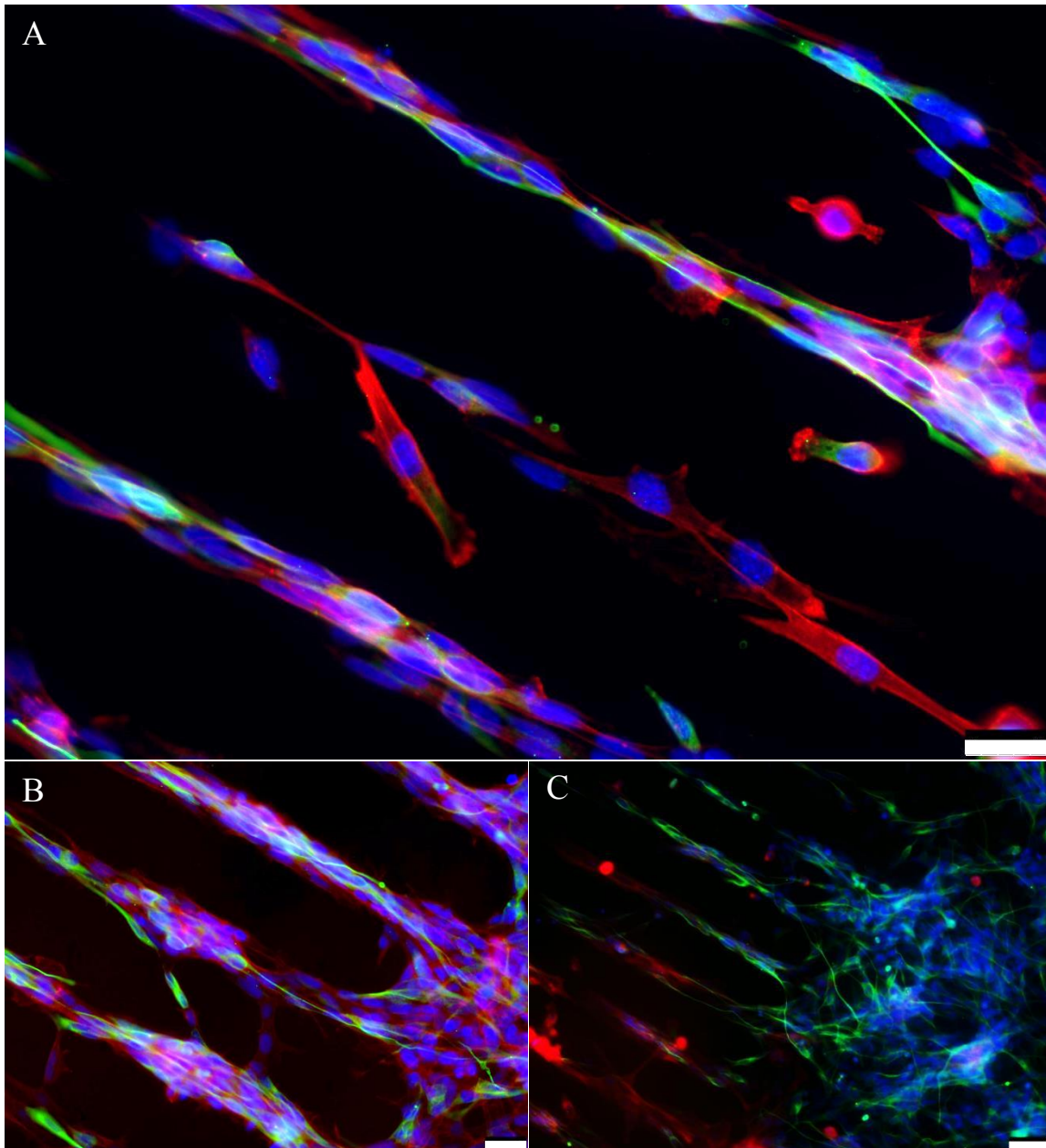


Figure 6.16. Patterned neuronal areas covered by C2C12's and SH-SY5Y's. A) In the channels, C2C12's grew on top of the already patterned neurons, creating a patterned co-culture. B) Similarly, layers of cells occupied the space of the channels. C) Likewise, the merging of both populations avoided the formation of a guided neuron-muscle interface. C2C12's were stained with rhodamine-phalloidin (red), neurons were stained with β tubulin III (green) and blue represents the nuclei stained with DAPI. Scale= 50 μ m.

6.4 Discussion

The study of nerve-muscle cultures has been of great interest for decades as these co-cultures could represent a functional model to analyse muscle innervation and maturation (Arnold *et al.*, 2012). The use of guided neurons towards skeletal muscle could be used as a tool for an improved co-culture system. With this, the study of the muscle-nerve communication and the consequent formation of NMJs could be analysed in a more segregated and specific environment.

6.4.1 Media compatibility and attempts to co-culture with patterned neurons

In vitro co-cultures are important for the study of interactions between different cell populations, and provide a more simplistic system to generate *in-vivo* like connections compared to current animal models (Goers *et al.*, 2014). Improving culture conditions in co-culture systems is needed, since the protocols for mono-cultures can vary across studies and cell lineages, preventing the use of a common media component for different cell types. To this end, the media compatibility data presented in this chapter aimed to determine a suitable differentiation media for both SH-SY5Y's and C2C12's to grow and differentiate. C2C12's have been shown to differentiate under growth factor reduction and/or withdrawal (Burattini *et al.*, 2004; Sharples *et al.*, 2012). Thus, a lower percentage of serum allowed for moderate differentiation of C2C12's, whilst promoting SH-SY5Y's survival in co-culture. Thereafter, the use of ATRA was required for neuronal differentiation and consequently, a suitable concentration of ATRA was determined for both cell types to proceed with future co-culture experiments. The effect of ATRA on neurite outgrowth is widely known (Encinas *et al.*, 2000; Clagett-Dame *et al.*, 2006; Xie *et al.*, 2010), however, results regarding its effect on myogenesis have been conflicting, showing a high dependence on the concentration used and the cell lineage utilised (Xiao *et al.*, 1995; Zhu *et al.*, 2009). RA acts within the nucleus, regulating differentiation and metabolism by its interaction with RA receptors, triggering the transcription of various RA-genes (Halevy and Lerman, 1993; Xiao *et al.*, 1995; Zhu *et al.*, 2009). The effect retinoic acid in muscle has previously been eluded to in various studies, highlighting the sensitivity of this tissue to this compound, as it is known to express high levels of retinoic acid receptors (Xiao *et al.*, 1995; Grey, 2011). A range of doses of ATRA were investigated in this work, and results indicated a decrease in myotube width, and

elongated-like myoblasts with high ATRA concentrations, suggesting that ATRA could cause impaired myotube development at high concentrations (Cong *et al.*, 2014; Li *et al.*, 2017). It could be speculated that ATRA acted by interacting through intermediates, such as molecules within the media, altering the effect of retinoic acid on cells and triggering an atrophic response. In addition, some of the RAR receptors have a precise restricted and dynamically changing pattern of expression, which may also be involved in the modifying effect of ATRA (Xiao *et al.*, 1995). Nevertheless, the main purpose of this study was to induce myotube formation for neuronal-muscle co-cultures, and this was achieved by reducing the concentration of ATRA used.

Neuromuscular co-culture systems with separated environments allow the control of the site of action at the muscle-neuron interface, facilitating a closer study of the heterotypic cell communication (Goubko and Cao, 2009). In the present study, the use of two different environments were used, including an area of patterned channels for neuronal guidance and an unpatterned zone, which was used for myotube growth. The ethos behind this set-up was that when myoblasts fused into myotubes, neurons would be attracted towards the myotubes, thus extending their processes through the channels and generating synapses. SH-SY5Y's and C2C12's were co-cultured and both cell differentiation processes were observed along with the co-habiting of both species with non-apparent negative effects. SH-SY5Y's were observed to extend long neurites (longer than observed in mono-cultures) towards C2C12's, suggesting attempts to initiate contact between both cell types. This observation is consistent with a study performed by Ostrovidov *et al.* (2014), who co-cultured C2C12's and PC12's within 50 μm channel patterns. In patterned mono-cultures, PC12's grew in small aggregates and extending very short neurites. For C2C12's, the pattern in mono-cultures produced myoblast alignment. When co-cultured, PC12's made contact with myoblasts and myotubes by extending neurites to perform connections, resulting in an increase in neurite outgrowth. Furthermore, the presence of neuronal cells in the co-culture improved myotube formation and aided myoblast differentiation. This study was based on the growth of both cell types within the same channel, whereas the work presented here illustrated the use of a semi-patterned surface for neuronal guidance towards unpatterned muscle cultures. Unfortunately, the invasive nature of the myoblasts prevented the formation of a guided co-culture due to the

continuous migration and proliferation towards the neuronal patterned channels. Furthermore, the lack of short-term availability to the equipment to create a different design to avoid the undesired myoblast migration, prevented the development of the set-up. These inconveniences prevented the development of the neuronal-guided muscle system and the further study of muscle- neuron interaction (pre and post synaptic markers, contractile behaviour in neural and aneural cultures, etc.), to examine whether heterotypical communication was carried out. For future experimentation, the use of a different cell types with slower growth rates could be used, as well as a pattern system with clearly separated areas to avoid the mixing of both populations. With adequate optimisation, this system could provide a simple neuronal-muscle co-culture model without the need for expensive differentiating components or the use of complex methodologies for cell guidance.

6.4.2 Chapter summary

The results presented in this chapter include the media optimisation for the co-culture of C2C12's and SH-SY5Y's, and the different methods to co-culture patterned neuronal cells towards skeletal muscle cells. The optimisation of differentiation media was accomplished, and both cell types differentiated within a single culture. With regards to the patterned co-culture, the difficulties in control and restraint of both cell populations prevented a directed synaptic contact with the myotubes. Preliminary results indicated the extension of long neurites and the positive co-habiting of both cell types during growth and differentiation. In some instances, initial observations also suggested the attempts of neuronal-muscle interaction. Although various limitations need to be refined in this set up (as mentioned throughout Section 6.3), the encouraging observations may represent a step forward in the development of a patterned neuronal co-culture system, where the study of neuromuscular interactions can be closely monitored.

7 Discussion

7.1 General discussion

The investigations conducted in this thesis allowed the identification, characterisation and patterning of instructive chemical cues for the control and guidance of SH-SY5Y neuronal cells. The combination of these cues with various patterning techniques were used to generate micro-chemical channels, with the aim to mimic the architecture of neuronal networks. The control of neuronal growth and directionality was achieved within this system, demonstrating the formation of a neuronal model that could be used to study neurodegenerative diseases and neuroregeneration, in a simpler and more controlled microenvironment than *in vivo* systems.

Whilst single-cell type patterns have been used in the literature (Chen *et al.*, 2008; Goubko and Cao, 2009; Tan *et al.*, 2013; Chelli *et al.*, 2014), the use of multiple-cell type patterns within the same surface are far less common (Goubko and Cao, 2009). To this end, a chimeric co-culture system was used in this thesis where patterned neuronal cells were co-cultured with skeletal muscle cells in an attempt to obtain an organised neuronal-muscle co-culture system. The use of a “cell line only” co-culture model could be a simpler and more affordable alternative to the *in vitro* NMJ models currently used (i.e. the use of stem cells or animal-derived cells), which are characterised by high cost, low availability, limited translation to human disease and ethical issues (Anderson *et al.*, 2004; Takazawa *et al.*, 2012).

The first part of this thesis involved the characterisation and confirmation of modified surfaces, including APTES, BIBB, PMMA, PHEMA, PKSPMA and PMETAC. The surface characterisation by XPS, FTIR and WCA resulted in surfaces displaying divergent characteristics, including different hydrophilicity, chemical functionality and charge. Therefore, SH-SY5Y's were cultured on the modified surfaces to identify which surfaces promoted or inhibited cell behaviour. There was a clear interaction at the cell material surface, with certain coatings either promoting cell behaviours, such as proliferation and neurite outgrowth, (APTES, BIBB) or inhibiting cell growth (PKSPMA, PMETAC). The cell attractive and repulsive characteristics of these coatings could be combined on the same surface to potentially promote cell directionality (Navarro *et al.*, 2008; Tong *et al.*, 2012). Indeed, the differing cell response was further demonstrated by the formation of a cell-

active/repulsive pattern, where the cell-repulsive properties of PKSPMA brushes were effectively displayed on a glass surface.

Polymer brushes are a unique method for surface modification and patterning. The covalent bonding, flexibility in the parameters for their synthesis, and the wide range of multifunctional end groups that can be used, make polymer brushes a suitable and convenient platform to modify materials (Moroni *et al.*, 2014; Tuft, 2014; Ibanescu, 2015; Pacelli *et al.*, 2016). Patterned PKSPMA brushes facilitated neural alignment and extension in this thesis, providing different channel sizes that were examined in Chapter 5 to demonstrate that channel width was influential in differing neuronal morphology.

The final aim of this thesis was to create chemical patterns that provide an organised neuronal system, in turn improving *in vitro* neural studies. This aim was achieved by the use of PKSPMA patterned brushes, and with this in mind, several research areas such as neural prosthetics could apply and benefit from this system. Novel prosthetic devices require an interface to re-direct neuronal growth towards specific targets, such as electrodes for neuronal stimulation or a different cell type to renew lost connections. The patterns developed in this thesis could be embedded in the prosthetic interface in proximity to the electrodes and the tissue. This could facilitate transected axons to grow in these patterns for neuronal tissue regeneration, and thus acting as a platform to replace missing biological functionality (Srinivasan *et al.*, 2015). Tuft (2014) used patterned polymerised surfaces to improve sensory prosthesis by increasing integration within the neural tissues, indicating the potential of these surfaces in bioprosthetic devices.

7.2 Key findings

The use of mechanical, physical, biochemical and chemically modified surfaces for *in vitro* studies has expanded over the years to find surfaces that facilitates desired cell responses such as adhesion, proliferation and differentiation (Charest *et al.*, 2006; Thevenot *et al.*, 2008; Tan *et al.*, 2013; Ballester-Beltran *et al.*, 2015). It has been consistently shown that cell responses are affected when parameters such as the functionality or wettability are altered (Lee *et al.*, 2003; Arima and Iwata, 2007). Whilst neuronal chemical patterns have been observed in the literature (Clark, *et al.*, 1993; Jang and Nam, 2012), only a small number of studies have used polymer brushes to direct cell growth towards specific targets. To this end, various SAMs and methacrylate brushes with differing chemical properties were used to analyse neuronal behaviour and address the attractive or repulsive characteristics of these coatings under cell culture conditions. The data collected in this work showed that a range of coatings (APTES and BIBB) promoted proliferation, and were viable for the culture of SH-SY5Y neuronal cells. In contrast, coatings such as PKSPMA and PMETAC prevented cell adhesion and growth, one of them even promoting cell toxicity (PMETAC; Section 4.3.1). Both cell-attractive and repulsive surfaces represent an improved alternative to standard tissue culture techniques. Firstly, this system incorporates a more complex environment than the homogeneous and simplistic surface present in conventional models. In addition, modified surfaces have the flexibility to be adapted onto different materials (see future directions, Section 7.4) and other surface strategies (combination of physical cues).

Understanding the cues affecting neuronal behaviour could aid the design of well-defined surfaces for biomedical applications and regenerative medicine, thus improving current systems and providing a step forward towards the next generation of cell culture materials. Equally important, the cell-repulsive effect of these surfaces could be advantageous when designing homogeneous bio-repulsive surfaces for certain applications (e.g. as antifouling coatings for marine fouling) or to act as an effective restrictive coating for cell growth to certain areas *in vitro*. A proof of concept was efficiently achieved in this thesis, where the cell repulsive PKSPMA brush combined with engineering technologies allowed for neuronal patterning. Neuronal directionality was achieved with the formation of these patterns, which

is a necessary step to begin building an *in vitro* model for mimicking the neuronal circuit found *in vivo*.

The progress made in microfabrication has allowed a multidisciplinary approach where biology, biotechnology and engineering work together to assess challenges in material design and biological approaches. Thus, its use in this thesis allowed for flexibility in the pattern design, providing a platform to achieve the rearrangement of neuronal cells in different channel sizes, and therefore obtaining neurite directionality and elongation. This patterning system can be applied to study neuronal communication by directing neurites to synapse with cells or components of interest (different engineering scaffold, electrical components or biochemical cues). Additionally, the set up could be utilised to underpin neurological processes behind neurodegenerative diseases and regeneration, by the specific study of single neuronal connections down a channel. When nerve damage occurred in mice at the peripheral nervous system (PNS), the regenerating axons appeared to retrace their original path before injury, reaching original branch points and innervating the same fibres (Nguyen *et al.*, 2002). Thus, this system could be used as a model to produce nerve damage and promote neuronal directionality to investigate whether neurons would successfully retrace their path to regenerate.

Preliminary results obtained in Chapter 6 for the co-culture of guided neuronal cells (SH-SY5Y's) with skeletal muscle cells (C2C12's) indicated a positive effect between both cell populations, by co-habiting together and differentiating. Furthermore, observations suggested some level of interaction when both cell types were contacting during culture. Nevertheless, this is based on qualitative observations, since synaptic contact was not analysed due to the lack of control in obtaining a discerned guided neuronal-myotube system. However, these observations may represent a step forward in the further investigation of a patterned neuronal co-culture for neuromuscular interactions. Prior to this, the optimisation of several parameters within the set up (specific mask design for co-culture, introduction of functional input, analysis of synaptic sites, etc.) needs to be assessed first to validate the observations attained in this thesis.

Importance of the findings

Despite micro-patterns having been previously used in cell culture, a vast majority of them are based on the use of extracellular matrix proteins or self-assembled monolayers, which lack of long term stability under cell culture conditions (Clark, Britland and Connolly, 1993; Staii *et al.*, 2009). Likewise, the use of micropatterns based on physical cues have been widely reported for neuronal alignment, however, the use of physical cues does not provide with repulsive cues which limit the growth of cells in certain areas in the long term (Marcus *et al.*, 2017). Alternatively, this work represents the use of a thick film made of PKSPMA polymer brush, which has been shown to display remarkable properties to resist cell attachment and thus to contributing to reliable micro patterns when using engineering techniques. The robustness of the brush architecture makes it attractive as a long term coating for bioapplications (Raynor *et al.*, 2009). Furthermore, brush patterns can be prepared on a wide range of materials, making it extremely advantageous as it allows for new avenues regarding implantation or functional testing.

In terms of the patterning method, the protocol used in this thesis describes a straight forward and simple method to deliver neuronal cells in different regions with defined geometries, ultimately leading to the control of cellular growth in specific areas. PKSPMA brushes have been previously used for cell patterning (Tan *et al.*, 2013), however, the micropattern also contained ECM proteins, and the pattern geometry was not based on neuronal alignment, but cell spreading across micro-circular geometries. Therefore, the use of PKSPMA as a repulsive cue to guide neurite extension and neural alignment has not been previously reported in the literature, making the system a novel and easy approach that could be used to underpin neurological processes behind neurodegenerative diseases by the specific study of single neuronal connections down the channel, resulting in several advantages in the field of neural tissue engineering.

Likewise, the use of co-cultures have been widely reported in the literature, however, there are few studies reporting the use of a partly chemical patterned culture system to direct neurons towards specific targets. Ostrovidov *et al.* (2014), co-cultured C2C12's and PC12's within 50 μm channel patterns, however, the growth of both cell types was within the same

pattern, rather than the direction of one cell type to the other. The use of neuromuscular in vitro systems with separated environments would allow the control of the site of action at the muscle-neuron interface, facilitating a closer study of the heterotypic cell communication (Goubko and Cao, 2009). In the present study, the use of two different environments were used, including an area of patterned channels for neuronal guidance and an unpatterned zone, which was used for myotube growth. Although the model presented in this thesis requires further optimisation, it is clear that this system could provide a simple neuronal-muscle co-culture model without the need for expensive differentiating components or the use of complex methodologies for cell guidance.

7.3 Limitation of this work

The work in this thesis presented a successful neuronal patterning method, and progressed in terms of using patterned neurons for neuronal-muscle co-cultures. However, further work is necessary to refine some of the models and improve the patterned co-culture process. As with all cell culture research, the studies in this thesis contain some limitations that should be mentioned.

Firstly, in Chapter 4, the study of neuronal behaviour on the different chemically modified surfaces was in the presence of serum. Thus, the mechanism of the cell-material interaction may remain uncertain, as the affects that were observed may have been influenced by the degree of protein-surface interaction, ultimately contributing to the diverse cell response.

The formation of reliable small channel sizes (5 and 10 μm) in the pattern described in Chapter 5, proved problematic. Whilst various pattern sizes were achieved and neurite directionality was accomplished to some extent, the smaller channel sizes (5 and 10 μm) could not be performed, due to lack of reproducibility of these sizes. This issue resided in the mask design, as all channel sizes were contained on a single mask, therefore rendering full optimisation of the conditions best suited to each channel size. Consequently, although optimisation for the photolithography procedure worked for the smaller channels widths, different parameters (UV exposure optimisation, conditions for pre and post baking) were required to obtain the higher resolution channels. The lack of readily available high-

resolution equipment dictated the use of the optimisation protocol for the majority of channel sizes. This could also be considered a limiting factor in the co-culture work described in Chapter 6, where an alternative pattern design for the co-culture could have been used to facilitate the separation of both cell types. Furthermore, the use of the invasive C2C12's, resulted in the rapid growth of this cell type on both the unpatterned and patterned areas, hindering the orientated co-culture. Perhaps, the use of a less invasive cell type such as human skeletal muscle cells, would help to prevent the mixing of both cell populations.

7.4 Future directions

The work in this thesis presents the characterisation and optimisation process of a simple and versatile patterned platform, where cell organisation can be achieved. This system was employed for neuronal organisation and the patterning of neuronal-muscle co-cultures. However, the system is not limited to neuronal cell applications, and thus further cell types such as astrocytes, Schwann cells, etc. could be incorporated. This could lead to a co-culture platform to support neuronal functionality, as well as a model to underpin the complexities of cell physiology in a more segregated environment. Prior to this, the system needs further development and thus, more work needs to be undertaken to refine the set up in terms of design and functionality to accurately mimic *in vitro* neuronal interactions.

Further analysis could be carried out in Chapter 3 to draw a more robust conclusion about the effect of the chemically modified surfaces on cells. Analysis could be performed not only at a chemical level but also in terms of the physical properties of the coatings (e.g. surface roughness, surface potential, polymer brush architecture), providing more information regarding effect of physicochemical properties on the cells (Chang and Wang, 2011; Gunkel *et al.*, 2011; Ishihara *et al.*, 2015). Similarly, the chemical modified coatings could be cultured in serum free media with defined supplements (N2, B27), allowing to underpin the mechanisms governing the cell-material interface (Kam *et al.*, 2001; Molnar *et al.*, 2007; Corey *et al.*, 2008).

The chemical patterns created in Chapter 5 were made of bare glass as the cell attractive surface, and PKSPMA as the cell repulsive actuator. In future work, the functionalisation of

the cell attractant surface with cell recognition molecules (natural polymers or motifs: collagen, laminin, chitosan, RGD, IKVAV) can be included. Alternatively, adapting engineered scaffolds within the system to enhance cell culture performance could also be attempted. In terms of the dimension and geometries of the pattern, further investigation should be carried out, as a different set up may be needed depending on its purpose. For example, if the aim of the application was the study of neuritogenesis, smaller channel sizes could be designed in order to obtain patterns where only neurites could pass through, similar to the effect given in microfluidic devices, although without the inconvenience of using PDMS as the gold standard material. In applications where two or more cell types were incorporated within the same system, various pattern designs could be applied with differing polymer features to obtain a potential lab on a chip system (neuron-muscle, neuron-glia, among others). For instance, when considering the pattern design in Chapter 6, a mask design where channels were longer (1 cm long in this thesis) to separate a large area for C2C12's to proliferate and differentiate, could perhaps facilitate the co-culture. Furthermore, the C2C12's could be cultured on different platforms, such as collagen gels or electrospun fibres, incorporating tissue engineered scaffolds to the system. Another change on the mask design for a successful co-culture system could involve the pattern of C2C12's perpendicular to a parallel array of neuronal channels. These neuronal channels would be designed in a size in which C2C12's could not enter (see Figure 7.1).

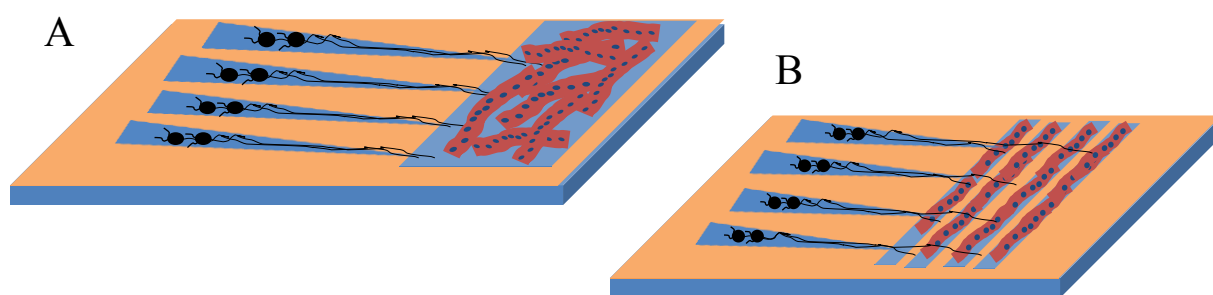


Figure 7.1. Alternative designs for neuron-muscle co-culture experimentation. A) Neurites would be patterned either in a conical geometry or with very thin channels, where only neurites could pass through. At the end, a pool of C2C12's would be randomly attached and differentiated for synapsing. B) Patterning both cell types could allow a more specific area to study synaptic contact.

Most importantly, patterns could be designed to enable excitation and regeneration of neurons. For example, the channels used in this thesis could be directed towards a multielectrode array, which could stimulate the neurons, collecting data regarding the electrical impulses from the cells. This could subsequently be used (once the improvement of the patterned co-culture system presented in Chapter 6 was complete) to examine the functionality of neurons on muscle. Such approach would be highly relevant in various applications regarding neural prostheses and nerve regeneration (Cui *et al.*, 2001; Stieglitz *et al.*, 2005; Biffi *et al.*, 2012). This, however, would require much work on the design and the optimisation process and would be a significant challenge.

The use of different materials can be manipulated depending on the purpose of the application. Brush patterns can be made of silicon oxide derivatives (PDMS, mica, silicon, silica), steel, titanium (Suknik *et al.*, 1990; Raynor, 2008), aluminium (Ma *et al.*, 2014), iron, textile, carbon based materials (carbon nanotubes) (Wei *et al.*, 2012), polytetrafluoroethylene, polyimide (Sheng *et al.*, 2015), and even there have been reports of brushes grown on hair (Wan *et al.*, 2013) and grapes (Sheng *et al.*, 2015). The flexibility of growing brushes on a wide range of materials is extremely advantageous as it allows for new avenues regarding implantation or functional testing. The ability to perform pattern modifications on titanium and silicon based materials allows for the formation of microelectrode-embedded patterns which could aid the study of neurophysiological processes and heterotypic communication, in terms of functional activity (Molnar *et al.*, 2007). Once the co-culture system has been optimised, targeted interest should be placed in the use of human cell types to provide a test bed for pre-clinical studies investigating neuronal disease modelling and treatment by drug screening.

7.5 Conclusions

The work described in this thesis aimed to improve neuronal *in vitro* systems for more accurate neurological studies. The work demonstrates the efficacy of combining chemically modified surfaces and microfabrication techniques as a potential system for directing neuronal growth towards a target (cell type, stimulating components). Chemically modified surfaces were chosen for their surface parameters, tested on neuronal cell cultures and

patterned at a micro scale level to enable close control over neuronal growth. Such a patterned system was further used in a chimeric co-culture as an attempt to control heterotypical communication between neurons and muscle cells. In the future, such a system may facilitate the further understanding of the mechanisms underpinning neurological processes as well as the investigation of heterotypical communication. More work is required for further development and thus, continued optimisation needs to be performed to obtain a defined system that allows the study of spatial neurite direction, synapse formation and neuromuscular junction formation. With further development in this system, the optimised co-culture models could be used in *in vitro* studies to better understand neuronal diseases and produce effective treatments.

8 References

- Acres, R. G., Ellis, A. V., Alvino, J., Lenahan, C. E., Khodakov, D. A., Metha, G. F. and Andersson, G. G. (2012) 'Molecular structure of 3-aminopropyltriethoxysilane layers formed on silanol-terminated silicon surfaces', *Journal of Physical Chemistry C*, 116 (10), pp. 6289–6297.
- Advincula, R. C., Brittain, W. J., Caster, K. C. and R  he, J. (2006) 'Polymer Brushes'. Wiley VCH. Weinheim.
- Alberts, B., Johnson, A., Lewis, J., Raff, M., Roberts, K. and Walter, P. (2002) 'Molecular Biology of the Cell', Garland Science, New York.
- Albutt, D. (2013) 'Surface Chemistry Modification of Glass and Gold for Low Density Neural Cell Culture', Thesis, University of Nottingham.
- Alswieleh, A. M., Cheng, N., Canton, I., Ustbas, B., Xue, X., Ladmiral, V., Xia, S., Ducker, R. E., El Zubir, O., Cartron, M. L., Hunter, C. N., Leggett, G. J. and Armes, S. P. (2014) 'Zwitterionic poly(amino acid methacrylate) brushes', *Journal of the American Chemical Society*, 136(26), pp. 9404–9413.
- Anderson, H. (1964) 'Alkyltin Methanesulfonates and ethanesulfonates', *Inorganic Chemistry*, 3(1), pp. 108–109.
- Anderson, K. N., Potter, A. C., Piccenna, L. G., Quah, A. K. J., Davies, K. E. and Cheema, S. S. (2004) 'Isolation and culture of motor neurons from the newborn mouse spinal cord', *Brain Research Protocols*, 12(3), pp. 132–136.
- Arima, Y. and Iwata, H. (2007) 'Effect of wettability and surface functional groups on protein adsorption and cell adhesion using well-defined mixed self-assembled monolayers', *Biomaterials*, 28(20), pp. 3074–82.
- Arnold, A. S., Christe, M. and Handschin, C. (2012) 'A functional motor unit in the culture dish: co-culture of spinal cord explants and muscle cells', *Journal of Visualized Experiments*, (62), p. e3616.
- Arslantunali, D., Budak, G. and Hasirci, V. (2014) 'Multiwalled CNT-pHEMA composite conduit for peripheral nerve repair', *Journal of Biomedical Materials Research - Part A*, 102(3), pp. 828–841.

- Azzaroni, O. (2012) ‘Polymer brushes here, there, and everywhere: recent advances in their practical applications and emerging opportunities in multiple research fields’, *Journal of Polymer Science, Part A: Polymer Chemistry*, 50(16), pp. 3225–3258.
- Bach, L. G., Islam, M. R., Gal, Y. S. and Lim, K. T. (2012) ‘Synthesis and characterization of TiO₂/Poly(methyl methacrylate) nanocomposites via surface Thiol-Lactam Initiated Radical Polymerization’, *Journal of Nanoscience and Nanotechnology*, 12(7), pp. 5976–5980.
- Ballester-Beltran, J., Biggs, M. J. P., Dalby, M. J., Salmerón-Sánchez, M. and Leal-Egaña, A. (2015) ‘Sensing the difference: the influence of anisotropic cues on cell behavior’, *Frontiers in Materials*, 2(May), pp. 1–12.
- Barbey, R., Lavanant, L., Paripovic, D., Schüwer, N., Sugnaux, C., Tugulu, S. and Klok, H.-A. (2009) ‘Polymer brushes via surface-initiated controlled radical polymerization: synthesis, characterization, properties, and applications’, *Chemical Reviews*, 109(11), pp. 5437–527.
- Belkaid, W., Thstrup, P., Yam, P. T., Juzwik, C. A., Ruthazer, E. S., Dhaunchak, A. S. and Colman, D. R. (2013) ‘Cellular response to micropatterned growth promoting and inhibitory substrates’, *BMC Biotechnology*, 13(1), pp. 86-94.
- Berkowski, K. L., Plunkett, K. N., Yu, Q. and Moore, J. S. (2005) ‘Introduction to photolithography: preparation of microscale polymer silhouettes’, *Journal of Chemical Education*, 82(9), pp. 1365–1369.
- Biffi, E., Piraino, F., Pedrocchi, A., Fiore, G. B., Ferrigno, G., Redaelli, A., Menegon, A. and Rasponi, M. (2012) ‘A microfluidic platform for controlled biochemical stimulation of twin neuronal networks’, *Biomicrofluidics*, 6(2).pp. 02410601-02410609.
- Binnig, G. and Quate, C. F. (1986) ‘Atomic Force Microscope’, *Physical Review Letters*, 56(9), pp. 930–933.
- Biosystems, A. (2008) ‘Guide to performing Relative Quantitation of gene expression using Real-Time Quantitative PCR’, pp. 1–60. Available at http://www3.appliedbiosystems.com/cms/groups/mcb_support/documents/generaldocuments/cms_042380.pdf.
- Borozenko, O., Machado, V., Skene, W. and Giasson, S. (2014) ‘Organophosphonic acids as viable linkers for the covalent attachment of polyelectrolyte brushes on silica and mica surfaces’, *Polymer Chemistry*, 5, pp. 5740–5750.

Briggs, D. and Seah, P. (1990) 'Practical Surface Analysis, Auger and X-ray Photoelectron Spectroscopy'. John Wiley and Sons Ltd, Chichester.

Brittain, W. J. and Minko, S. (2007) 'A structural definition of polymer brushes', *Journal of Polymer Science Part A: Polymer Chemistry*, 45(16), pp. 3505–3512.

Burattini, S., Ferri, R., Battistelli, M., Curci, R., Luchetti, F. and Falcieri, E. (2004) 'C2C12 murine myoblasts as a model of skeletal muscle development: morpho-functional characterization', *European Journal of Histochemistry*, 48(3), pp. 223–233.

Buttiglione, M., Vitiello, F., Sardella, E., Petrone, L., Nardulli, M., Favia, P., d'Agostino, R. and Gristina, R. (2007) 'Behaviour of SH-SY5Y neuroblastoma cell line grown in different media and on different chemically modified substrates', *Biomaterials*, 28(19), pp. 2932–2945.

Campbell, N.A., and Reece, J. B. (2008) 'Biology', Pearson Learning Solutions, California.

Chan, K. H. and Ho, S. L. (2000) 'An update on myasthenia gravis', *Hong Kong Practitioner*, 22(1), pp. 8–20.

Chang, H.-I. and Wang, Y. (2011) 'Cell responses to surface and architecture of tissue engineering scaffolds', *Regenerative Medicine and Tissue Engineering - Cells and Biomaterials*, 27, pp. 569–588.

Charest, J. L. (2007) 'Topographic and chemical patterning of cell- surface interfaces to influence cellular functions', Thesis, Georgia Institute of Technology.

Charest, J. L., Eliason, M. T., Garcia, A. J. and King, W. P. (2006) 'Combined microscale mechanical topography and chemical patterns on polymer cell culture substrates', *Biomaterials*, 27(11), pp. 2487–2494.

Chau, T. T. (2009) 'A review of techniques for measurement of contact angles and their applicability on mineral surfaces', 22(3), *Minerals Engineering*, pp. 213–219.

Chelli, B., Barbalinardo, M., Valle, F., Greco, P., Bystrenova, E., Bianchi, M. and Biscarini, F. (2014) 'Neural cell alignment by patterning gradients of the extracellular matrix protein laminin', *Interface Focus*, 4(1), p. 20130041.

- Chen, J. K., Chen, Z. Y., Lin, H. C., Hong, P. Da and Chang, F. C. (2009) 'Patterned poly(2-hydroxyethyl methacrylate) brushes on silicon surfaces behave as "tentacles" to capture ferritin from aqueous solution', *ACS Applied Materials and Interfaces*, 1(17), pp. 1525–1532.
- Chen, J. K., Hsieh, C. Y., Huang, C. F., Li, P. M., Kuo, S. W. and Chang, F. C. (2008) 'Using solvent immersion to fabricate variably patterned poly(methyl methacrylate) brushes on silicon surfaces', *Macromolecules*, 41(22), pp. 8729–8736.
- Chen, T., Amin, I. and Jordan, R. (2012) 'Patterned polymer brushes', *Chemical Society Reviews*, 41, pp. 3280–3296.
- Chen, Z., Kang, L., Wang, Z., Xu, F., Gu, G., Cui, F. and Guo, Z. (2014) 'Recent progress in the research of biomaterials regulating cell behavior', *RSC Advances*, 4(109), pp. 63807–63816.
- Chiang, E. N., Dong, R., Ober, C. K. and Baird, B. A. (2011) 'Cellular responses to patterned poly(acrylic acid) brushes', *Langmuir*, 27(11), pp. 7016–7023.
- Clagett-Dame, M., McNeill, E. M. and Muley, P. D. (2006) 'Role of all-trans retinoic acid in neurite outgrowth and axonal elongation', *Journal of Neurobiology*, 66(7), pp. 739–756.
- Clark, P., Britland, S. and Connolly, P. (1993) 'Growth cone guidance and neuron morphology on micropatterned laminin surfaces', *Journal of Cell Science*, 105(Pt 1), pp. 203–212.
- Comelles, J., Estévez, M., Martínez, E. and Samitier, J. (2010) 'The role of surface energy of technical polymers in serum protein adsorption and MG-63 cells adhesion', *Nanomedicine: Nanotechnology, Biology, and Medicine*, 6(1), pp. 44–51.
- Cong, W., Liu, B., Liu, S., Sun, M., Liu, H., Yang, Y., Wang, R. and Xiao, J. (2014) 'Implications of the Wnt5a/CaMKII pathway in retinoic acid-induced myogenic tongue abnormalities of developing mice', *Scientific Reports*, 4, p. 6082.
- Cooper, S. T., Maxwell, a. L., Kizana, E., Ghoddusi, M., Hardeman, E. C., Alexander, I. E., Allen, D. G. and North, K. N. (2004) 'C2C12 co-culture on a fibroblast substratum enables sustained survival of contractile, highly differentiated myotubes with peripheral nuclei and adult fast myosin expression', *Cell Motility and the Cytoskeleton*, 58(3), pp. 200–211.

- Corey, J. M., Gertz, C. C., Wang, B. S., Birrell, L. K., Johnson, S. L., Martin, D. C. and Feldman, E. L. (2008) 'The design of electrospun PLLA nanofiber scaffolds compatible with serum-free growth of primary motor and sensory neurons', *Acta Biomaterialia*, 4(4), pp. 863–875.
- Cosa, G., Focsaneanu, K. S., McLean, J. R., McNamee, J. P. and Scaiano, J. C. (2001) 'Photophysical properties of fluorescent DNA-dyes bound to single- and double-stranded DNA in aqueous buffered solution', *Photochemistry and Photobiology*, 73(6), pp. 585–599.
- Cui, X., Lee, V. a, Raphael, Y., Wiler, J. a, Hetke, J. F., Anderson, D. J. and Martin, D. C. (2001) 'Surface modification of neural recording electrodes with conducting polymer/biomolecule blends', *Journal of Biomedical Materials Research*, 56(2), pp. 261–72.
- Dadsetan, M., Knight, A. M., Lu, L., Windebank, A. J. and Yaszemski, M. J. (2009) 'Stimulation of neurite outgrowth using positively charged hydrogels', *Biomaterials*, 30(23–24), pp. 3874–3881.
- Deng, J., Ren, T., Zhu, J., Mao, Z. and Gao, C. (2014) 'Adsorption of plasma proteins and fibronectin on poly(hydroxylethyl methacrylate) brushes of different thickness and their relationship with adhesion and migration of vascular smooth muscle cells', *Regenerative Biomaterials*, 1(1), pp. 17–25.
- Dhandayuthapani, B., Yoshida, Y., Maekawa, T. and Kumar, D. S. (2011) 'Polymeric scaffolds in tissue engineering application: a review', *International Journal of Polymer Science*, (2011).
- Dong, R., Molloy, R. P., Lindau, M. and Ober, C. K. (2010) 'Direct synthesis of quaternized polymer brushes and their application for guiding neuronal growth', *Biomacromolecules*, 11(8), pp. 2027–2032.
- Dowell-Mesfin, N. M., Abdul-Karim, M.A., Turner, A. M. P., Schanz, S., Craighead, H. G., Roysam, B., Turner, J. N. and Shain, W. (2004) 'Topographically modified surfaces affect orientation and growth of hippocampal neurons', *Journal of Neural Engineering*, 1(2), pp. 78–90.
- Dragan, A. I., Casas-Finet, J. R., Bishop, E. S., Strouse, R. J., Schenerman, M. A. and Geddes, C. D. (2010) 'Characterization of PicoGreen interaction with dsDNA and the origin of its fluorescence enhancement upon binding', *Biophysical Journal*, 99(9), pp. 3010–3019.

- Dworak, A., Utrata-Wesołek, A., Szweda, D., Kowalczyk, A., Trzebicka, B., Anioł, J., Sieroń, A. L., Klama-Baryła, A. and Kawecki, M. (2013) 'Poly[tri(ethylene glycol) ethyl ether methacrylate]-coated surfaces for controlled fibroblasts culturing', *ACS Applied Materials & Interfaces*, 5(6), pp. 2197–207.
- Edmondson, S., Osborne, V. L. and Huck, W. T. S. (2004) 'Polymer brushes via surface-initiated polymerizations', *Chemical Society Reviews*, 33, pp. 14–22.
- Encinas, M., Iglesias, M., Liu, Y., Wang, H., Muhaisen, A., Cena, V., Gallego, C. and Comella, J. X. (2000) 'Sequential treatment of SH-SY5Y cells with retinoic acid and brain-derived neurotrophic factor gives rise to fully differentiated, neurotrophic factor-dependent, human neuron-like cells', *Journal of Neurochemistry*, 75(3), pp. 991–1003.
- Engler, A. J.; Sen, S.; Sweeney, H. L.; Discher, D. E (2006) 'Matrix Elasticity Directs Stem Cell Lineage Specification'. *Cell*, 126 (4), pp. 677–689.
- Falconnet, D., Csucs, G., Michelle Grandin, H. and Textor, M. (2006) 'Surface engineering approaches to micropattern surfaces for cell-based assays', *Biomaterials*, 27(16), pp. 3044–3063.
- Fan, Y. W., Cui, F. Z., Chen, L. N., Zhai, Y., Xu, Q. Y. and Lee, I. S. (2002) 'Adhesion of neural cells on silicon wafer with nano-topographic surface', *Applied Surface Science*, 187(3–4), pp. 313–318.
- Faucheux, N., Schweiss, R., Lützow, K., Werner, C. and Groth, T. (2004) 'Self-assembled monolayers with different terminating groups as model substrates for cell adhesion studies', *Biomaterials*, 25(14), pp. 2721–30.
- Förch, R., Schönherr, H. and Jenkins, A. T. A. (2009) 'Surface Design: Applications in Bioscience and Nanotechnology', Wiley-VCH Verlag GmbH & Co, Weinheim.
- Fowler, S., Roush, R. and Wise, J. (2013) 'Concepts of Biology', OpenStax College. Available at: <https://openstax.org/details/books/concepts-biology>.
- García, A. J. (2005) 'Get a grip: integrins in cell-biomaterial interactions', *Biomaterials*, 26(36), pp. 7525–7529.
- Gerhardt, L.-C. and Boccaccini, A. R. (2010) 'Bioactive glass and glass-ceramic scaffolds for bone tissue engineering', *Materials*, 3(7), pp. 3867–3910.

- Gibbs, J. W., Sombati, S., DeLorenzo, R. J. and Coulter, D. (1997) 'Physiological and pharmacological alterations in postsynaptic GABA(A) receptor function in a hippocampal culture model of chronic spontaneous seizures', *Journal of Neurophysiology*, 77, pp. 2139–2152.
- Gilmore, I. S. (2009) 'Surface Analysis-The Principal Techniques', John Wiley & Sons, Ltd.
- Goers, L., Freemont, P. and Polizzi, K. M. (2014) 'Co-culture systems and technologies: taking synthetic biology to the next level', *Journal of the Royal Society, Interface*, 11(96), p. 20140065.
- Gomez, N., Chen, S. and Schmidt, C. E. (2007) 'Polarization of hippocampal neurons with competitive surface stimuli: contact guidance cues are preferred over chemical ligands', *Journal of the Royal Society, Interface*, 4(13), pp. 223–233.
- Gonzalez, R. J. and Tarloff, J. B. (2001) 'Evaluation of hepatic subcellular fractions for Alamar blue and MTT reductase activity', *Toxicology in Vitro*, 15(3), pp. 257–259.
- Gordon, J., Amini, S. and White, M. K. (2013) 'General overview of neuronal cell culture', *Neuronal Cell Culture: Methods and Protocols*, 1078, pp. 1–8.
- Goubko, C. A. and Cao, X. (2009) 'Patterning multiple cell types in co-cultures: a review', *Materials Science and Engineering C*, 29(6), pp. 1855–1868.
- Govindarajan, T. and Shandas, R. (2014) 'A survey of surface modification techniques for next-generation shape memory polymer stent devices', *Polymers*, 6(9), pp. 2309–2331.
- Greco, F., Fujie, T., Ricotti, L., Taccola, S., Mazzolai, B. and Mattoli, V. (2013) 'Microwrinkled conducting polymer interface for anisotropic multicellular alignment', *ACS Applied Materials and Interfaces*, 5(3), pp. 573–584.
- Grey, M. (2011) 'Bio-engineering of Muscle Tissue in Culture: Influence of Neural, Cartilage or Kidney Cells and the Effect of Retinoic Acid on Muscle Cell Growth', Thesis, University of Victoria.
- Gunkel, G., Weinhart, M., Becherer, T., Haag, R. and Huck, W. T. S. (2011) 'Effect of polymer brush architecture on antibiofouling properties', *Biomacromolecules*, 12(11), pp. 4169–4172.

- Guo, X., Das, M., Rumsey, J., Gonzalez, M., Stancescu, M. and Hickman, J. (2010) 'Neuromuscular junction formation between human stem-cell-derived motoneurons and rat skeletal muscle in a defined system', *Tissue Engineering. Part C, Methods*, 16(6), pp. 1347–1355.
- Halevy, O. and Lerman, O. (1993) 'Retinoic acid induces adult muscle cell differentiation mediated by the retinoic acid receptor-alpha', *Journal of Cellular Physiology*, 154(3), pp. 566–572.
- Hayes, J. S., Czekanska, E. M. and Richards, R. G. (2011) 'The cell-surface interaction', *Advances in Biochemical Engineering/Biotechnology*, 126(October), pp. 1–31.
- Henrie, J., Kellis, S., Schultz, S. and Hawkins, A. (2004) 'Electronic color charts for dielectric films on silicon', *Optics Express*, 12(7), pp. 1464–1469.
- Hon, K. K. B., Li, L. and Hutchings, I. M. (2008) 'Direct writing technology-advances and developments', *CIRP Annals - Manufacturing Technology*, 57(2), pp. 601–620.
- Howarter, J. A. and Youngblood, J. P. (2006) 'Optimization of silica silanization by 3-aminopropyltriethoxysilane', *Langmuir*, 22(26), pp. 11142–11147.
- Ibanescu, S. A. (2015) 'Surface Grafted Polymer Brushes: A Versatile Platform for Antibacterial Applications', Thesis, École Polytechnique Fédérale de Lausanne.
- In, H. Y., Co, C. C. and Ho, C. C. (2005) 'Alteration of human neuroblastoma cell morphology and neurite extension with micropatterns', *Biomaterials*, 26(33), pp. 6599–6609.
- Ishihara, K., Kitagawa, T. and Inoue, Y. (2015) 'Initial cell adhesion on well-defined surface by polymer brush layers with varying chemical structures', *ACS Biomaterial Science and Engineering*, 1(2), pp. 103–109.
- Ito, T. and Okazaki, S. (2000) 'Pushing the limits of lithography', *Nature*, 406, pp. 1027–1031.
- Ito, Y. (1999) 'Surface micropatterning to regulate cell functions', *Biomaterials*, 20(23-24) pp. 2333–2342.
- Jakubowski, W. and Matyjaszewski, K. (2005) 'Activator generated by electron transfer for atom transfer radical polymerization', *Macromolecules*, 38(10), pp. 4139–4146.

- Jakubowski, W., Min, K. and Matyjaszewski, K. (2006) 'Activators regenerated by electron transfer for atom transfer radical polymerization of styrene', *Macromolecules*, 39(1), pp. 39–45.
- Jalili, N. and Laxminarayana, K. (2004) 'A review of atomic force microscopy imaging systems: application to molecular metrology and biological sciences', *Mechatronics*, 14(8), pp. 907–945.
- Jang, M. J. and Nam, Y. (2012) 'Geometric effect of cell adhesive polygonal micropatterns on neuritogenesis and axon guidance', *Journal of Neural Engineering*, 9(4), p. 46019.
- Jans, K., Van Meerbergen, B., Reekmans, G., Bonroy, K., Annaert, W., Maes, G., Engelborghs, Y., Borghs, G. and Bartic, C. (2009) 'Chemical and biological characterization of thiol SAMs for neuronal cell attachment.', *Langmuir: the ACS Journal of Surfaces and Colloids*, 25(8), pp. 4564–4570.
- Jiang, S. and Cao, Z. (2010) 'Ultralow-fouling, functionalizable, and hydrolyzable zwitterionic materials and their derivatives for biological applications', *Advanced Materials*, 22, pp. 920–932.
- Joshi, S., Guleria, R., Pan, J., DiPette, D. and Singh, U. S. (2006) 'Retinoic acid receptors and tissue-transglutaminase mediate short-term effect of retinoic acid on migration and invasion of neuroblastoma SH-SY5Y cells', *Oncogene*, 25, pp. 240–247.
- Jung, D. R., Kapur, R., Adams, T., Giuliano, K. a, Mrksich, M., Craighead, H. G. and Taylor, D. L. (2001) 'Topographical and physicochemical modification of material surface to enable patterning of living cells', *Critical Reviews in Biotechnology*, 21(2), pp. 111–154.
- Junkin, M. and Wong, P. K. (2011) 'Probing cell migration in confined environments by plasma lithography', *Biomaterials*, 32(7), pp. 1848–1855.
- Kam, L., Shain, W., Turner, J. N. and Bizios, R. (2001) 'Axonal outgrowth of hippocampal neurons on micro-scale networks of polylysine-conjugated laminin', *Biomaterials*, 22(10), pp. 1049–1054.
- Kane, R. S., Takayama, S., Ostuni, E., Ingber, D. E. and Whitesides, G. M. (1999) 'Patterning proteins and cells using soft lithography', *Biomaterials*, 20(23-24), pp. 2363–2376.

- Kanning, K. C., Kaplan, A. and Henderson, C. E. (2010) 'Motor neuron diversity in development and disease.', *Annual Review of Neuroscience*, 33, pp. 409–440.
- Khan, S. and Newaz, G. (2010) 'A comprehensive review of surface modification for neural cell adhesion and patterning', *Journal of Biomedical Materials Research - Part A*, 93(3), pp. 1209–1224.
- Kilby, J. (1964) 'Miniaturized electronic circuits', *US Patent 3,138,743*.
- Kim, B. S. and Mooney, D. J. (1998) 'Development of biocompatible synthetic extracellular matrices for tissue engineering', *Trends in Biotechnology*, 16(5), pp. 224–229.
- Kim, E., Xia, Y. and Whitesides, G. M. (1996) 'Micromolding in capillaries: applications in materials science', *Journal of the American Chemical Society*, 118 (24), pp. 5722–5731.
- Kim, J., Seidler, P., Wan, L. S. and Fill, C. (2009) 'Formation, structure, and reactivity of amino-terminated organic films on silicon substrates', *Journal of Colloid and Interface Science*, 329(1), pp. 114–119.
- Klein, C. L., Scholl, M. and Maelicke, A. (1999) 'Neuronal networks in vitro: formation and organization on biofunctionalized surfaces', *Journal of Materials Science: Materials in Medicine*, 10(12), pp. 721–727.
- Kleinfeld, D., Kahler, K. H. and Hockberger, P. E. (1988) 'Controlled outgrowth of dissociated neurons on patterned substrates', *Journal of Neuroscience*, 8(11), pp. 4098–4120.
- Kobayashi, M., Terayama, Y., Yamaguchi, H., Terada, M., Murakami, D., Ishihara, K. and Takahara, A. (2012) 'Wettability and antifouling behavior on the surfaces of superhydrophilic polymer brushes', *Langmuir*, 28, pp. 7212–7222.
- Kovalevich, J. and Langford, D. (2013) 'Considerations for the use of SH-SY5Y neuroblastoma cells in neurobiology', *Neuronal Cell Culture: Methods and Protocols*, 1078, pp. 9–21.
- Krishnamoorthy, M., Hakobyan, S., Ramstedt, M. and Gautrot, J. E. (2014) 'Surface-initiated polymer brushes in the biomedical field : applications in membrane science, biosensing, cell culture, regenerative medicine and antibacterial coatings', *Chemical Reviews*, 114 (21), pp. 10976–11026.

- Kumar, A., Srivastava, A., Galaev, I. Y. and Mattiasson, B. (2007) 'Smart polymers: physical forms and bioengineering applications', 32(10), *Progress in Polymer Science*, pp. 1205–1237.
- Kuzmyn, A. R., de los Santos Pereira, A., Pop-Georgievski, O., Bruns, M., Brynda, E. and Rodriguez-Emmenegger, C. (2014) 'Exploiting end group functionalization for the design of antifouling bioactive brushes', *Polymer Chemistry*, 5(13), pp. 4124–4131.
- Lafranzo, N. A. (2013) 'Use of Self-Assembled Monolayers to Tailor Surface Properties: From Lubrication to Neuronal Development', Thesis, Washington University.
- Larkin, L. M., Van der Meulen, J. H., Dennis, R. G. and Kennedy, J. B. (2007) 'Functional evaluation of nerve-skeletal muscle constructs engineered in vitro', *In Vitro Cellular & Developmental Biology. Animal*, 42(3–4), pp. 75–82.
- Lee, B. S., Chi, Y. S., Lee, J. K., Choi, I. S., Song, C. E., Namgoong, S. K. and Lee, S. G. (2004) 'Imidazolium Ion-Terminated Self-Assembled Monolayers on Au: Effects of counteranions on surface wettability', *Journal of the American Chemical Society*, 126(2), pp. 480–481.
- Lee, J. W., Lee, K. S., Cho, N., Ju, B. K., Lee, K. B. and Lee, S. H. (2007) 'Topographical guidance of mouse neuronal cell on SiO₂ microtracks', *Sensors and Actuators, B: Chemical*, 128(1), pp. 252–257.
- Lee, S. J., Khang, G., Lee, Y. M. and Lee, H. B. (2003) 'The effect of surface wettability on induction and growth of neurites from the PC-12 cell on a polymer surface', *Journal of Colloid and Interface Science*, 259(2), pp. 228–235.
- Letsche, S. A., Steinbach, A. M., Pluntke, M., Marti, O., Ignatius, A. and Volkmer, D. (2009) 'Usage of polymer brushes as substrates of bone cells', *Frontiers of Materials Science in China*, 3(2), pp. 132–144.
- Li, L., Wu, J. and Gao, C. (2011) 'Surface-grafted block copolymer brushes with continuous composition gradients of poly(poly(ethylene glycol)-monomethacrylate) and poly(N-isopropylacrylamide)', *Science China Chemistry*, 54(2), pp. 334–342.
- Li, N., Tang, Y., Liu, B., Cong, W., Liu, C. and Xiao, J. (2017) 'Retinoid acid-induced microRNA-27b-3p impairs C2C12 myoblast proliferation and differentiation by suppressing α -dystrobrevin', *Experimental Cell Research*, 350(2), pp. 301–311.

- Lih, E., Oh, S. H., Joung, Y. K., Lee, J. H. and Han, D. K. (2015) 'Polymers for cell/tissue anti-adhesion', *Progress in Polymer Science*, 44(May), pp. 28–61.
- Lim, E., Tu, G., Schwartz, E., Cornelissen, J. J. L. M., Rowan, A. E., Nolte, R. J. M. and Huck, W. T. S. (2008) 'Synthesis and characterization of surface-initiated helical polyisocyanopeptide brushes', *Macromolecules*, 41, pp. 1945–1951.
- Lindquist, N. C., Nagpal, P., McPeak, K. M., Norris, D. J. and Oh, S.-H. (2012) 'Engineering metallic nanostructures for plasmonics and nanophotonics', *Reports on Progress in Physics*, 75(3), p. 36501.
- Livet, J., Weissman, T. A., Kang, H., Draft, R. W., Lu, J., Bennis, R. A., Sanes, J. R. and Lichtman, J. W. (2007) 'Transgenic strategies for combinatorial expression of fluorescent proteins in the nervous system', *Nature*, 450(7166), pp. 56–62.
- Lodish, H., Berk, A., Zipursky, S. L., Matsudaira, P., Baltimore, D. and Darnell, J. (2000) 'Molecular Cell Biology', W. H. Freeman and Company, New York.
- Luzinov, I. and Minko, S. (2012) 'Soft Matter Gradient Surfaces: Methods and Applications', John Wiley & Sons, Inc., New Jersey.
- Ma, H. W., Hyun, J. H., Stiller, P. and Chilkoti, A. (2004) "'Non-fouling" oligo(ethylene glycol)-functionalized polymer brushes synthesized by surface-initiated atom transfer radical polymerization', *Advanced Materials*, 16(4), pp. 338–341.
- Ma, S., Liu, J., Ye, Q., Wang, D., Lianga, Y. and Zhou, F. (2014) 'A general approach for construction of asymmetric modification membranes for gated flow nanochannels', *Journal of Materials Chemistry A*, 2(C), pp. 8804–8814.
- Ma, Y., Cao, X., Feng, X., Ma, Y. and Zou, H. (2007) 'Fabrication of super-hydrophobic film from PMMA with intrinsic water contact angle below 90°', *Polymer*, 48(26), pp. 7455–7460.
- Mager, M. D., LaPointe, V. and Stevens, M. M. (2011) 'Exploring and exploiting chemistry at the cell surface', *Nature Chemistry*, 3, pp. 582–589.
- Mahoney, M. J., Chen, R. R., Tan, J. and Mark Saltzman, W. (2005) 'The influence of microchannels on neurite growth and architecture', *Biomaterials*, 26(7), pp. 771–778.

Massia, S. P.; Hubbell, J. A. (1991). 'An Rgd Spacing of 440Nm Is Sufficient for Integrin Alpha-V-Beta-3-Mediated Fibroblast Spreading and 140Nm for Focal Contact and Stress Fiber Formation' *J. Cell Biol.*, 114 (5), pp 1089–1100.

Martin, N. R. W., Passey, S. L., Player, D. J., Mudera, V., Baar, K., Greensmith, L. and Lewis, M. (2015) 'Neuromuscular junction formation in tissue engineered skeletal muscle augments contractile function and improves cytoskeletal organisation', *Tissue Engineering Part A*, 21, pp. 2595-2604.

Matyjaszewski, K. and Xia, J. (2001) 'Atom transfer radical polymerization', *Chemical Reviews*, 101, pp. 2921–2990.

McBeath, R., Pirone, D. M., Nelson, C. M., Bhadriraju, K. and Chen, C. S. (2004) 'Cell shape, cytoskeletal tension, and RhoA regulate stem cell lineage commitment', *Developmental Cell*, 6(4), pp. 483–495.

McCrackin, F. L.; Passaglia, E.; Stromberg, R. R.; Steinberg, H. L. (1963) 'Measurements of the thickness and refractive index of very thin films and the optical properties of surfaces by ellipsometry' *Journal of Research of the National Bureau Of Standards and Technology*, 67, pp. 363-377.

Mehling, M. and Tay, S. (2014) 'Microfluidic cell culture', *Current Opinion in Biotechnology*, 25, pp. 95–102.

Mei, Y., Wu, T., Xu, C., Langenbach, K. J., Elliott, J. T., Beers, K. L., Amis, E. J., Washburn, N. R. and Henderson, L. (2005) 'Control of protein absorption and cell adhesion: effect of polymer graft density', *Polymer Preprints (American Chemical Society, Division of Polymer Chemistry)*, 46(2), pp. 1227–1228.

Mei, Y., Wu, T., Xu, C., Langenbach, K. J., Elliott, J. T., Vogt, B. D., Beers, K. L., Amis, E. J. and Washburn, N. R. (2005) 'Tuning cell adhesion on gradient poly(2-hydroxyethyl methacrylate)-grafted surfaces', *Langmuir*, 21(26), pp. 12309–12314.

Mendelsohn, J. D., Yang, S. Y., Hiller, J. A., Hochbaum, A. I. and Rubner, M. F. (2003) 'Rational design of cytophilic and cytophobic polyelectrolyte multilayer thin films', *Biomacromolecules*, 4(1), pp. 96–106.

Metavarayuth, K., Sitasuwan, P., Zhao, X., Lin, Y. and Wang, Q. (2016) 'Influence of surface topographical cues on the differentiation of mesenchymal stem cells in vitro', *ACS Biomaterials Science & Engineering*, 2(2), pp. 142–151.

Milner, S. (1991) 'Polymer brushes', *Science*, 251, pp. 905–914.

- Mittal, V. (2012) 'Polymer Brushes: Substrates, Technologies, and Properties', Taylor & Francis, CRC Press.
- Molnar, P., Wang, W., Natarajan, A., Rumsey, J. W. and Hickman, J. J. (2007) 'Photolithographic patterning of C2C12 myotubes using vitronectin as growth substrate in serum-free medium', *Biotechnology Progress*, 23(1), pp. 265–268.
- Moroni, L., Gunnewiek, M. K. and Benetti, E. (2014) 'Polymer brush coatings regulating cell behavior: passive interfaces turn into active', *Acta Biomaterialia*, 10(6), pp. 2367–2378.
- Mrabet, B., Nguyen, M. N., Majbri, A., Mahouche, S., Turmine, M., Bakhrouf, A. and Chehimi, M. M. (2009) 'Anti-fouling poly(2-hydroxyethyl methacrylate) surface coatings with specific bacteria recognition capabilities', *Surface Science*, 603, pp. 2422–2429.
- Mullis, K., Faloona, F., Scharf, S., Saiki, R., Horn, G. and Erlich, H. (1986) 'Specific enzymatic amplification of DNA in vitro: the polymerase chain reaction', *Cold Spring Harbor Symposia on Quantitative Biology*, 51, pp. 263–273.
- Nam, K., Jamilpour, N., Mfoumou, E., Wang, F., Zhang, D. D. and Wong, P. K. (2014) 'Probing mechanoregulation of neuronal differentiation by plasma lithography patterned elastomeric substrates', *Scientific Reports*, 4, p. 6965.
- Navarro, M., Benetti, E. M., Zapotoczny, S., Planell, J. A. and Vancso, G. J. (2008) 'Buried, covalently attached RGD peptide motifs in poly(methacrylic acid) brush layers: the effect of brush structure on cell adhesion', *Langmuir*, 24 (19), pp 10996–11002.
- Nguyen, Q. T., Sanes, J. R. and Lichtman, J. W. (2002) 'Pre-existing pathways promote precise projection patterns', *Nature Neuroscience*, 5(9), pp. 861–867.
- Nolan, T., Anders Bergkvist, C., Carvallo, C., Peter Chereson, M. H., Daley, L., Heath, A., Hibbs, S., Stacey Hoge, M., Elena Jouravlena, B., Kreader, C., Mohammed, M., Mueller, E., Richardson, G., Tom Russell, M., Ward, B., Weber, S. A. and Marina Wiklander, B. (2014) 'PCR technologies, A Technical Guide'. Sigma Aldrich. Available at: http://www.sigmaaldrich.com/content/dam/sigma-aldrich/docs/Sigma-Aldrich/General_Information/1/pcr-technologies-guide.pdf
- O'Brien, J., Wilson, I., Orton, T. and Pognan, F. (2000) 'Investigation of the Alamar Blue (resazurin) fluorescent dye for the assessment of mammalian cell cytotoxicity', *European Journal of Biochemistry*, 267, pp. 5421–5426.

Offenhausser, A., Bocker-Meffert, S., Decker, T., Helpenstein, R., Gasteier, P., Groll, J., Moller, M., Reska, A., Schafer, S., Schulte, P. and Vogt-Eisele, A. (2007) 'Microcontact printing of proteins for neuronal cell guidance', *Soft Matter*, 3(3), p. 290.

Ogaki, R., Alexander, M. and Kingshott, P. (2010) 'Chemical patterning in biointerface science', *Materials Today*, 13(4), pp. 22–35.

Ohring, M. (2001) 'Materials Science of Thin Films – Deposition & Structure, Materials Science', Academic Press.

Olivier, A., Meyer, F., Raquez, J. M., Damman, P. and Dubois, P. (2012) 'Surface-initiated controlled polymerization as a convenient method for designing functional polymer brushes: From self-assembled monolayers to patterned surfaces', *Progress in Polymer Science*, 37(1), pp. 157–181.

Ostrovidov, S., Ahadian, S., Ramon-Azcon, J., Hosseini, V., Fujie, T., Parthiban, S. P., Shiku, H., Matsue, T., Kaji, H., Ramalingam, M., Bae, H. and Khademhosseini, A. (2014) 'Three-dimensional co-culture of C2C12/PC12 cells improves skeletal muscle tissue formation and function', *Journal of Tissue Engineering and Regenerative Medicine*, 11(2), pp. 582–595

Pacelli, S., Manoharan, V., Desalvo, A., Lomis, N., Jodha, K. S., Prakash, S. and Paul, A. (2016) 'Tailoring biomaterial surface properties to modulate host-implant interactions: implication in cardiovascular and bone therapy', *Journal of Materials Chemistry B*, 4(9), pp. 1586–1599.

Paguirigan, A. L. and Beebe, D. J. (2009) 'From the cellular perspective: exploring differences in the cellular baseline in macroscale and microfluidic cultures', *Integrative Biology : Quantitative Biosciences from Nano to Macro*, 1(2), pp. 182–195.

Palyvoda, O., Bordenyuk, A. N., Yatawara, A. K., McCullen, E., Chen, C. C., Benderskii, A. V. and Auner, G. W. (2008) 'Molecular organization in SAMs used for neuronal cell growth', *Langmuir*, 24(22), pp. 4097–4106.

Pasternack, R. M., Amy, S. R. and Chabal, Y. J. (2008) 'Attachment of 3-(aminopropyl)triethoxysilane on silicon oxide surfaces: dependence on solution temperature', *Langmuir*, 24, pp. 12963–12971.

Patten, T. E. and Matyjaszewski, K. (1998) 'Atom transfer radical polymerization and the synthesis of polymeric materials', *Advanced Materials*, 10(12), pp. 901–915.

Perez Roldan, M. J. (2011) 'Chemical patterning of surfaces for the development of biofunctional interfaces', Thesis, Universidad Autonoma de Madrid.

Peyrin, J.-M., Deleglise, B., Saias, L., Vignes, M., Gougis, P., Magnifico, S., Betuing, S., Pietri, M., Caboche, J., Vanhoutte, P., Viovy, J.-L. and Brugg, B. (2011) 'Axon diodes for the reconstruction of oriented neuronal networks in microfluidic chambers.', *Lab on a Chip*, 11(21), pp. 3663–73.

Pliskin, W. A. and Conrad, E. E. (1964) 'Nondestructive determination of thickness and refractive index of transparent films', *IBM Journal of Research and Development*, 8(1), pp. 43–51.

Podrygajlo, G. (2009) 'Investigation of cellular phenotype in vitro and in transplantation studies', Thesis, University of Veterinary Medicine Hannover.

Poudel, I., Lee, J. S., Tan, L. and Lim, J. Y. (2013) 'Micropatterning-retinoic acid co-control of neuronal cell morphology and neurite outgrowth', *Acta Biomaterialia*, 9(1), pp. 4592–4598.

Poudel, I., Menter, D. E. and Lim, J. Y. (2012) 'Directing cell function and fate via micropatterning: role of cell patterning size, shape, and interconnectivity', *Biomedical Engineering Letters*, 2(1), pp. 38–45.

Purves, D., Augustine, G., Fitzpatrick, D., Katz, L., LaMantia, A.-S., McNamara, J. and Williams, M. (2001) 'Neuroscience', Sinauer Associates, Sunderland.

Rajnicek, A., Britland, S. and McCaig, C. (1997) 'Contact guidance of CNS neurites on grooved quartz: influence of groove dimensions, neuronal age and cell type', *Journal of Cell Science*, 110, pp. 2905–2913.

Ramstedt, M., Cheng, N., Azzaroni, O., Mossialos, D., Mathieu, H. J. and Huck, W. T. S. (2007) 'Synthesis and characterization of poly(3-sulfopropylmethacrylate) brushes for potential antibacterial applications', *Langmuir*, 23(6), pp. 3314–3321.

Raynor, J. E. (2008) 'Surface Modification of Titanium Substrates With Polymer Brushes To Control Cell Adhesion for Surface Modification of Titanium Substrates With Polymer Brushes To Control Cell Adhesion for Bioapplications', Thesis, Georgia Institute of Technology.

- Raynor, J. E., Capadona, J. R., Collard, D. M., Petrie, T. A. and García, A. J. (2009) 'Polymer brushes and self-assembled monolayers: versatile platforms to control cell adhesion to biomaterials (Review)', *Biointerphases*, 4(2), p. FA3-A16.
- Reece, J. B., Urry, L. A., Cain, M. L., Wasserman, S. A., Minorsky, P. V. and Jackson, R. B. (2010) 'Biology', Benjamin Cummings, San Francisco.
- Ren, T., Mao, Z., Guo, J. and Gao, C. (2013) 'Directional migration of vascular smooth muscle cells guided by a molecule weight gradient of poly(2-hydroxyethyl methacrylate) brushes', *Langmuir*, 29(21), pp. 6386–6395.
- Ren, Y. J., Zhang, H., Huang, H., Wang, X. M., Zhou, Z. Y., Cui, F. Z. and An, Y. H. (2009) 'In vitro behavior of neural stem cells in response to different chemical functional groups', *Biomaterials*, 30(6), pp. 1036–1044.
- Roach, P., Eglin, D., Rohde, K. and Perry, C. C. (2007) 'Modern biomaterials: a review - bulk properties and implications of surface modifications', *Journal of Materials Science: Materials in Medicine*, 18(7), pp. 1263–1277.
- Roach, P., Parker, T., Gadegaard, N. and Alexander, M. R. (2010) 'Surface strategies for control of neuronal cell adhesion: a review', *Surface Science Reports*, 65(6), pp. 145–173.
- Ross, R. A., Spengler, B. A. and Biedler, J. L. (1983) 'Coordinate morphological and biochemical interconversion of human neuroblastoma cells', *Journal of the National Cancer Institute*, 71(4), pp. 741–747.
- Rosso, F., Marino, G., Giordano, A., Barbarisi, M., Parmeggiani, D. and Barbarisi, A. (2005) 'Smart materials as scaffolds for tissue engineering', *Journal of Cellular Physiology*, 3, pp. 465–470.
- Rühe, J., Yano, R., Lee, J. S., Köberle, P., Knoll, W. and Offenhäusser, A. (1999) 'Tailoring of surfaces with ultrathin polymer films for survival and growth of neurons in culture', *Journal of Biomaterials Science. Polymer Edition*, 10(8), pp. 859–874.
- Scallan, K. F. (2007) 'The Detection of Elemental Mercury by Gold Nanoparticles', Thesis, University of California, Berkeley.
- Schmidt, C. E. and Leach, J. B. (2003) 'Neural tissue engineering: strategies for repair and regeneration', *Annual Review of Biomedical Engineering*, 5(1), pp. 293–347.

Senaratne, W., Andruzzi, L. and Ober, C. K. (2005) 'Self-assembled monolayers and polymer brushes in biotechnology: current applications and future perspectives', *Biomacromolecules*, 6(5), pp. 2427–2448.

Shah, S., Solanki, A. and Lee, K. B. (2016) 'Nanotechnology-based approaches for guiding neural regeneration', *Accounts of Chemical Research*, 49(1), pp. 17–26.

Sharples, A. P., Player, D. J., Martin, N. R. W., Mudera, V., Stewart, C. E. and Lewis, M. P. (2012) 'Modelling in vivo skeletal muscle ageing in vitro using three-dimensional bioengineered constructs', *Aging Cell*, 11(6), pp. 986–995.

Sheng, W., Li, B., Wang, X., Dai, B., Yu, B., Jia, X. and Zhou, F. (2015) 'Brushing up from “anywhere” under sunlight: a universal surface-initiated polymerization from polydopamine-coated surfaces', *Chemical Science*, 6, pp. 2068–2073.

Sherwood, L. (2001) 'Human Physiology: From Cells to Systems', Brooks/Cole, Pacific Grove.

Shim, H. W., Lee, J. H., Hwang, T. S., Rhee, Y. W., Bae, Y. M., Choi, J. S., Han, J. and Lee, C. S. (2007) 'Patterning of proteins and cells on functionalized surfaces prepared by polyelectrolyte multilayers and micromolding in capillaries', *Biosensors and Bioelectronics*, 22, pp. 3188–3195.

Shirley, D. A. (1972) 'High-resolution x-ray photoemission spectrum of the valence bands of gold', *Physical Review B*, 5(12), pp. 4709–4714.

Sigma-Aldrich Co. LLC. (2013) *PCR/qPCR/dPCR Assay Design*. Available at: <http://www.sigmaaldrich.com/technical-documents/articles/biology/pcr-qpcr-dpcr-assay-design.html>. (Accessed: 20 July 2016).

Silver, J. and Sidman, R. L. (1980) 'A mechanism for the guidance and topographic patterning of retinal ganglion cell axons', *The Journal of Comparative Neurology*, 189(1), pp. 101–111.

Sjöström, T.; Mcnamara, L. E.; Meek, R. M. D.; Dalby, M. J.; Su, B (2013) '2D and 3D nanopatterning of titanium for enhancing osteoinduction of stem cells at implant surfaces'. *Adv. Healthc. Mater.* 2 (9), pp 1285–1293

Smith, A. S. T., Passey, S. L., Martin, N. R. W., Player, D. J., Mudera, V., Greensmith, L. and Lewis, M. P. (2016) 'Creating interactions between tissue-engineered skeletal muscle and the peripheral nervous system', *Cells Tissues Organs*, 202(3–4), pp. 143–158.

Srinivasan, A., Tahilramani, M., Bentley, J. T., Gore, R. K., Millard, D. C., Mukhatyar, V. J., Joseph, A., Haque, A. S., Stanley, G. B., English, A. W. and Bellamkonda, R. V. (2015) 'Microchannel-based regenerative scaffold for chronic peripheral nerve interfacing in amputees', *Biomaterials*, 41, pp. 151–165.

Srivastava, D. K. (1991) 'Surface Phenomena and Fine Particles in Water-Based Coatings and Printing Technology'. Plenum Press. Edited by F. J. Sharma, M.K. and Micale. New York.

Srl, E. E. (2003) 'Ordyl dry film alpha 900 Photoresist', Technical sheet.

Staii, C., Viesselmann, C., Ballweg, J., Shi, L., Liu, G. yu, Williams, J. C., Dent, E. W., Coppersmith, S. N. and Eriksson, M. A. (2009) 'Positioning and guidance of neurons on gold surfaces by directed assembly of proteins using Atomic Force Microscopy', *Biomaterials*, 30, pp. 3397–3404.

Stanton, M. M. (2014) 'Regulation of Cell Behavior at the Cell-Surface Interface', Thesis, Worcester Polytechnic Institute.

Stevens, M. M. and George, J. H. (2005) 'Exploring and engineering the cell surface interface.', *Science*, 310, pp. 1135–1138.

Stieglitz, T., Schuettler, M. and Koch, K. P. (2005) 'Implantable biomedical microsystems for neural prostheses', *IEEE Engineering in Medicine and Biology Magazine: the Quarterly Magazine of the Engineering in Medicine & Biology Society*, 24(5), pp. 58–65.

Sukenik, C. N., Balachander, N., Culp, L. A., Lewandowska, K. and Merritt, K. (1990) 'Modulation of cell adhesion by modification of titanium surfaces with covalently attached self-assembled monolayers', *Journal of Biomedical Materials Research*, 24, pp. 1307–1323.

Takahashi, H., Nakayama, M., Itoga, K., Yamato, M. and Okano, T. (2011) 'Micropatterned thermoresponsive polymer brush surfaces for fabricating cell sheets with well-controlled orientational structures', *Biomacromolecules*, 12(5), pp. 1414–1418.

Takano, H., Kenseth, J. R., Wong, S. S., O'Brien, J. C. and Porter, M. D. (1999) 'Chemical and biochemical analysis using scanning force microscopy', *Chemical Reviews*, 99(515), pp. 2845–90.

- Takazawa, T., Croft, G. F., Amoroso, M. W., Studer, L., Wichterle, H. and MacDermott, A. B. (2012) 'Maturation of spinal motor neurons derived from human embryonic stem cells', *PLoS ONE*, 7(7), pp. e40154.
- Tan, K. Y., Lin, H., Ramstedt, M., Watt, F. M., Huck, W. T. S. and Gautrot, J. E. (2013) 'Decoupling geometrical and chemical cues directing epidermal stem cell fate on polymer brush-based cell micro-patterns', *Integrative Biology: Quantitative Biosciences from Nano to Macro*, 5, pp. 899–910.
- Teixeira, A. I., Ilkhanizadeh, S., Wigenius, J. A., Duckworth, J. K., Ingans, O. and Hermanson, O. (2009) 'The promotion of neuronal maturation on soft substrates', *Biomaterials*, 30, pp. 4567–4572.
- Thevenot, P., Hu, W. and Tang, L. (2008) 'Surface chemistry influence implant biocompatibility', *Current Topics in Medicinal Chemistry*, 8(4), pp. 270-280.
- Tonazzini, I., Cecchini, A., Elgersma, Y. and Cecchini, M. (2014) 'Interaction of SH-SY5Y cells with nanogratings during neuronal differentiation: comparison with primary neurons', *Advanced Healthcare Materials*, 3(4), pp. 581–587.
- Tong, W., Liu, X., Pan, F., Wu, Z. and Jiang, W. (2012) 'Protein adsorption and cell adhesion on RGD-functionalized silicon substrate surfaces', *Chinese Journal of Polymer Science*, 31(3), pp. 495–502.
- Tong, Y. W. and Shoichet, M. S. (2001) 'Enhancing the neuronal interaction on fluoropolymer surfaces with mixed peptides or spacer group linkers', *Biomaterials*, 22(10), pp. 1029–1034.
- Tuft, B. W. (2014) 'Photopolymerized materials and patterning for improved performance of neural prosthetics', Thesis, University of Iowa.
- Tugulu, S., Silacci, P., Stergiopulos, N. and Klok, H.-A. (2007) 'RGD-Functionalized polymer brushes as substrates for the integrin specific adhesion of human umbilical vein endothelial cells', *Biomaterials*, 28, pp. 2536–2546.
- Ulman, A. (1996) 'Formation and structure of self-assembled monolayers', *Chemical Reviews*, 96(4), pp. 1533–1554.

- Vega-Avila, E. and Pugsley, M. K. (2011) 'An overview of colorimetric assay methods used to assess survival or proliferation of mammalian cells', *Proceedings of the Western Pharmacology Society*, 54, pp. 10–14.
- Ventre, M., Causa, F. and Netti, P. A. (2012) 'Determinants of cell-material crosstalk at the interface: towards engineering of cell instructive materials', *Journal of the Royal Society Interface*, 9(74), pp. 2017–2032.
- Vroman, L.; Adams, A. L.; Fischer, G. C.; Munoz, P. C. (1980) Interaction of high molecular weight kininogen, factor XII, and fibrinogen in plasma at interfaces. *Blood* 55 (1), pp 156–159.
- Wan, F., Pei, X., Yu, B., Ye, Q., Zhou, F. and Xue, Q. (2012) 'Grafting polymer brushes on biomimetic structural surfaces for anti-algae fouling and foul release', *ACS Applied Materials and Interfaces*, 4, pp. 4557–4565.
- Wan, F., Ye, Q., Yu, B., Pei, X. and Zhou, F. (2013) 'Multiscale hairy surfaces for nearly perfect marine antibiofouling', *Journal of Materials Chemistry B*, 1(29), pp. 3599–3606.
- Wang, J.-S. and Matyjaszewski, K. (1995) 'Controlled/"living" radical polymerization. halogen atom transfer radical polymerization promoted by a Cu(I)/Cu(II) redox process', *Macromolecules*, 28(23), pp. 7901–7910.
- Wei, J., Igarashi, T., Okumori, N., Igarashi, T., Maetani, T., Liu, B. and Yoshinari, M. (2009) 'Influence of surface wettability on competitive protein adsorption and initial attachment of osteoblasts', *Biomedical Materials*, 4(4), p. 045002.
- Wei, Q., Wang, X. and Zhou, F. (2012) 'A versatile macro-initiator with dual functional anchoring groups for surface-initiated atom transfer radical polymerization on various substrates', *Polymer Chemistry*, 3(8), pp. 2129–2137
- Wei, X. and Ngai, T. (2012) 'Ion-induced hydrophobic collapse of surface-confined polyelectrolyte brushes measured by total internal reflection microscopy', *Polymer Chemistry*, 3(8), p. 2121.
- Xia, Y. and Whitesides, G. M. (1998) 'Soft lithography', *Annual Review of Materials Science*, 28, pp. 153–184.
- Xiao, Y., Grieshammer, U. and Rosenthal, N. (1995) 'Regulation of a muscle-specific

transgene by retinoic acid', *Journal of Cell Biology*, 129(5), pp. 1345–1354.

- Xie, H., Hu, L. and Li, G. (2010) 'SH-SY5Y human neuroblastoma cell line: in vitro cell model of dopaminergic neurons in Parkinson's disease', *Chinese Medical Journal*, 123, pp. 1086–1092.
- Yaffe, D. and Saxel, O. (1977) 'Serial passaging and differentiation of myogenic cells isolated from dystrophic mouse muscle', *Nature*, 270(5639), pp. 725–727.
- Yamamoto, H., Demura, T., Morita, M., Banker, G. A., Tanii, T. and Nakamura, S. (2012) 'Differential neurite outgrowth is required for axon specification by cultured hippocampal neurons', *Journal of Neurochemistry*, 123, pp. 904–910.
- Yang, F., Murugan, R., Wang, S. and Ramakrishna, S. (2005) 'Electrospinning of nano/micro scale poly(l-lactic acid) aligned fibers and their potential in neural tissue engineering', *Biomaterials*, 26(15), pp. 2603–2610.
- Yom, J., Lane, S. M. and Vaia, R. A. (2012) 'Multi-component hierarchically structured polymer brushes', *Soft Matter*, 8(48), pp. 12009–12016.
- Yu, L. M. Y., Leipzig, N. D. and Shoichet, M. S. (2008) 'Promoting neuron adhesion and growth', *Materials Today*, pp. 36–43.
- Yuan, Y. and Lee, T. R. (2013) 'Contact angle and wetting properties', *Surface Science Techniques*, pp. 1–34.
- Zahavi, E. E., Ionescu, A., Gluska, S., Gradus, T., Ben-Yaakov, K. and Perlson, E. (2015) 'A compartmentalized microfluidic neuromuscular co-culture system reveals spatial aspects of GDNF functions.', *Journal of Cell Science*, 128(6), pp. 1241–1252.
- Zeng, X., Xu, G., Gao, Y. and An, Y. (2011) 'Surface wettability of (3-Aminopropyl)triethoxysilane self-assembled monolayers', *Journal of Physical Chemistry B*, 115, pp. 450–454.
- Zhang, F., Sautter, K., Larsen, A. M., Findley, D. A., Davis, R. C., Samha, H. and Linford, M. R. (2010) 'Chemical vapor deposition of three aminosilanes on silicon dioxide: surface characterization, stability, effects of silane concentration, and cyanine dye adsorption', *Langmuir*, 26(18), pp. 14648–14654.
- Zhang, Z., Chao, T., Chen, S. and Jiang, S. (2006) 'Superlow fouling sulfobetaine and carboxybetaine polymers on glass slides', *Langmuir*, 22(24), pp. 10072–10077.

Zhao, B. and Brittain, W. J. (2000) 'Polymer brushes : surface-immobilized macromolecules', *Progress in Polymer Science*, 25, pp. 677–710.

Zhao, C., Li, L., Wang, Q., Yu, Q. and Zheng, J. (2011a) 'Effect of film thickness on the antifouling performance of poly(hydroxy-functional methacrylates) grafted surfaces', *Langmuir*, 27, pp. 4906–4913.

Zhao, X. M., Xia, Y. and Whitesides, G. M. (1996) 'Fabrication of three-dimensional microstructures. Microtransfer molding', *Advanced Materials*, 8, pp. 837–840.

Zhao, Y. H., Zhu, X. Y., Wee, K. H. and Bai, R. (2010) 'Achieving highly effective non-biofouling performance for polypropylene membranes modified by UV-induced surface graft polymerization of two oppositely charged monomers', *Journal of Physical Chemistry B*, 114(7), pp. 2422–2429.

Zhou, Z., Yu, P., Geller, H. M. and Ober, C. K. (2012) 'The role of hydrogels with tethered acetylcholine functionality on the adhesion and viability of hippocampal neurons and glial cells', *Biomaterials*, 33, pp. 2473–2481.

Zhou, Z., Yu, P., Geller, H. M. and Ober, C. K. (2013) 'Biomimetic polymer brushes containing tethered acetylcholine analogs for protein and hippocampal neuronal cell patterning', *Biomacromolecules*, 14, pp. 529–537.

Zhu, B. (2012) 'Surface initiated polymerisation for applications in materials science', Thesis, Loughborough University.

Zhu, B., Eurell, T., Gunawan, R. and Leckband, D. (2001) 'Chain-length dependence of the protein and cell resistance of oligo(ethylene glycol)-terminated self-assembled monolayers on gold.', *Journal of Biomedical Materials Research*, 56(3), pp. 406–16.

Zhu, G. H., Huang, J., Bi, Y., Su, Y., Tang, Y., He, B. C., He, Y., Luo, J., Wang, Y., Chen, L., Zuo, G. W., Jiang, W., Luo, Q., Shen, J., Liu, B., Zhang, W. L., Shi, Q., Zhang, B. Q., Kang, Q., Zhu, J., Tian, J., Luu, H. H., Haydon, R. C., Chen, Y. and He, T. C. (2009) 'Activation of RXR and RAR signaling promotes myogenic differentiation of myoblastic C2C12 cells', *Differentiation*, 78(4), pp. 195–204.

9 Appendices

9.1 LIVE/DEAD® assay optimisation

Prior to identifying live and dead cell populations on the modified surfaces created, it was necessary to optimise the dye concentrations to ensure that the live cell dye (calcein AM) did not interfere with dead cell staining (ethidium homodimer-1, EthD-1) and *vice versa*. Therefore, cells were treated with 0.1, 0.5 and 1.0 μM concentrations of both calcein AM and EthD-1. Representative images with the ratio of the concentrations used for both dyes have been illustrated in Figure 9.1. For the lowest concentration of EthD-1 (0.1 μM) the cells had a faint red colour. For a concentration of 0.5 μM , ethidium homodimer omitted stronger fluorescence (images 4, 5 and 6), whereas the concentration of 1 μM seemed to be overexposed (images 7, 8 and 9; note that exposure settings were kept constant for all the images). As a result, 0.5 μM of ethidium homodimer was chosen as the concentration for future experimentation. For all of the concentrations, no traces of calcein AM were found and thus, the same range of concentrations were used on samples of live cells to optimise the concentration of calcein AM. Images A, B and C from Figure 9.1 represent the concentration of Calcein AM at 0.1, 0.5 and 1.0 μM , respectively. Cells treated with a concentration of 0.1 μM of calcein AM (A) displayed very faint staining, whilst cells exposed at a concentration of 1 μM (C) were stained intensely. At a concentration of 0.5 μM (B), an good amount of fluorescence was obtained from the cells and therefore this concentration was used for further experiments.

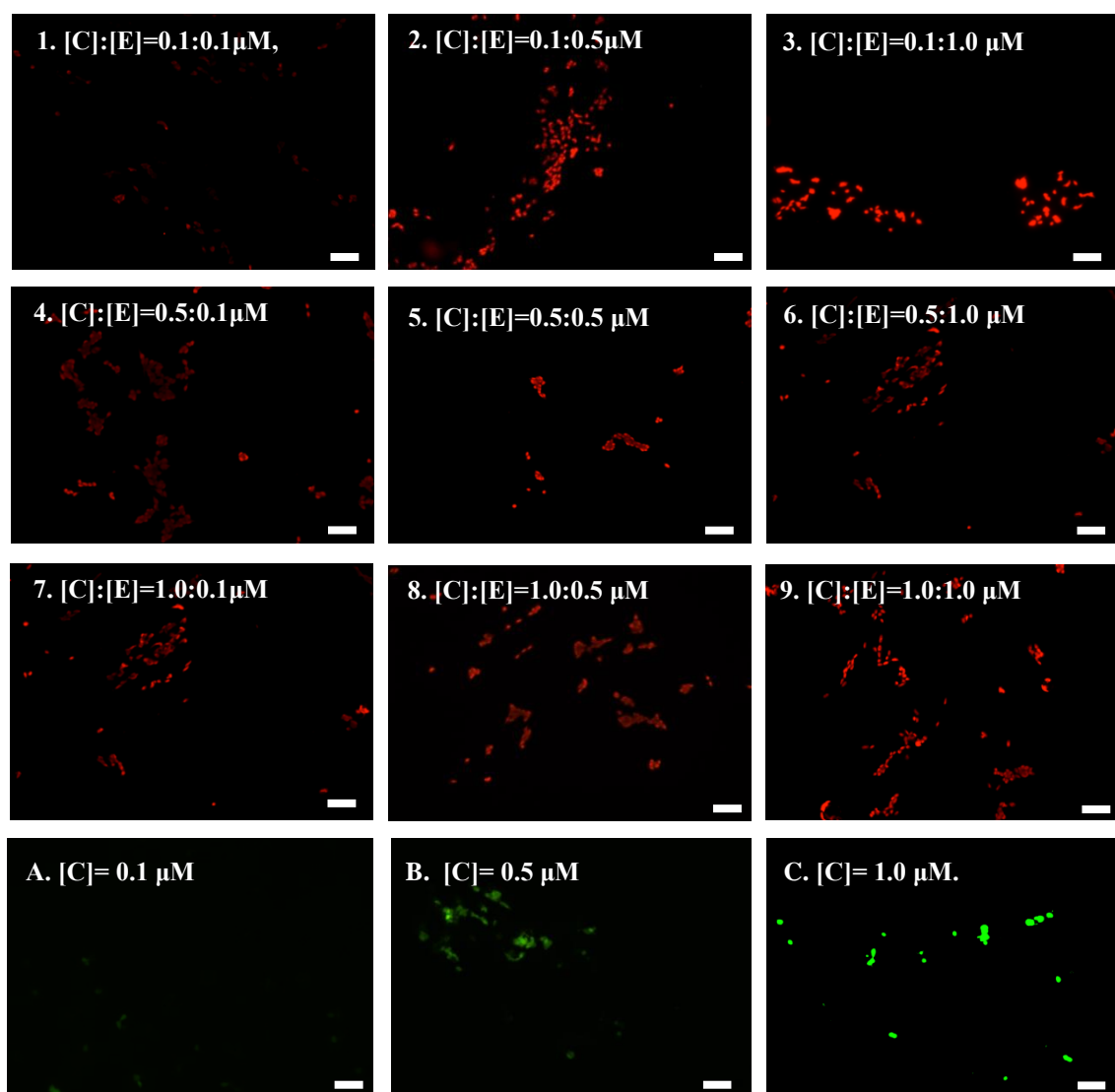


Figure 9.1. Representative fluorescence microscope images of SH-SY5Y for dye optimisation. Images 1-9 represent samples of dead cells used to determine EthD-1 concentration. The amount of calcein AM that did not fluoresce in dead samples was applied on samples of live cells (Image A, B and C). The specific concentrations used for each treatment have been specified in the images. [C]= concentration of calcein AM [E]= concentration of ethidium homodimer⁻¹. Scale bar= 100 μm.

9.2 alamarBlue® assay optimisation

Firstly, the dye was optimised so that the appropriate incubation time and cell density could be used for further experimentation. To achieve this, cells were seeded at three different cell densities (2500, 5000 and 10000 cells/cm²) and the assay was conducted over a 7 day culture period using different dye incubation times (1, 2 and 4 hours). Whilst exponential growth occurred for the various cell densities (Figure 9.2) the data at both 2500 (Figure 9.2A) and 5000 cells/cm² (Figure 9.2B) during day 5 and day 7, showed no clear indication of fluorescence increasing. This may be due to the cell density being insufficient to produce further fluorescence. This issue did not occur when the cell density was 10000 cells/cm² (Figure 9.2C), as the cell population increased exponentially over the course of the experiment until day 7. As a result, a seeding density of 10000 cells/cm² was used for further experimentation.

Regarding alamarBlue® incubation times (see Figure 9.3), data showed that all the dye incubation times tested (1, 2 and 4 hours) were suitable for experimentation since there was an overall increase in fluorescence for all the different cell densities, with no indication of a saturation period. An incubation of 4 hours was selected as fluorescence increased to a greater extent throughout the time course of the experiment.

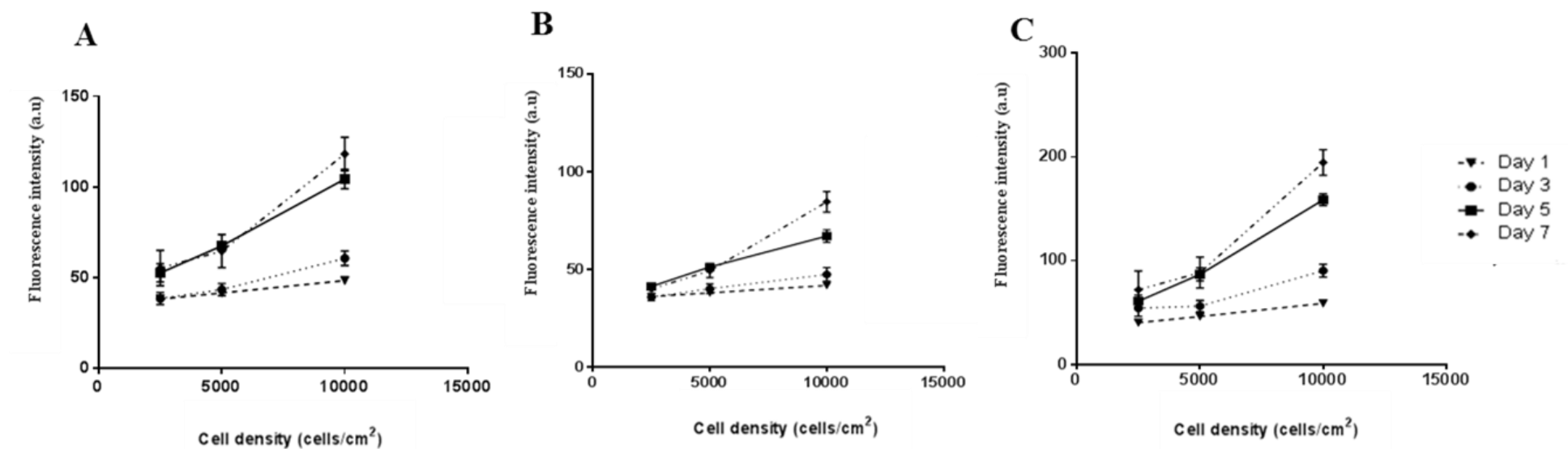


Figure 9.2. Optimisation of alamarBlue® assay for different cell densities for SH-SY5Y's. The dye was incubated for 1 hour (A), 2 hours (B) and 4 hours (C) at cell densities of 2500, 5000 and 10000 cells/cm² and at days 1, 3, 5 and 7. Error bars correspond to SD of the mean (n= 3).

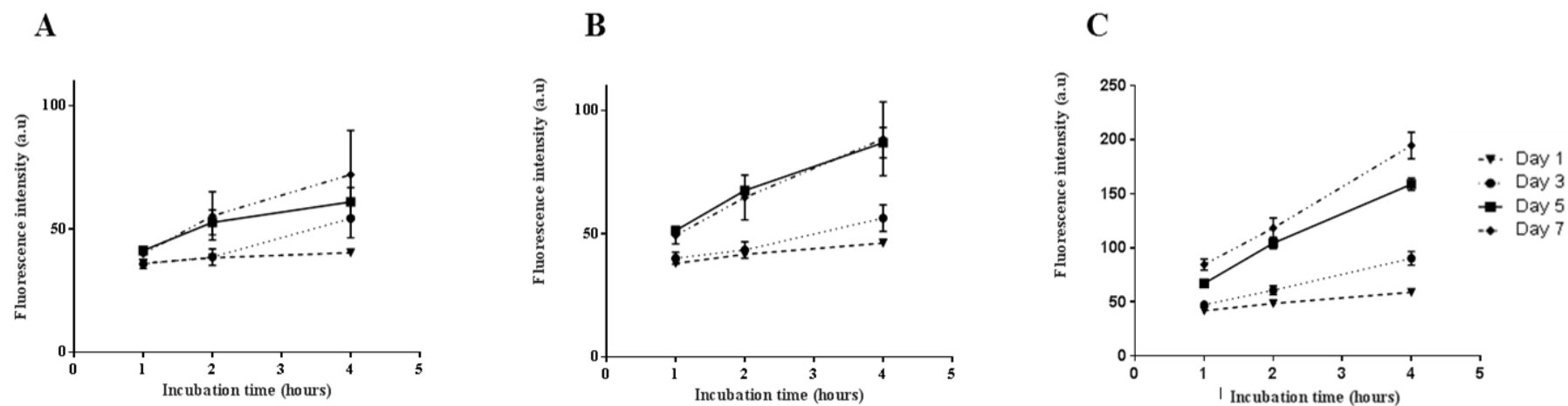


Figure 9.3. Optimisation of alamarBlue® assay at different incubation periods for SH-SY5Y's. The dye was used on 2500 (A), 5000 (B) and 10000 (C) cells/cm² and at days 1, 3, 5 and 7. Error bars correspond to SD of the mean (n= 3).

9.3 Guidance to estimate brush thickness

This thin-film colour chart was used as a qualitative guide for brush thickness estimation.

Available at <https://sites.google.com/site/stevedmondson/Home>.

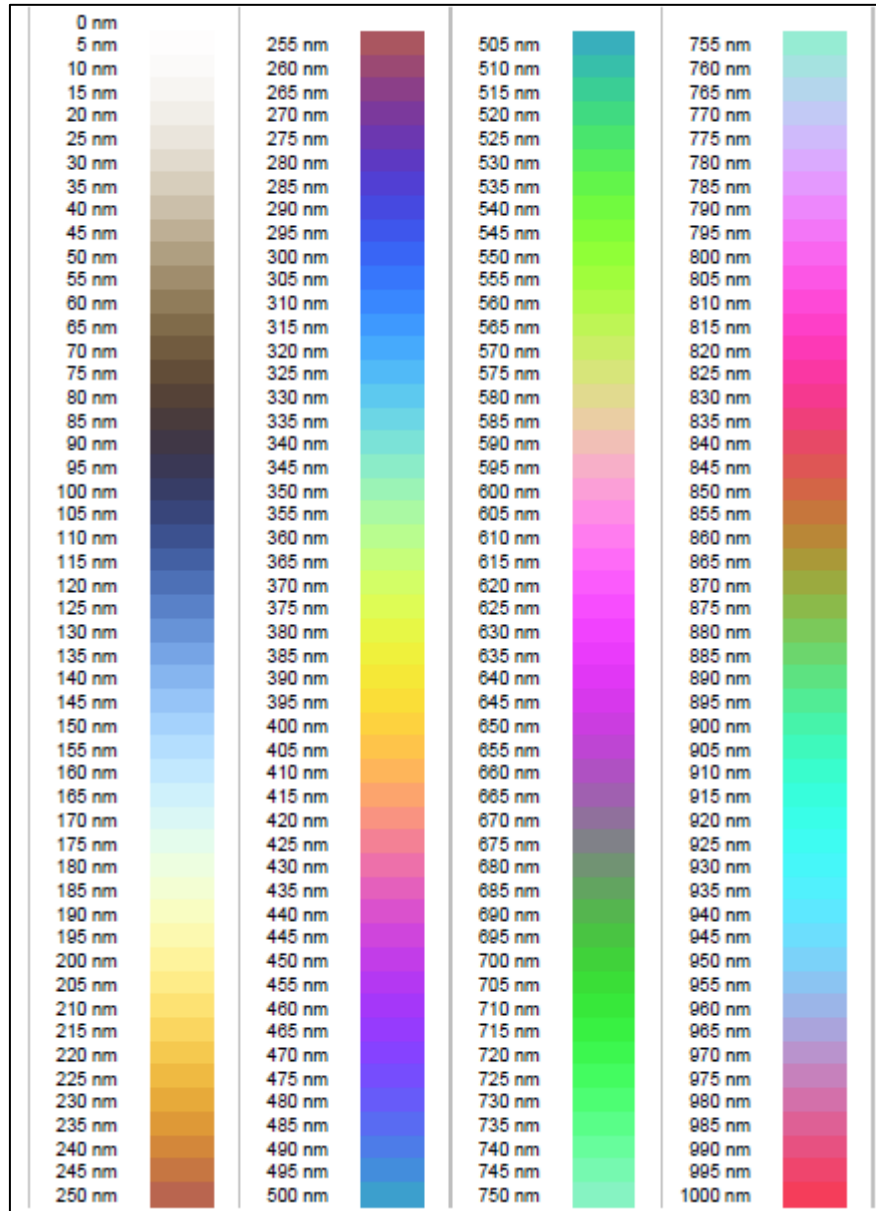


Figure 9.4. Colour chart to estimate brush thickness. Film with refractive index 1.5 on silicon.

9.4 List of abbreviations

a.u.	Arbitrary unit
AFM	Atom force microscopy
ANOVA	Analysis of variance
APTES	3-aminopropyltriethoxysilane
ARGET-ATRP	Activators regenerated by electron transfer atom transfer radical polymerization
ATRA	<i>All-trans</i> retinoic acid
ATRP	Atom transfer radical polymerisation
BE	Binding energy
BIBB	α -Bromoisobutyryl bromide
bp	Base pair
Bpy	2, 2'-bipyridine
BUM	Undecyl mercaptan
cDNA	Complementary deoxyribonucleic acid
cm	Centimeter
cm²	Centimeter squared
CNS	Central nervous system
CNT	Carbon nanotubes
CO₂	Carbon dioxide
C_T	Cycle threshold
CuBr	Copper (I) bromide
CuBr₂	Copper (II) bromide
CVD	Chemical vapour deposition
DAPI	4',6-Diamidino-2-Phenylindole

dH₂O	Distilled water
DM	Differentiated media
DMEM	Dulbecco's modified Eagle's medium
DMSO	Dimethyl sulfoxide
DNA	Deoxyribonucleic acid
dNTPs	Deoxynucleotides
DRG	Dorsal root ganglia
dsDNA	Double stranded DNA
ECM	Extracellular matrix
EDTA	Ethylenediaminetetraacetic acid
EK	Kinetic energy
EthD-1	Ethidium homodimer-1
eV	Electronvolt
FTIR	Fourier transform infrared
g	Gravity
GC	Guanine cytosine
GM	Growth media
GS	Goat serum
HEMA	2-hydroxyethyl methacrylate
hMSC	Human mesenchymal stem cells
HS	Horse serum
HUVEC	Human umbilical vein endothelial cells
<i>hν</i>	X-ray photon energy
IKVAV	Ile-Lys-Val-Ala-Val
IMS	Industrial methylated spirit

IR	Infrared
KSPMA	3-sulfopropyl methacrylate potassium salt
MAPT	Microtubule-associated protein tau
MeOH	Methanol
METAC	[2-(Methacryloyloxy)ethyl]trimethylammonium chloride
MFBS	Foetal bovine serum
MHDA	16-Mercaptohexadecanoic acid
MIMIC	Micromolding in capillaries
mL	Milliliter
mm	Millimeter
MMA	Methyl methacrylate
mmol	Millimol
mRNA	Messenger ribonucleic acid
NFBS	Heat-inactivated foetal bovine serum
NF-H	Neurofilament-H
ng	Nanogram
nm	Nanometer
NMJ	Neuromuscular junction
NMP	Nitroxide-mediated radical polymerization
NS	Nervous system
NSCs	Neuronal stem cells
OTS	Octadecyltrichlorosilane
P/S	Penicillin/Streptomycin
PAcMo	Poly(N-acryloylmorpholine)
PAH	Polyallylamine hydrochloride

PBS	Phosphate buffered saline buffer
PCR	Polymerase chain reaction
PDMS	Polydimethylsiloxane
PE	Polyethylene
PEG	Polyethylene glycol
PHEMA	Poly (2-hydroxyethyl methacrylate)
PIPAAm	Poly(N-isopropylacrylamide)
PKSPMA	Poly(potassium 3-sulfopropyl methacrylate)
PLA	Poly(L-lactic acid)
PLL	Poly-L-lysine
PMETAC	Poly([2-(Methacryloyloxy)ethyl]trimethylammonium chloride)
PMMA	Poly(methyl methacrylate)
PMPC	Poly(2-Methacryloyloxyethyl phosphorylcholine)
PNS	Peripheral nervous system
PSPMA	Poly(potassium 3-sulfopropyl methacrylate)
PTHFEMA	Poly(2,2,2-Trifluoroethyl methacrylate)
PTMAEMA	Poly(2-methacryloyloxy ethyl trimethyl ammonium chloride)
RAR	Retinoid acid receptor
RBL	Rat basophilic leukaemia cells
RGD	Arg-Gly-Asp
RNA	Ribonucleic acid
ROMP	Ring-opening metathesis polymerization
R_p	Reflection ratio of p polarised light
RPIIβ	RNA polymerase II
rpm	Revolutions per minute

R_s	Reflection ratio of s polarised light
RT	Room temperature
RT-qPCR	Real time quantitative polymerase chain reaction
RXR	Retinoid X receptor
SAMs	Self-assembled monolayers
SD	Standard deviation
SEM	Standard error of the mean
SI-ARGET ATRP	Surface initiated activator regenerated by electron transfer atom transfer radical polymerization
SI-ATRP	Surface initiated atom transfer polymerization
SIP	Surface initiated polymerisation
SPL	Scanning probe lithography
TBS	Tris-buffered saline
THF	Tetrahydrofuran
T_m	Melting temperature
UV	Ultraviolet
VSMC	Vascular smooth muscle cells
XPS	X-ray photoelectron spectroscopy
γ_{lv}	Surface tension at the liquid-vapour interface
γ_{sl}	Surface tension at the solid-liquid interface
γ_{sv}	Surface tension at the solid-vapour interface
Δ	Change
θ	Angle
μL	Microliter
μM	Micromolar

μm	Micrometer
μTM	Microtransfer molding
μM	Micromolar
°	Degrees
°C	Degrees centigrade
Ψ	Amplitude
%	Percentage

9.5 Achievements related to this thesis

Conference abstracts

M. M. Pardo-Figuerez, N. R. W. Martin, D. J. Player, S. D. R. Christie and M. P. Lewis. eCM Meeting Abstracts 2015, Collection 3; TCES (page 88).

M. M. Pardo-Figuerez, N. R. W. Martin, D. J. Player, A. J. Capel, S. D. R. Christie and M. P. Lewis. eCM Meeting Abstracts 2016, Collection 5; TCES (page 109).

Original articles

M. M. Pardo-Figuerez, N. R. W. Martin, D. J. Player, A. J. Capel, S. D. R. Christie and M. P. Lewis. Neural and aneural regions generated by the use of chemical surface coatings (2017). ACS Biomater. Sci. Eng., Just Accepted Manuscript. DOI: 10.1021/acsbiomaterials.7b00663

M. M. Pardo-Figuerez, N. R. W. Martin, D. J. Player, A. J. Capel, S. D. R. Christie and M. P. Lewis. Micro-patterned polymer brushes leading neuronal guidance (2017). **In preparation.**

Awards

Winner Poster Competition, Science Matters conference, Loughborough University (2014).

‘Honourable Mention Award’ in ‘Reflections of Research Photo Competition’, Loughborough University (2016).